Resources

Improving returns from southern pine plantations through innovative resource characterisation

Project number: PNC361-1415

April 2019

Forest & Wood Products Australia

Improving returns from southern pine plantations through innovative resource characterisation

Prepared for

Forest & Wood Products Australia

Henri Bailleres and David Lee*

Chandan Kumar, Steven Psaltis, Gary Hopewell, Loic Brancheriau

Scientific contributions:
Ian Turner, Troy Farrell, Elliott Carr, Geoff Downes, Bruce Hogg, Adam Redman, William Leggate and Lesley Francis

* Project leader

Publication: Improving returns from southern pine plantations through innovative resource characterisation

Project No: PNC361-1415

Researchers:
David Lee
University of the Sunshine Coast
90 Sippy Downs Drive
Sippy Downs Qld 4556

Henri Bailleres, Gary Hopewell, Chandan Kumar, Adam Redman, William Leggate*, Bruce Hogg, Lesley Francis
Department of Agriculture & Fisheries
50 Evans Road
Salisbury Qld 4107

Steven Psaltis, Ian Turner, Troy Farrell, Elliott Carr
Queensland University of Technology
Gardens Point campus, L8 Y block

Geoff Downes
Forest Quality Pty. Ltd.
Tasmania

Loic Brancheriau
CIRAD, Montpellier
France

* Formerly DAF, currently Koppers Performance Chemicals Australia

Final report received by FWPA in May, 2018

1 Executive summary

The southern pine resource includes slash pine (*Pinus elliottii* var. *elliottii*) [PEE], Caribbean pine (*P. caribaea* var. *hondurensis*) [PCH] and a locally-developed hybrid [PEE × PCH] (hybrid pine). These pines as well as smaller areas of loblolly pine (*P. taeda*) have been the main taxa planted in the coastal areas of southern Queensland and subcoastal areas of northern New South Wales for the last 25 years.

The standard structural grade ranking of the southern pine resource is limited by its stiffness as characterised by the measurement of the Modulus of Elasticity (MOE). The MOE dictates the mechanical grade of the board (or other structural products, extracted from the log). A board's market value is directly linked to its stress grade based on individual grading performance (e.g. MGP10). For example, 1 m³ of structural board (i.e. MGP10 and above) is worth about \$350 whereas non-structural board (i.e. <MGP10) is worth about \$80. Based on the importance of MOE, this report focusses on it as the key attribute for the southern pine.

Non-destructive tools that accurately measure board MOE will allow enhanced genetic selection, site matching, harvest planning schedules, improved allocation of the resource to different processors and facilitate improved processor settings and product performance.

Key findings from the study were:

- Sigmoid curves (S shaped curves) capture the variation in wood properties from the pith to the bark.
  - The cambial age versus ultrasound MOE (USMOE) sigmoids, referred to here as 'fingerprint curves', measured along sampled cores, are independent of the silviculture, size and growth of the trees. These curves vary depending on genetics and environment. They allow the grower and processor to determine the performance potential of genetic material in a given environment.
  - The radial growth versus USMOE curves, referred to as 'radial sigmoids', are influenced by silviculture as well as genetics and environment. These curves estimate the quantity of wood of a given performance (e.g. >10,000 MPa).
  - Both of these curves provide useful information to manage plantation growth and processing, improving the growers' and processors' abilities to value stands of trees.
- Of the three technologies tested the USMOE provided the most accurate measure of sawlog MOE ($R^2 = 0.78$) and the least biased (9% bias). The Resistograph was the second most accurate tool at predicting log MOE ($R^2 = 0.68$) and a 9% bias. The ST300 was the least accurate tool to predict log MOE ($R^2 = 0.42$) and had a large bias of 41%. The large bias on the ST300 resulted in this tool over-predicting the MOE of the trees in the stands.
- The USMOE using a 2D integration approach can reconstruct an estimate of MOE for individual boards that can be sawn from trees with moderate accuracy ($R^2 = 0.53$) and very little bias (2%). Similar results were achieved using 3D approaches. These correlations are robust, since they are based on a deterministic approach that directly connects products to the trees from which they were derived. This has potential to improve the growers' and processors' abilities to value stands of trees and the trees within these stands.
- The ST300 (time of flight of stress waves) and Resistograph (resistance to drilling) technologies only give a single measurement or prediction of sawlog MOE, and this

number is based on calibrations and approximations. Hence, they cannot be used to accurately predict the value of different parts of the plantation estate, but they may be useful for a general ranking of stands. They are useful at segregating the extreme high or low MOE range.

- Changing the sawing pattern used on a log can have a dramatic impact on the recovery of MGP10 or better boards. This could improve product value with flow-on effects across the whole value chain.

Key recommendations

- The sawlog and board MOE estimated by the USMOE should be further validated by destructively sampling a broad range of the plots.
- Southern pine growers should use the fingerprint curves obtained from USMOE measured on cores at age 17, along with LiDAR information to better manage their plantation estates to maximise sales of high value products.
- Processors should use the USMOE to optimise their setting to maximise recovery of high value products improving returns across the whole value chain.

Table of contents

2 List of figures

3   List of tables

4 Glossary

5PL	Five parameter logistic function.
Accuracy	Accuracy describes the difference between the measurement and the part's actual value.
Allometric	Describes change in characteristics with change in size.
Asymptote	A value that you get closer and closer to, but never quite reach. In mathematics, an asymptote is a line that a graph approaches but never touches.
Bias	A measure of the distance between the value of the measurements and the true value of the sample.
BING	Beam Identification by Non-destructive Grading; a resonance acoustic method for estimating MOE.
Box plot	Also known as a box and whiskers graph. A box plot, is a simple way of representing statistical data in which a box is drawn to represent the second and third quartiles, usually with a horizontal line inside to indicate the median value. The lower and upper quartiles are shown as vertical lines either side of the box. Values outside the vertical line are considered anomalous.
CA (cambial age)	The age of the cambium when the wood was formed. On a seasonal basis it corresponds to the ring number when counting outwards from the pith.
Cambial sigmoid or CA sigmoid	A 5PL sigmoid curve fitted between MOE vs weighted average cambial age for each segments
Clone	Vegetatively produced copies of an organism (in this case pine hybrid trees).
Fingerprint curve	The 5PL curve fitted between MOE as a function of cambial age
Fingerprint function	The 5PL function fitted between MOE as a function of cambial age.
Genotype	Genetically similar organisms (trees)
Integral or Integration	The general meaning is "to put together parts or elements and combine them into a whole". Integration is the process of finding the "area under the curve" in the one-dimensional context, i.e. integrating a single-variable function over an interval.
Integral average	The average of a function calculated by integration. In this report, a 'shell integration' was performed to calculate the integral average MOE.
Metrology	The science of measurement to manufacturing and other processes and their use, ensuring the suitability of measurement instruments, their accuracy, calibration and quality control.
MPa	Megapascal, is equal to 10^6 Pascal, a unit of measure for Modulus of Elasticity (MOE) (mega = 10^6)
MGP	Machine-graded pine
MGP10+	Wood or boards having MOE of 10,000 MPa or greater
MOE (modulus of elasticity)	Modulus of elasticity infers about material's important property against any external stress. It is the resistance given by material against deformation.
NDE	Non-destructive evaluation (testing)
NLE	Non-lethal evaluation (testing).
NIR	Near infrared spectroscopy.
PCT	Pre-commercial thin.

Plot fingerprint	The characteristics of a plot given by its cambial sigmoid.
Precision	Precision describes the variation you see when you measure the same part repeatedly with the same device.
Qualitative assessment	Assessment of wood quality that focuses on USMOE without accounting for the quantity of wood. The qualitative assessments in this report were performed using a cambial sigmoid.
Quantitative assessment	Assessment of wood quality that focuses on the quantity of wood with a particular USMOE. The quantitative assessments in this report were performed using a radial sigmoid.
Radial sigmoid	A sigmoid curve fitted between MOE and radial position for each segment from a core.
Regularisation	Creating models that generalise performance of a plot by fitting the segments' MOE data in a plot against cambial age.
ResiMOE	The MOE predicted by the IML Resistograph when the default (*P. radiata*) calibration was used.
Sigmoid	'S' shape curve defined by five parameter logistic function (5PL).
Static bending MOE	Board MOE obtained by a static bending test.
Static bending test	A four-point bending test also known as flexural test that provides values for MOE in according to the Australian standard.
ST300MOE	The MOE predicted from the squaring the acoustic velocity measured by the ST300 and a nominal green density of 1,000 kg/m³.
Stiffness	A measure of a board's/beam's resistance to deflection; see MOE.
Stress Grade	Structural grading is the process by which timber is sorted into groups - or stress grades - with ideally, similar structural properties in each group. Inevitably there is a very substantial range of properties within a group and significant overlap in properties between the groups. Structural grading can be performed in a number of ways including the following: • visual stress-grading • machine stress-grading • machine proof-grading The two most commonly used methods in Australia are visual stress-grading and machine stress-grading, with use of machine proof-grading being limited.
Stocking rate	The approximate number of stems per hectare (spha).
Taxon (plural taxa)	Species, varieties or hybrids of trees
US	Ultrasound
USMOE	The MOE predicted from the core by integration of the core segments predicted from ultrasound measurement of MOE at 8% moisture content.
Virtual board	A board that was reconstructed mathematically by mimicking the actual sawing pattern.
Violin plot	Violin plots are similar to box plots, except that they also show the kernel probability density of the data at different values. Typically, violin plots will include a marker for the median of the data.
Weighted average cambial age	The average cambial age resulting from the multiplication of each cambial rings age in a core segment by the relative corresponding area in the segment.

5 Rationale for the project approach

5.1 Forest value chain

The Australian forest sector's prosperity is becoming less and less dependent on the traditional volume production target. As in many countries, the economic viability of fibre sources increasingly depends on end-product value, performance and diversity. The value of the products in the market are dictated by the products' performance. This project aims to improve the assessment and prediction of the performance of the final products such as boards or veneer from measurements taken on standing trees. Making this link will improve returns across the forest value chain.

Currently the main product manufactured from the southern pine resource in Australia is sawn timber in the form of standard board sizes (Figure 1). The value of this product depends on its mechanical performances assessed using Australian Standard procedures. They specify non-structural and structural grades based on product stiffness quantified by the Modulus of Elasticity (MOE) and its strength quantified by the Modulus of Rupture (MOR). The standard structural grade rating of the southern pine resource is limited by its stiffness. The MOE dictates the mechanical grade of the board. A board's market value is directly linked to its grade based on individual grading performance (e.g. MGP10). For example, 1m³ of structural board (i.e. MGP10 and above) is worth about ≥$350 whereas non-structural board (i.e. <MGP10) is worth about $80.

In order to extract the best value from the wood fibre, it is essential that the performance of the forest resource be assessed as soon as possible along the wood value chain. Consequently, in the case of the southern pine resource, the structural performance assessment of the board MOE from in-field tree measurements is the key element to estimate resource value and optimise value extraction.
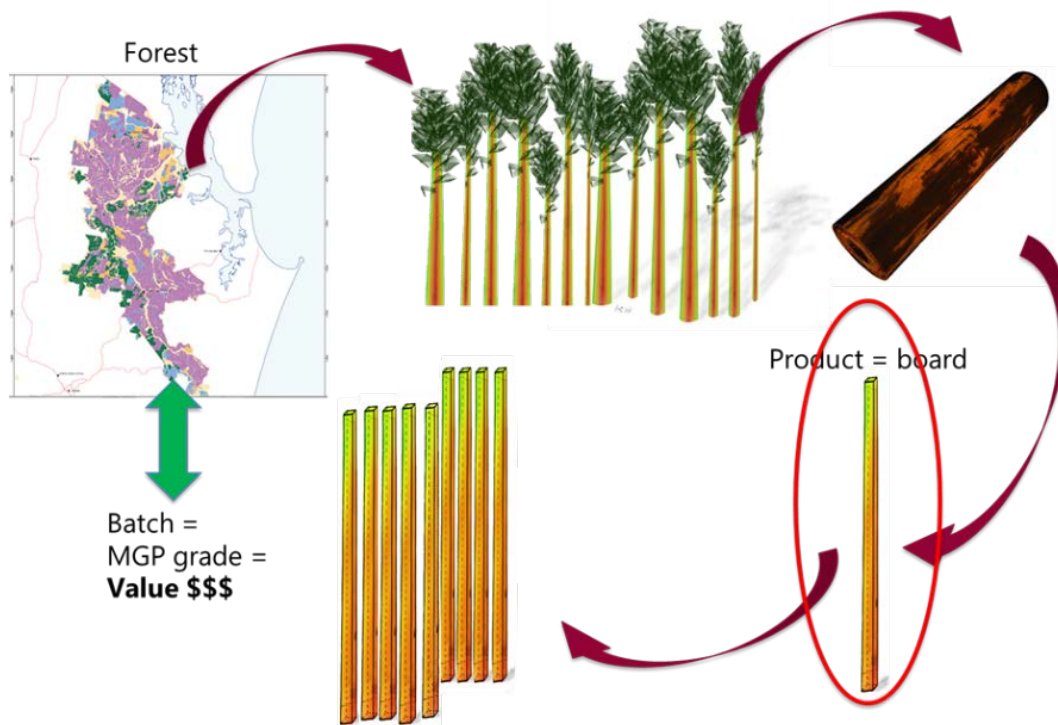
Figure 1. Schematic showing the process to obtain final product (board) from forest and the profit associated with the final product.

Many factors contribute to the variability in the quality of the final product cut from a plantation. The variability of the southern pine plantation estate in space and time is complex. The variability is expressed in different ways:
- at the stand, compartment, or plot level;
- within and between tree in terms of size and properties;
- within a log, where the greatest variation occurs from the pith to the bark (along the radius)
- within and between boards sawn from a log

Here is an example of the variability in southern pine at the tree and forest level: in southern pine plantations, the variability of MOE at the end of the rotation ranges from 8,700 to 14,400 MPa. Within a single tree the MOE of clear wood can range from 3,000 MPa to 26,000 MPa. This MOE gradient is observed across the radius of the tree with the MOE increasing from the pith to the bark. The variation up the tree is much lower. The MOE variation around the circumference of the tree is even lower. The latter is essentially due to the presence of reaction wood (compression wood) caused by competition, wind or mechanical stress.

5.2   From log to board

Bearing in mind the variation of MOE within a tree, when a board is sawn across the log MOE gradient, the prediction of a single board's MOE requires information about the position of the board within the log which gives the MOE distribution within the board (Figure 2).
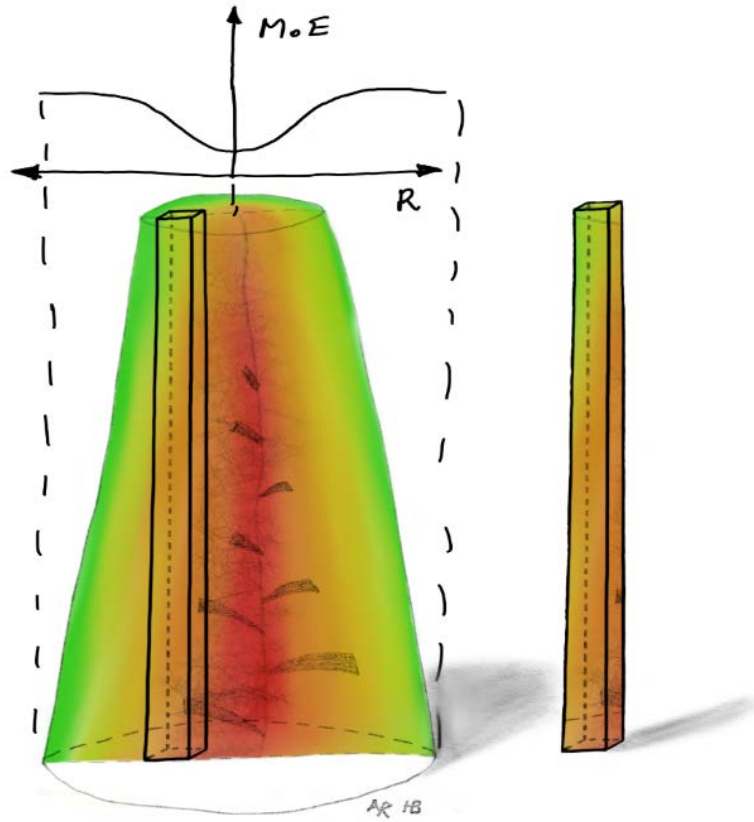
Figure 2. Within log MOE variability from low (red) to high (green) MOE and the consequence of this on the board MOE gradient.

It is not possible to predict the MOE of a board from the log level information such as average log MOE. The position of the board and the description of MOE gradients within the log are essential for predicting the MOE of an individual board. To further illustrate the importance of gaining access to MOE gradients, the individual board MOE, based on static bending, obtained from each log is plotted against log stiffness that has been accurately measured through a resonance acoustic method (Figure 3). It is clear that log stiffness is poorly correlated ($R^2= 0.14$) with stiffness of individual boards cut from the log.
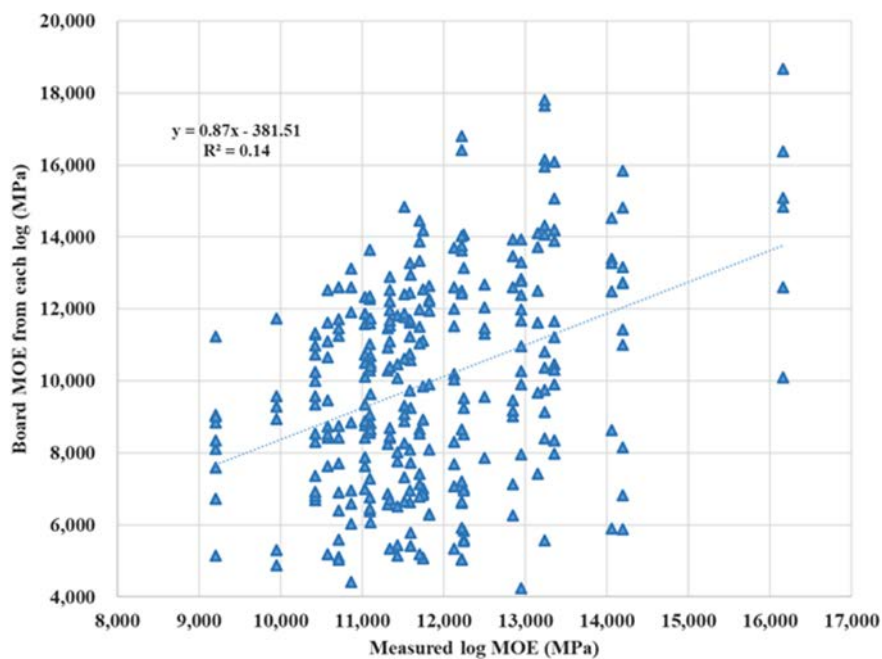
Figure 3. Relationship between the whole log MOE (n=30) and individual board MOE (n=294; static bending). Each vertical array depicts static MOE for a sub-sample from each board from a single log.

However, using the same dataset, the correlation between the average stiffness of all the boards obtained from a log and the log stiffness (Figure 4) is quite high (R^2=0.75). This latter correlation however is useless to predict the performances of individual boards, as it does not represent the actual value i.e. the individual board performance to the log. The only time this correlation can help growers and processors select logs are those instances of logs with very low or very high MOE. These logs should provide a high proportion of either very low or very high MOE boards. Unfortunately, these extreme cases represent a small proportion of the resource. Since the variability between logs is lower than the variability between boards, each log would provide a different distribution of board MOE. For the processor, the value of the board is based on a ranking system (with boards being graded into various MOE stress grades or classes). A single MOE prediction for a whole log will not provide useful information about the MOE of boards that could be cut from that log and therefore the value of the boards and consequently the value of production.
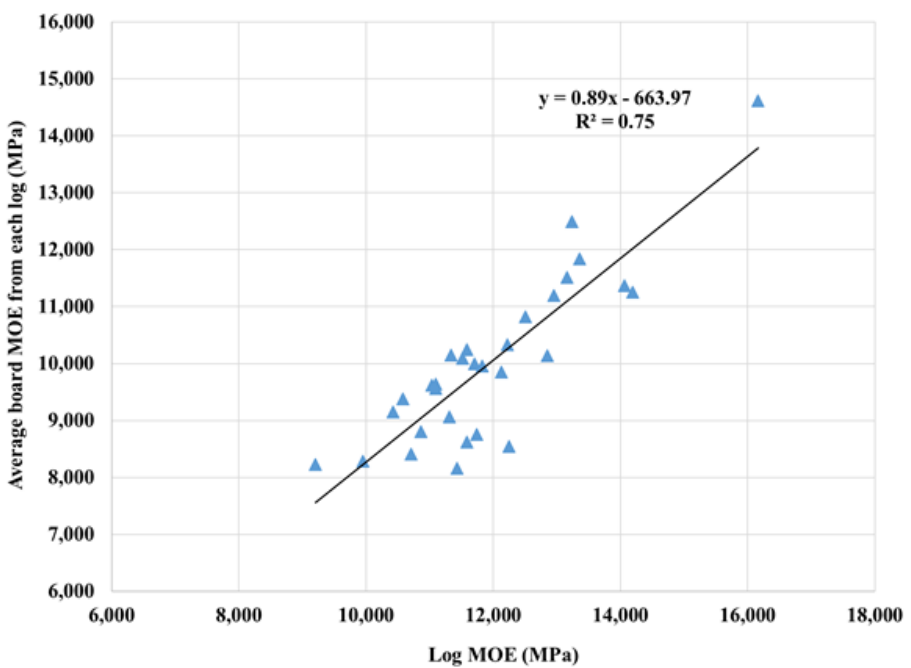
Figure 4. Relationship between the whole log MOE and mean board MOE/sawlog from 30 southern pine logs.

The example above highlights the importance of developing a reliable method to assess the individual board stiffness for resource value assessment purposes, as the money the processor makes from selling boards (or other products e.g. veneer), can be linked to the grower's potential profit from the sale of the logs. **Since we observe the largest variation in MOE across the tree radius, the knowledge of this variation is the key element of any value analysis as MOE variation is by far the main factor defining value. This is the focus of this study.**

6 Material and methods

The southern pine resource characterisation study included a comprehensive stratified sampling process to select representative plots for the test material and data collection. Figure 5 provides a simplified depiction of the material flows.
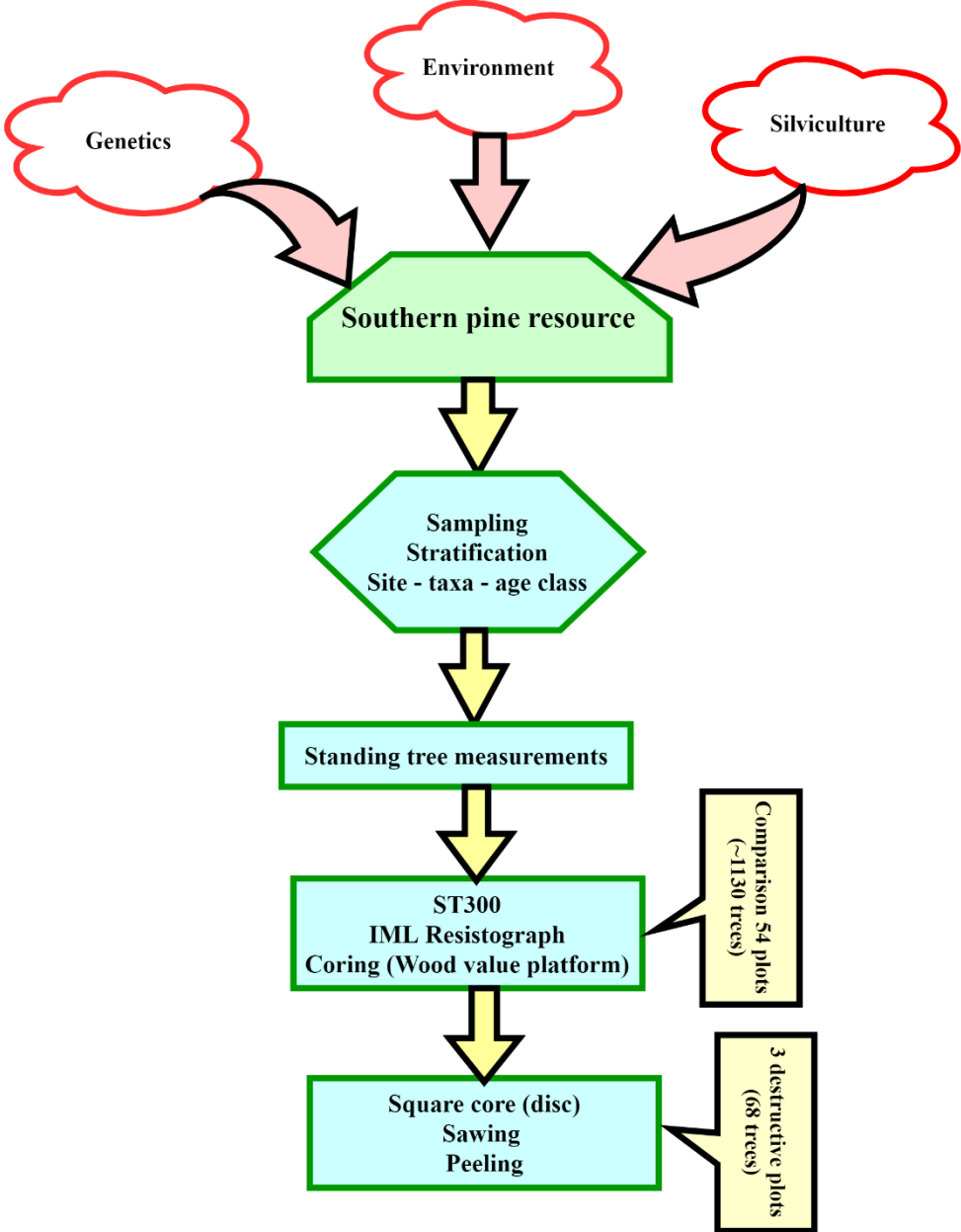
Figure 5. Southern Pine Resource Characterisation project materials flow chart.

An overview of the project showing the three non-destructive evaluation tools and how each component of the wood value platform is interlinked is shown in Figure 6 and Figure 12. Details of these phases of work are included in section 6.1 (Wood Value Platform), 6.5.1 (Measurement of field plots), and 6.5.2 (Destructive sampling).
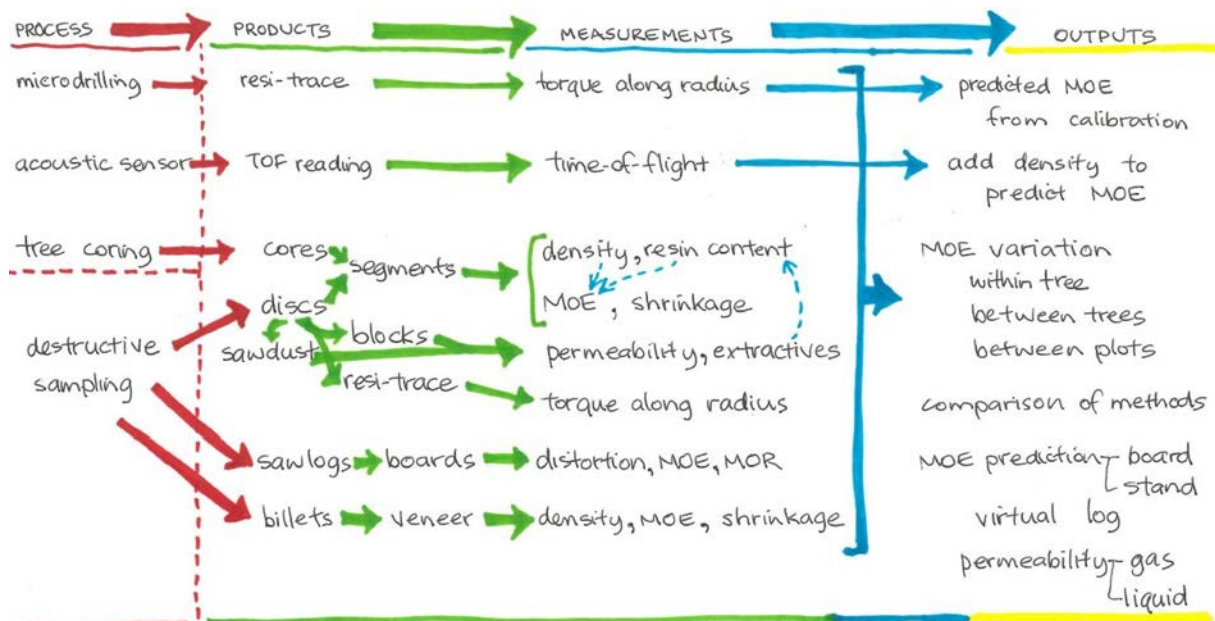
Figure 6. Project methods flow chart and outputs. Note: the acoustic sensor used on standing trees in the plots to provide TOF readings was an ST300; the microdrill was an IML Resistograph PD400.

The project has been designed around the accurate measurement of the ultrasound MOE of cores at 8% moisture (hereafter called USMOE). In a core, the ultrasound (US) actually measures the local longitudinal MOE (along the fibres) of small clear wood specimens, based on a measurement of the time of flight of US stress waves. This USMOE was measured on 20 mm segments taken along a radius of cores extracted from a standing tree or on discs from logs. The measurement of USMOE has been found to be unbiased when modelled and compared with the longitudinal MOE measured through conventional resonance methods (see for example American standard ASTM E1875).

Using a measure of local longitudinal MOE measured by ultrasound, which is much smaller than standard boards, allows the reconstruction (not prediction based on calibration) of the log and board MOE. This is important, as the value of the resource is primarily based on this board MOE. For example, when valuing the structural products manufactured from southern pine, the reference method used by processors is the static bending MOE of kiln-dried boards or veneer. These boards are cut from 'localised' positions within a log and this is measured and valued as a 'local longitudinal MOE' of that part of the log. The local longitudinal MOE is determined by the origin (e.g. genetics, location and growth history) of the tree, the location within the tree or log where the board was cut from and the size of the board.

A system that is based on a measurement of local longitudinal MOE should therefore be the reference method for all other types of measurements using indirect and/or non-local measurements (e.g. on a log or a tree) of MOE. Ultimately, the usefulness of each method must be evaluated through its capacity to accurately predict the MOE of boards from trees and stands. Other key properties or characteristics have been measured locally in the log/tree because they can impact the value of the southern pine resource were: density, shrinkage, resin content and liquid permeability.

6.1 Wood value platform

One of the objectives of the project was to develop and test a high throughput, relatively low-cost platform for accurate and direct measurement of wood properties and characteristics from radially sampled, small, clear wood specimens. Traditional wood quality laboratories and

equipment such as Silviscan have the disadvantages of high capital costs or long waiting periods for results. Moreover, they often rely on indirect measurements of the fundamental properties through calibration procedures and/or unstable physical relationships. The wood value platform includes a patented tree corer bit used with a rechargeable hammer drill to extract cores from standing trees and a suite of plug-in laboratory modules that provide predictions of extractives content and direct measures of wood density, stiffness (Modulus of Elasticity MOE), shrinkage and permeability. Tests for stiffness, density, resin content and shrinkage were conducted on 20 mm (radial length) segments derived from cores and discs extracted from selected trees across the southern pine plantation estates of Queensland and New South Wales. Permeability test samples were cut from discs from destructively sampled trees representing a range of taxa, ages and sites across sub-tropical southern Queensland and northern New South Wales. The details about each component of the wood value platform are presented in Appendix 2. This Appendix includes information about the tree coring, wood discs collected, cambial age referencing of the cores; measurement of the MOE of the cores using ultrasound and measurement of wood density, shrinkage and extractives.

6.2   Static bending – the reference method for board MOE

Board static bending tests were performed using a testing method in accordance with AS/NZS 4063.1:2010. The position of the board to be tested was randomly selected. From this MOE was calculated.

The load for the reference testing was applied and measured with a Shimadzu universal testing machine. In the middle of the span the deflection was digitally imaged. The bending test span was 1,620 mm with load applied at four points and the span-to-depth ratio was 18:1. The load deflection curve was measured up to 1.6 kN for all specimens. The Modulus of Elasticity was determined from the slope of the linear relationship between the applied load and the resulting deflection.

6.3   Stiffness evaluation technologies

This component of the study compared several technologies: time of flight (ToF) acoustics using the Director ST300 (Fibre-gen, Christchurch, New Zealand), resonance acoustics with the HM200 (Fibre-gen, Christchurch, New Zealand) and BING (CIRAD, France), micro-drill torque resistance using the IML Resistograph PD-400 (IML, United States of America) and transverse increment cores with the aim of developing cost-effective wood performance screening systems to allow the characterisation of the southern pine resource for wood properties and value. As discussed earlier, the key wood property that determines southern pine timber value is stiffness or Modulus of Elasticity (MOE). Southern pines typically have higher MOE values than radiata pine, which gives southern pine timber a higher structural grade for the same dimensions. Understanding the MOE variation using simple tools will allow growers to better manage their plantation estate and allow processors to optimise settings in the mill to maximise recovery of the highest quality product.

The different technologies used to measure MOE have to be analysed from a metrological (the science of measurement) point of view. Metrology is used across many industries to determine the accuracy, precision and bias of measurement. We are aware that we did not have the time and resources to perform a full metrological analysis on all of the equipment, however we have enough data to correctly assess each method (e.g. we did repeatability and operator effect studies and within log variation assessment on the ST300, see Appendix 2).

The key attributes and outputs for each technology are summarised in Table 1.

Table 1 Key attributes and outputs for stiffness evaluation technologies.

Tools	Technology	Output/s
ST300	stress wave velocity	stress wave velocity of outer wood of trees, MOE can be predicted if density is known or estimated
IML Resistograph	resistance of drilling (torque) along a radius	resistance to drilling along a radius which can be used to predict MOE and density following a calibration process based on HM200 measurements on logs as the reference measurement
BING	resonance frequency	provides a dynamic MOE based on frequency and density measurements (if density is known, measured separately or estimated) – measurement can be performed on logs, boards and veneer
HM200	resonance frequency	provides a velocity (**different from the velocity obtained with ST300**) from the fundamental longitudinal resonance frequency – measurement can only be performed on logs
Wood quality platform - ultrasound	ultrasound time of flight density position on the radius and cambial age resin content shrinkage	the key measurement is the ultrasound (US) MOE based on us time of flight and density measurements on 20 mm segments taken along the radius (core) used to re-construct MOE for logs and boards

Additional information including a brief review of the literature and background information describing how each technology works is provided in Appendices 2-6 (section 14) and in Figure 6.

6.4 Accuracy and precision

This whole study is about the accuracy and precision of the tools used to measure or predict wood quality. Accuracy refers to the closeness of a measured value to a standard or known value. For example, if you obtain a weight measurement of 3.2 kg for a given substance, but the actual or known weight is 10.0 kg, then your measurement is not accurate. In this case, your measurement is not close to the known value.

Precision refers to the closeness of two or more measurements to each other. Using the example above, if you weigh a given substance five times, and get 3.2 kg each time, then your measurement is very precise. Precision is independent of accuracy. You can be very precise but inaccurate, as described above. You can also be accurate but imprecise.

In other words, accuracy describes the difference between the measurement and the part's actual value, while precision describes the variation you see when you measure the same part repeatedly with the same device (see Figure 7).

A measurement system is considered valid if it is both accurate and precise.
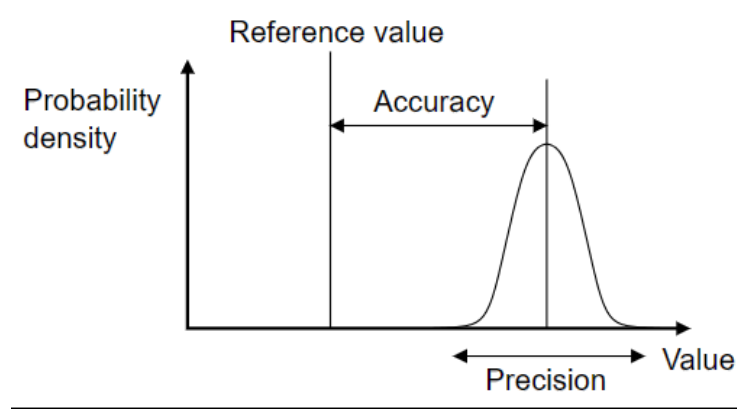
Figure 7: Definition of precision and accuracy

6.5 Sampling strategy

Sampling was undertaken across plots of the southern pine estate to give an initial characterisation of the resource. Destructive sampling was undertaken in three plots allowing accurate reporting of the MOE variation in trees.

6.5.1 Measurements of field plots

Field measures, assessments and coring were undertaken from three sources: existing growth plots stratifying the southern pine resources in Queensland, new growth plots established by project staff in New South Wales and two genotype × spacing trials (also called plots for convenience in this report). Five plantation nodes across Queensland and New South Wales were sampled (Figure 8). Within each plot the range of size classes were also stratified to capture information about the full range of logs available within the plots. We focussed the project to the three major southern pine taxa (PCH = *P. caribaea* var. *hondurensis*, PEE = *Pinus elliottii* var. *elliottii* and hybrid pine (PEE × PCH, both F_1 and F_2 hybrids) across age ranges: thinning age (15 to 20 years old) and harvest age (25-36 years). One plot of loblolly pine (LBP = *P. taeda*) was included to allow assessment and comparison with previous studies. Full details about what was measured and sampled in each plot is presented in Appendix 1.
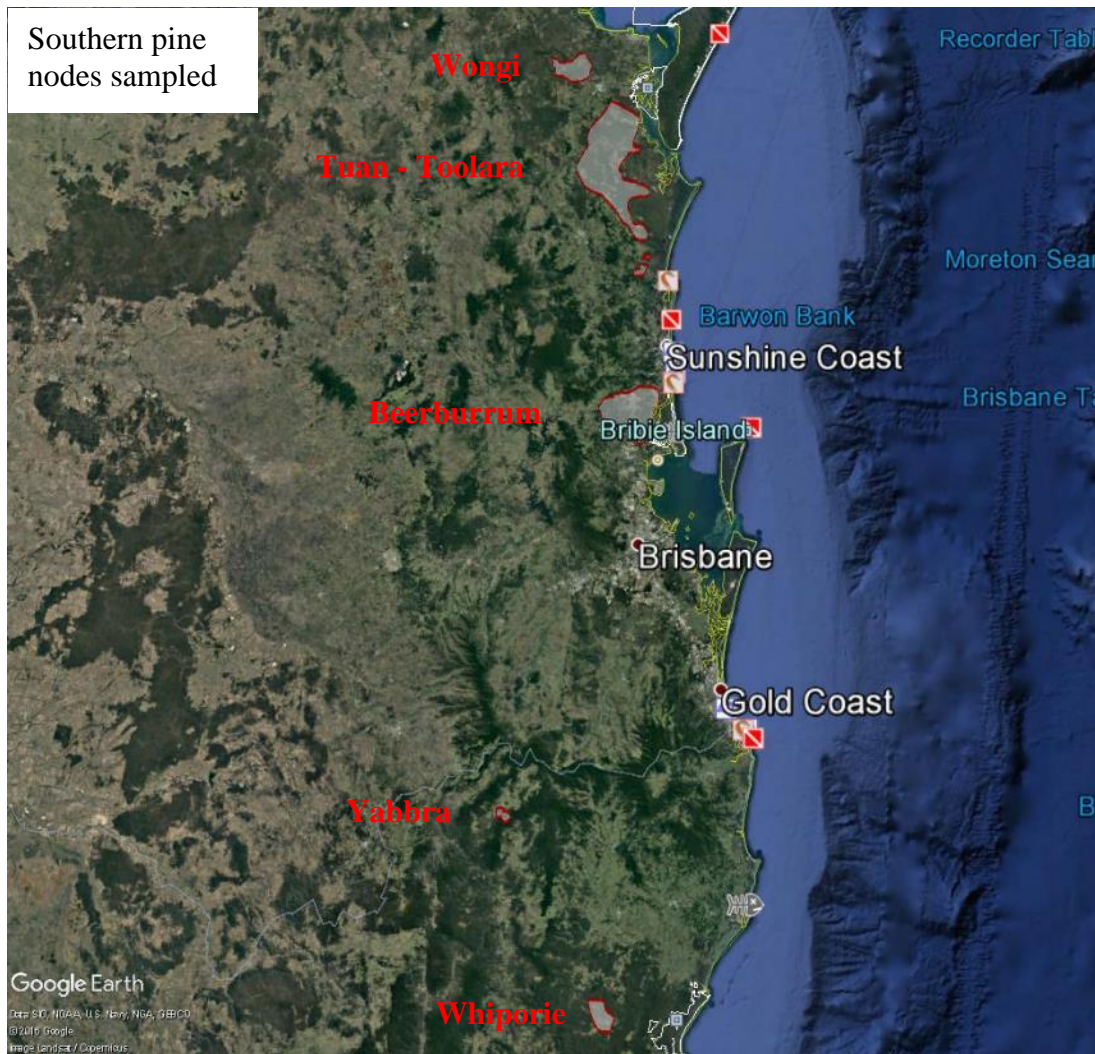
Figure 8. The five southern pine plantation nodes (outlined in red) included in the resource characterisation project.

6.5.2 Destructive sampling

Several of the project objectives required intensive data collection from destructive sample trees. For example, the aims of the project included predicting whole log value from assessments on breast height increment cores and developing 3-dimensional (3D) visualisation models for virtual processing; and to evaluate the value of the data collected by the ST300 and IML Resistograph. These activities required collection of data from a wide range of locations within the stem and from batches of logs from three different sites (detailed in Appendix 1). In addition to the standard breast height increment core from the standing stem, each destructively sampled tree provided four transverse discs from different heights in the tree, a sawlog and two peeler billets (Figure 9).
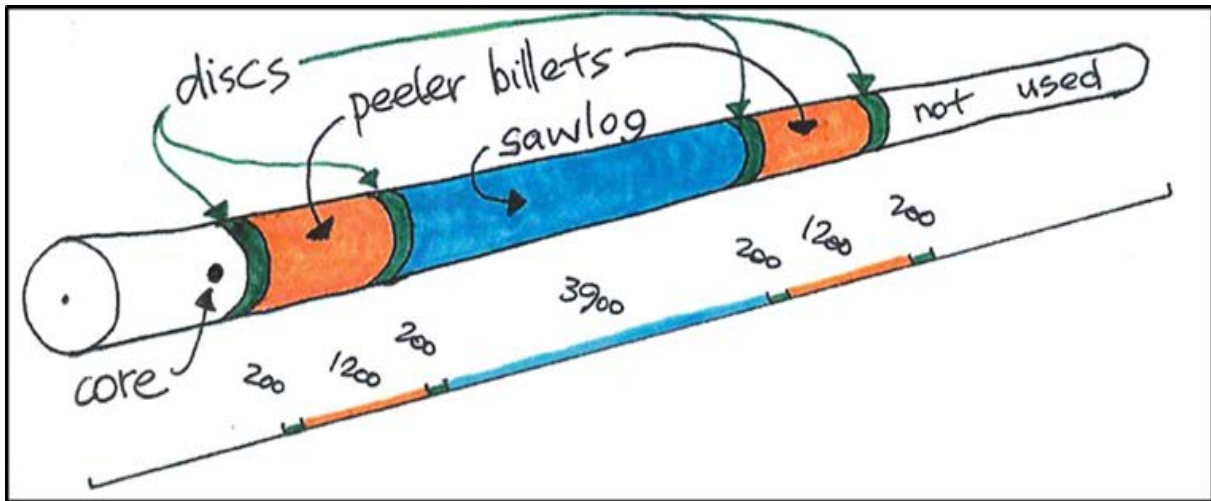
Figure 9. Sacrificial tree merchandising template. The butt of the log is towards the left in the diagram.

Note: the discs were sub-sampled to provide 'square' cores and radial Resistograph traces as depicted in Figure 10.

The four transverse discs were sub-sampled to provide diametrical planks for wood value platform processing providing pseudo core samples for dynamic stiffness, density and shrinkage tests from four heights up the tree. These specimens underwent identical measurement processing to the increment cores described in Appendix 2. In addition, a radial Resistograph trace was captured from below the core position along the same axis, but only for one radius, as depicted in Figure 10.
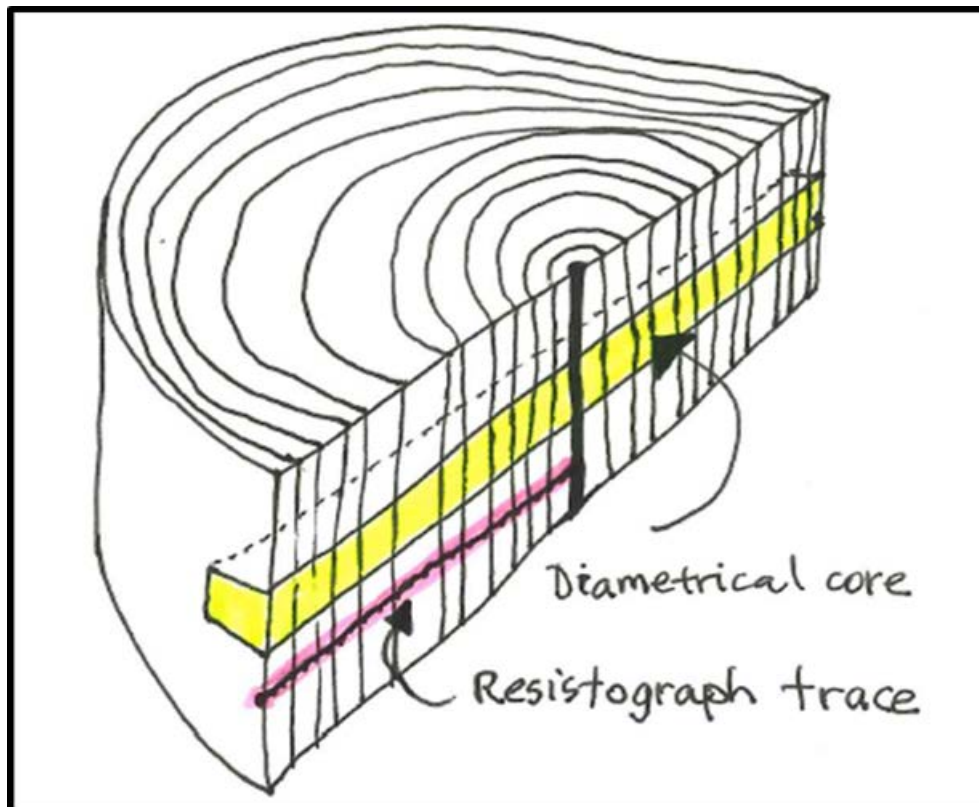
Figure 10. Disc treatment: diametrical strip for wood value platform processing (top) and Resistograph trace (below).

The 3.9 m sawlogs were weighed, measured and green stiffness properties were determined using BING and HM200 (both resonance acoustic tools). Details of these technologies are provided in Appendices 4 and 5.

The 3.9 m logs were sawn and dried in accordance with industry recommendations for nominal structural framing dimensions. Full length boards were also tested using the BING equipment to provide stiffness data (MOE) and measured for distortion (twist, spring and bow), then sub-sampled for static bending (Modulus of Elasticity MOE; Figure 11) as briefly described in section 6.2 and more fully described in Appendix 7.

Figure 11. Static bending testing for MOE from a sub-sample cut from a 3.9 m board.

The 1.2 m peeler billets were also weighed, measured and tested with BING equipment, then processed using a spindle-less lathe to produce 3 mm veneer ribbons. The entire veneer sheet was photographed over a light table to provide data for the log visualisation components of the project (see section 8.1), then clipped to provide 100 mm test strips at approximately 1.0 m intervals for dynamic stiffness, density and shrinkage measurements.

Measurements of the veneer strip wood properties and characteristics were undertaken using similar methods to those used on the core segments. The $100 \times 1,200$ mm veneer strips were weighed and measured then tested using the BING module for wood stiffness (see Figure 128 14.5). They were then docked to 100×100 mm for the shrinkage testing, using the digital scanning and image analysis methods described section 14.2.7.

The overall project sample and measurement flow is shown in Figure 12. The performance of the southern pine resource is affected by factors such as soil, rainfall, temperature, genetics that are listed in the top row of Figure 12. Sampling was based on site, taxa and age class with the resource being sampled non-destructively (Standing tree measurements) and destructively (Sacrificial tree measurements). Ninety three plots were assessed with ST300, 83 plots were assessed by Resistograph and 54 plots were assessed through coring and wood value platform. For sacrificial tree measurement, the full stems were cut to obtain 2 peeler billets, 1 sawlog and 4 discs, as highlighted in Figure 12.
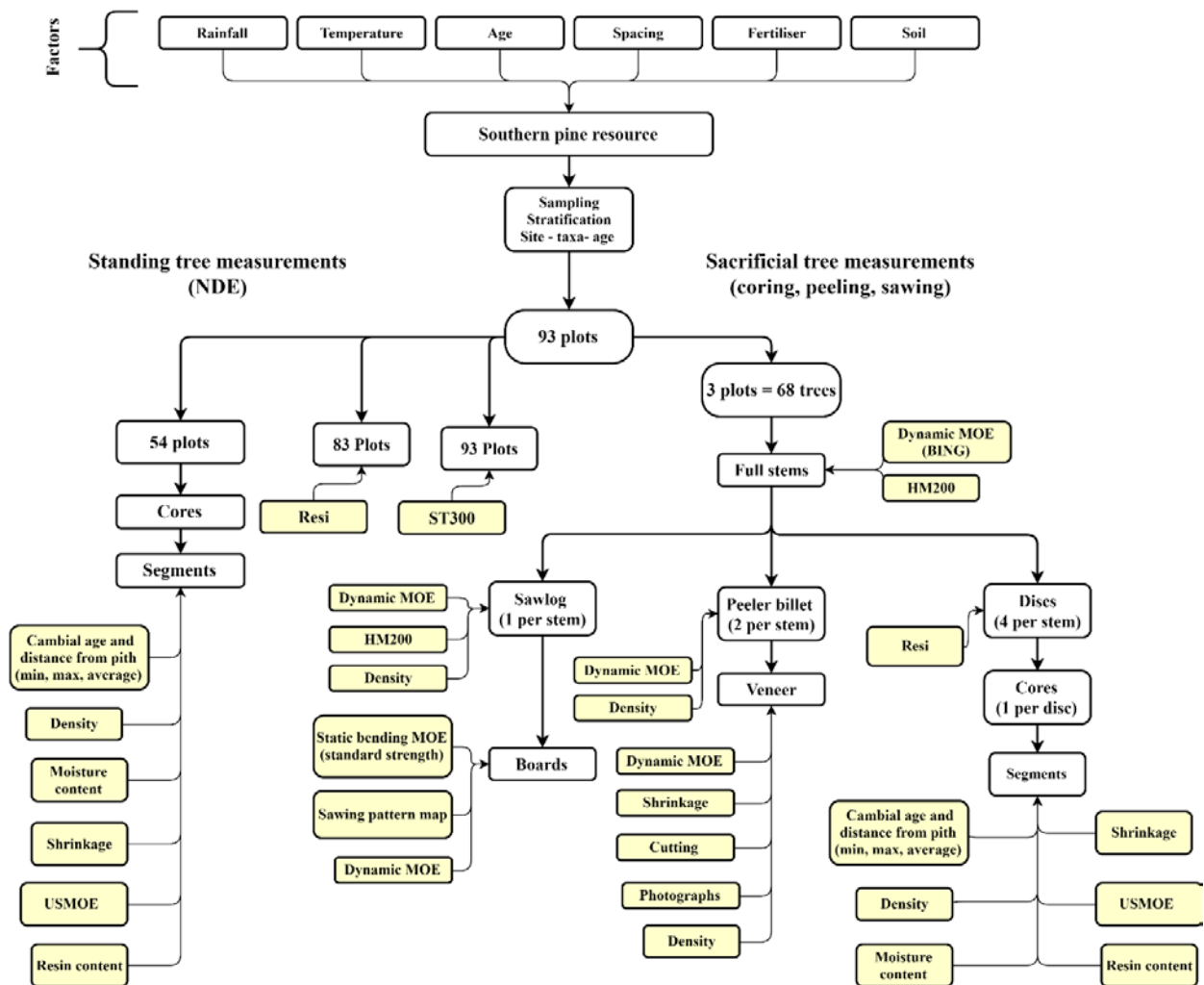
Figure 12. Overview of the project samples and measurements flow. The yellow filled boxes are the measurements.

6.6 Spatial and time referencing of wood

Each cell of wood can be referenced according to its spatial (location within a tree) and time locus (age).

The wood cells can be referenced by the age of the tree from germination, whereby each year the apical meristem produces a new shoot which regularly increases the height of the tree. Adjacent to the apical meristem, which produces the pith, the vascular cambium is formed. At this point of time it starts to produce new cells of wood which leads to the radial expansion of the tree. The new wood cells can therefore be referenced by the age of the apical meristem that has produced the new pith (apical age) and the age of the vascular cambium that has produced the observed wood cells (cambial age). When annual growth rings are formed, each ring encompasses a year of growth of vascular cambium, which is one year of cambial age growth. Figure 13 provides a schematic representation of the different ages of an element of wood.
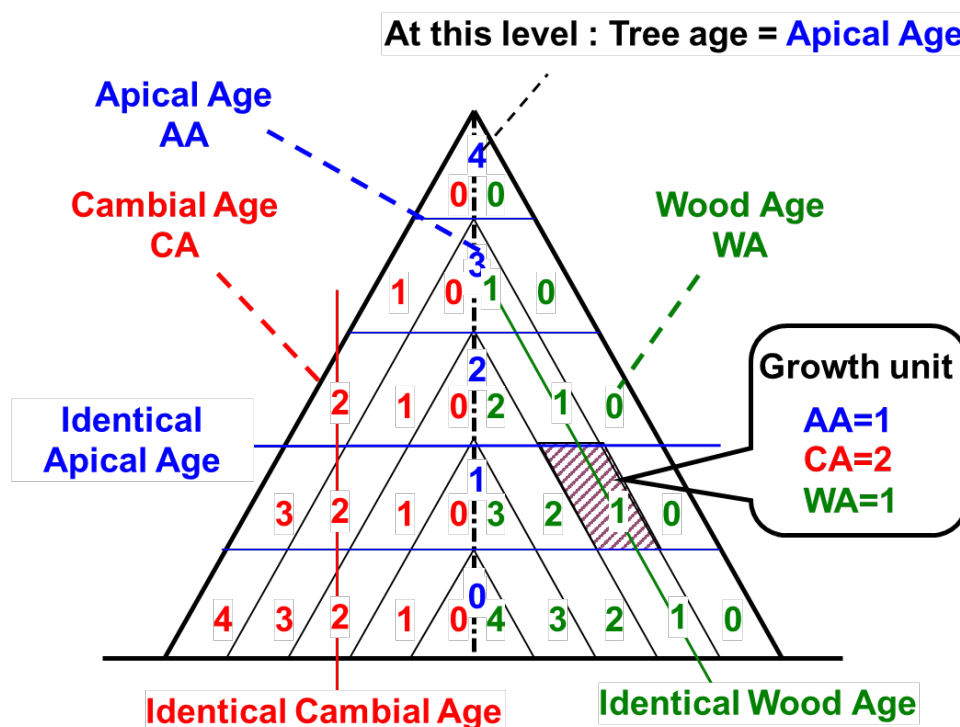
Figure 13. The different wood 'ages' for any location within a stem.

Once a cell has been produced by the cambium, this cell is situated at a certain distance from the ground (height) and from the pith (radius). Height and radius characterize a spatial reference of that wood cell. The third spatial reference of given wood cells is from either its circumferential position or its cardinal position relative to the pith. **In this project we assume that the wood formed at a given cambial age has the same properties whatever its position around the circumference or cardinal position.**

To further illustrate the difference between radial position and cambial age, Figure 14 displays two cores sampled in the same plot from a small and a larger tree. The cambial age scale is the same for these two trees since they were planted at the same time and they have grown during the same period. Noticeably, the radial position of a portion of wood of the same cambial age is significantly different between these two trees.
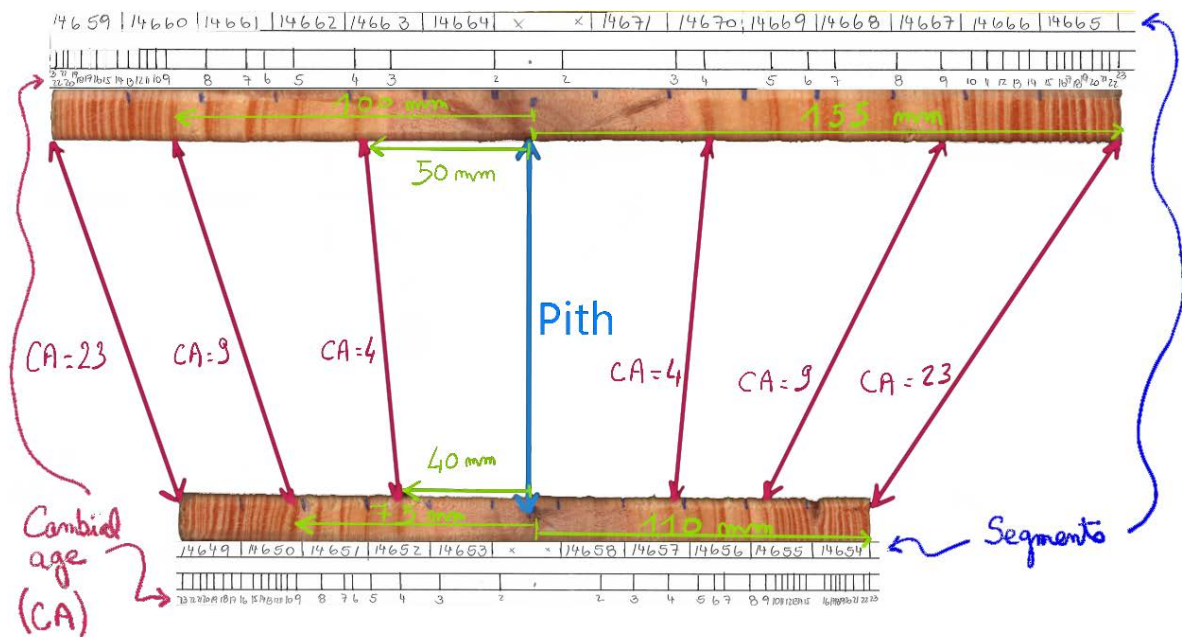
Figure 14. Comparison of cambial and radial position scales from two trees sampled in the the same plot.

Indeed, the reference scales described above are used to describe the internal pattern of variation. They provide useful approaches to analyse the performance of a stand from different points of view or with distinctive objectives.

On one hand **apical and cambial age** provide regular scales with fixed intervals (e.g. one year) for counting and ordering the growth. All the trees planted at the same time follow the same time scale independently of the geometric (height and diameter) growth. As this scale is not directly related to the quantity of wood formed, it represents a **qualitative metric** of a given element of wood.

On the other hand, **height and radial positions** provide the actual spatial location of an element of wood in each individual tree. It relates to the actual geometry of the stem which will be processed. As such it links the geometry of any products to the **quantity of wood** taken from the stem. The relationship between age and geometry is embodied in growth curves.

6.7 Analysis strategy and data reconstruction approach

In this section, we explain the basic principles and the techniques used to model and reconstruct the performances of wood within and between trees.

6.7.1 Weighted average of cambial age

Our data is directly measured on the segment data as this provides the most fine-grained information on the variation of wood properties within the tree. We have utilised the ring markings recorded for each of these cores to account for the different contributions of cambial age to the 20 mm segments. Figure 15 shows an example of a square core segment with ring markings.

24
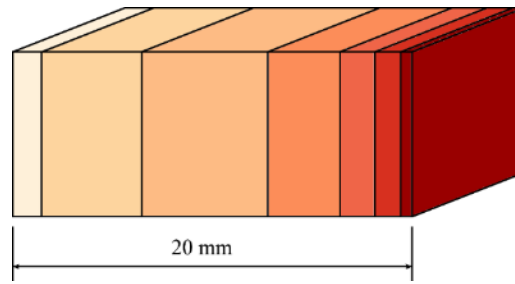
Figure 15. Square core segment diagram showing different proportions of each ring.

To calculate a more accurate average cambial age for each segment, we have used a volume averaging approach where the proportion of each growth ring cambial age comprising the 20 mm segment is calculated. Let the volume corresponding to cambial age i be V_i and the total volume of the segment be V_T. The proportion by volume for ring i is then $\varepsilon_i = \frac{V_i}{V_T}$. Then, the average cambial age for the segment is given by:

$$\sum_{i=1}^{n} \text{ca}_i \varepsilon_i, \tag{1}$$

where ca_i is the cambial age of ring i. This gives a new average cambial age for the segment, and these new data were used to model the variation in wood properties with cambial age. Through the study we use this weighted average cambial age.

6.7.2 Sigmoidal shape fitting

As indicated earlier, within each tree, the most significant variation of properties, such as MOE and density, are found along the radial axis compared to lesser variations in the longitudinal direction and assumed negligible variation in tangential direction (around the circumference of the tree). In this section, we present the method to compress the dataset and model the radial variation of MOE within a tree and between trees.

Within-tree radial variation (pith to bark) of wood characteristics was described by Larson (1967, cited by Zobel and van Buijtenen 1989), as being very large and more variable than between trees growing on the same or on different sites. Several equations have been reported in previous studies to describe ontogenetic variation for tree characteristics (developmental history of a tree), largely based on the best fit rather than on clear biological mechanisms (e.g., Koch 1972; Downes *et al.,* 1997; Zobel and Sprague 1998). On the other hand, West *et al.* (2001) derived a general quantitative model based on fundamental principles for the allocation of metabolic energy between the maintenance of existing tissue and the production of new biomass. They predicted the parameters governing growth curves from basic cellular properties and derived a universal family of curves that describes the growth of many species. These curves represent a classical S shape curve or sigmoidal shape. The model provides the basis for deriving allometric relationships for growth rates and time. Specific properties related to biomass increase, such as tree density or stiffness, follow the same patterns. Indeed, the specific wood density is a simple measure of the total dry mass per unit volume of wood. It is also related to basic wood mechanical properties such as MOE (Kollmann and Côté, 1968; Koch, 1972). While not necessarily recognised, in most experimental studies, wood mechanical property trajectories have the characteristic sigmoidal shape that is observed empirically (e.g., Zobel and Van Buijtenen 1989; Zobel and Sprague 1998). Bailleres *et al.* (2005) reported the use of sigmoidal profiles as an effective method to describe some select key wood properties in planted *Eucalyptus* species.

To model this variation, we accept that wood properties vary with cambial age or radial position according to a five-parameter logistic (5PL) model which represents a family of sigmoidal curves. This type of model is widely used in biological literature, and exhibits rapid initial growth (increase) before approaching a plateau. It is commonly shown that wood properties such as density and MOE follow this type of pattern, due to normal plant physiology and wood formation processes. The five-parameter logistic model used in this study for MOE is given by

$$MoE(x) = A + \frac{B - A}{\left(1 + \left(\frac{x}{C}\right)^D\right)^E}. \tag{2}$$

Here, x is weighted average cambial age (discussed in 6.7.1) or radial position for the segment, A is the asymptotic maximum, B is the asymptotic minimum, C is the transition point midway between A and B (when E=1), D is the slope factor which refers to the steepness of the curve, and E is the asymmetry factor.

We have utilised an orthogonal distance regression (ODR) algorithm (Boggs and Rogers, 1990) to obtain the best fit of the 5PL function to the measured data. ODR is preferred over standard regression techniques when there may be error in both the measured property and error in the independent variable (cambial age in this case) (Boggs and Rogers, 1990). Figure 16 demonstrates ODR, where δ_i and ϵ_i are the errors in the independent and dependent variables respectively, and r_i is the orthogonal distance between data point i and the fitted curve.
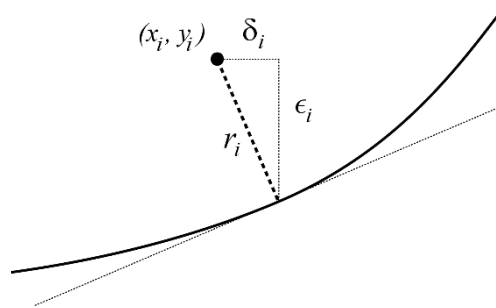
Figure 16. Representation of orthogonal distance regression, where the orthogonal distance, r_i, between the data point and the curve is minimised.

An example of the fitted 5PL for MOE is given in Figure 17, where the orthogonal distance between the curve and the data points is minimised. A bounded minimisation scheme was used, allowing us to apply bounds on the values of the function parameters. Each curve represents the fitted MOE at a single apical age of the tree. Note that this function gives a value of the MOE for a given cambial age only, at the given apical age. The sigmoid fitted between MOE and cambial age is defined as 'cambial age sigmoid' in this report.
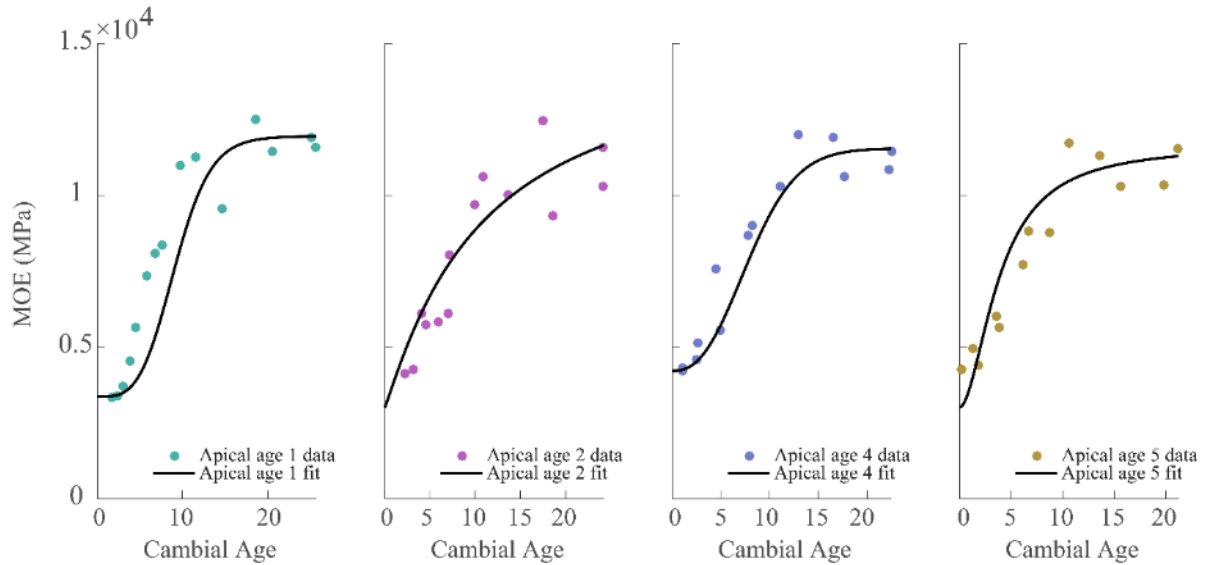
Figure 17. Fitted five-parameter logistic functions to the four square core's segment data for Tree 3.

The five parameter logistic function (sigmoid) in equation (2) can also be fitted between MOE and segment radial position for a single core. The sigmoid fitted between MOE and radius is defined as 'radial sigmoid' in this report. Figure 18 shows examples of such radial sigmoids for two cores. As discussed earlier, the MOE increases from pith towards bark and the sigmoid function we used here can accurately describe this variation.
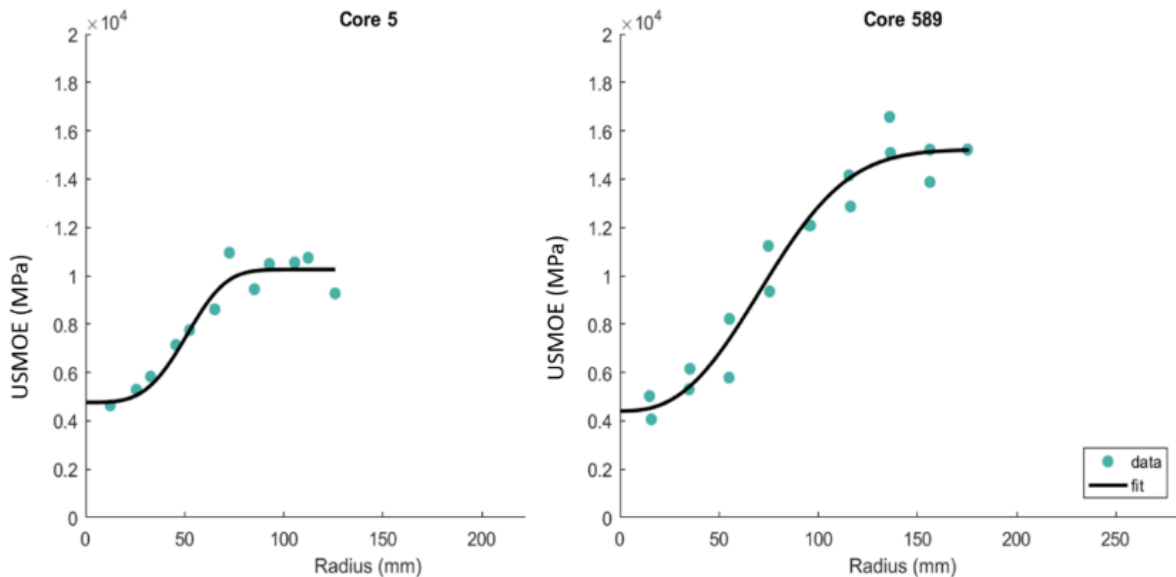
Figure 18. Example of radial sigmoids for two cores.

6.7.3   Intrinsic performance through time scale fitting

The radii of trees in a plot/coupe/compartment vary depending on inter-tree competition, variation in genetic origin and microsite variation. Therefore, the representation of MOE variation with the radius is not practical, as the change in MOE, i.e. trajectory of the curves will follow a different pattern depending on the size of the tree. In other words a given MOE

will be observed at a different radial position for different size trees (see section 6.6 and Figure 14).

Since all the trees in a stand have the same age span, **a characteristic curve** of the stand can be obtained by fitting the weighted average cambial age calculated for each segment and the MOE of the segments. An example of the fitted five parameter logistic function (5PL) for a plot (15 trees) is shown in Figure 19. The MOE increases with cambial age through the **juvenile phase** of growth, with wood of higher cambial age towards the bark generally having higher MOE, though an asymptote is often reached and the gradient flattens at higher cambial ages (the **mature phase**), in the case of plot 8 (Figure 19) at approximately 18 years old. Given that factors such as genetics, soil and environment can be considered the same in a homogeneous plot, **we assume** that this 5PL curve fitting obtained from sampled trees in a single plot represents all the trees on the stand of the same genetic material growing in similar environmental conditions. Under these conditions, this type of cambial age sigmoid is thus representative of all the trees in a plot or a coupe and is **independent of silvicultural regime.** It can be then considered as a **"fingerprint" of the performance** of the stand.
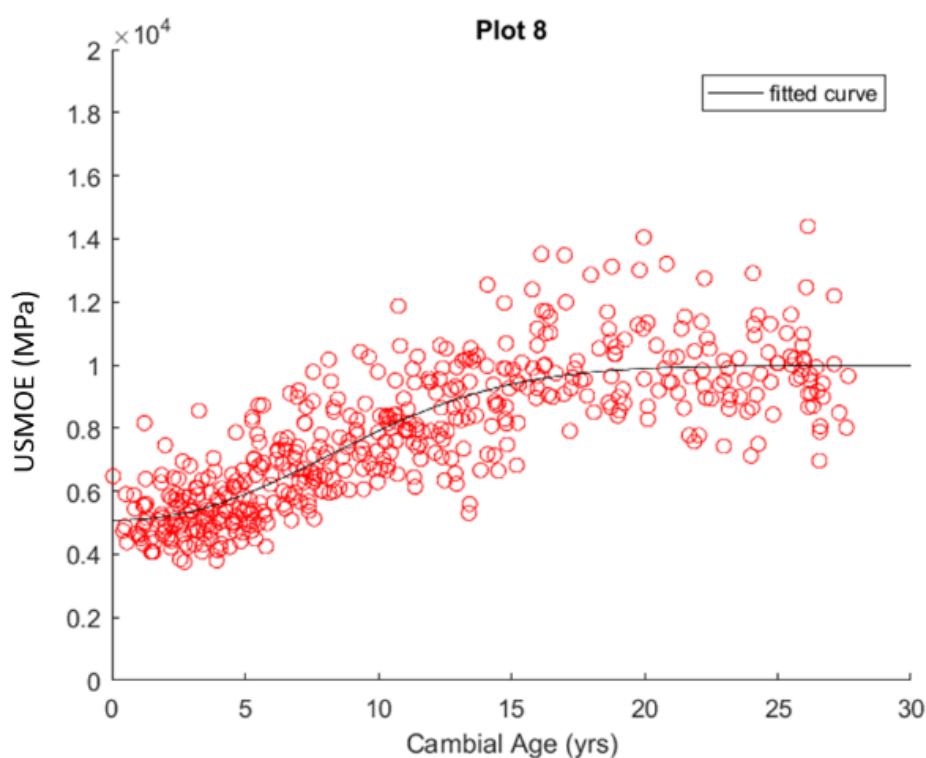
Figure 19. Example of a 5PL sigmoid fitting for a plot, the 'fingerprint' graph (15 trees × 2 cores, 453 MOE radial measurements on 20 mm segments).

The validation (spacing) trial with five stockings rates from 200 to 1,000 stem/ha illustrates and consolidates this postulate. Figure 20 shows the MOE variation with cambial age (a) and radius or distance from pith (b) in the validation plot with same genetic material but with different stocking rates. The solid lines represent the 5PL sigmoid curves fitted for a specific stocking rate.

The MOE variation with radius shows that the trees in the higher stocking rates (666 and 1,000 spha) have smaller diameters at breast height (DBH) with maximum diameters around 100 mm (Figure 20b). The maximum MOE of these trees occurs at this diameter. The trees in the lower stocking rates of 200 and 333 spha have diameters over 200 mm and maximum MOE occurs at the maximum diameter (Figure 20b). Therefore, the MOE of all the trees at

the site cannot be characterised as a function of radius. Conversely, each tree from the same genetic material planted in the same environment, displays a performance (here MOE) at each cambial age (CA) (Figure 20a).

The sigmoid fitted for the MOE vs radius data shows greater spread (Figure 20b), i.e. the vertical distance between the sigmoids is higher. For example, the grey and red sigmoids expressed in radius versus MOE (graph b) are wide apart whereas, remarkably, the same stocking rates represented through MOE vs cambial age display similar sigmoidal trajectories and are closely aligned irrespective of spacing (graph a). Consequently, the MOE vs CA sigmoids can be considered as analogous for all trees in this trial. Spacing and microsite variation do not impact significantly the overall shape of the sigmoids. This observation provides a solid ground for considering the cambial age sigmoid at the plot/coupe or trial level as a 'fingerprint' since it accurately represents all the trees in a plot/coupe or trial planted independently of the growing pattern.
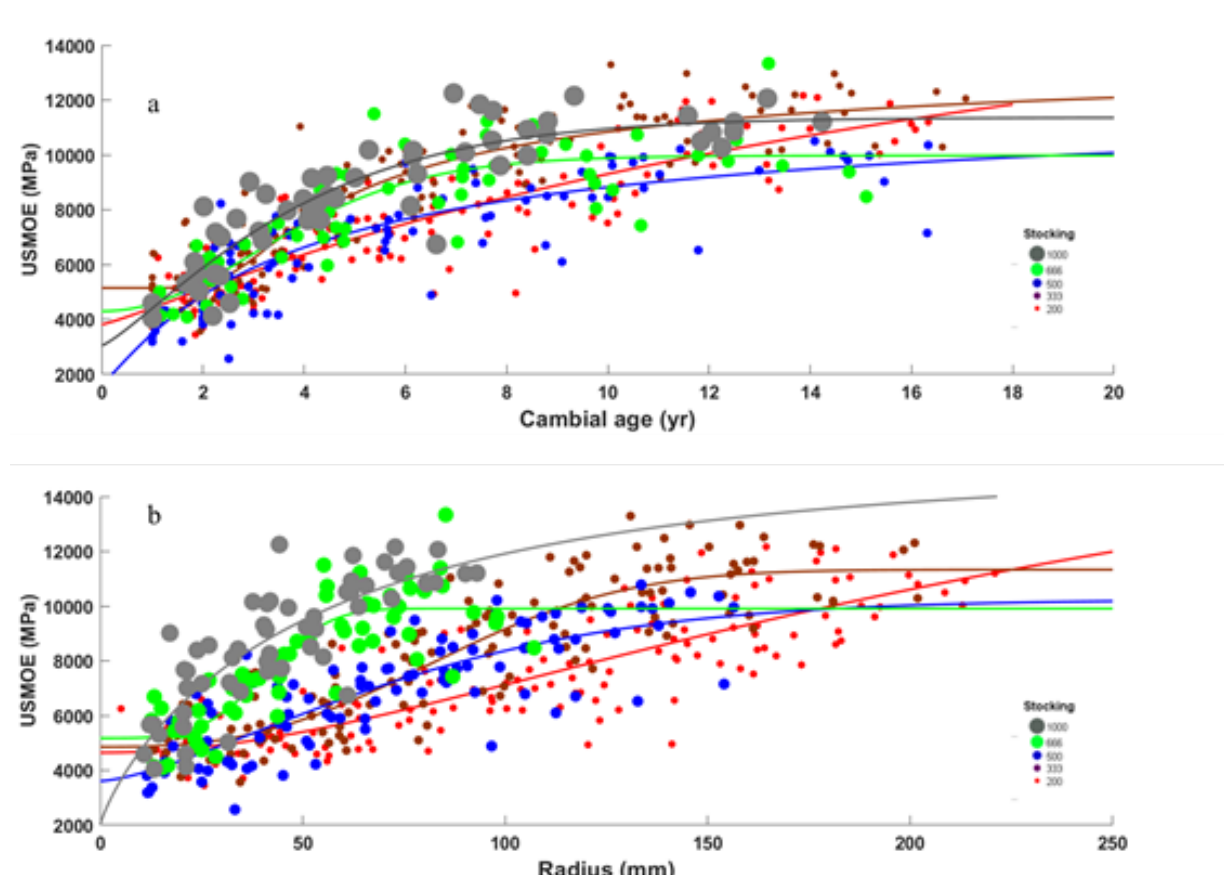
Figure 20. MOE variation with (a) cambial age and (b) radial distance from pith.

The fitted 5PL between MOE vs CA (fingerprint curve) can be used to extract some useful information about **the intrinsic quality of a stand**. For example, the MOE of the wood produced at different ages of the tree (e.g. the MOE at 5 years, 10 years), age at which the trees start producing quality wood (e.g. 10,000 MPa), independently of the dimensional growth pattern for given genetic material and environment. The results obtained using this fingerprint curve are discussed in section 7.1.3.1.

6.7.4 Characteristic performance values through sigmoid integration

6.7.4.1 Radial sigmoid method

This section describes the methods applied to extract **quantitative** characteristics values such as the quantity of wood for a given level of performance (e.g. above 10,000 MPa) or the average MOE for a given age interval.

The average MOE of a log section can be assessed by double integration of the sigmoid curve on the full radius of the log and its circumference (shell integration) as shown in Figure 21 and through the following equation:

$$Integral\ average\ MOE\ on\ Log\ section = \frac{1}{\pi R^2} \int_0^{2\pi} \int_0^R MOE(r)\, r\, dr\, d\theta \qquad (3)$$
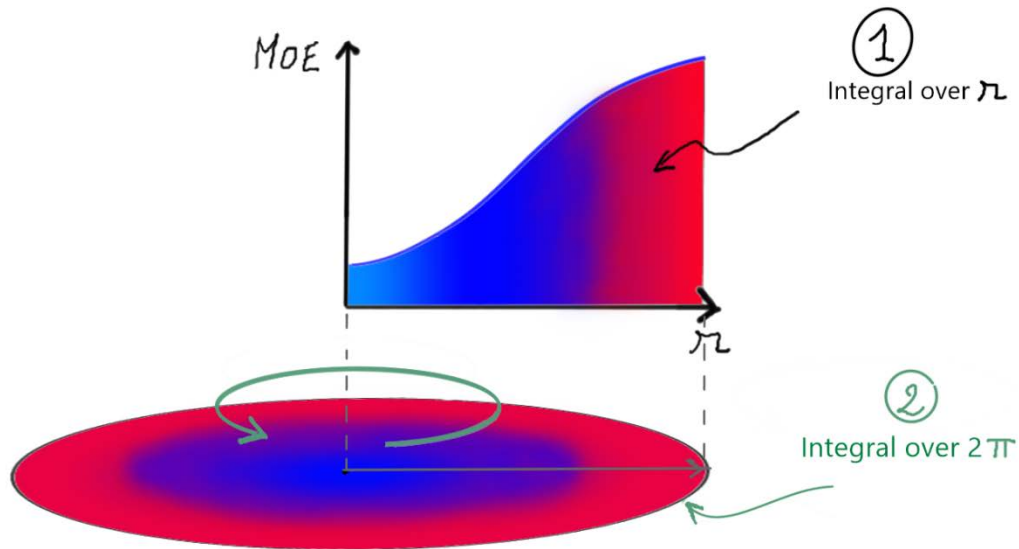
Figure 21. Shell integration from radial sigmoid over log section (2D)

The value obtained by this method, defined in this report as the **integral average MOE** on the radius, is directly compared to the MOE measured by resonance method (BING in section 14.5).

In order to extract an average MOE of a given area of wood a similar approach was used by applying a definite integration. The average MOE for the ring area between ring i and $i + 1$ position was obtained by using the following equation:

$$Average\ MOE\ within\ interval = \frac{1}{\pi r_{i+1}^2 - \pi r_i^2} \int_0^{2\pi} \int_{r_i}^{r_{i+1}} MOE(r)\, r\, dr\, d\theta \qquad (4)$$

6.7.4.2 Cambial sigmoid method

The fingerprint function at the plot level (5PL function MOE vs cambial age) provides the ability to extract useful **qualitative characteristics** independently of the growth of the individual trees. The integration of this function does not provide a structural capacity according to a quantity of wood but instead provides an average MOE over time as the cambium ages (ontogenetic effect). **It expresses the average MOE related to a given period of growth, arising from the cambial activity, independent of the quantity of wood formed. As such it is an indicator of the potential performance irrespective of growth patterns in diameter and height.**

6.7.5 Product performance reconstruction methods

The processors convert logs (larger volumes of wood) into boards (smaller volumes of wood) in a sawmill. The method to extract the MOE from these smaller volumes is to reconstruct them from the radial sigmoid curves (1D) by revolving these curves around the pith for a 2D approach (see section 6.7.4.1 above), and "extruding" or interpolating on height for 3D approach (see Figure 22).
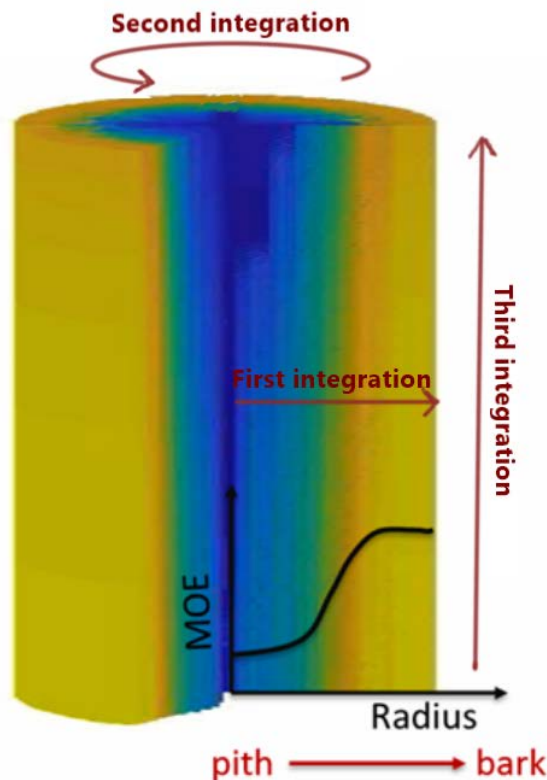
Figure 22. Shell integration from radial sigmoid over entire log (3D)

From these spatial distributions of MOE (maps) on the cross section of log or the entire log volume, a mesh (grid) is generated with each node having spatial coordinates and a MOE. The next step is to isolate a board sections or volume from these maps (virtual board) using a conventional sawing pattern and calculate 2D (Figure 23) or 3D (Figure 24) average MOE. The 3D reconstruction approach is further explained in section 7.3.2.2.
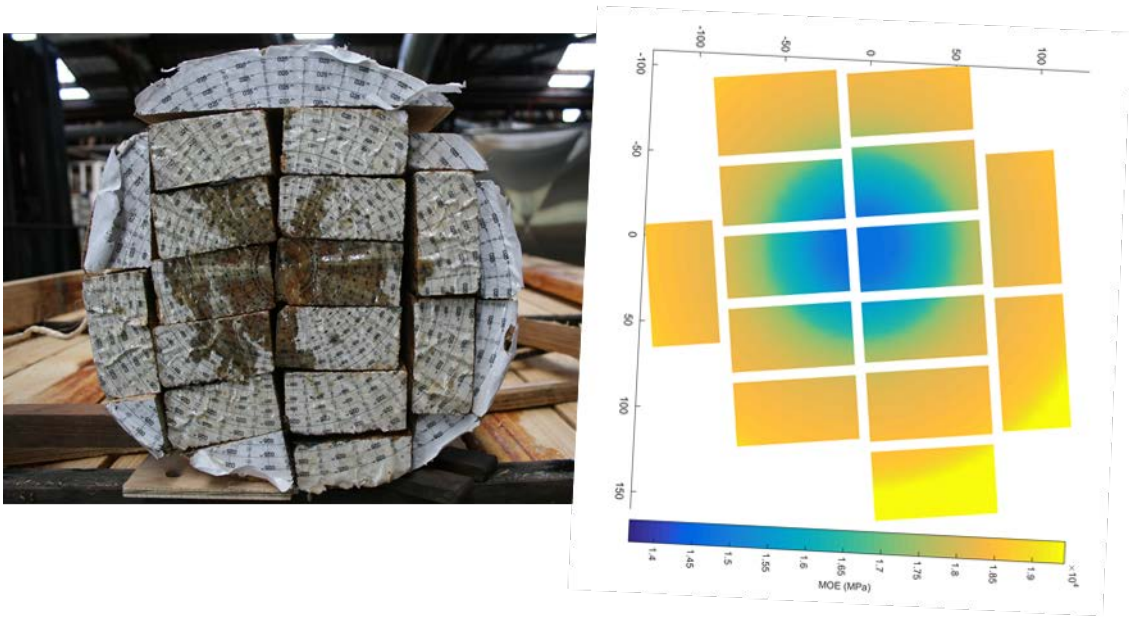
Figure 23. Left picture: actual sawing pattern from a sacrificial plot log. Right picture: virtual sawing pattern and MOE map in 2D from the actual log on the right.
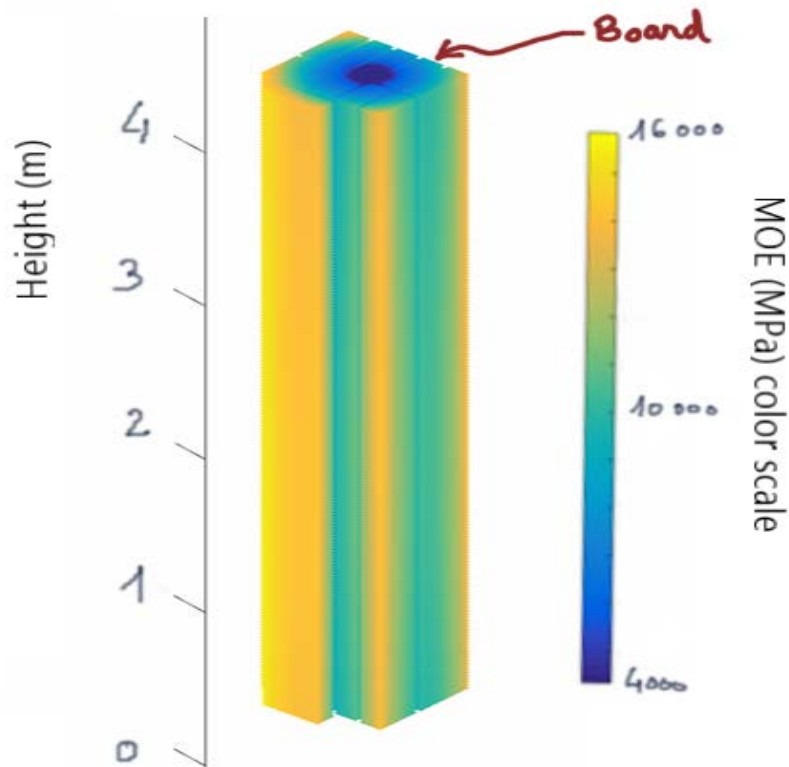
Figure 24. Virtual sawing pattern and MOE map in 3D

A simulation of the standard static bending test can be simulated on the 3D virtual boards (Figure 25).
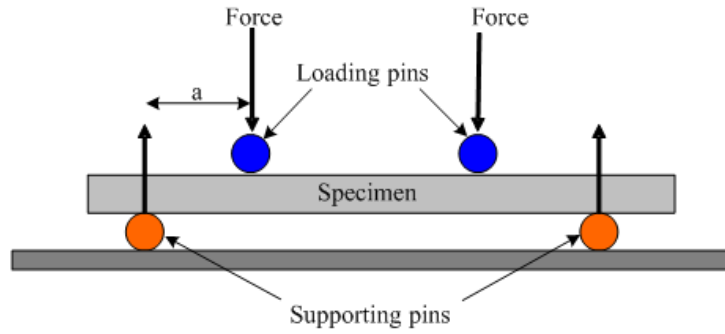
Figure 25. Standard 4 points static bending test

Finally, these MOE based on a reconstruction approach can be compared to actual board static bending tests and used to assess the value of the resource through a grading process. This is shown and discussed in section 7.3.

The methods for board MOE prediction from log section (2D) or entire log (3D) is described in Figure 26.
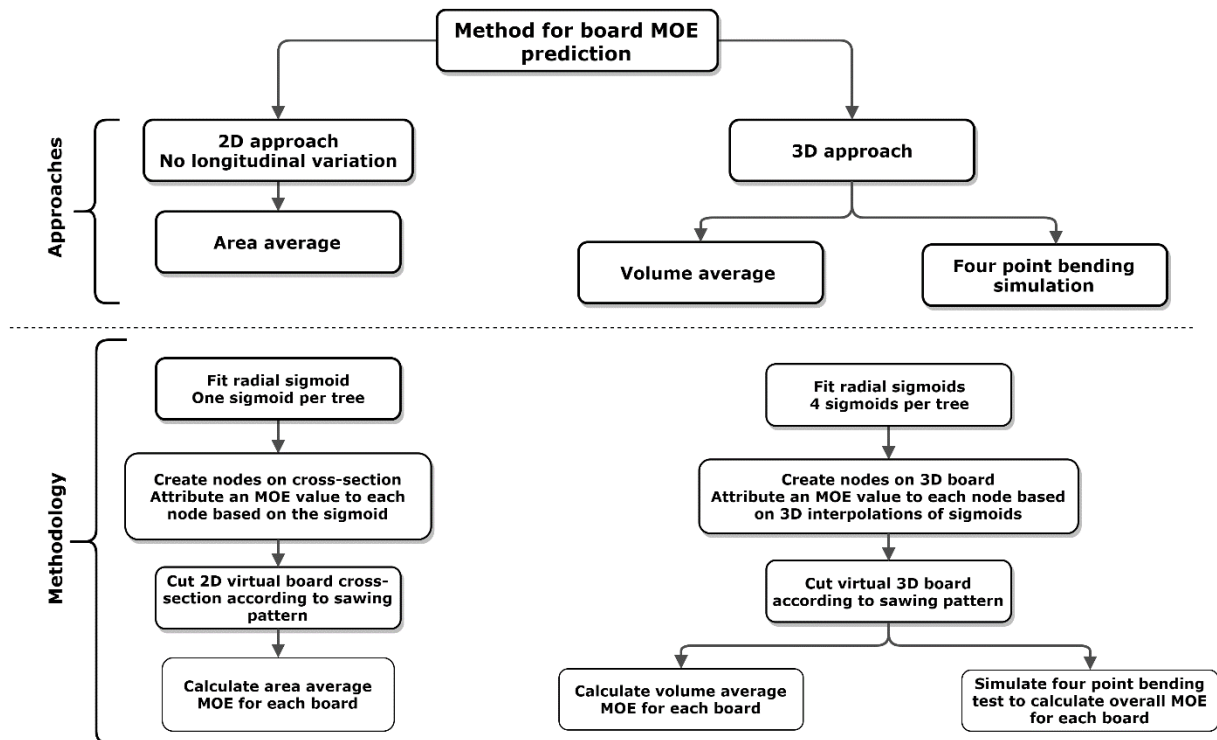
Figure 26. Methods for board MOE prediction from log section (2D) or entire log (3D)

When converting a round log into sawn boards from the sawing patterns only a fraction of the wood is recovered from the log since the sawing operation converts a conical shape (log) into parallelepiped (boards). Figure 27 shows a violin plot the of actual board area percentage recovered including a 10 mm saw cut width (kerf). The sawn board area covers approximately 70% of the area of whole log which corresponds to 84% of the radius of the tree (based on the area of a circle $= \pi r^2$). Therefore, we assume that the percentage of area within 84% radius of the log represents the wood available for sawn boards.
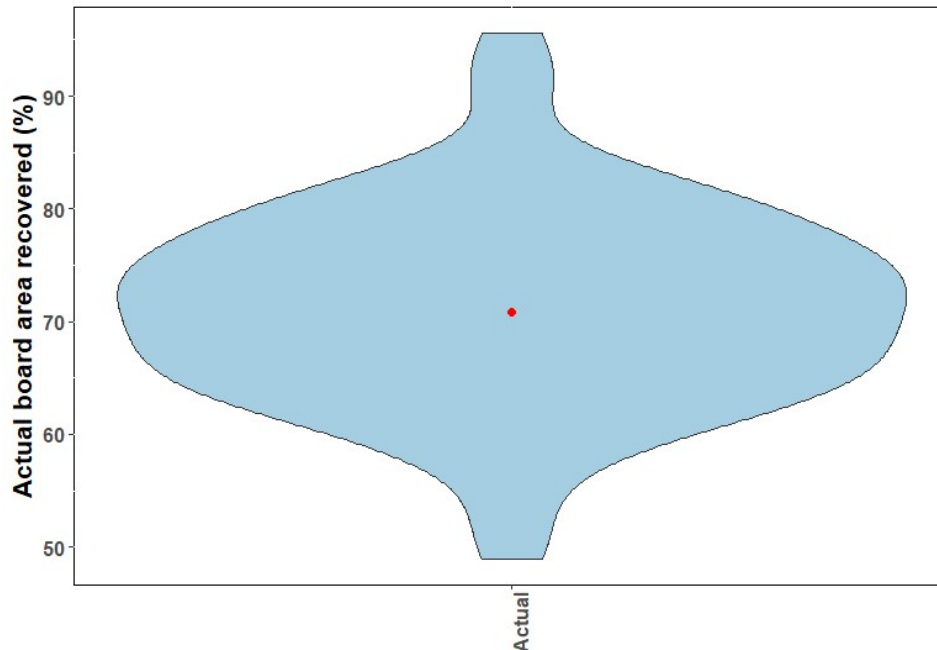
Figure 27. Actual board area recovered from destructive samples of 68 trees (note: the area includes sawcut width). Red dot in the centre is the median.

7 Stiffness or Modulus of Elasticity (MOE)

MOE is the key factor driving forest value for the southern pine plantations in Australia, hence it is the focus of this report. This section reports on the variability within trees, between trees and between plots and compares MOE measured or predicted by three technologies (ultrasound, ST300 and Resistograph).

7.1 Variability analysis of MOE

The measurement of ultrasound MOE (USMOE) from 20 mm segments provided spatial distributions of properties along the radius and, in the case of destructive sampling, up the tree. First, the variation within a tree (radial and longitudinal) is discussed in section 7.1.1 for the destructively sampled trees. Subsequently the variability between trees is explored (section 7.1.2) then the variability between plots (section 7.1.3). For comparing plots two new approaches have been developed using the cambial age as a reference (a qualitative approach, explained in section 6.7.4.2) and based on radial position as the reference (a quantitative assessment, explained in section 6.7.4.1). Finally, the USMOE is compared to MOE predicted by the ST300 and Resistograph (section 7.1.4).

7.1.1 Intra-tree variation

Figure 28 shows that the MOE varies significantly with a steep rise as the distance from the pith increases for a single tree at four heights. For this tree, MOE in radial direction varies from 3,300 MPa near the pith to almost 12,000 MPa near the bark (range=8,700 MPa).

The slope of the sigmoid also increases with increasing height of the tree. The maximum MOE (maximum asymptote of the sigmoid) at each height is however almost the same for all heights even though diameter of the tree decreases with height. Therefore, the MOE increases sharply with radius at higher positions in the tree, reaching the same plateau or maximum with the smaller diameter as we go up the tree.
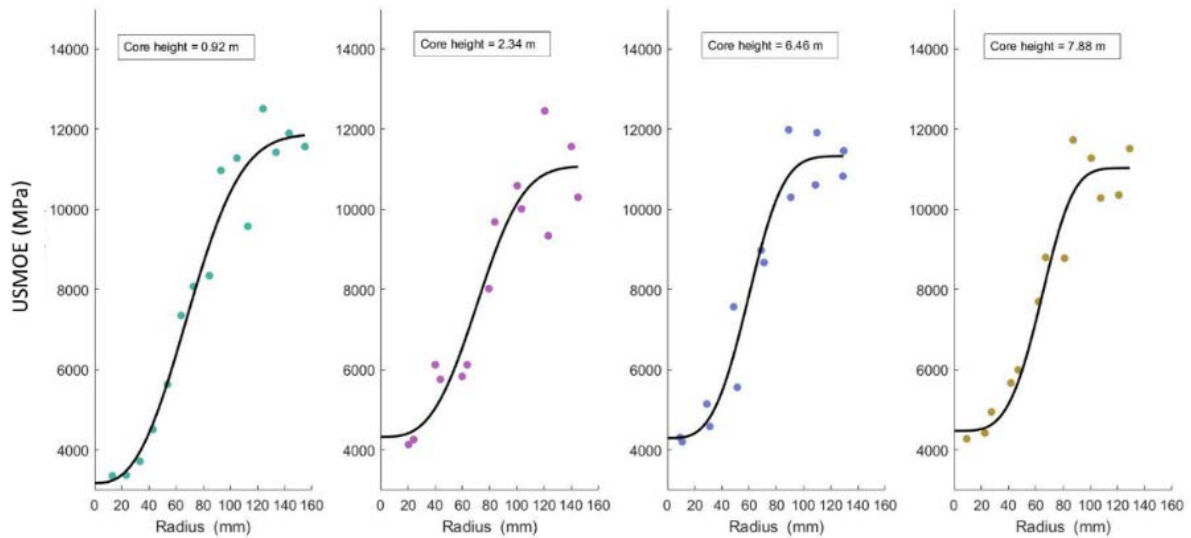
Figure 28. Radial and longitudinal variation of USMOE within a tree (destructively harvested tree number 3).

In addition, the MOE increases slightly at the same radius from the pith of the tree. For example, in tree 3 (above), MOE varies from 10,140 MPa to 11,200 MPa at 100 mm radius (range = 1,060 MPa) for each core height as we go up the tree.

Figure 29 shows the variation of MOE at given cambial ages extracted from the sigmoids of each core at four different heights of 30 trees from the destructively harvested F_2 hybrid commercial plantation at Tuan at fixed cambial ages of 5, 10 and 20 years. This highlights that the variation up the tree is greater near the pith. For example, at cambial age 5, the median MOE of 30 logs varies from 6,000 MPa to 8,000 MPa from height 0.92 m to 2.34 m. However, the variation above 2.34 m at cambial age 5 is negligible. The variation up the log away from pith (nearer to the bark) of the tree is insignificant, for example, at cambial age 10 and 20 years, all the trees have MOE of approximately 10,000 MPa and 12,000 MPa respectively as shown by the median values in the boxplots.
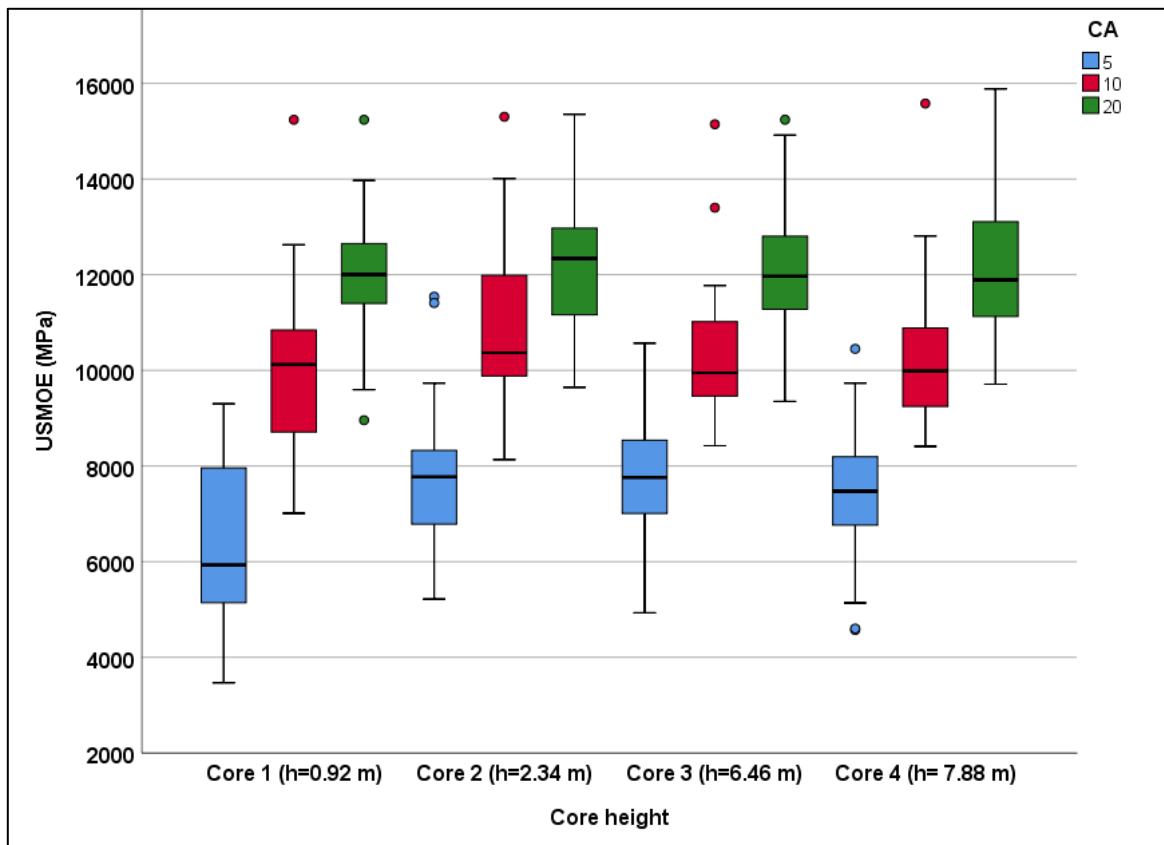
Figure 29. Longitudinal variation of USMOE of 30 destructively sampled trees from a 29 year old commercial F_2 hybrid plot from Tuan. The centre horizontal line of box is the median.

7.1.2 Variation between trees

The properties of individual trees from a given plot, planted with the same genetic material and a set spacing can vary significantly. Figure 30 shows the variation of measured log MOE of 30 trees in a commercial plot. The MOE of logs measured by resonance method (BING) varied from 9,000 MPa to 16,000 MPa (range = 7,000 MPa).
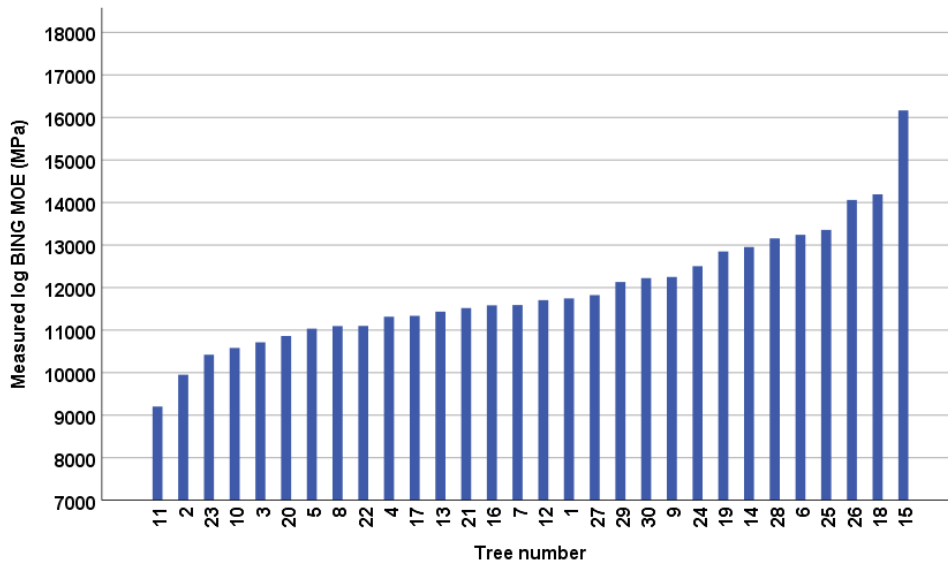
Figure 30. Variation of log MOE measured by a resonance method (BING) for 30 trees from a 29 year old commercial F₂ hybrid plot from Tuan planted with the same genetic material.

The range of USMOE measured on the core segments of these 30 trees is shown in Figure 31. The boxplots in Figure 31 are sorted by mean USMOE and the centreline of each box represents the median of segment USMOE for the tree. The maximum MOE of the segments varies from 11,000 MPa (for tree 15) to approximately 17,000 MPa (for tree 23) and the minimum segment MOE varies from approximately 2,500 MPa (tree 23) to 5,500 MPa (tree 15). For some trees the variation in segment MOE (i.e. intra tree variation) is large, for example in tree 18, USMOE of segments varies from 3,000 to over 16,000 MPa (range=13,000 MPa). In contrast, the variation in some trees is small, for example in tree 11, USMOE varies from 4,000 to 12,000 MPa (range=8,000 MPa).
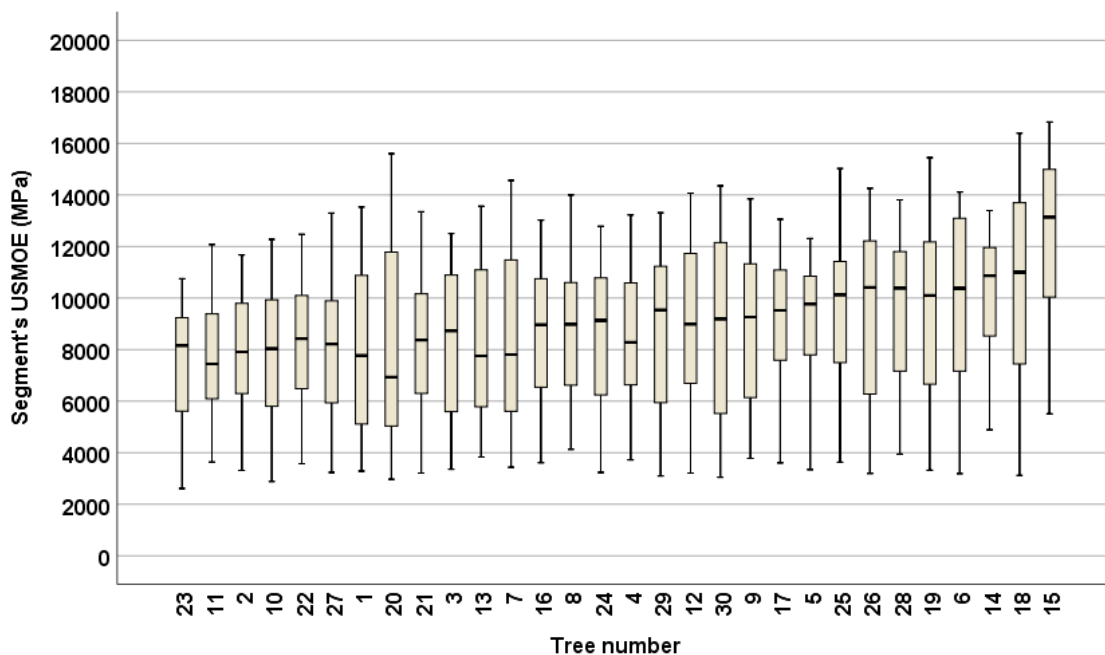
Figure 31. Variation of segments' USMOE within for 30 trees from a 29 year old commercial F₂ hybrid plot at Tuan. The centre horizontal line of box is the median.

37

Figure 32 shows the variation of segment MOE of some trees obtained from two different plots based on the average USMOE (plot 32 and 210) having similar genetic material (F_2) and at same age (18 years old). In these plots individual trees display a wide range of segment USMOE values despite the performance of the plot based on mean results.
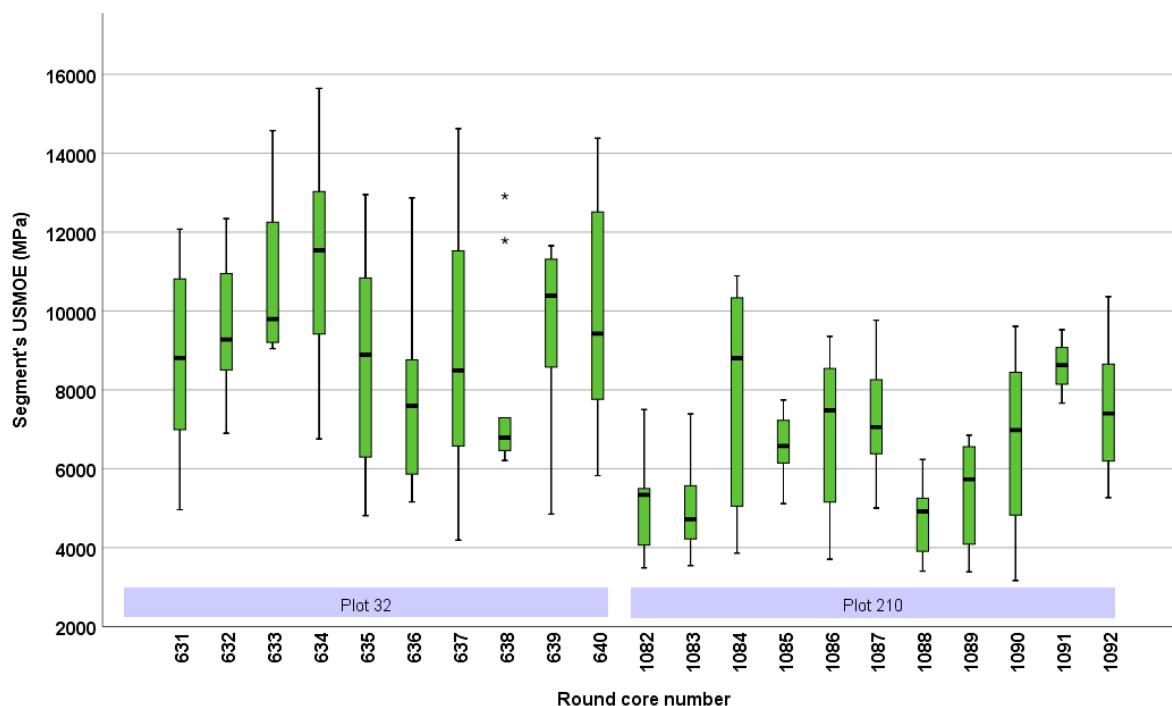
Figure 32. Intra-tree variation of segments' USMOE for plot 32 and 210, planted with F_2 hybrids. The segment MOE are restricted to below 18 yrs for comparison purposes. The centre horizontal line of each box is the median.

7.1.3   Variation between plots

This section examines the variation of USMOE at the plot level and assessment of the potential performance of the plots independently of the growth pattern. The fitted 5PL function between USMOE vs cambial age for a plot graph was used for qualitative assessment and the fitted 5PL function between MOE vs radius for individual trees was used for quantitative assessment.

7.1.3.1   Qualitative assessment of plots (2D approach)

In this study qualitative assessment indicates that volume or size is not considered in the analysis. The focus is on wood intrinsic performance. The approach involved simplification and regularisation methods (section 6.7) to model the average wood properties at the plot level using individual tree information.

This section discusses the usefulness of the fingerprint curve through some examples. Figure 33 shows fingerprint sigmoids for plots 1, 209 and 59, showing the variation of MOE with cambial age of the sampled trees. These three sigmoids (fingerprint curves) display the overall performance of the plots. Plot 1 (CA 29) shows a typical radial pattern of a gradual increase of MOE with age, levelling out at approximately age 30. Plot 209 (CA 20) has a lower slope and the MOE never attains 10,000 MPa, which implies these trees will not provide any structural boards having MOE 10,000 MPa or more. On the other hand, in plot 59, which is three years younger (CA 17) than Plot 209, the sigmoid curve has sharply increased from

38

cambial age 5 to 10 and the MOE exceeds 10,000 MPa during this time. Wood produced by these trees beyond age 10 should be structural grade, as it achieves 10,000 MPa or better.
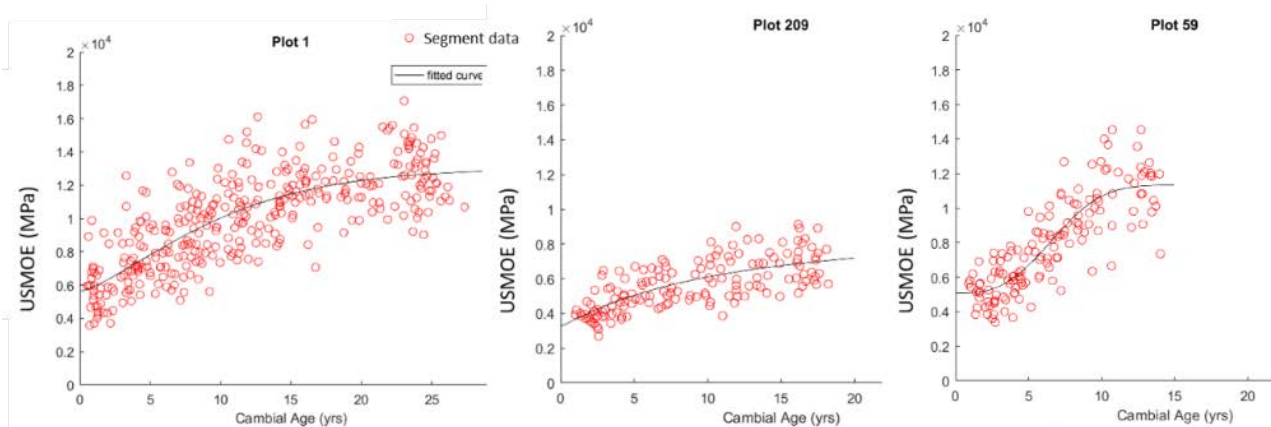
Figure 33. MOE vs CA sigmoid of plots to provide 'fingerprint' of the quality of the plots.

One of the tangible benefits of the plot fingerprint curves are that they can be used to calculate the average intrinsic MOE of the plots at any age independently of the growth patterns of the trees. The bar graph Figure 34 shows the average plot MOE at 17 years of age for all 54 plots measured for USMOE. The graph clearly displays considerable variation between the plots, the MOE varying from 6,200 MPa to over 13,000 MPa (range=6,800 MPa). This approach offers an assessment of the intrinsic plot quality or performance allowing comparison or ranking of plots, coupes and stands.
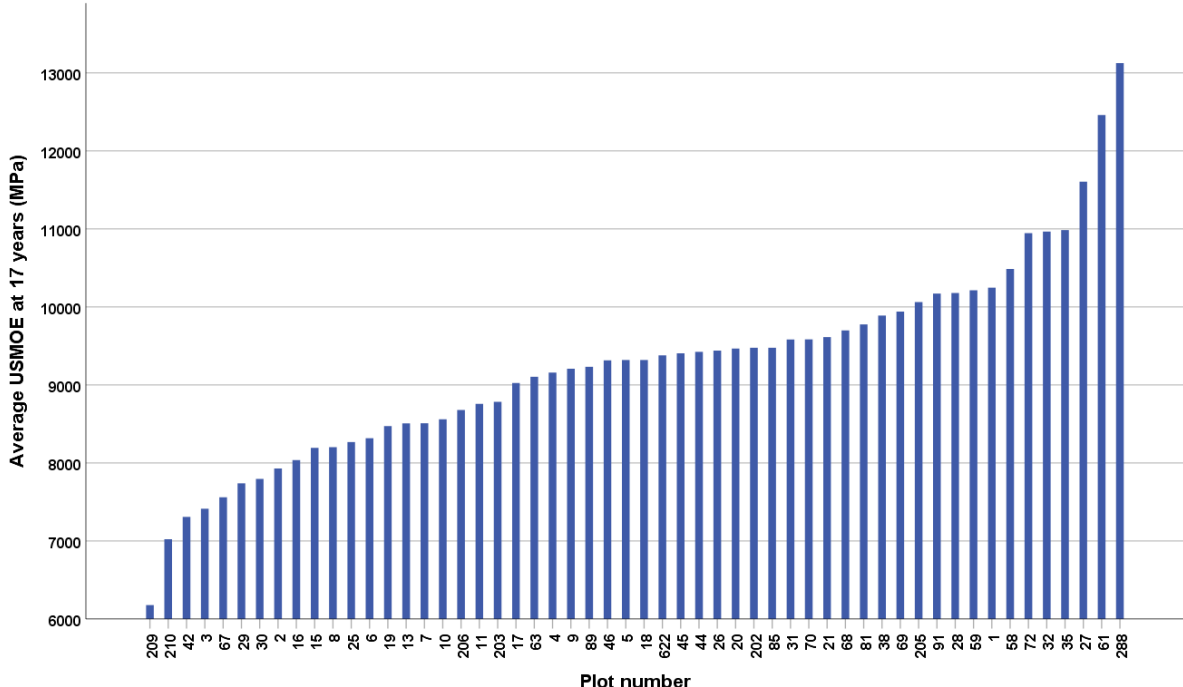
Figure 34. Average plot MOE at 17 years age calculated from cambial sigmoid (i.e. 'fingerprint' curve) per plot. Plot number is sorted by its USMOE value (low to high).

The same fingerprint curve can also be used to find the age at which the plots start producing any specified wood quality. Figure 35 shows the cambial age of the plots when the plot

reaches a threshold of 10,000 MPa. Some plots, e.g. plot 61, 288, 27 and 72, achieve an average MOE of 10,000 MPa in 6-8 years, whereas two plots only reach 10,000 MPa between ages 35-40 years (plot 3 and 67). The six plots highlighted by the yellow bar with dashed lines do not attain a MOE of 10,000 MPa.
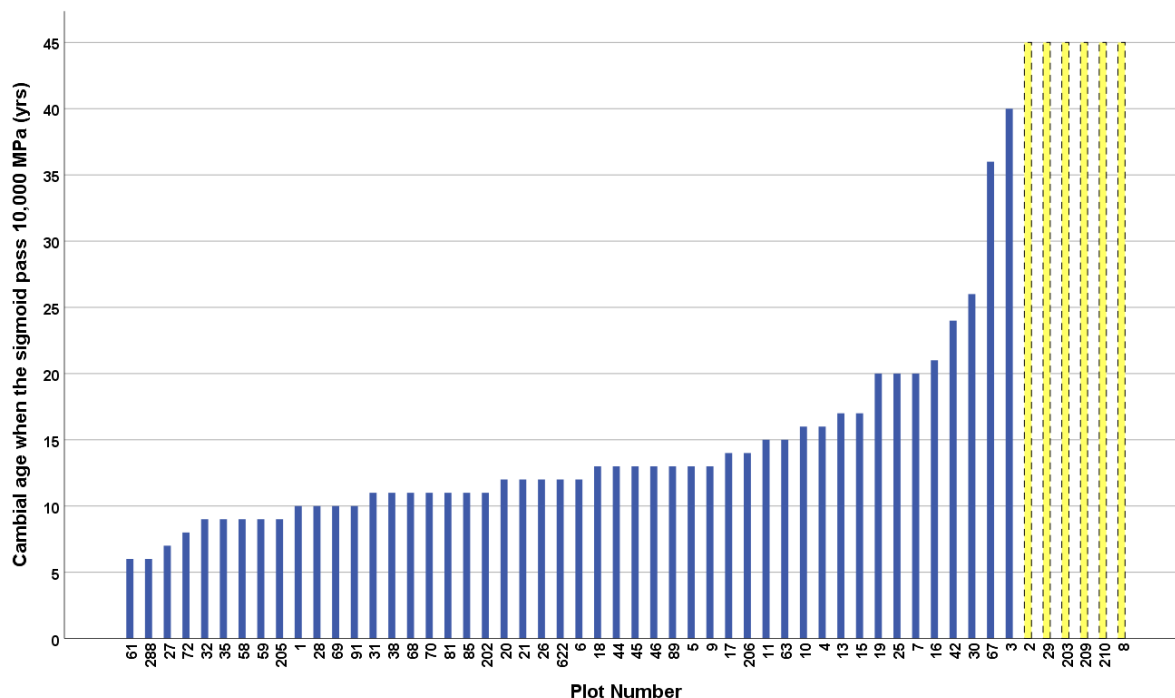
Figure 35. Cambial age of plot when the plot on average reached an average MOE of 10,000 MPa. Note: average MOE was calculated by fitting a sigmoid curve through the data for all segments in a plot.

In conclusion, the plot fingerprint (sigmoid of MOE vs CA) can be used to calculate:
- MOE at any age
- average MOE of any age range such as average MOE between 0-5 years, 17-28 years
- average MOE at any given age, and
- the age trees in a plot will reach any given MOE.

7.1.3.2 Quantitative assessment of plots (2D approach)

Unlike the qualitative assessment in the previous section, the quantitative assessment approach calculates the **actual** average MOE of an individual log since the size of the log is considered for the MOE calculation. Thus, the variation of individual logs MOE in a plot can be analysed. Figure 36 shows the variation of log MOE calculated from radial sigmoids from individual trees for 54 plots considering the full diameter of the logs.
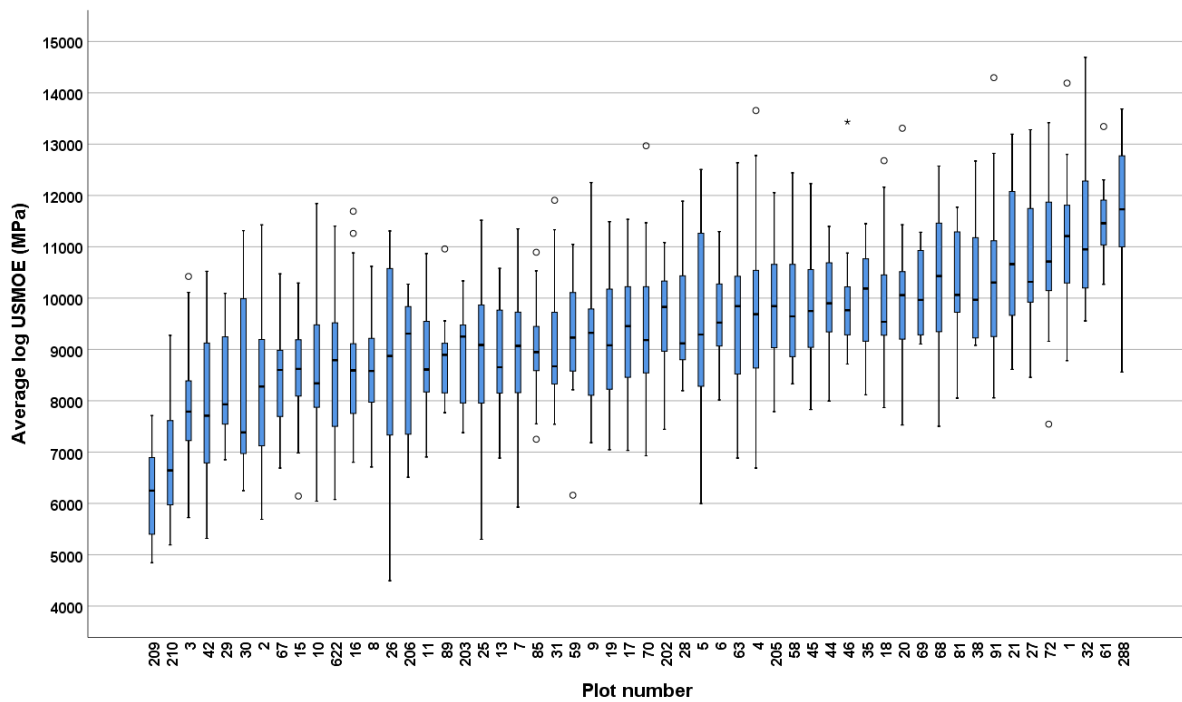
Figure 36. Average plot MOE variation from radial sigmoids of each log. Centre horizontal line of box is the median.

The radial sigmoid first shown (Figure 18) can also be used to calculate the cross-sectional area of wood having a given range of MOE values. For example, Figure 37 shows the quantity (percentage area) of wood having MOE of 10,000 MPa or more for each plot obtained from the individual tree radial sigmoids. The box plots are presented in ascending order of plot for the mean area percentage of MOE of 10,000 or more MPa. Plots 209 and 210 did not produce any wood having a MOE value of 10,000 MPa or more. Therefore, these plots are unlikely to produce any structural boards of 10,000 MPa. We note some considerable variations of this percentage between trees within each plot. For example, plot 63 and plot 16 display a variation from 0 to nearly 100%, indicating some trees will produce no 10,000 MPa boards and others will produce a lot of 10,000 MPa boards.
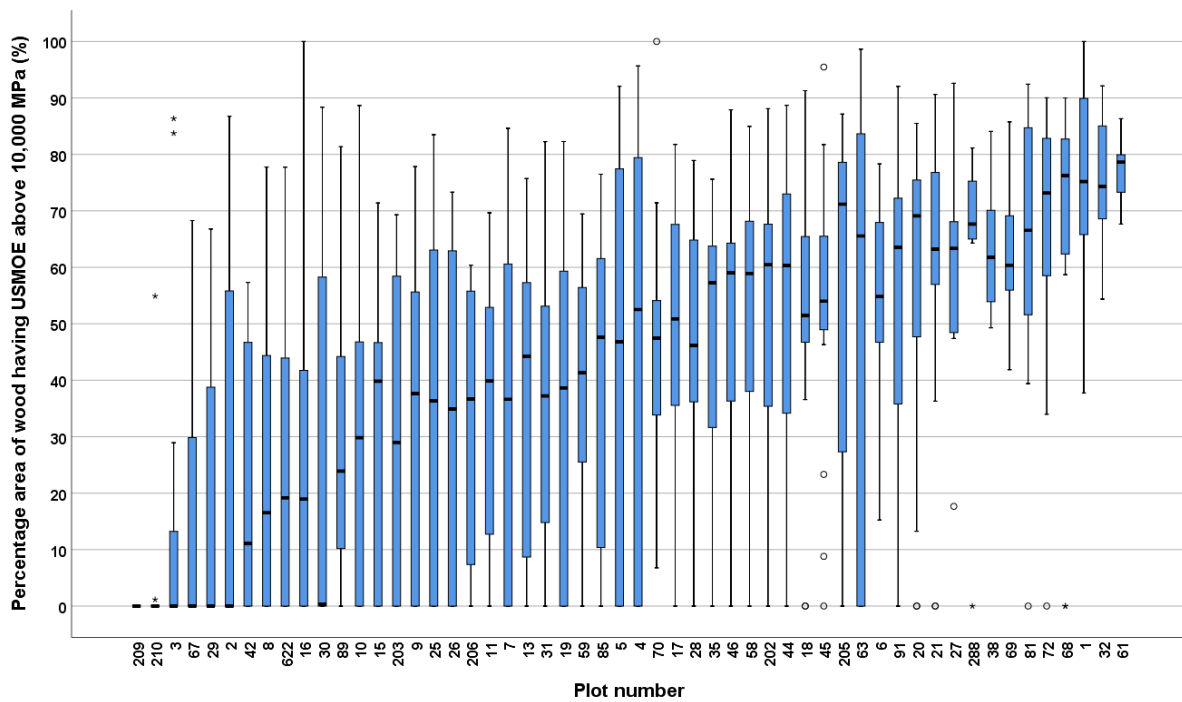
Figure 37. Quantity (% area) of wood having an MOE value of 10,000 MPa or more. Boxplots sorted by mean; middle line of the box = median value of cores per plot.

The boards' cross sections are rectangular whereas the logs' section shape is almost circular. This difference in shape generates off-cuts close to the circumference of the log, consequently some high MOE wood is discarded near the periphery. Depending on the diameter and the overlaying sawing pattern of the log, the quantity of off-cuts can vary significantly.

As a rule, the boards are sawn within 84% of the maximum radius of the log (see section 6.7.5). This approach can be used to approximate the percentage of boards having a MOE of 10,000 MPa or more. Figure 38 shows the percentage area of wood having MOE above 10,000 MPa within 84% of the radius of the log. Comparatively with the calculation performed on the full log, the restriction of the surface to 84% has a dramatic effect on the recovery, showing a decrease of about 30 to 40% in recovery of 10,000 MPa and above. Interestingly, the rank of some of the plots is affected as well indicating that some plots are more affected than other plots by the radius restriction. This is mainly due to the size of the log and the radial sigmoid pattern.
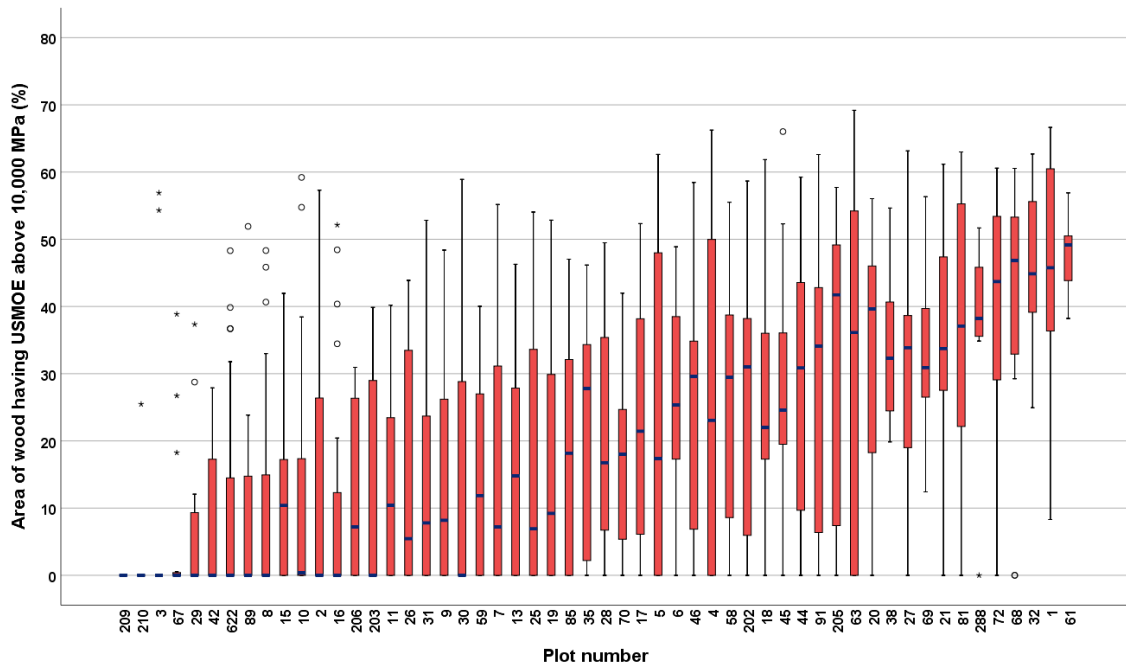
Figure 38. Percentage area of wood having an MOE value of 10,000 MPa, within 84% of inner radius of log. Box plots sorted by mean: The centre horizontal blue line of each box is the median.

7.1.4 Comparison of USMOE, ST300MOE and ResiMOE

When the data from all plots are combined, it is possible to assess if the various technologies are measuring or predicting similar levels of information. In the violin plots in Figure 39, where the width (along the x-axis of each violin plot indicates the frequency and the y-axis indicates the range of MOE values from each technology), the USMOE (integral average) has a median just above 10,000 MPa and a range from 5,000 to 16,613 MPa. The ST300 has a much wider range of predicted MOE values from 7,535 to 27,573 MPa and a median 19,000 MPa. The ResiMOE has a range from 5,300 to 21,500 MPa and a median MOE of approximately 12,000 MPa. The different shapes and MOE ranges of the technologies indicate they are not capturing the same information. To calculate the MOE in each of these instances density is either measure (e.g. USMOE), assumed (e.g. ST300MOE where green density is assumed to be 1000kg/m^3) or predicted (ResiMOE).

43
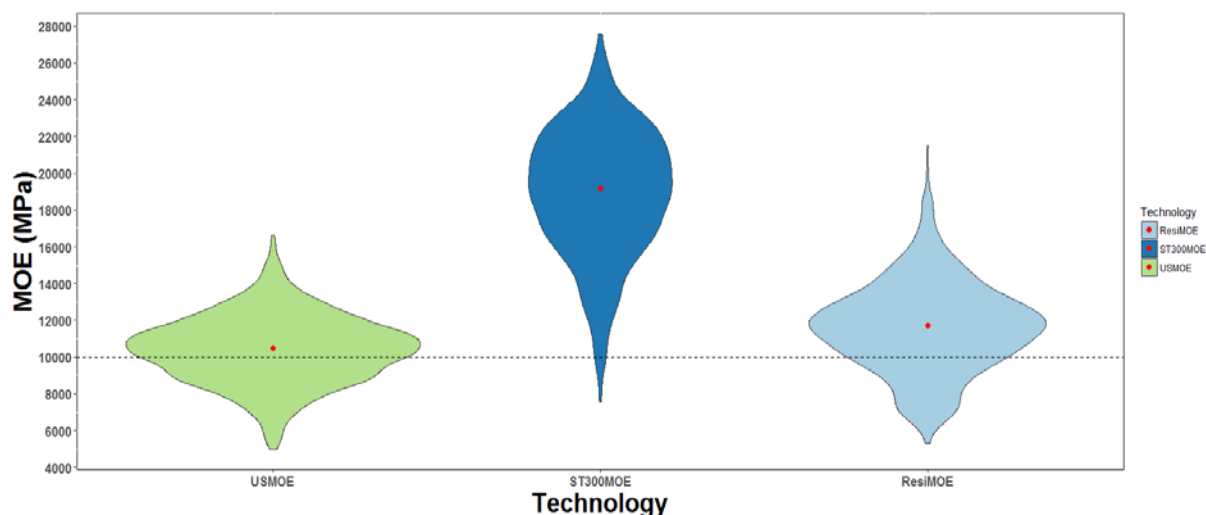
Figure 39. Variation in MOE across all plots sampled by the three technologies. Red dot = the median.

This is further explored using individual plots sorted by increasing USMOE (Figure 40). All three technologies USMOE, ST300MOE and ResiMOE have similar overall trends, but there are clear differences.

The ST300 method is based on measurement of the outer and stiffer log wood, therefore the ST300 MOE over-predicts the actual average MOE of the logs. All plots sampled with the ST300 are shown in Appendix 9 (see Figure 131). Hence most of the predicted ST300MOE plot values are above 10,000 MPa. This over-prediction of MOE by the ST300 is well known. Each plot sampled with the ST300 also has a wider range of ST300MOE values as indicated by the longer violin plot. The shape of the ST300MOE boxplot differs notably from the shape of the MOE provided by the two other technologies.

Despite the calibration applied on the Resistograph traces being developed from radiata pine populations, the overall shape and level of ResiMOE predicted is relatively close to the USMOE violin plot. However variation in ResiMOE, particularly the plots that have low ResiMOE predictions (e.g. Plots 622, 26 and 35) when compared to USMOE (Figure 40) appears to be random. They are not associated with taxon, age or locational effects. This could be due to trees in these plots being outside the calibration population set for the Resistograph. This would mean that the training set needs to be extended to include trees with new Resistograph trace characteristics to improve the calibration prediction. Moreover, the development of the calibration could be reviewed to take into account specific characteristics observed in the traces. This implies new reference measurements (HM200) will need to be completed for these trees (they must be destructively sampled). All plots sampled with the Resistograph are shown in Appendix 9 (see Figure 132).
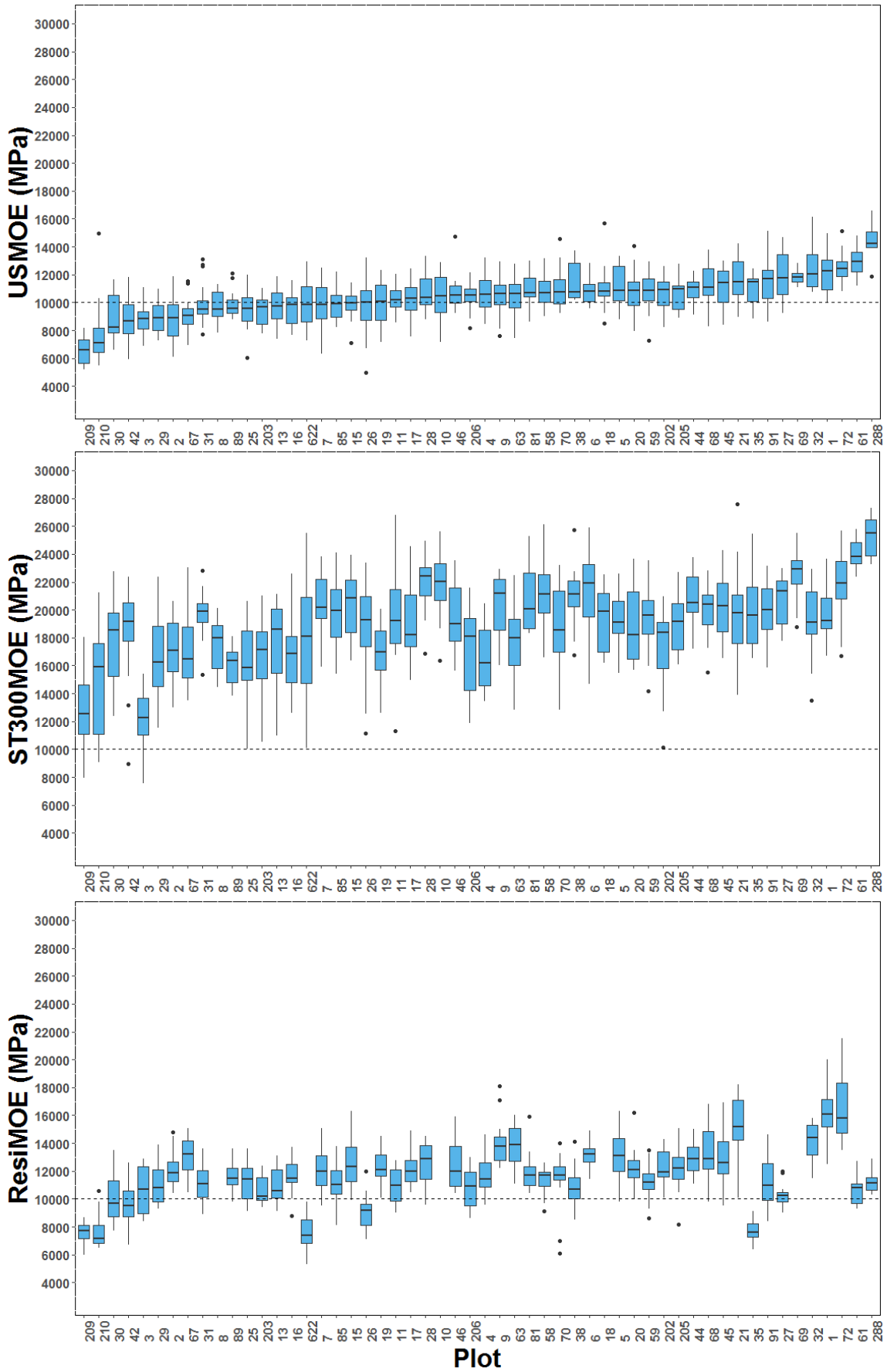
Figure 40. Comparison of the plot MOE predicted by the three technologies. In each chart, plots are ordered by USMOE ranking from low to high (top chart). Dashed line indicates 10,000 MPa.

7.1.5   Key points from the quantitative assessment and comparison of tools

The cambial age sigmoid or fingerprint curve allows the grower and processor to determine when or if plots, compartments or stands will produce high quality wood independently of the size growth of the trees.

The radial sigmoid curve can be used to determine how much of a specific wood MOE grade has been produced from a given location inside a tree. As the ST300 and Resistograph currently only give a single measurement or prediction per log, and this number is based on calibrations and approximations, they cannot be used to accurately predict the value of different parts of the plantation estate, but they may be useful for general ranking of stands, especially at the extremes.

7.2 Log MOE

In this section, the log MOE obtained from three different techniques (i.e. USMOE, ST300, and ResiMOE) are compared with reference log MOE obtained by the resonance method (BING). The log MOE (log dynamic MOE) from 68 destructively sampled trees were used for the comparison. (Note Bing and HM200 resonance acoustic methods were well correlated $R^2 = 0.91$).

We have evaluated linear regression models by regressing the predicted values with observed values to compare the slope and intercept against a 1:1 (i.e. y=x) line. The slope of regression line with zero intercept (y=mx), means the change in actual MOE is directly proportional to the predicted MOE. For ideal prediction, the slope of regression line, m, with intercept zero is one (1, i.e. y=x). The slope closer to one (1) means the bias in the prediction is minimal. This evaluation method is used throughout the report.

7.2.1 Ultrasound MOE (USMOE)

Calculated MOEs obtained from ultrasound (US) measurement from cores taken at breast height were correlated with the reference log MOE (BING). Predicted USMOE values of the logs were calculated using two methods (i) simple arithmetic average of segments' USMOE for each core and (ii) integral (weighted) average of the radial sigmoid from the segments' USMOE for each core.

7.2.1.1 Arithmetic average of core segment's MOE

The simplest method to obtain the average MOE of the log is to calculate the arithmetic average of the core segments' MOE data. This method provides a simple estimate of dynamic log MOE (Figure 41). With $R^2 = 0.76$ the regression explains 76% of the variation observed in the dynamic log MOE (obtained by BING). It under predicts the dynamic log MOE by 24% (y=1.24x). The relative proportion of the area or volume of the wood represented by each segment explains this discrepancy. Indeed, with the arithmetic average, the wood from the periphery of the log, with the highest MOE, has the same weight as the wood near the pith. In fact, the proportion of wood in a log changes according to the square of the radius. Thus, the arithmetic average has the effect of under representing the wood having high MOE. In contrast, the next section discusses the integral average method, which considers the proportional area of the wood.
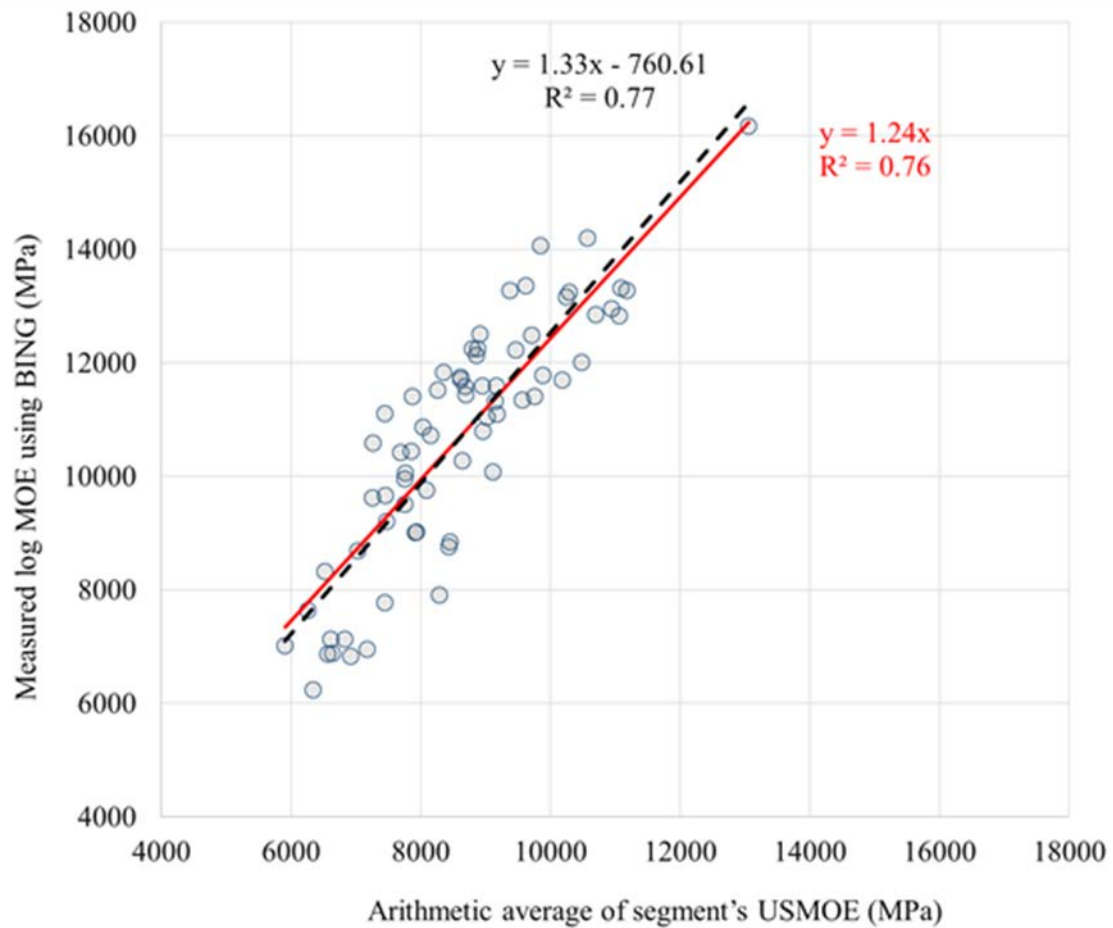
Figure 41. Regression of measured log MOE and segment arithmetic average of USMOE from the second core of the 68 destructively sampled trees.

7.2.1.2 Integral average of segments' MOE

In this method, the average log MOE was calculated using the fitted radial sigmoidal curve (i.e. MOE vs radius 5PL fitted curve). This radial sigmoid was integrated over the whole cross-sectional surface area to take into account the relative proportion of the wood at a given value of MOE. In other words, this method of calculation of the MOE of the log considers the proportion of wood relative to the log surface or volume corresponding to a given MOE since the annular quantity of wood increases with the square of the radius.

Figure 42 shows the correlation of the predicted log MOE using the integral average of segments' MOE and the measured log MOE. The $R^2 = 0.77$ for the integral average is marginally higher than the prediction made by arithmetic average ($R^2 = 0.76$). However, the integral average approach significantly improves the prediction capacity since the slope of the regression line with an intercept zero is 1.09 (Figure 42). The integral average underestimates the actual MOE by 9%. In contrast, the slope of the correlation using the arithmetic average MOE was 1.24 (Figure 41).
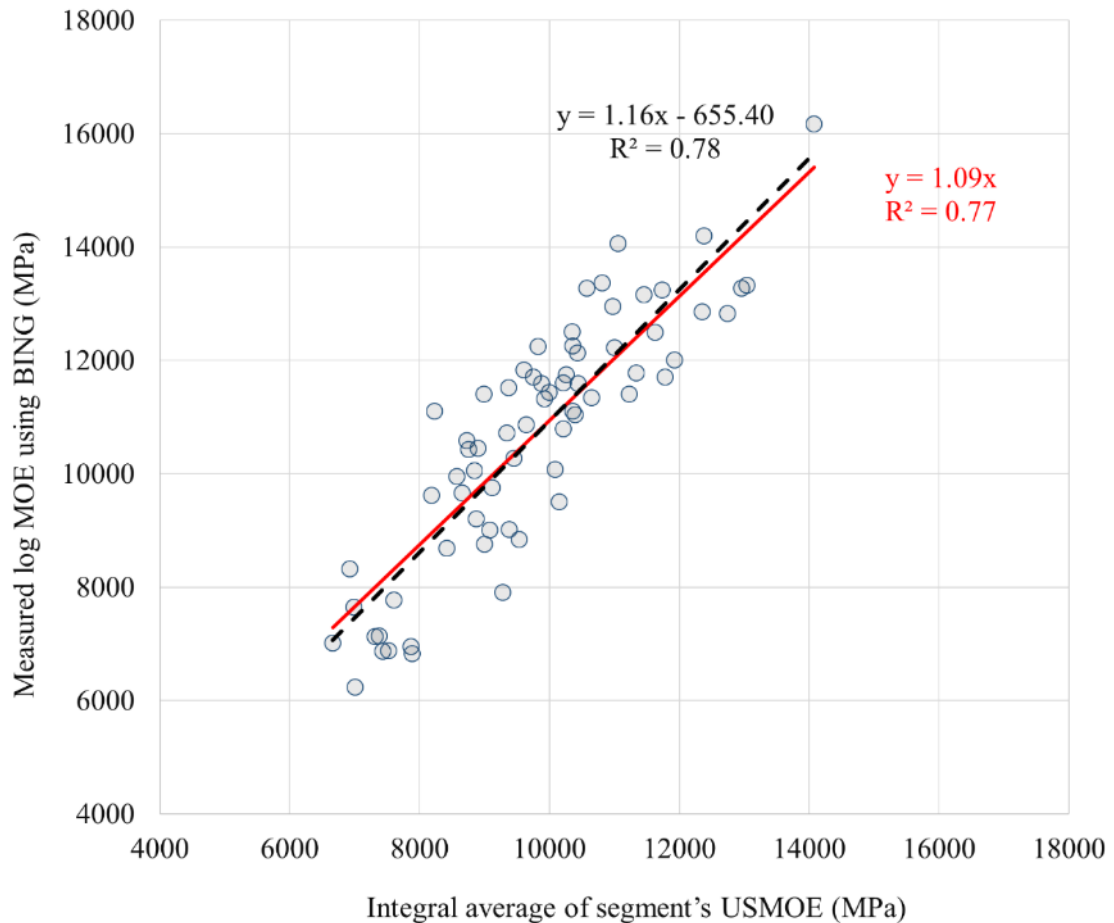
Figure 42. Regression of measured log MOE against integral average of USMOE radial sigmoid from the second core of the 68 destructively sampled trees.

The graphs above show the trees from both commercial stand and spacing trials. Separate correlations for commercial and spacing trials are shown in Figure 43. It shows marginally improved correlation between prediction (integral average) and actual values (BING) with R^2 = 0.76 for the commercial stand and R^2 = 0.80 for the spacing trial. We note that the variation of log MOE in the spacing trial is much higher than in the plot from the commercial stand which explains partly the lower coefficient of determination of the latter. The slope for the spacing trial is close to 1 (1.04) whereas the slope for the commercial stand is1.15 implying that for this plot the integral average MOE under predicts the log dynamic MOE by 15%.
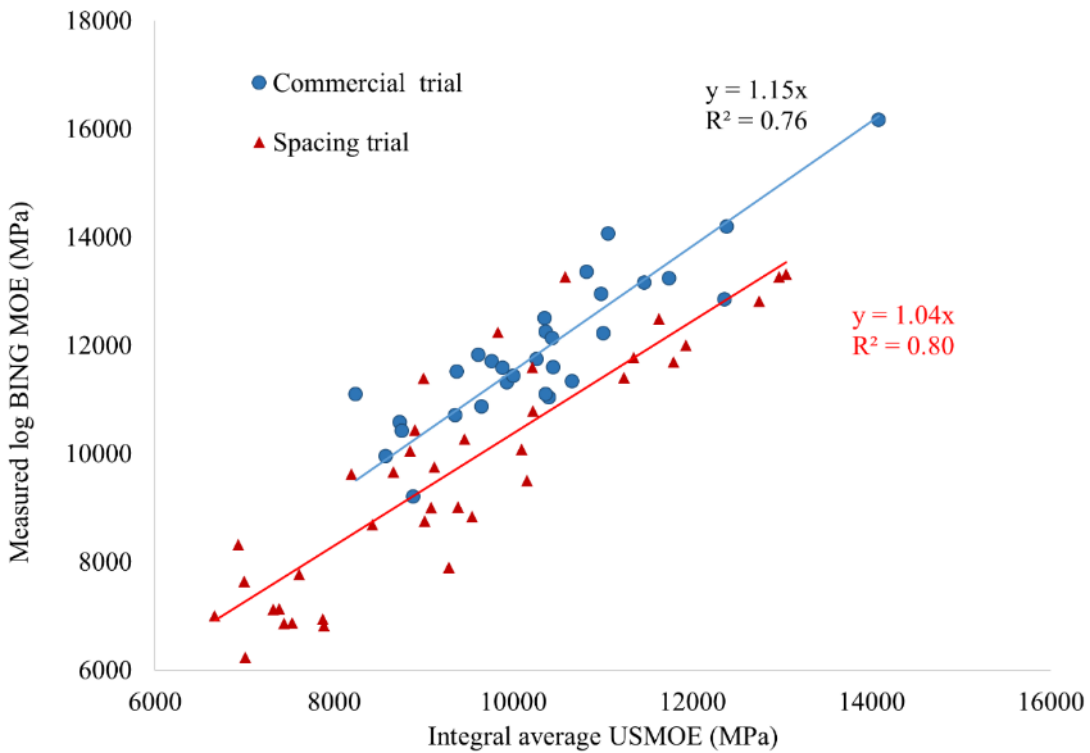
Figure 43. Separate correlations of log MOE prediction for commercial stand and the two spacing trials.

7.2.1.3 Genetics and spacing effects on log MOE

Figure 44 shows the effect of germplasm and stocking on log MOE. The effect of stocking is not very prominent as can be seen from the 68 destructively sampled trees. Instead the trees are generally clustering based on their genotypes. The exception to this may be the F2 seedlings from the thinned commercial stand.
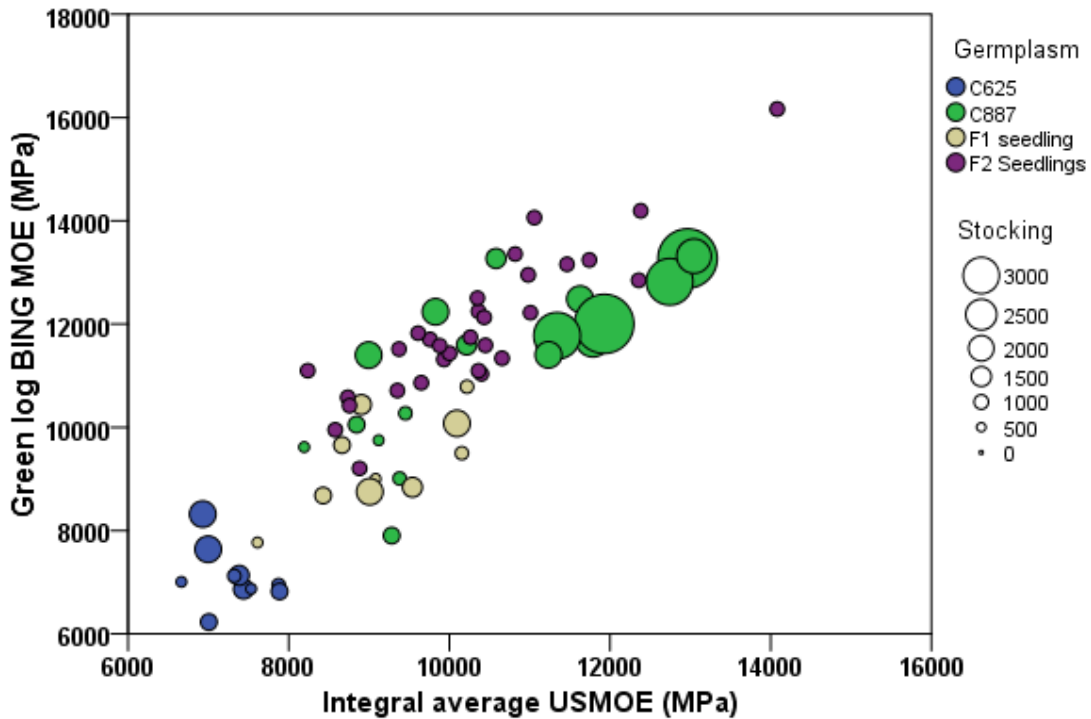
Figure 44. Effect of germplasm and stocking on log MOE for the sacrificial trials.

Interestingly, we observe that integral average USMOE tends to overestimate log MOE for the higher stocking (i.e. small diameter trees). The segment sampling methodology that starts to cut the segments sequentially from the bark to the pith may explain this tendency. Often the segment close to the pith could not be measured because of defects or undersize (<20 mm). Therefore, the segments having lower MOE segment were less represented when the reconstruction method was applied on small logs. Consequently, the higher MOE segments (outer segments) have higher weight and could explain the overestimation on the smaller log.

However, a clear effect of germplasm on log MOE was observed. The clone C887 and F_2 hybrid seedlings exhibit the highest quality, C625 has the lowest quality, and the F_1 seedlings germplasm is intermediate in Figure 44. The effect of germplasm can be established by observing the trajectories of the cambial sigmoid curves. In Figure 45, three different genotypes grown in the same plot exhibit distinctive MOE patterns relative to cambial age. This explains the performance of this material. The longer juvenile phase of clone C625 clearly undermines its performance. The usefulness of the fingerprint curve approach (discussed in section 7.1.3.1) is further confirmed here.
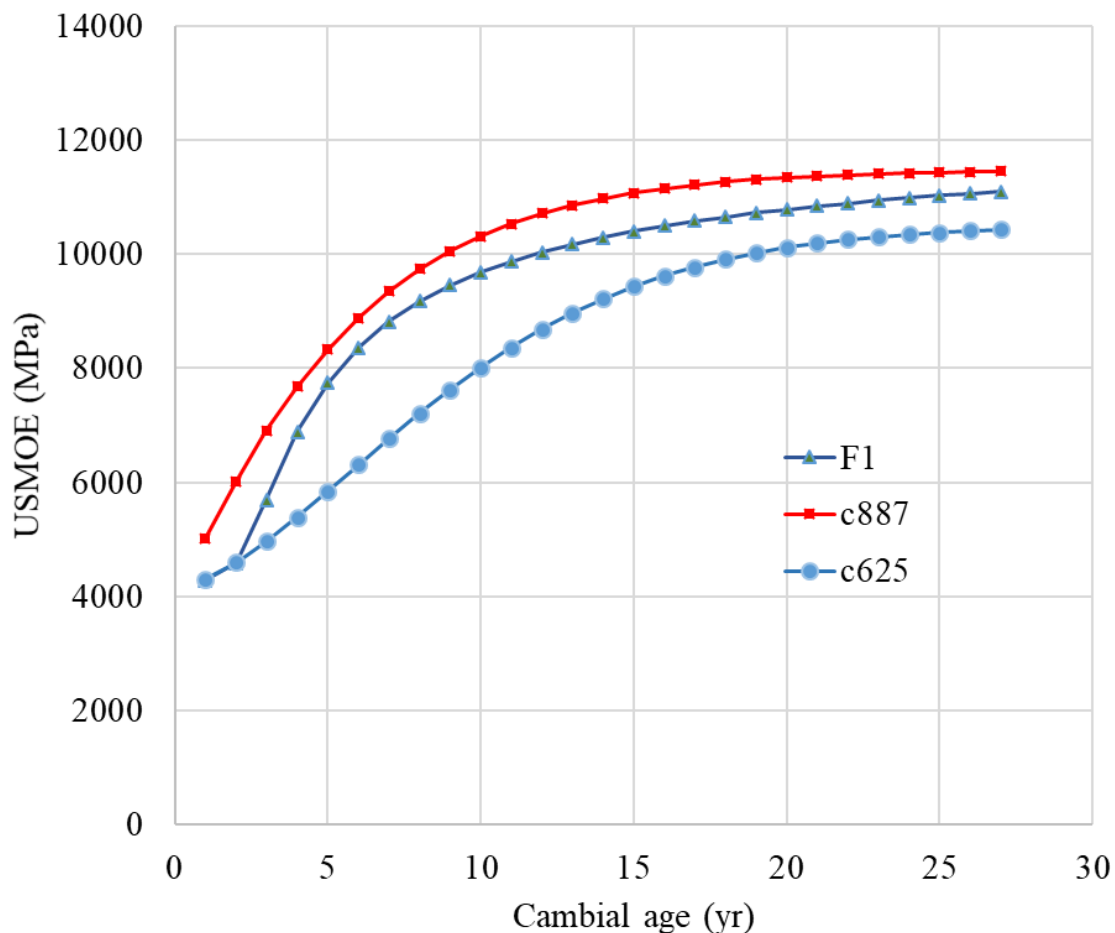
Figure 45. The sigmoid curve of three different genotypes obtained from a spacing trial (plot 622).

7.2.2 ST300 predicted MOE (ST300MOE)

ST300MOE was calculated from stress wave velocity and an arbitrarily established density through the formula velocity^2 $\times$1,000 kg/m^3. When forced through the origin (red line, Figure 46), the regression line for the 68 destructively sampled trees shows that ST300MOE over-predicts the dynamic log MOE by 41% (y=59x). The regression explains only 19% of the variance of the log MOE measured by resonance acoustics. When the regression is not forced through the origin, the level of explained variance increases significantly to 42% however the

prediction bias from the regression equation slope increases to 65%. This over prediction is to be expected since the ST300 only samples the stiffer outer wood of the trees.
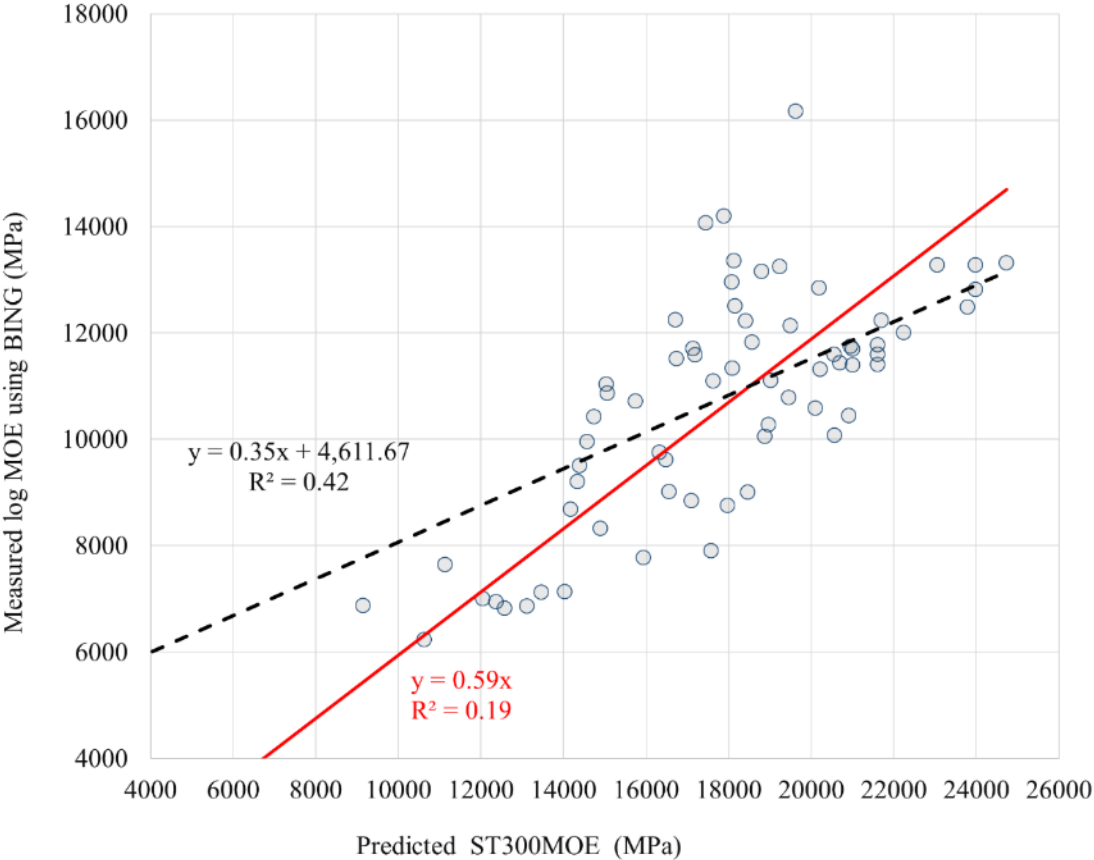
Figure 46. The relationship between the ST300MOE and the log MOE measured using a resonance acoustic tool for the second core of the 68 destructively sampled trees. The red line is the regression line forced through the origin; dotted line is the normal regression line.

7.2.3 Resistograph predicted MOE (ResiMOE)

As there is no calibration equation for southern pine, the regression line for the ResiMOE was predicted using the current settings for the Resistograph which were based on resonance method data (from HM200) from over 2,000 radiata pine logs (Downes and Lausberg 2016). When forced through the origin (red line) for the 68 destructively sampled trees the slope is slightly biased (Figure 47). The regression explains 56% of the variance of the log dynamic MOE, the ResiMOE under predicts the log MOE by 9% (y=1.09x). When not forced through the origin, the level of variance explained increases to 68% however the bias due to the slope also increases inducing an over prediction of ResiMOE by 22%. In the Resistograph study, all of clone 625 (one of four genotypes sampled) results fall below the 8,000 MPa log MOE value (see blue circle Figure 47). Downes *et al.* (2017) attributed this to abnormal behaviour of this particular clone. In fact the observed discrepancy is due to the calibration process since there is nothing atypical with this clone – it simply has low MOE (see section 7.2.1.3).
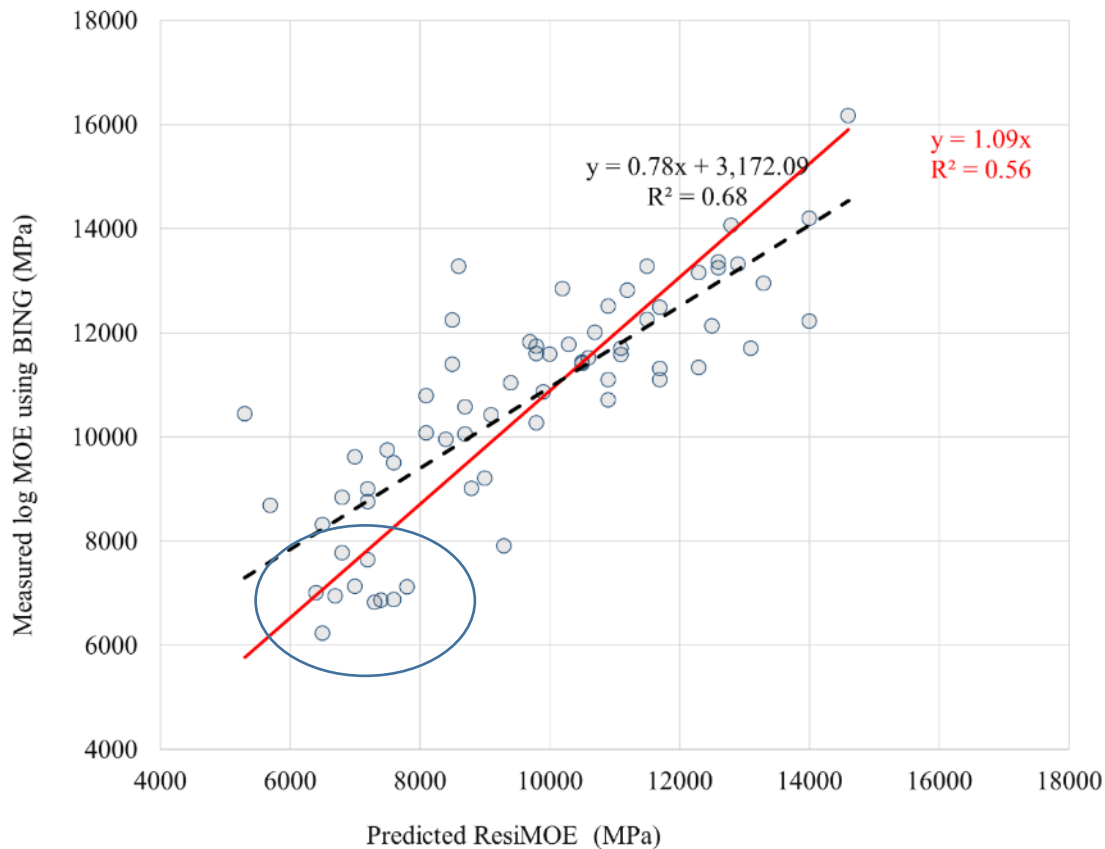
Figure 47. The relationship between the ResiMOE and the log MOE measured using a resonance acoustic tool.

7.2.4 MOE comparison between tools

Figure 48 provides a comparison of the regressions between predicted and measured MOE obtained from three methods: USMOE, ST300MOE and ResiMOE. Overall, the USMOE, ResiMOE and ST300MOE explain 78%, 68% and 42% of the variance in dynamic log MOE data respectively. This indicates that USMOE is the most precise method. Another important observation from this graph is that the slope of the regression lines with intercept zero (the solid line, equation format $y=mx$) are 1.09, 1.09 and 0.59 for USMOE, ResiMOE and ST300MOE, respectively. Therefore, the bias in USMOE and ResiMOE is relatively small (9%), whereas bias in ST300 is approximately 41% indicating a poor accuracy of this method. Although the slopes for USMOE and ResiMOE are similar, ResiMOE explains less of the dynamic MOE variation (68%) compared to USMOE (78%).
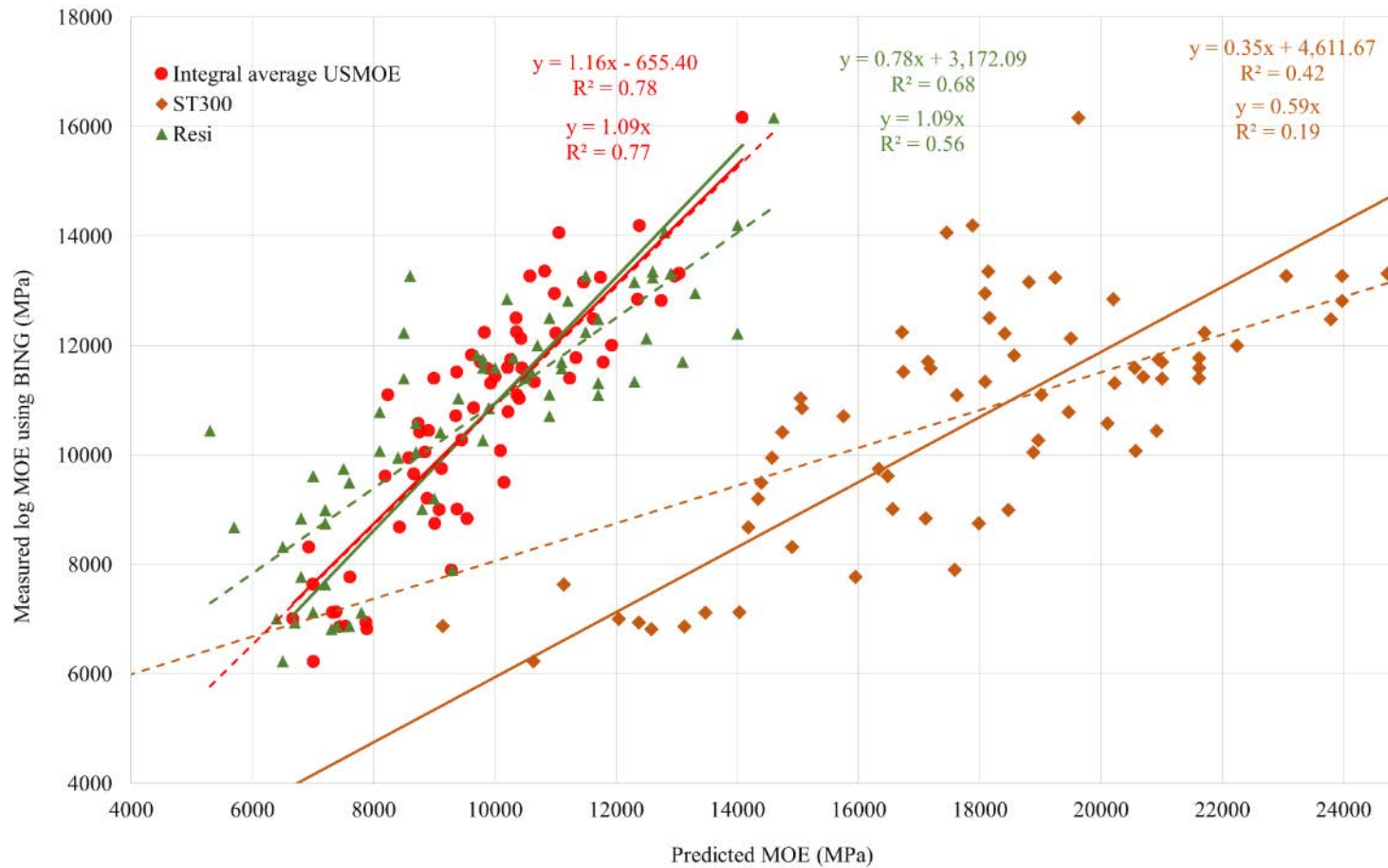
Figure 48. Comparison of log MOE between integral average, ST300 and Resistograph.

7.3 Board MOE

The boards are the marketable products that are directly linked to the value of the southern pine resource.

Boards from the sacrificial plots were sawn according to standard sawing patterns provided by Hyne and tested according to the Australian standard four point static bending test. This section compares the predicted board MOE reconstructed from USMOE data with static bending MOE. The ST300MOE and ResiMOE are not designed to access the local (i.e. within tree) MOE variation. As such they are not able to predict the actual board MOE. Consequently they are not part of this section. All the boards sawn from the 68 destructively sampled trees obtained from the commercial stand and two spacing trials were used for this part of the study.

In the first part of this section (Section 7.3.1), the average static bending MOE of the boards was calculated for each log. It was then compared with the log MOE calculated from the radial sigmoid curves.

In the second part of this section (section 7.3.2), the static bending MOE for each board was compared with predicted boards from the local measurement of USMOE using two approaches:

1) 2D (2-dimensional) approach using board projections from a disc (explained in section 6.7.5), and
2) 3D (3-dimensional) approach which provides the full volumetric reconstruction of the board (explained in section 6.7.5).

7.3.1 Average MOE of the boards per log

The average static bending MOE of boards obtained from each log from the commercial and spacing trials were plotted against i) the log dynamic MOE obtained from BING as a reference prediction and ii) USMOE calculated from two different methods.

Figure 49 shows the regression between measured log dynamic MOE (BING) and average boards' static bending MOE. Although the R^2 of the correlation is relatively high (0.80), it is 13% biased as the slope is 0.87. The over prediction is partly due to the sawing patterns which discards the outer high stiffness wood of the log, whereas the resonance method measured dynamic MOE of the full log. Moreover, this over prediction of the dynamic MOE over the static MOE is a well-known phenomenon in solid mechanics. Since wood is a viscoelastic material part of the mechanical energy is dissipated in the viscous components of wood. The higher the loading speed or the displacement frequency the higher the energy dissipated and the higher the measured MOE. The experimental data indicates 45 of the 68 logs had MOE values over 10,000 MPa, which equates to 66%, whereas only 33% of boards obtained from these trees had MOE 10,000 and more MPa.
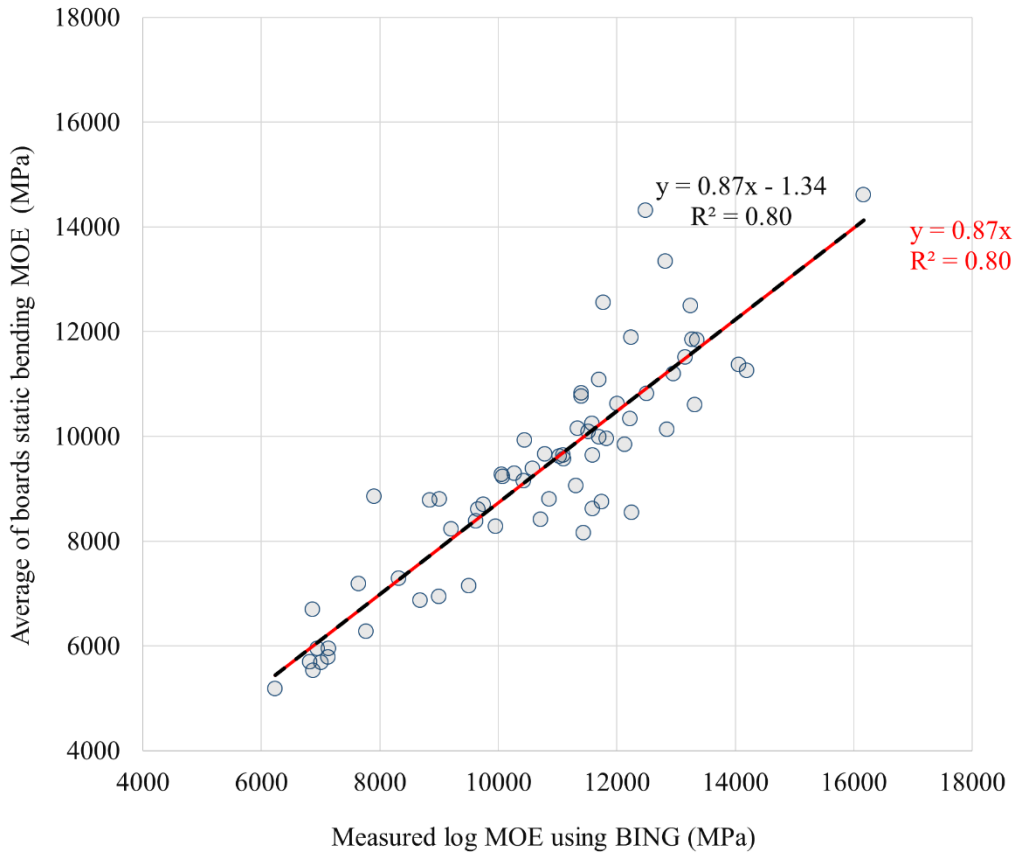
Figure 49. Average board MOE (static bending) vs log BING MOE from the second core of the 68 destructively sampled trees.

Figure 50 shows the correlation between the average static bending MOE of the boards of each log and the integral average USMOE (radial sigmoid) of the same log. Although the slope of the regression line with intercept at zero is 1.03, the R^2 is only 0.44. In the same way as above, this observation is due to the difference between the cross section surface of wood measured by each method. The integral average calculation considers the whole diameter of the logs, however, wood near the bark is discarded during the sawing process. Conversely in the lower part of the graph, a group of logs displays a higher average static bending MOE than the integral average USMOE this may be due to loss of outer wood from heavy log debarking resulted in damage or loss of the outer section of some cores.

In Figure 51 we examine what occurs when only the inner 84% of the radius is used for the calculation of the integral average MOE as explained in section 6.7.5. When the area directly associated to the sawing pattern is considered, the correlation improved to $R^2 = 0.77$.
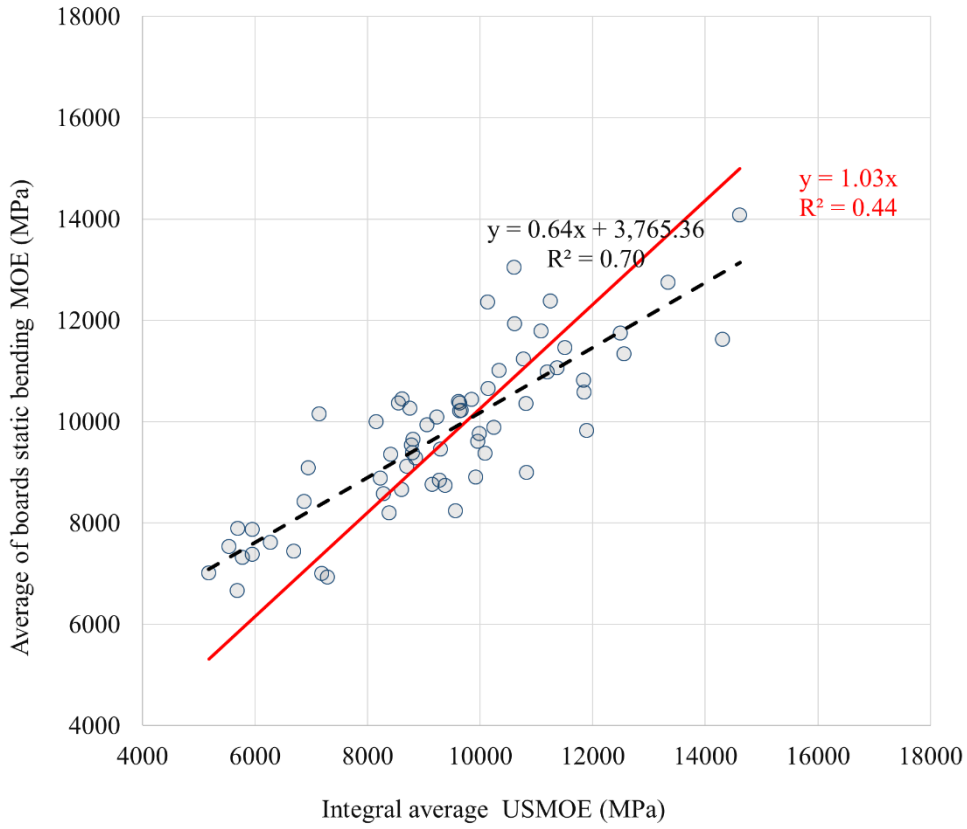
Figure 50. Weighted average (integral average 100% of radius) with average static bending MOE.
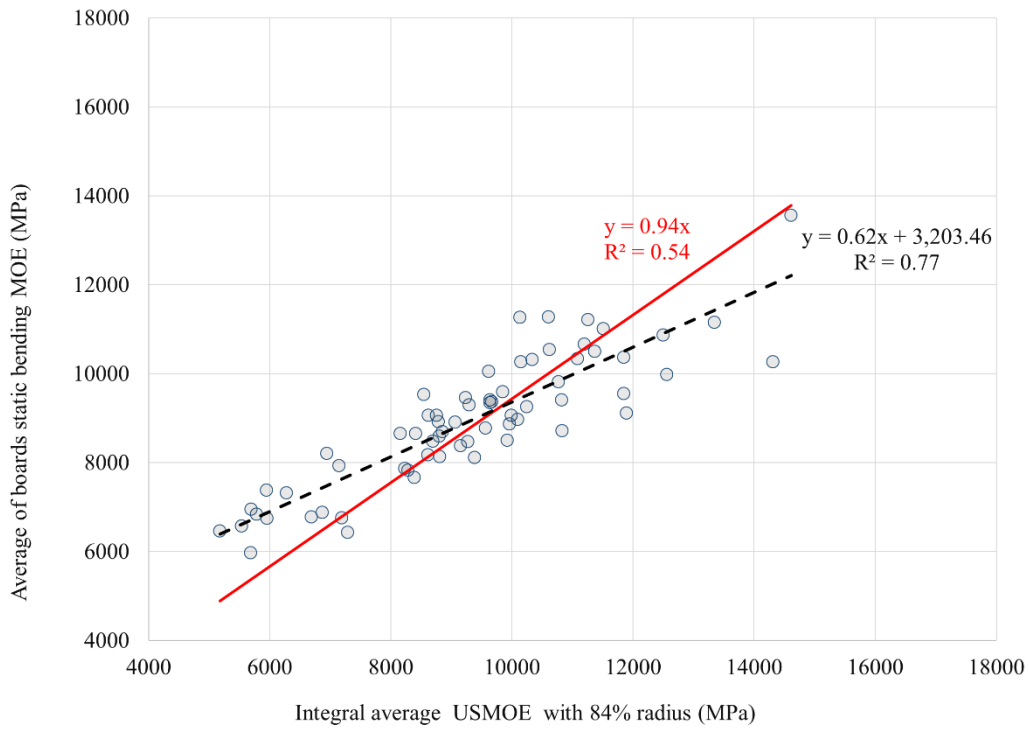
Figure 51. Weighted average (integral average 84% of radius) with average static bending MOE

7.3.2   Individual board MOE prediction

The prediction of individual board MOE is discussed in this section. The results from three different approaches, namely, area average (2D), volume average (3D) and four point bending simulation (3D) are presented and discussed. The principles of these three approaches were presented in section 6.7.5.

7.3.2.1   Area average (2D) with sawing pattern approach

A 5PL sigmoid function between MOE and radius (i.e. "radial 5PL") was used to calculate the board MOE for individual boards (e.g. Figure 18). The shell integration of the radial 5PL function followed by surface mapping allowed us to calculate the MOE at any location in the log for any section shape. In this 2D approach, first the actual board locations were calculated from the actual sawing pattern. Afterward discrete nodes from the map (a node is a point in a spatial location) were created on the cross-sectional surface of the board. The 5PL function was then used to calculate the MOE at each node. The node MOE is then assigned to a finite area created around each node. Finally the average MOE of each board was calculated using the calculated MOE of each finite area. The flowchart of predicting 2D area average MOE is shown in Figure 26.

Comparisons between predicted MOE and static bending MOE for individual board sawn from six selected trees are shown in Figure 52. Two of these trees were from a commercial plantations and four from the spacing trials.
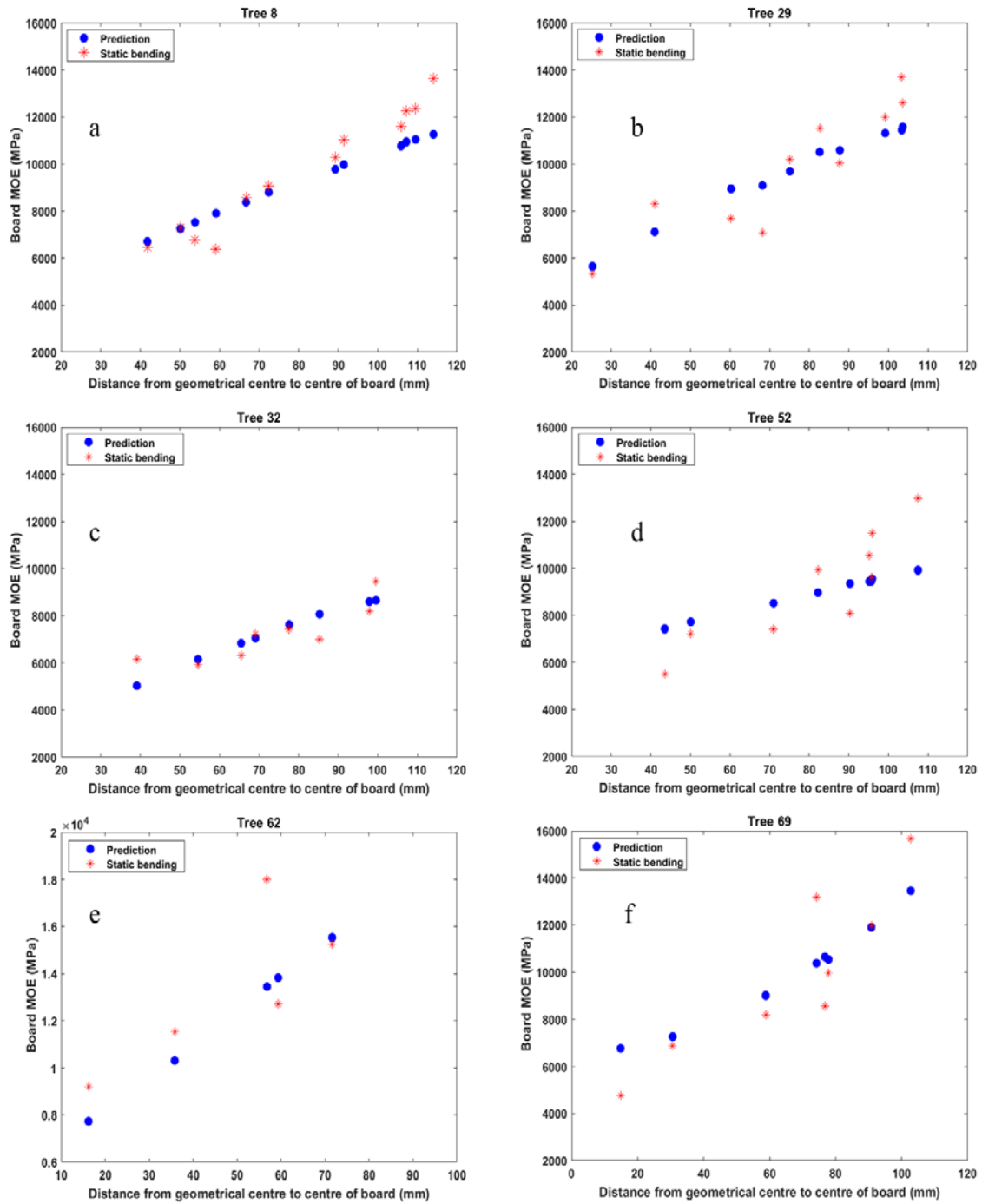
Figure 52. Comparisons between predicted MOE and static bending MOE for individual boards sawn from six trees. Figures a and b show two trees from commercial stand (tree 8 and 29 respectively), and c, d, e and f show four trees from the spacing trials (tree 32, 52, 62 and 69 respectively).

Figure 53 shows the correlation between the reconstructed board MOE using the 2D approach and static bending MOE for 625 individual boards obtained from the 68 destructively sampled trees. A good correlation was obtained with $R^2 = 0.53$ considering:

1. The reconstruction was based on USMOE measured on defect free samples. The static bending MOE can be significantly affected by the knots and defects present in the board.
2. The relative errors on the measurements of static bending MOE (for example the 11% relative error of measurement, see Appendix 7.
3. The potential errors due to the inaccurate location mapping of sawing pattern of the boards.

Remarkably, the correlation displays only marginal bias i.e. the predicted MOE is directly proportional to static bending MOE as the slope of the regression line is 1.02. As a consequence this method provides a simple and accurate approach to predict the range of board MOE values obtainable from each log. The precision can still be improved by introducing a model for knots.
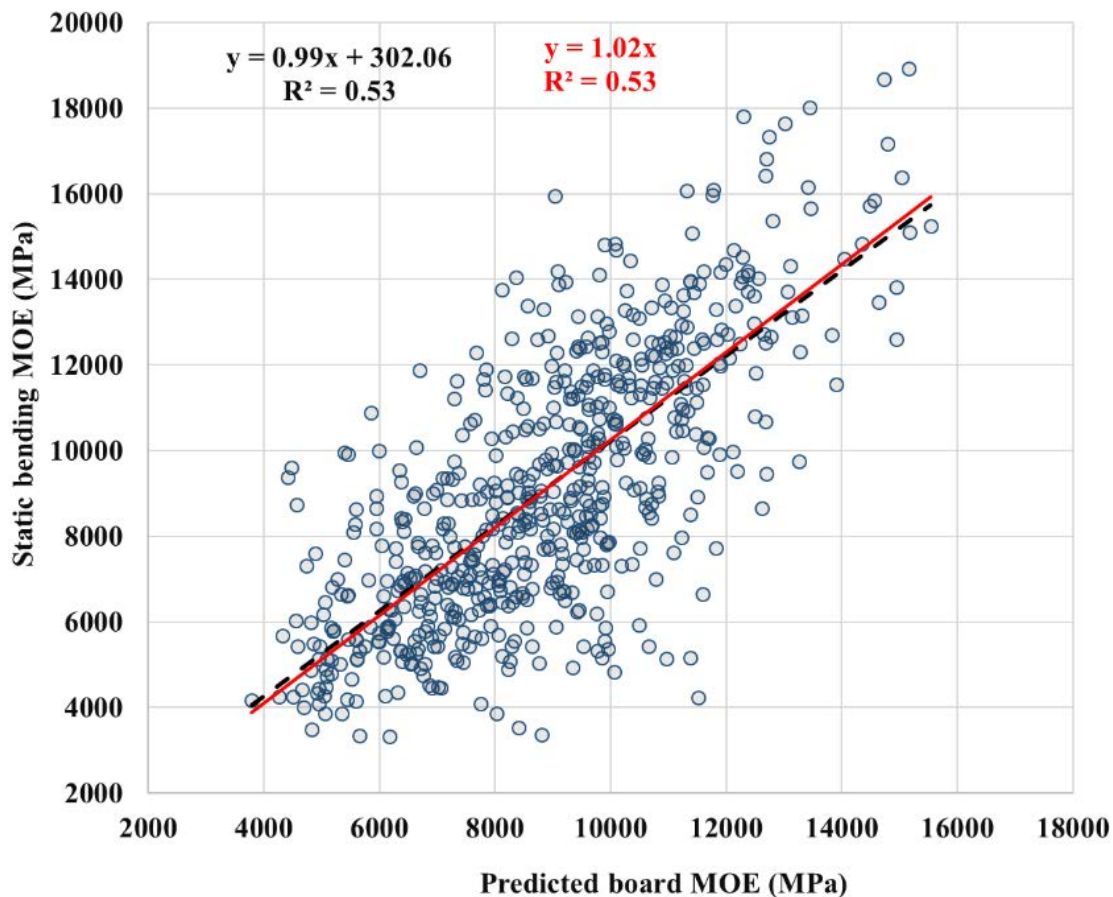
Figure 53. Correlation between measured and predicted MOE for all boards sawn from commercial and spacing trial combined. N= 625.

The efficiency of this method can be further demonstrated by displaying the linear regression charts for the commercial plot and spacing trials in Figure 54 and Figure 55. The 2D reconstruction is able to explain 50% and 52% variation in board MOE for calibration and validation plots respectively, and slopes of 1.06 and 0.99 respectively. The validation plot

includes trees from low stocking to very high stockings. The model still predicts the board MOE with the same level of accuracy. This stability proves the robustness of the model.
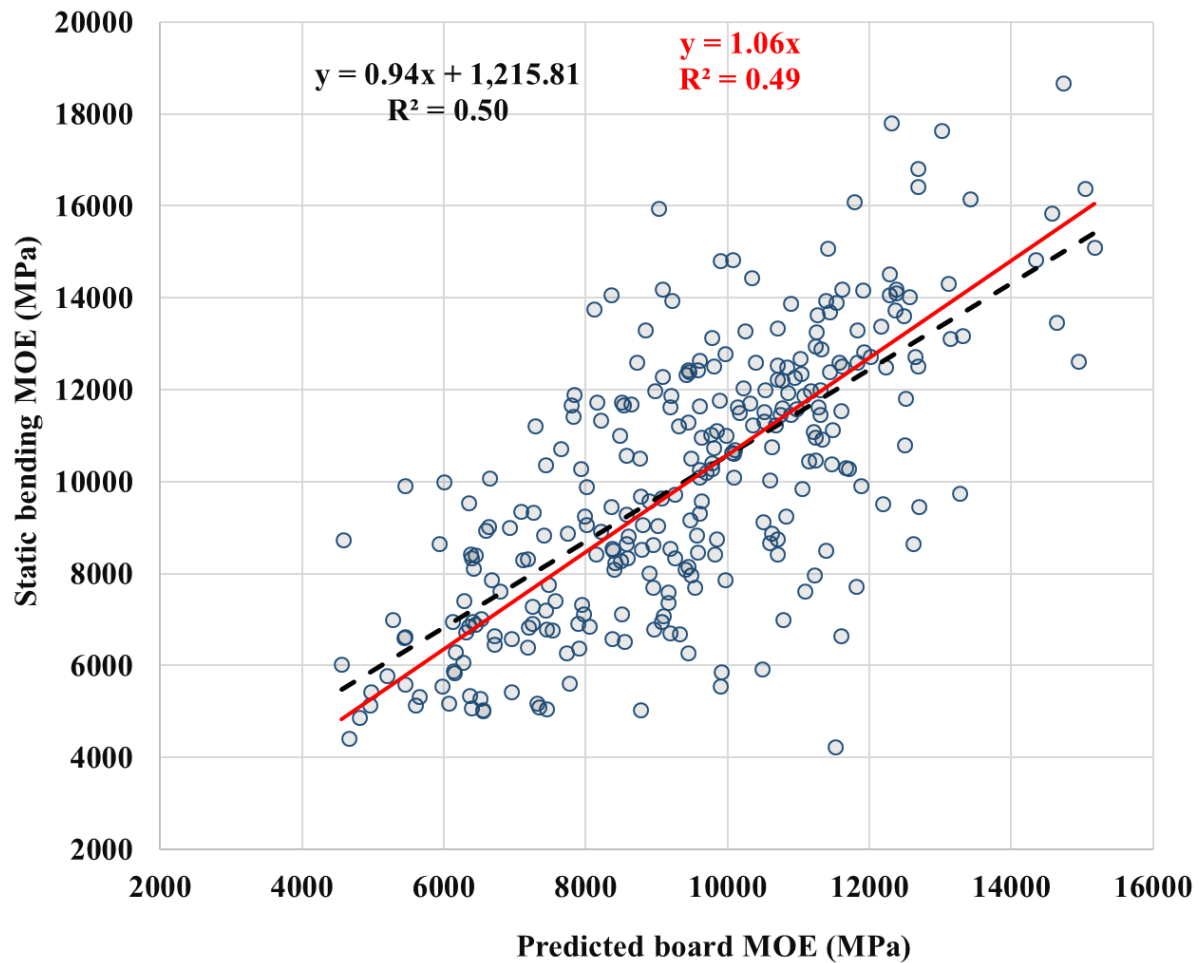
Figure 54. Correlation between measured and predicted MOE for boards sawn from the commercial F₂ hybrid plot
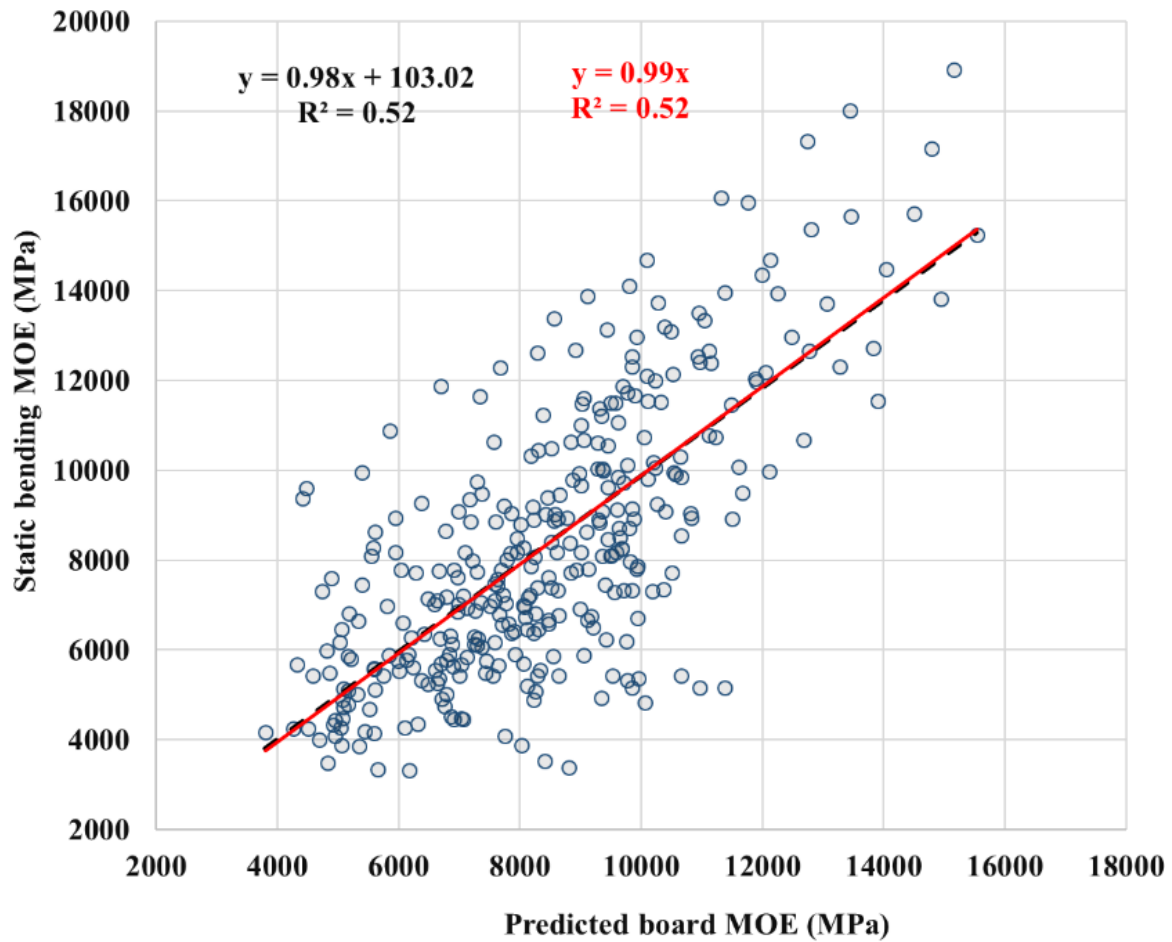
Figure 55.Correlation between measured and predicted MOE for boards sawn from the spacing trials.

Correlations of predicted and static bending MOE for selected trees are shown in Figure 56. They further confirm the robustness of the 2D approach. The R^2 of the correlation is often greater than 0.80 and the slope within 10% of the y=x line. However, on some trees the 2D reconstruction method displays lower precision and accuracy. The errors are most likely due to lower MOE values in the actual bending test due to the presence of knots, error in the location mapping of the board or high eccentricity of the pith.
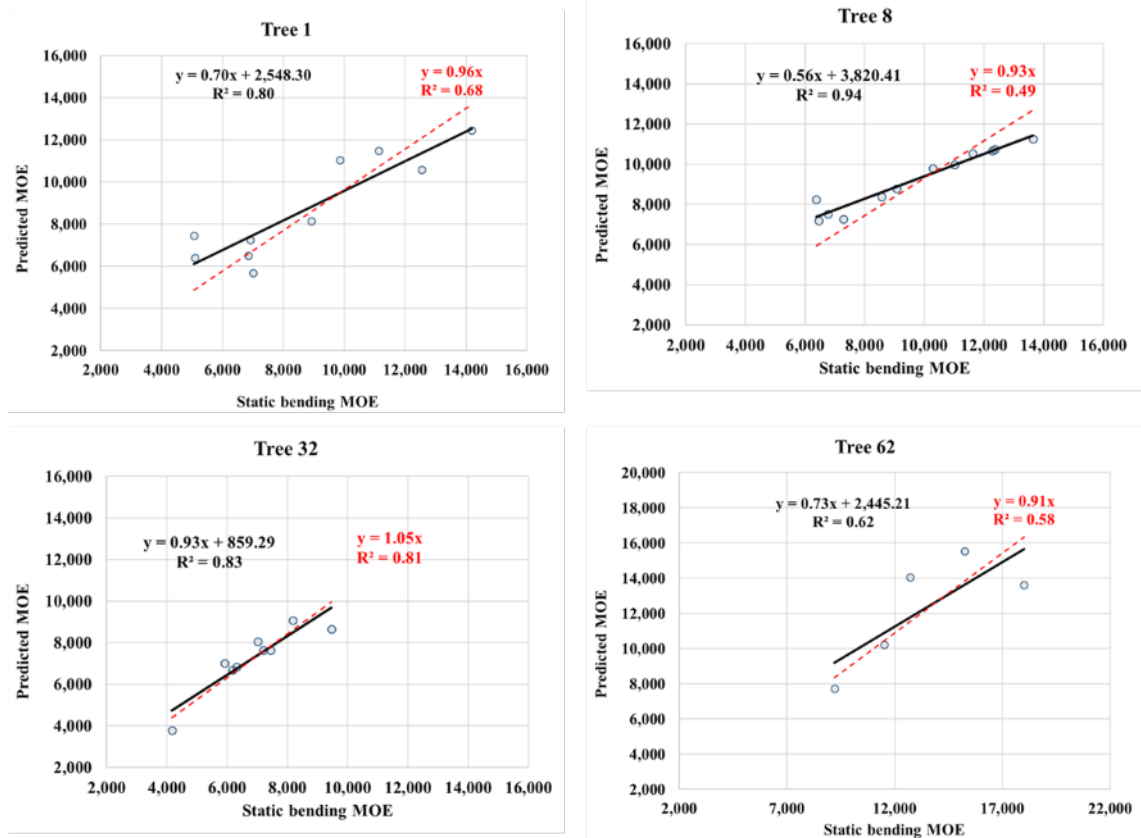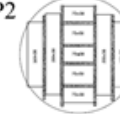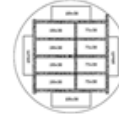
Figure 56. Correlation between predicted and actual MOE for selected individual trees.

This approach can be applied to investigate the impact of the shape of the radial sigmoid curve, sawing patterns and MOE cut-off as shown in Table 2. It exhibits the high impact on structural grade recovery of the interactions between these parameters. As an example, for a given radial sigmoid curve and cut-off of desired MOE class, the recovery can change by 40% depending on the sawing pattern. When all the other parameters remain constant, the radial sigmoid curve can have a dramatic effect on the recovery.

Table 2. Percentage recovery of wood above 10,000 or 9,000 MPa for three sawing patterns (P1-P3) and 5 radial sigmoid trajectories taken from sampled trees. Small end log diameter = 290 mm.

Sigmoid		MOE Cutoff (MPa)	P1	P2	P3
Tree 10		9,000	42%	50%	40%
		10,000	19%	27%	29%
Tree 29		9,000	42%	50%	40%
		10,000	19%	27%	34%
Tree 52		9,000	42%	50%	40%
		10,000	0%	0%	0%
Tree 38		9,000	50%	50%	55%
		10,000	50%	50%	40%
Tree 44		9,000	32%	26%	43%
		10,000	0%	0%	16%

63

7.3.2.2 3D sawing pattern approach

In this section, we outline the development of the mathematical model used to predict the wood properties at a board level based entirely on measurements taken from the cores. The model of wood properties is based on the segment data collected from the cores ('square' cores cut from the discs see Figure 9) obtained at four different heights within each destructively sampled tree.

A key component of the model development was being able to relate cambial age with radial position. To do this, we utilised the core maps recorded for each square core taken from the trees in the destructive sampling trials. These core maps show the ring positions on both the left and right side of the pith. By developing an algorithm in MATLAB, we were able to read the ring locations from the scanned images of the core maps. This gave us direct information on the growth of the tree at four different heights, and allowed us to transform between cambial age and radius.

Utilising information from the tree ring markings, we were then able to map cambial age and apical age back to a radial and height position within each individual tree. This allowed us to build a profile of the tree structure, and use as an approximation, piece-wise linear functions to connect the rings at each height within the tree. Note that not all rings were present throughout the tree, and we assumed a radius of zero for the rings that were no longer present. Figure 57 shows an example of the tree profile obtained from tree ring markings. Note that the inner-most ring is only present in the bottom core, so we set a value of zero for the radius at each subsequent core position.
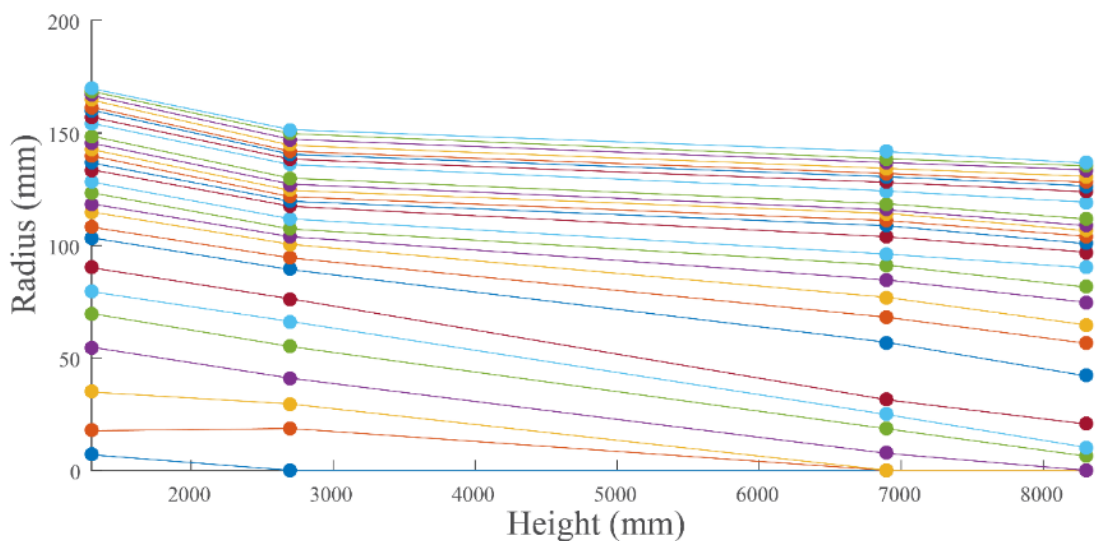
Figure 57. Tree ring profiles based on core measurements (cores from four heights along the stem). The first core was taken at approximately 0.7 m.

The next step was to connect the property between points of measurement up the height of the tree. To do this, we used an approach based on radial basis functions (RBFs) (Carr *et al.*, 2001). RBFs have been used in a wide range of fields, from computer graphics to medical imaging (Carr *et al.*, 2001; Carr, *et al.*, 1997). RBFs provide a functional description of the data, and hence the surface can be evaluated at any location. They do not require that data points be located on a regular grid, allowing for increased flexibility. We used a thin-plate spline radial basis function, given by:

$$\phi(r) = r^2 \log(r),$$ (5)

where r is the distance between a data point and a point on the surface. The surface is then given by a linear combination of these RBFs, together with a polynomial term. We interpolated between the fitted 5PL functions to obtain a surface describing the variation in MOE with cambial age and apical age. Figure 58 shows the measured data points, fitted sigmoid curves and the resulting interpolating surface for tree one. Note that we added an additional sigmoid between curves two and three (shown in red). This was the average of the sigmoids at either end of the sawlog, and included to reduce the overshooting that was observed initially when fitting the surface. This allowed us to smoothly connect the sigmoids obtained at different heights in the tree, to get an estimate of the property at any cambial age and apical age.
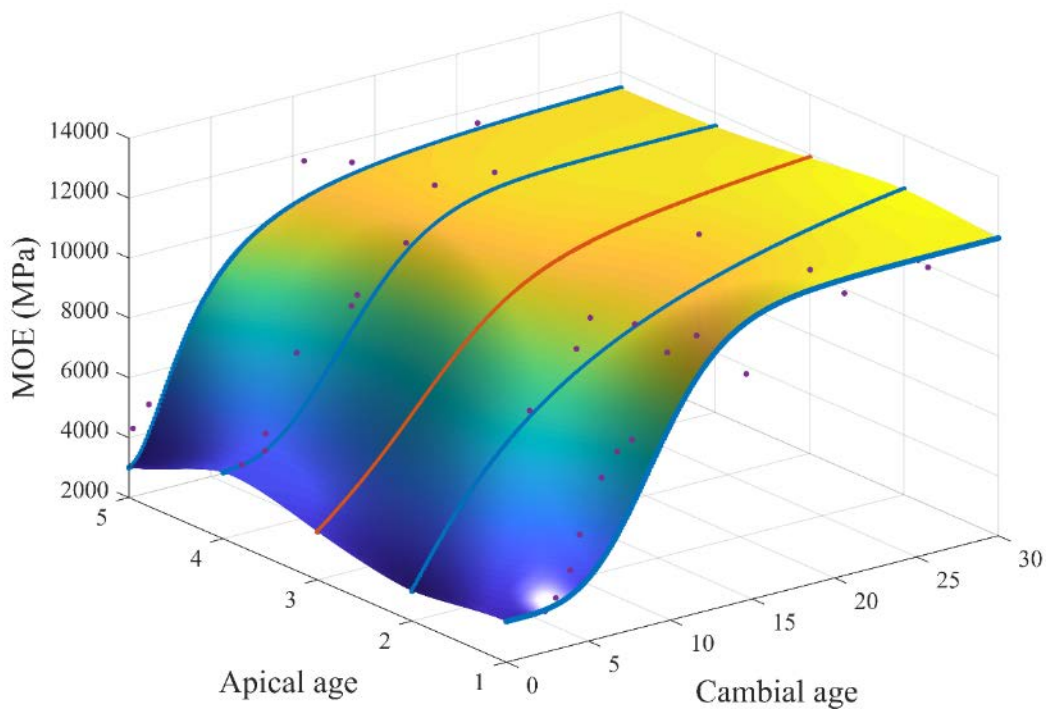
Figure 58. MOE surface showing variation with cambial age and apical age.

Using the tree ring profiles, we built a three-dimensional representation of the log. This is shown in Figure 59 where the colours represent the calculated MOE from our model. Near the centre of the tree we have wood with low MOE values, which increase towards the outer

edge. We can also see that there is a gradient of MOE longitudinally along the height of the tree, however this variation is much less than the radial variation.
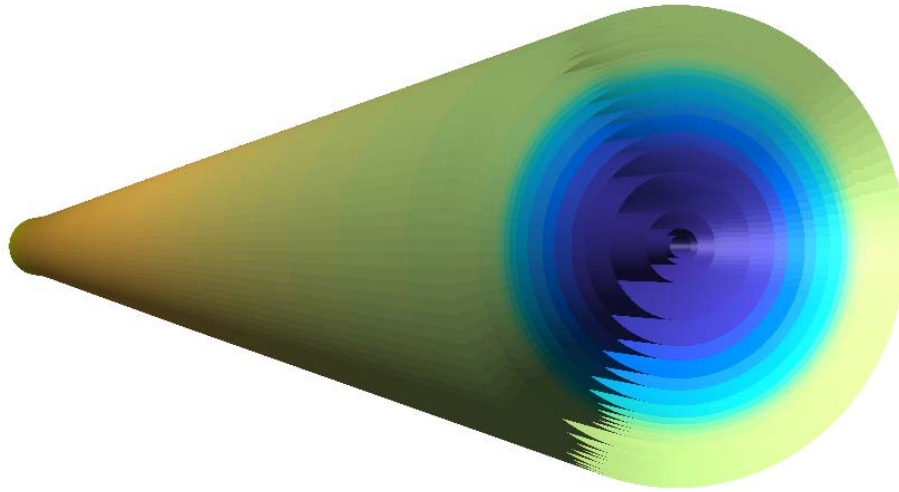
Figure 59. Three-dimensional representation of log based on tree ring profiles. The colour gradient indicates low MOE in blue to higher MOE in yellow.

This three-dimensional representation of the log allows us to perform virtual sawing to extract the timber boards, calculate their MOE, and compare this value to the MOE obtained from static bending.

To virtually saw boards from the log, we must digitise each individual sawing pattern provided for the trees in the calibration and validation trials. To do this, we have implemented an image processing algorithm to identify the locations of the board centres from the scanned template images. These board centres are loaded into a MATLAB script that generates a mesh for each individual board. This script requires information on what boards are aligned with each other, their dimensions and orientation. The alignment can be seen in Figure 60, where we have two rows of aligned boards (board A1 to A5 and board B1 to B5), with board A6 being unaligned. The code then optimises their positions by minimising the shift of centres, change in dimensions and the difference between the board spacing and spacing given the true saw kerf width. The board spacing has been weighted

more heavily to ensure an appropriate saw kerf width is obtained. Figure 60 shows the sawing pattern and the corresponding digitised board layout for tree one.
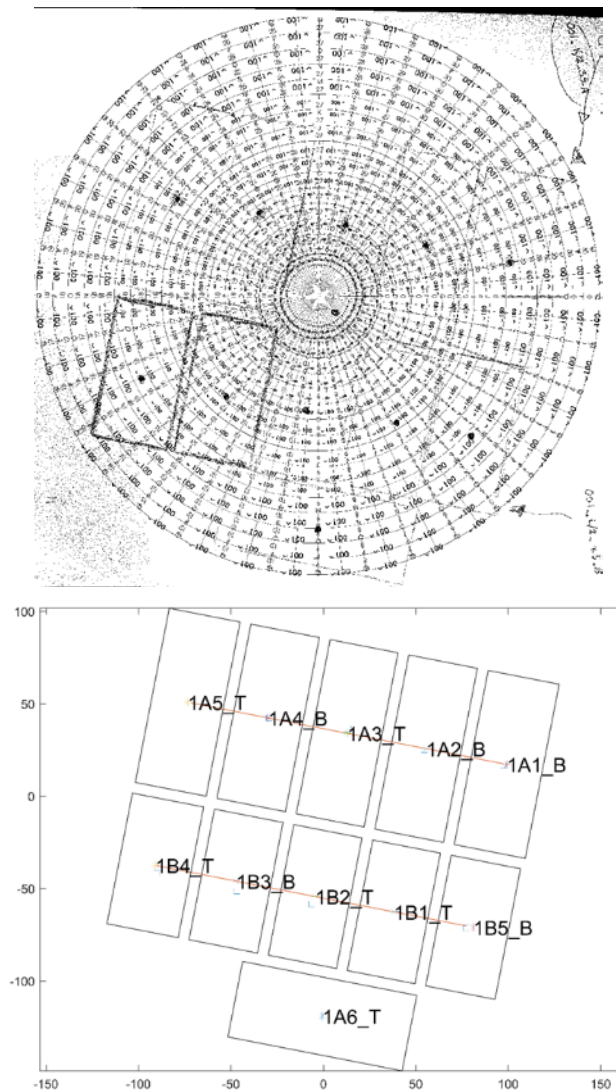
Figure 60. Example of actual sawing pattern and corresponding digitised sawing pattern obtained from tree 1.

This layout is then extruded through the length of the sawlog to obtain the digital representation of each board, described by discrete (x, y, z) coordinates. At each coordinate in the board, a value of MOE is obtained through interpolation of the MOE distribution in the log. To compare the measured MOE values with those predicted from the virtual boards, we use the MOE obtained from static bending. The static bending was performed on a shorter test sample, with the length of this test sample being determined by the cross-section dimensions of the board. For 96×40 mm boards, the test sample is 2 m long, while for the 72×40 mm boards it is 1.5 m. Each of these test samples is taken from the butt or top end, as determined by a coin toss. The virtual boards obtained from tree 1 are shown in Figure 61, indicating their geometry and MOE gradient from low (blue) to high (yellow).
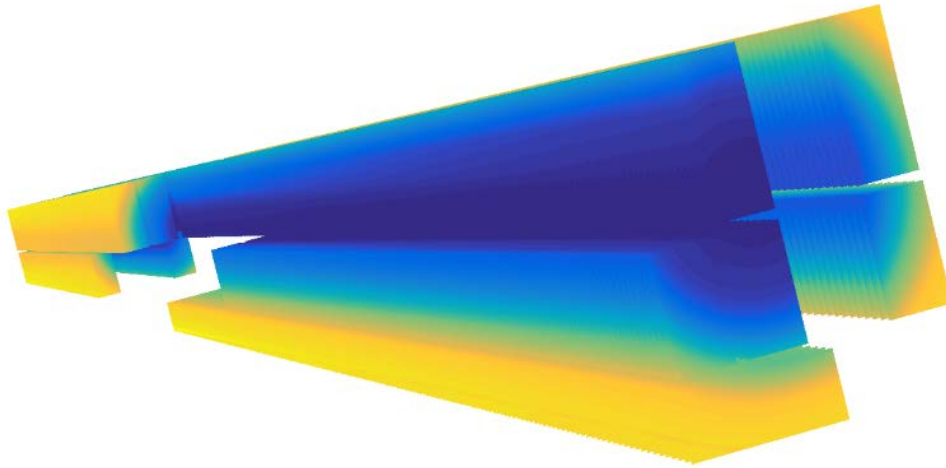
Figure 61. Virtual boards sawn from the log model. We have accounted for the end that the board was taken from for static bending testing. MOE gradient from low (blue) to high (yellow).

7.3.2.2.1 3D volume average

To evaluate our reconstructed MOE base on the volume average in comparison to the measured MOE, we plotted the measured MOE vs reconstructed MOE (Figure 62) and performed a linear regression analysis. Interestingly the correlation between the measured

and reconstructed MOE (R^2 = 0.53, slope = 1.01) is quite close to the same regression obtained from 2D reconstruction display in Figure 53.
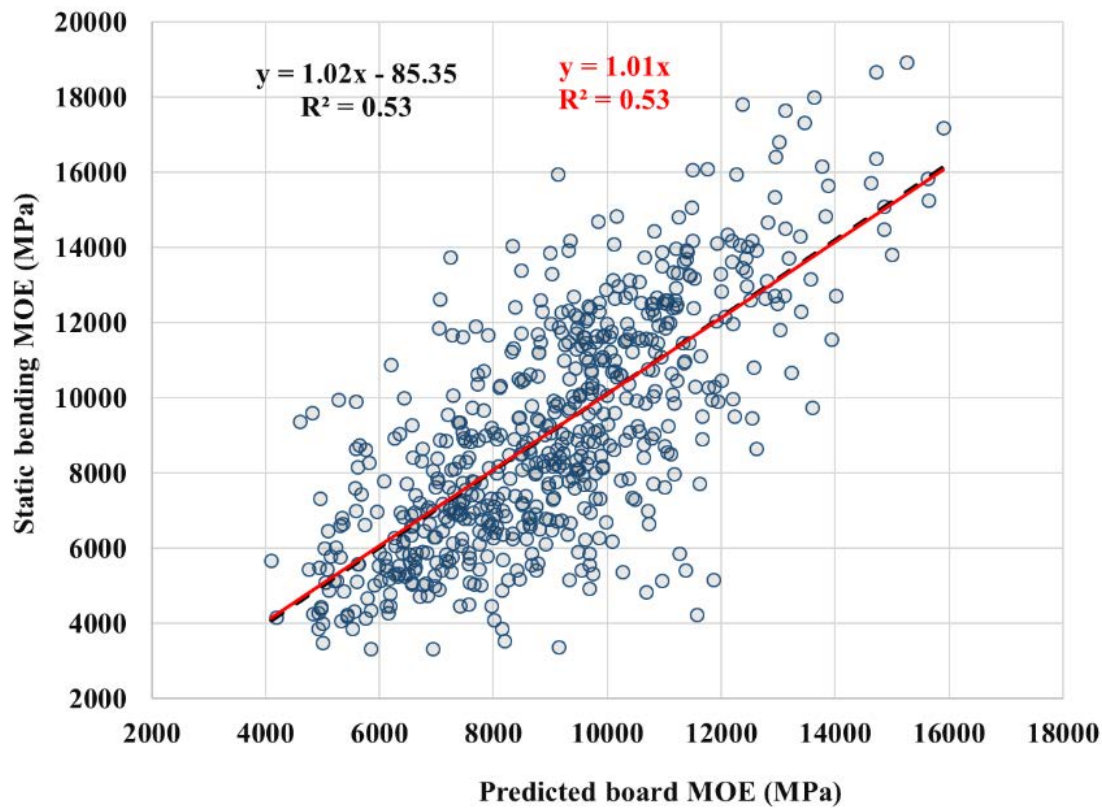
Figure 62. Correlation between measured and predicted MOE for calibration and validation trials combined - 3D volume average

The same observation arises when a linear regressions were applied to the 30 trees in the commercial plot and 38 trees in the spacing trials with R^2 = 0.50 and 0.51 respectively and slopes of 1.05 and 0.97 (figures not shown). This again is very similar to that of the 2D approach shown in Figure 54 and Figure 55. The straightness of the tree and the low variation of MOE with height partially explains this observation.

7.3.2.2.2 3D four-point static bending simulation

In this approach, we utilise the distribution of MOE to calculate reconstructed board MOE values to compare with the measured values. The MOE of the sawn boards was measured through a four-point static bending test according to the AS/NZS 4063.1:2010 standard method (see Figure 130).

Using this standard method, whereby the apparent modulus of elasticity in bending, E, is determined from the measurement of the vertical displacement, e, at mid-span (point B) using the equation:

$$E = \frac{23}{108} \left(\frac{L}{d}\right)^3 \left(\frac{\Delta F}{\Delta e}\right) \frac{1}{b}$$

(6)

where F is the applied load. If the board is sufficiently slender it allows us to neglect the effect of the shear deformation (Euler-Bernoulli beam theory), we are able to simulate the four-point bending test to predict the sawn board MOE. This configuration has been used to develop a mechanical model to calculate the MOE of the boards. A MATLAB function was developed to perform the static bending test using the middle portion of the board to obtain a value of the board MOE that we can compare to the measured values.

The regressions between the simulated MOE from the radial sigmoid and the actual static bending MOE are displayed in Figure 63.

The accuracy or the prediction of this 3D reconstruction method hasn't significantly improved compared to the 3D volume-based or 2D surface-based methods (sections 7.3.2.1 and 7.3.2.2.1).

The same observation arises when a linear regressions were applied separately to the 30 trees in the commercial plot and 38 trees in the spacing trials with $R^2 = 0.48$ and the slope was 1.03 (for both commercial and spacing trials; figures not shown). Again, this is very similar to that of the 2D approach shown in Figure 54 and Figure 55.
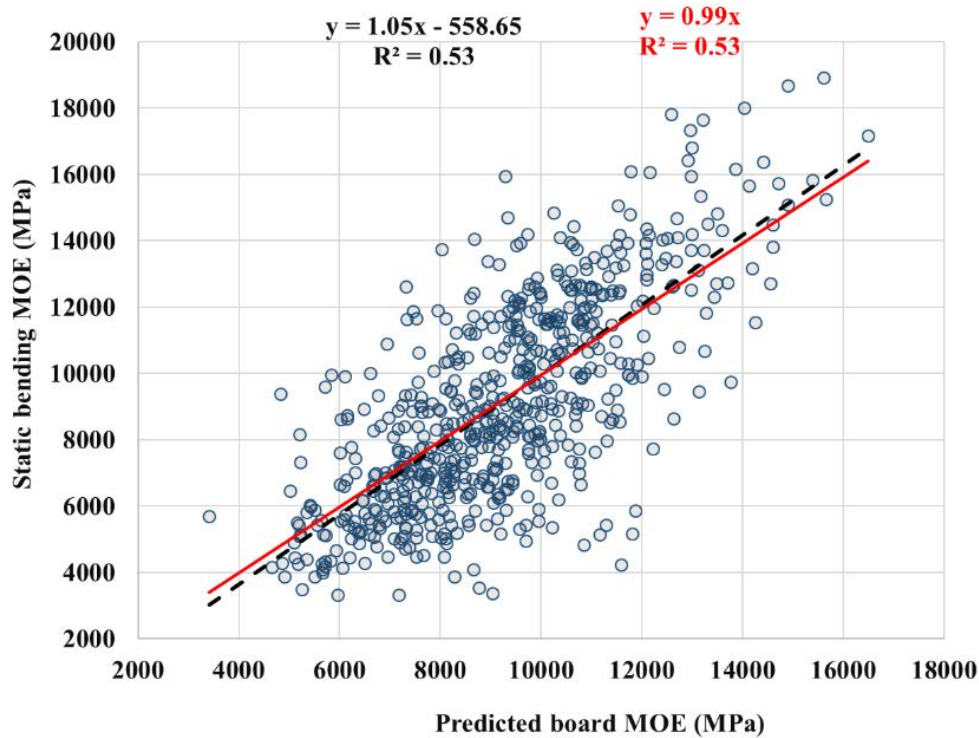
Figure 63. Correlation between measured and predicted MOE for the calibration and validation trials - 3D four-point bending simulation.

7.3.2.3 Board MOE comparison – key points

The regressions based on three levels of complexity of board MOE reconstruction have similar R^2 of 0.53 (for the 68 trees destructively sampled), therefore they can explain 53% of the variation observed on individual static bending MOE (Table 3). This metric is associated with the precision of the prediction. When the differences are considered from the metrological point of view, the influence of knots and wood defects on static bending measurement and the fact that USMOE is directly measured on small clear samples (core), this result is an excellent prediction. The key result is the high level of accuracy revealed in this study associated with the small bias of the linear regression measured by the slope of regression line with intercept at zero. Both 3D methods have only 1% bias which is marginally better than 2D model where bias is 2%.

Table 3. Number of MGP10+ boards obtained by experiment and model.

Coefficient of determination and slope of the linear regression without constant	2D area average	3D volume average	3D static bending simulation
R^2	0.53	0.53	0.53
Slope	1.02	1.01	0.99

The number of boards having a MOE of 10,000 MPa or greater (designated here MGP10+) calculated from the three approaches discussed above were compared with static bending test in Table 4. A total 625 actual boards (from the destructively harvested trees) were measured by standard static bending. They were also reconstructed using the three models described above (1 × 2D and 2 × 3D). There was a total of 232 MGP10+ boards observed in the static bending test. The 2D area average, 3D volume average and 3D static bending simulation methods estimated 192, 190 and 205 MGP10+ boards, respectively. The 2D area average and

3D volume average provided similar predictions for both commercial and spacing trials. The 3D static bending simulation had a better prediction capacity when it comes to rating the boards. From the comparative observation of Figure 53, Figure 62 and Figure 63, it emerges that the static bending simulation tends to under predict static bending MOE in the lower MOE range of the distribution.

It is noticeable that the error in the prediction of number of boards rated is considerable. It is important to note that the prediction cut-off for the rating calculation was exactly 10,000 MPa which means the board with predicted MOE of 9,999 MPa or below were not included. The adjustment of this parameter may result in the ability to find a value that will perfectly align the prediction with the actual rating. However, this type of adjustment could be risky, since lowering the cut-off will increase the number of boards which are predicted to be MGP10+ when legitimately they are not.

Table 4. Number of boards having a MOE of 10,000 MPa or greater from three reconstruction methods and standard static bending test.

	Total number of boards	Number of boards having a MOE of 10,000 MPa or greater			
		Static bending test	Predicted		
			2D area average	3D volume average	3D static bending
All destructive samples	625	232	192	190	205
Commercial trial	291	146	116	116	123
Spacing trial and Nelder wheel	334	86	76	74	82

In conclusion, both 2D and 3D approaches based on USMOE can be used to estimate the individual board MOE. For the three approaches evaluated, there was little bias (the slope of the regression lines being approximately 1) and correlations between the estimated board MOE and static bending MOE were moderate (R^2=0.53). The 3D static bending simulation had a better prediction capacity for rating the boards.

7.4 MOE prediction of full stands from sample trees

This section deals with the potential of the reconstruction approaches to predict a full stand from the information gathered on a sample of a few trees which have the same growing environment as the stand. The method is based on cambial age fitting ("fingerprint curve", see section 6.7.3) from sampled trees and the use of growth curves on other trees to assess individual tree MOE radial variations. This can be done with either the 2D or 3D approaches. These two approaches were designed to predict the value of full stands or compartment from sample trees.

7.4.1 2D approach without sawing pattern

The 'fingerprint' curve allows the calculation of MOE at any given cambial age. This curve can then be combined with the growth curves (radius vs cambial age) to provide the MOE at any given radius. Foresters routinely measure the growth curves in stands. The MOE vs radius data can be used to calculate MOE vs ring area of each tree in a plot.

The principle of this reconstruction lies on combining the fingerprint curve with individual growth curves of **new trees** as shown in Figure 64. The growth curves can be built from growth curves and diameter histogram of the stands.
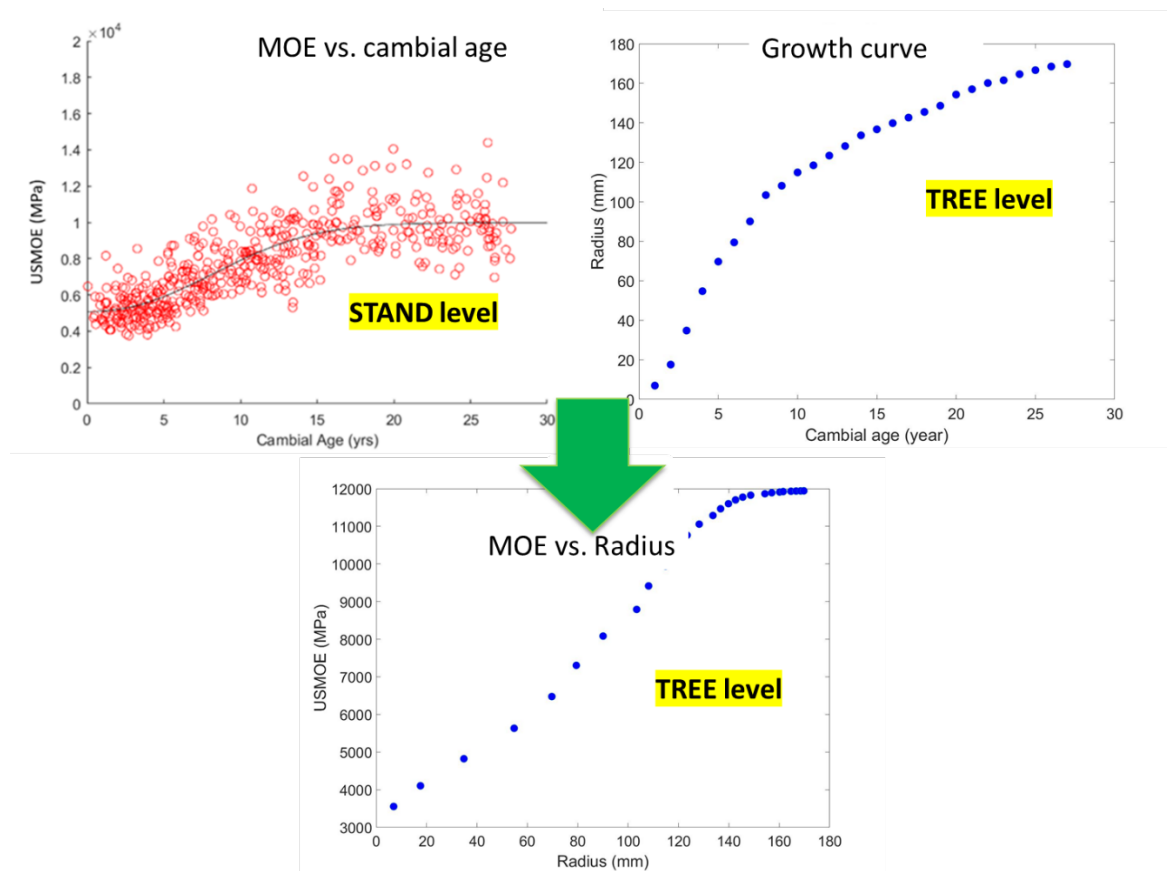
Figure 64. Extraction of individual radial MOE curve from fingerprint and growth curves.

The radial MOE curve is then used to extract the average MOE corresponding to the surface of a growth unit (e.g. growth ring) as shown in Figure 65.
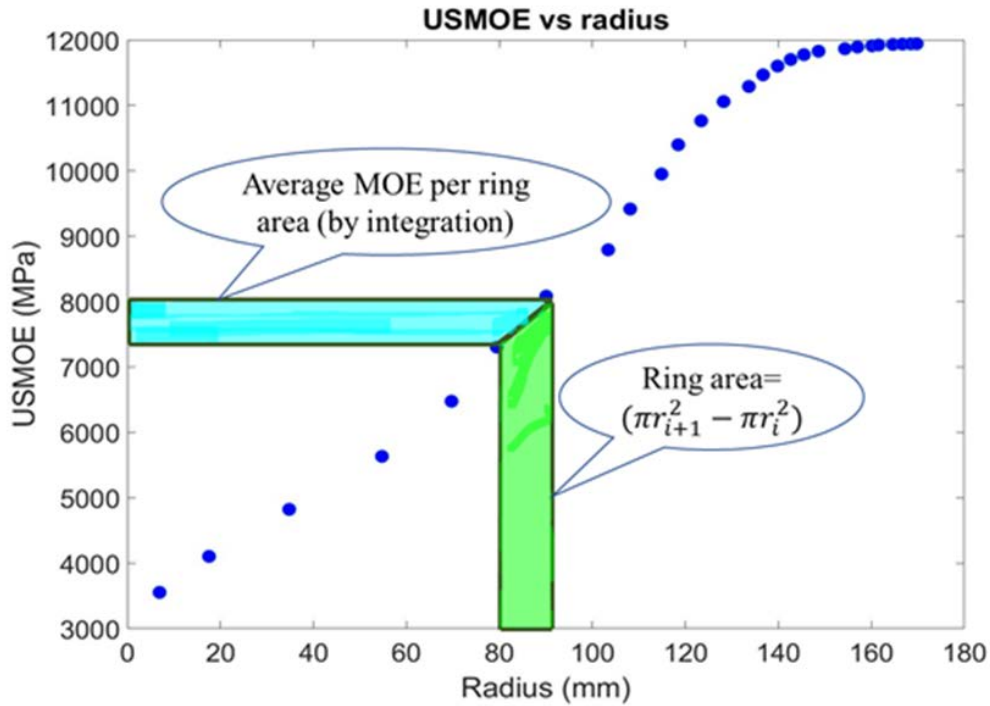
Figure 65. Extraction of average MOE corresponding to the surface of a growth ring for each tree.

For each tree a table can be extracted as shown in Figure 66.
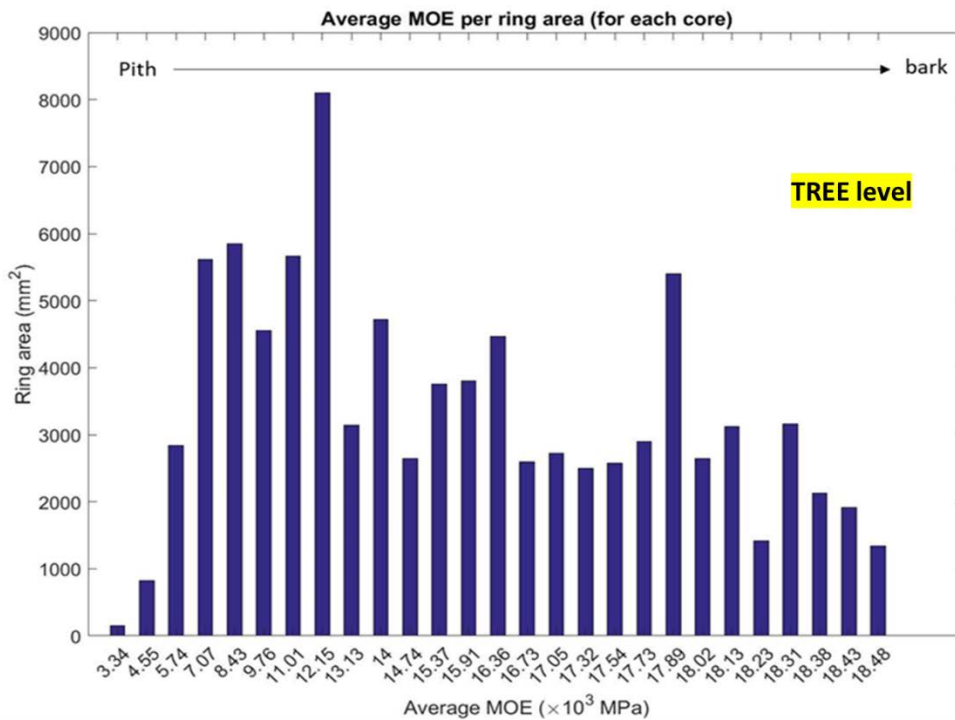
Figure 66. Surface and corresponding average MOE of each ring for a tree section.

Finally, the area or volume of wood having any specified range of MOE can be calculated for each tree and then for each stand. An example is given in Figure 67.
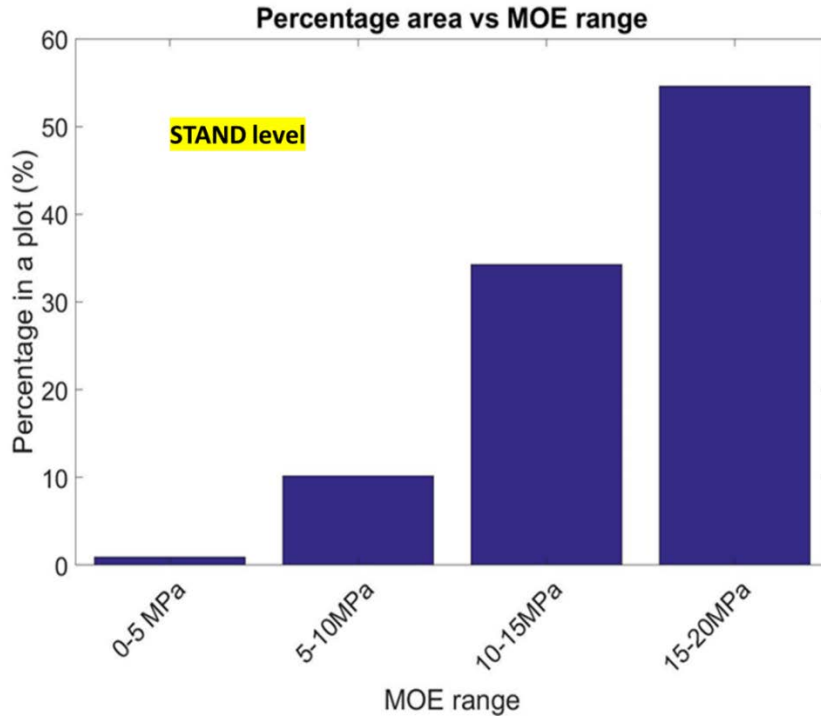
Figure 67. Histogram of MOE at the stand level from sampled trees and the rest of the stand growth curves.

From this method the percentage of area of wood in each plot having USMOE of 10,000 MPa or greater can be displayed (Figure 68). Since we do not have the growth curve for all trees, we predicted the plot/coupe from the 'fingerprint' curve combined with the growth curve from all sampled trees.
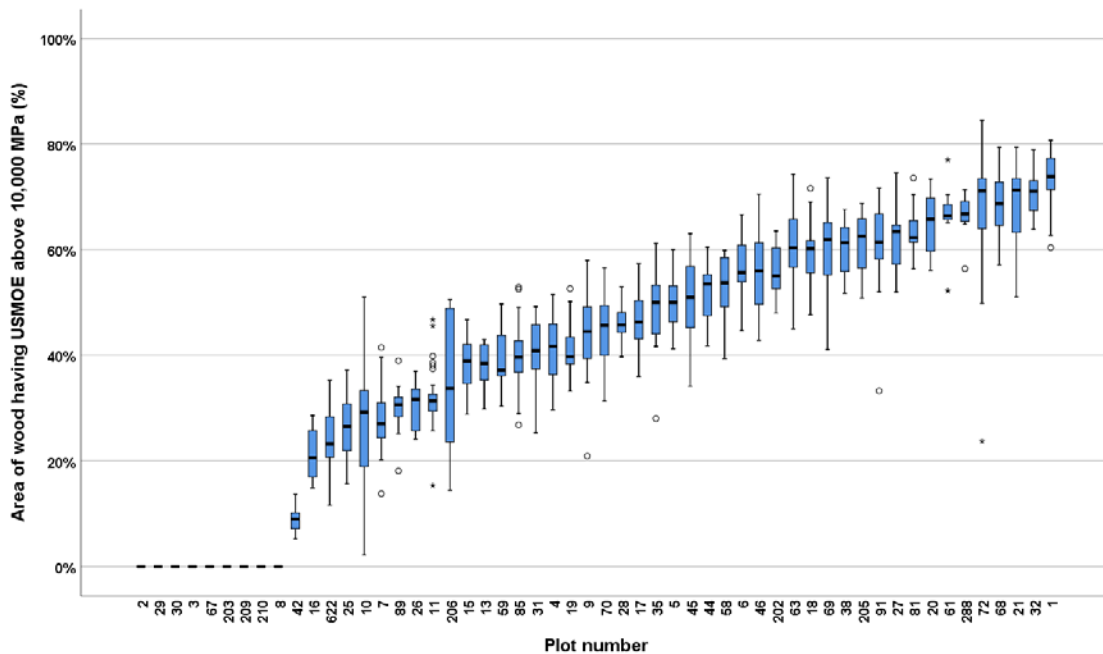
Figure 68. Percentage of wood area having MOE of 10,000(+) MPa (in the full log radius) across 54 plots (age range 16 – 35 years old).

In Figure 69 we compared the area of boards having a MOE of 10,000 MPa and above (designated MGP10+) obtained from 2D prediction with the actual static bending MOE. The percentage area of MGP10+ boards obtained from the destructive samples from three different plots shows good agreement between actual and predicted % area of MGP10+ boards. However, there are discrepancies in predicting the spacing trials. This is because the spacing trial contains three genotypes (i.e. clone 887 (C887), clone 625 (C625) and F_1 hybrid seedlings). The performance of these genotypes is different (dissimilar fingerprint curves), with C887 the best and C625 the worst, as we have shown in Figure 45. Mixing the sigmoids resulted in lower predicted values when fitted. If the genotypes are detached, meaning using a fingerprint curve associated with each clone, the prediction capability is improved. Figure 70 shows the percentage area of MGP10+ boards in spacing trials when the genotypes are separated.
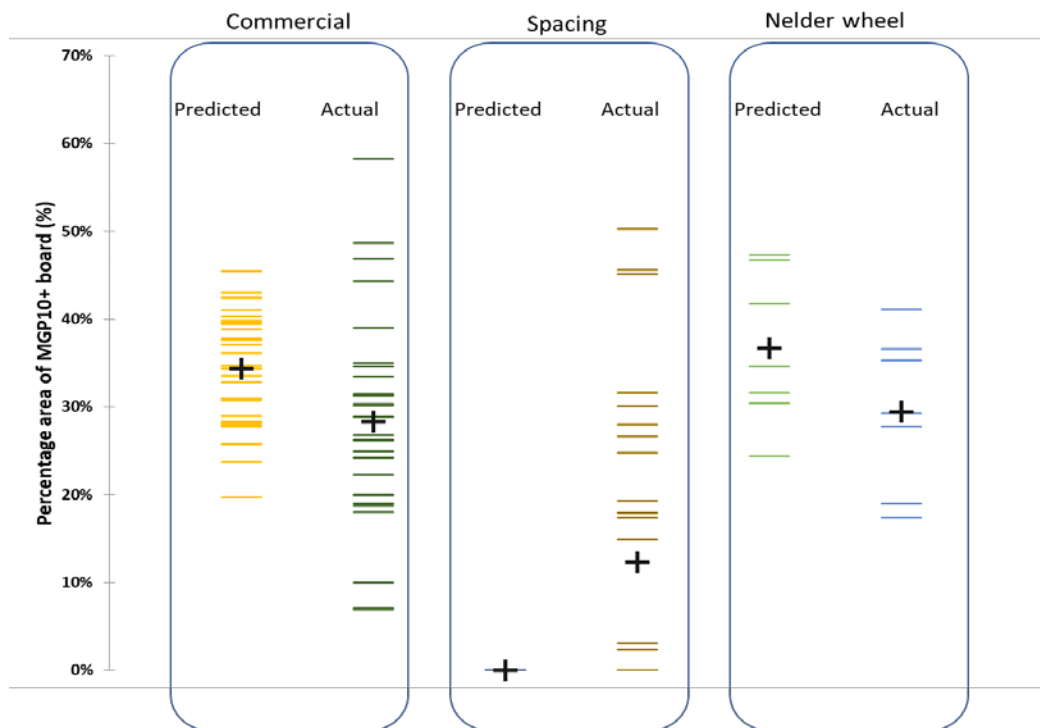
Figure 69. Percentage area of boards having a MOE of 10,000 MPa and above (within 84% of the radius) from destructive samples (30 trees from commercial trial, 30 trees from spacing trial and 8 trees from Nelder wheel trial; '+' indicates the mean). Each horizontal color line represents a tree.
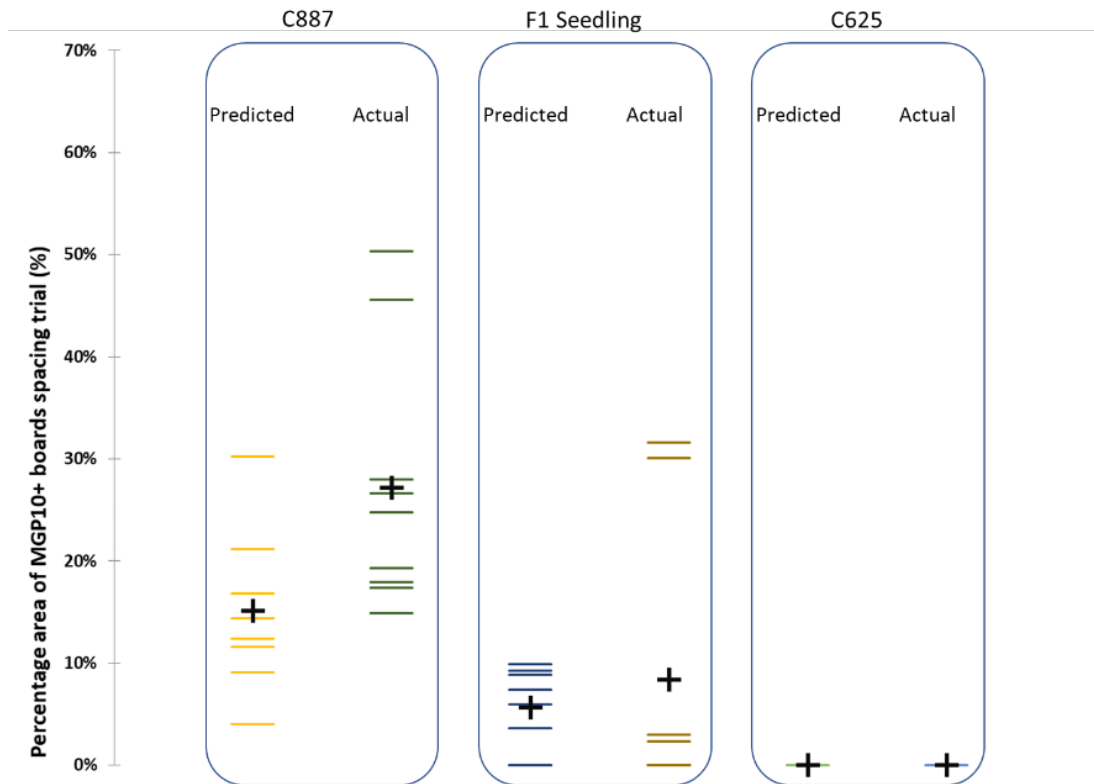
Figure 70. Percentage area of MGP10(+) boards (within 84% of the radius) for three genotypes from a spacing trial (10 trees from C887, 10 trees from F$_1$ seedling, and 10 trees from C625; '+' sign indicates the mean).

The accuracy and precision of the method needs to be assessed on a larger population of tree as only these 30 trees were available for this component of the study. Further investigation and validation is recommended.

As an example of potential application, this method was applied on the 54 southern pine plots sampled for USMOE. The result is displayed in Figure 71. It is worthwhile noting that only the sampled trees were included in this analysis. However, as discussed earlier, the reconstruction could be done for trees outside of the plots if the growth curves were available (e.g. from LiDAR and field measurements combined).

The simulation displayed in Figure 71 shows that 16 plots don't effectively provide any MGP10+ boards (plots 16 to 7 along the x-axis). Of these 16 plots with no operational MGP10+ board recovery the following applies:

- Five of these plots are in the age range of 16-21 year old. In this group plots 209 and 210 are predicted to never start producing any MGP10+ board (see Figure 35). The other three 16-21 year old plots (622, 89 and 26) began producing wood with MOE of 10,000 MPa or better between the ages of 10 to 15 years old so they should produce MGP10+ boards in the future.
- The other 11 plots are at or near harvest age (24 to 36 years old). This information can be useful to better allocate this resource in order to maximise value across the supply chain.

77

The top sixteen plots in Figure 71 (plots 205 to plot 1 on the right hand side of the x-axis) should produce around 30% to 40% of MGP10+ boards. The top plot (plot 1) is a 29 year old F_2 hybrid. In this group there are three 16-21 year old plots (205 [F_1], 27 [PCH], 61 [F_1]) that could potentially be harvested earlier while producing high value products. This could increase returns for both the growers (shorter rotations) and processors higher value (MGP10+) timber produced.

The ability to directly link USMOE (combined cambial age and growth parameters) to final product value is the real benefit of this technology.
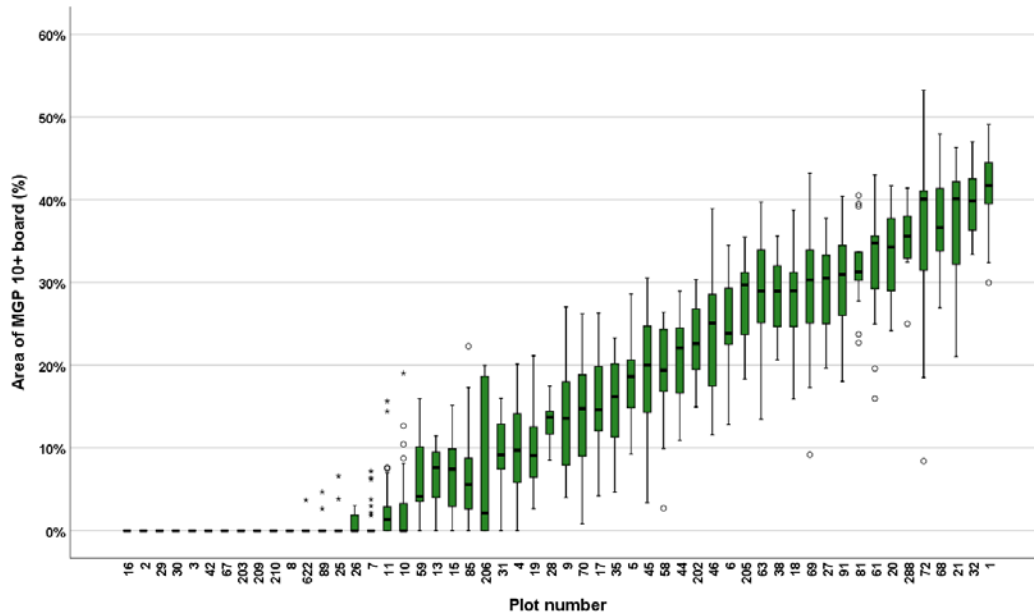
Figure 71. MGP10 area with 84% radius of log– (for plots) across 54 plots (age range 16 – 35 years old). Note this is ranked by increasing area of MGP10+ board recovery.

7.4.2   3D approach

In this section, we present a proof-of-concept for a 3D approach to predict board performance from a single breast-height core. We emphasise here that we have not conducted a comprehensive study on this approach, nor its robustness.

It is not feasible for multiple cores at different heights to be taken from standing trees to obtain the level of data collected from the destructive sampling. We propose an initial method that may provide an avenue from which timber properties of additional trees can be modelled based on the extensive data collection effort undertaken in the project. We will refer to the tree that we are attempting to predict the board performance from as the 'target' tree. We emphasise here that we have not performed this process using the cores taken from the standing trees, we are using cores from the destructively sampled trees as an initial demonstration.

To predict board performance, in addition to property information from a breast-height core we require information regarding the growth of the target and an intended sawing pattern for the tree. In this study, the target tree was one of the destructively sampled trees and the remaining destructively sampled trees were used to develop the prediction. From the sigmoid fitting outlined previously, we have mathematical descriptions of the MOE for each tree in

the destructive sampling, at discrete apical ages. We also know information about the tree rings within the target tree, allowing us to build a profile of the tree's structure. Note that we believe this information could be approximated through measured growth curves, and from tree rings measured on the breast-height core. This is the same process in 2D or 3D reconstruction approaches.

We assume that for our target tree we have only a single sigmoid that has been fitted to data obtained from a breast-height core. Using this sigmoid, we identify the trees from the destructive sampling that have fitted sigmoids that most closely match to the target tree. To calculate this, we take the definite integral of the squared difference between the target tree's sigmoid and the tree being compared as a match. This gives a measure of how similar the two curves are. We also assume that these are the trees that most closely resemble the target tree. We then take an average of the fitted sigmoid parameters for the remaining cores up the tree, to obtain new sigmoids for the target tree. **This then gives us an approximation for the variation of MOE for the target tree with apical age,** and we are able to utilise our existing algorithm to obtain the MOE distribution throughout the tree. Given that the target tree is one from the existing destructive sampling trials, we have information on the sawing pattern and measured board MOE, allowing us to perform a comparison of initial results.

Figure 72 shows results from the initial predictions using a single core and the models developed for the destructive samples. We see that in most cases the new prediction quite closely follows the original prediction, indicating that the closely-matched trees are a good representation of the target tree. However, we note for Tree 3 there is a significant difference between the new and original predictions, indicating that this target tree is not well represented by the closely-matched trees. The new predictions appear to significantly under-predict the MOE towards the outer diameter of the tree. The reason for this can be seen in Figure 73, where the sigmoids for the subsequent cores in the apical direction of the tree are significantly different than the original sigmoids for the target tree. Note that core one is quite accurately represented by the closely-matched trees.

Recall that to determine the trees that most closely match the target tree we are only using the cores near breast height. There may be additional information that needs to be taken into account in the 3D approach to predict board performance when identifying the closely-matched trees, such as location, species, physical dimensions, and silvicultural treatment. Nevertheless, we feel this approach shows promise in being able to predict board performance from breast height cores by utilising the information collected from the destructive sampling. Further analysis needs to be undertaken on this approach to justify its predictive capability, and this scope of work is recommended for further research.

a) Tree 3

b) Tree 4

c) Tree 10

d) Tree 11
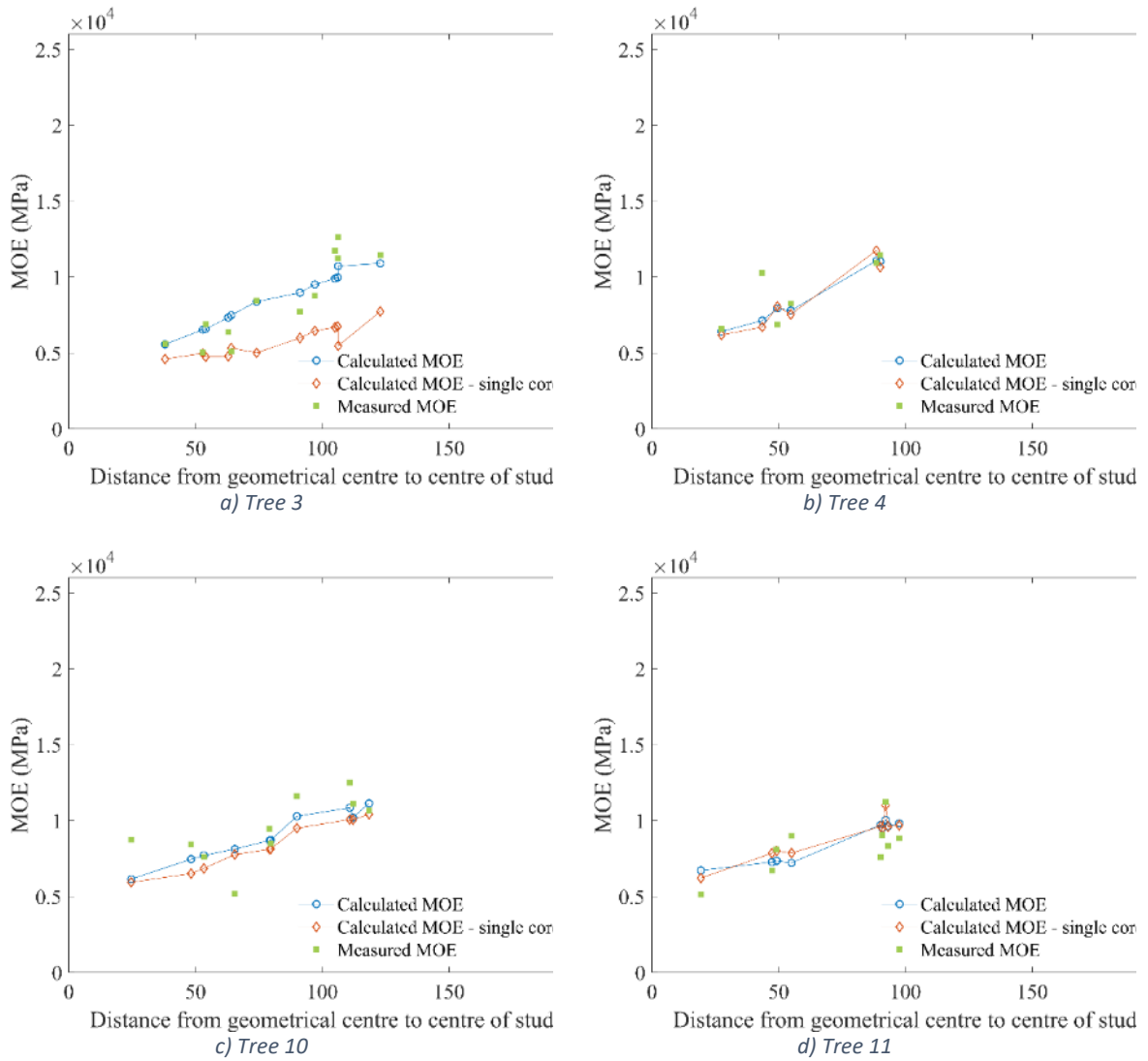
Figure 72. Example board predictions based on a single core, compared with original predictions using four cores and measured data.
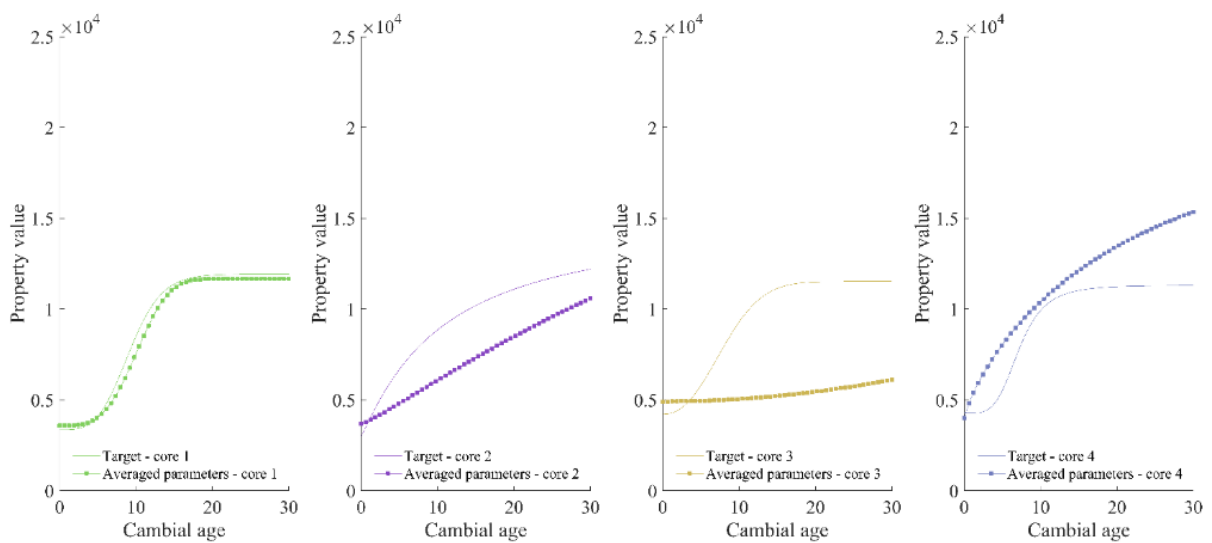
Figure 73 Tree 3 sigmoid comparison, showing the original fitted sigmoid (target) compared to the sigmoids obtained from averaging the sigmoid parameters from the closely-matched trees.

7.5 Factors involved in the performance variability

From a wood performance point of view, the value of the resource is essentially based on MOE. Density is not a criterion taken into account for product grading in any standard performance requirements by the southern pine processing industry and is therefore not discussed here.

7.5.1 Ultrasound MOE (USMOE)

At the taxon level, the USMOE cambial age integral average of the cores (i.e. the trees) ranged from a minimum of 5000 to 16,613 (MPa) with a mean of 10,442 MPa and median of 10,468 MPa, (Figure 74). The median USMOE of the PEE is slightly higher than the other taxon and there are more trees at this median range. However there is a large overlap in the values indicating all species have potential to produce wood with similar stiffness. It appears that the F_1 and F_2 hybrids may actually have more trees (indicated by the long tail above the median) in the higher MOE ranges than PEE. However PEE has more trees above 10,000 MPa.
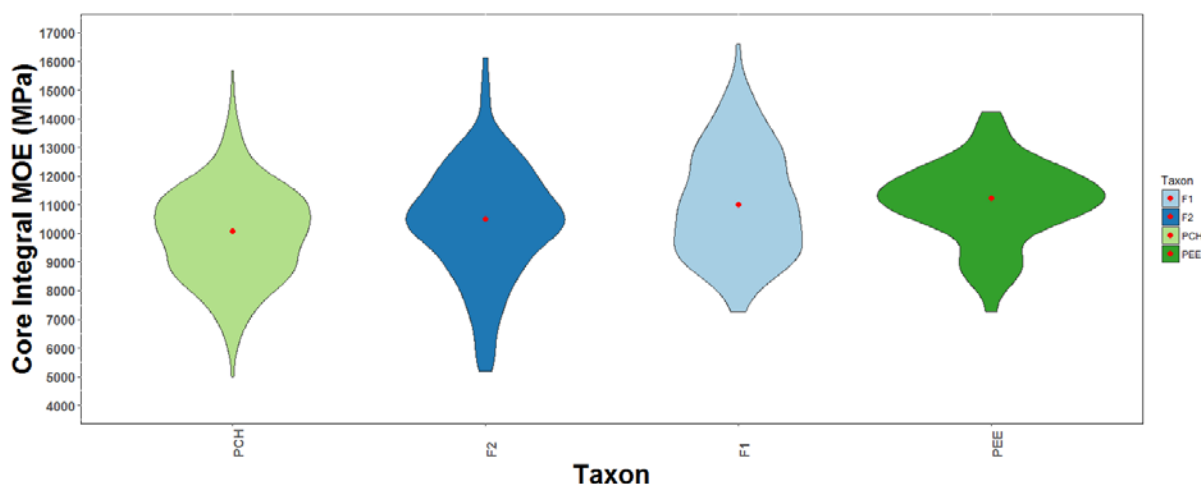
Figure 74. Violin plot showing the variation in USMOE from cambial age integral average of southern pine taxon sampled across multiple plots. The red dot is the median for that taxon. Width of the violin plot indicates the frequency of trees in a particular MOE class.

7.5.2 Investigating factors involved in the performance of USMOE

The wood quality data collected in the field and laboratory are known as variates (e.g. USMOE, ResiMOE). We also collected growth (e.g. height) and collated environmental and site information to investigate which of these factors could be associated with southern pine wood performance. Details of the growth, site and environmental factors investigated are provided in section 14.8 (Appendix 8). As a first look at this we have displayed the variation in USMOE (ordered by increasing mean plot integral USMOE) of three overarching factors (taxon, state forest and age range). As shown in Figure 75 none of these appeared to be strongly associated with USMOE when ordered by increasing plot mean USMOE. The exception to this may be the F_2 hybrids from Yabbra State Forest (plots 209 and 210) that have low MOE. As indicated earlier in the report, trees in these plots never produce wood with an MOE above 10,000 MPa. Of interest, these plots display the 'S' curve or sigmoid curves typical of biological systems (particularly for the lower and upper USMOE plots).
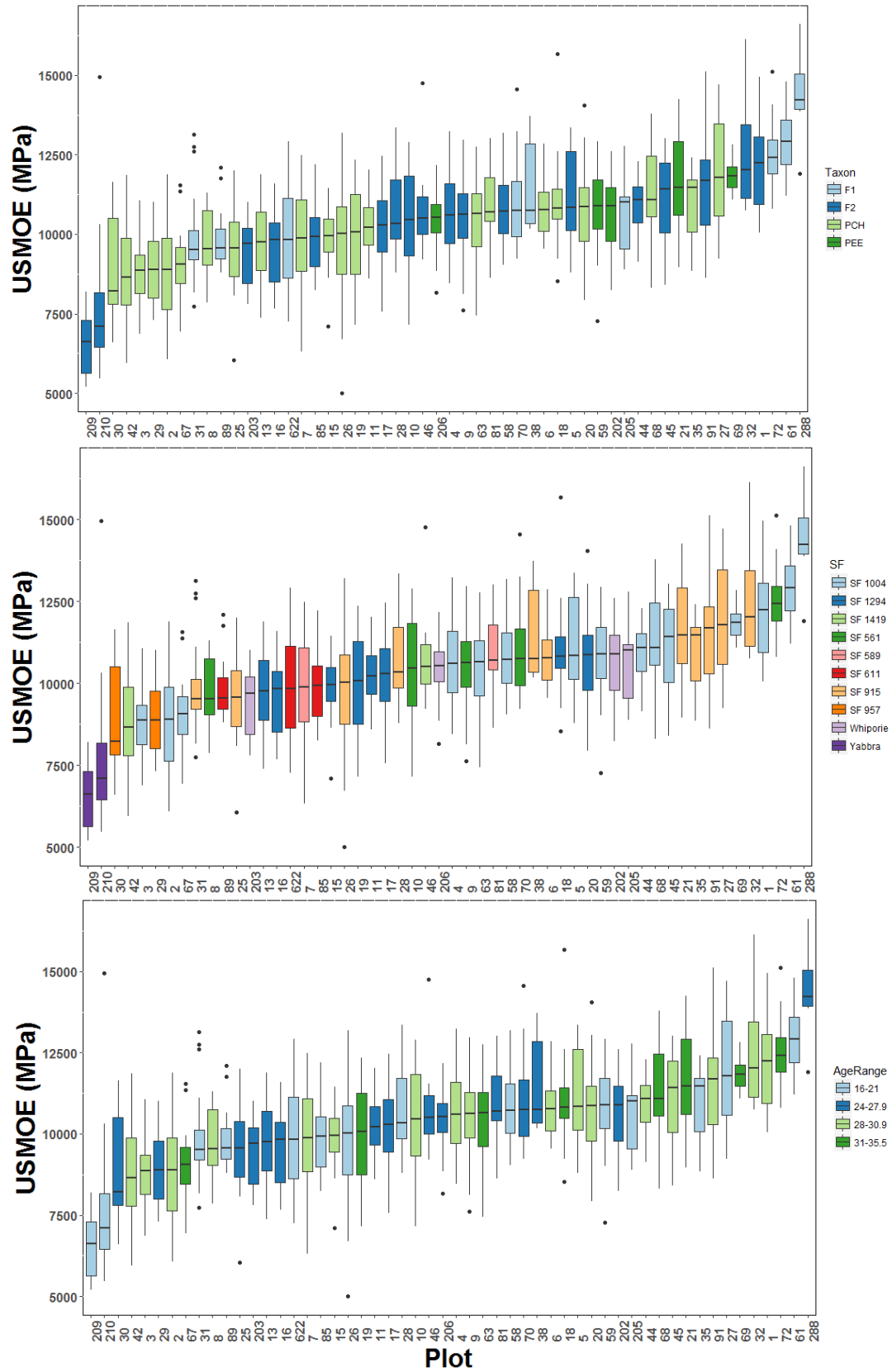
Figure 75. Variation in whole core USMOE cambial age integral mean sorted by median USMOE across 54 plots coloured by Taxon (top), State Forest (middle) and Age range (bottom).

7.5.3 Descriptive statistics

Following the above overview, we used descriptive statistics, to explore how the wood quality traits correlate to each other, growth and age factors and climate factors. Here we used linear correlations (Pearson's correlation coefficient). Positive correlations are displayed in blue and negative correlations in red. The colour intensity and the size of the circle are proportional to the correlation coefficients. If the correlations are not significant at the 0.05 level then no correlation is shown.

Correlation between the three technology platforms, site index, age and growth factors

Correlations between wood quality traits collected using the three technology platforms (wood quality platform - cores, ST300 and Resistograph) are presented (Figure 76). All of the Resistograph predictions: basic density (PRDens), log MOE (PRHM200) and MOE (ResiMOE) were moderately to strongly correlated[1] with each other. The correlation between PRHM200 and ResiMOE ($r = 0.95$) indicated that they are effectively the same trait. These correlations between the Resistograph predictions should be expected, since the parameters from the Resistograph trace were calibrated against PRHM200. The model used to predict PRHM200 and ResiMOE includes age in the calibration equation (Downes and Lausberg 2016). The moderate positive correlation between these traits and age therefore was expected. This may also partially explain why the Resistograph seems to under predict the MOE (ResiMOE) relative to USMOE of some plots in Figure 27 (e.g. plots 26, 35 and 622 which have median ResiMOEs well below the 10,000 MPa line). These three plots are all under 20 years old. The USMOE is moderately and significantly correlated with the three variables predicted by the Resistograph. USMOE is also moderately correlated with the MOE predicted by the ST300 (ST300MOE). USMOE is not correlated with any of the growth factors (site index (SI), Age, diameter at breast height (DBH) or height (Ht)). This means this measure of MOE is independent of these factors since the USMOE is a reconstructed performance characteristic from local measurement on the cambial age. This is one of the advantages of this technology. ST300MOE is not correlated with the Resistograph predicted variables.

Resin (ResinPercent) is moderately and significantly correlated with age and DBH of the trees. This may indicate older plots are more likely to have higher levels of resin.

---

[1] A correlation does not equal causality (also known as cause and effect relationship) (Esbensen *et al.*, 2004).
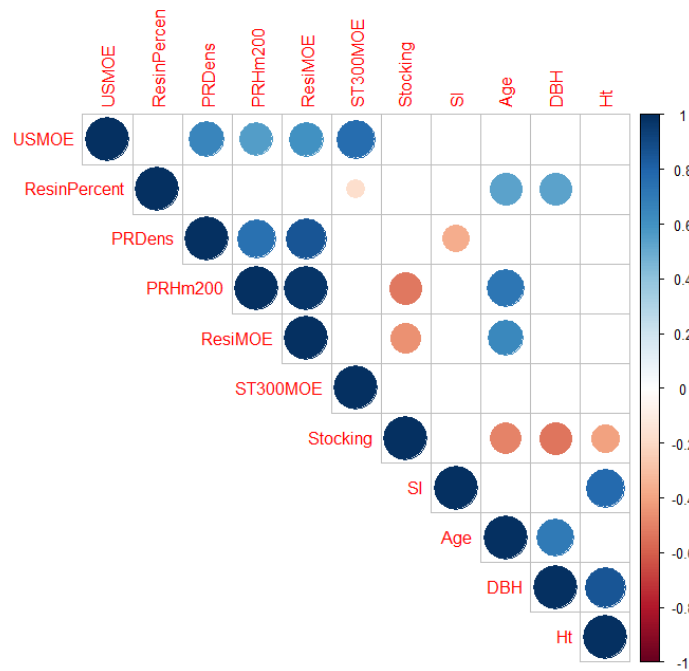
Figure 76. Correlation matrix for the wood quality variables measured or predicted in this study. Only correlations significant at the P = 0.05 level are dispalyed. Positive correlations are displayed in blue and negative correlations in red.

Many of the climatic variables are strongly and significantly correlated to each other (Figure 77). For example the following climatic factors are highly positively correlated (e.g. rainfall (Rain) and wetness index (Wetindex); mean daily maximum temperature (Tmax) and Evapotranspiration (Evapotrans) and some are highly negatively correlated (e.g. Average yearly number of raindays (RainDays) and average annual number of dry months with <= 30 mm of rain (DryMonths) and the relative humidity of the mean daily maximum temperature (RHmaxT) and Average annual number of dry months with <= 30mm of rain (DryMonths). USMOE is correlated with nine climate factors, being moderately positively correlated with mean daily minimum temperature (Tmin), mean relative humidity at the mean daily maximum temperature (RHmaxT) and extreme minimum temperature for the growing period (minT).

Resin (ResinPercent) correlated with six climate factors. For example, it is moderately positively correlated with the total number of months with less ≤ 30 mm of rain (NoDroughts) and moderately negatively correlated with Raindays.

The high level of collinearity shown in these collation matrices (in which one variable predicts another with a substantial degree of accuracy) limits the type of regression analysis that can be undertaken to investigate what factors are causing or effecting the wood properties of the southern pine.
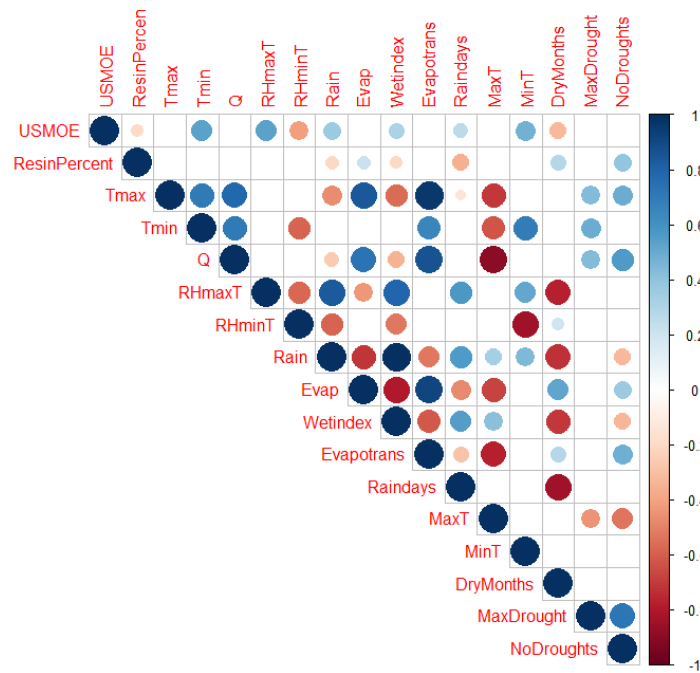
Figure 77. Correlation matrix showing USMOE and resin along with the climatic variables available. Only correlations significant at the P = 0.05 level are dispalyed. Positive correlations are displayed in blue and negative correlations in red.

7.5.4 Factor analysis of the commercial plots

In order to limit the impact of collinearity, Principal Component Analysis was applied to extract the important variables from the large number of numerical based (quantitative) variables available that could impact on USMOE.

7.5.4.1 Description of the quantitative variables

Number of observations (plots) = 50 (Note plots 209 and 210 were discarded as outliers) Number of quantitative variables = 20 (numerical variables). Quantitative variables represent a measurable quantity. Note, that growth related variables (e.g. height and diameter) were excluded from the analysis when investigating average USMOE at 17 years based on MOE Vs cambial age integral.

Description of the quantitative variables:
- Plot characteristics (Slope_prc, Soil_moist, Lidar_elev, SI, Stocking)
- Climatic variables for each plot location (Tmax, Tmin, Q, RHmaxT, RHminT, Rain, Evap, Wetindex, Evapotrans, Raindays, MaxT, MinT, DryMonths, MaxDrought, NoDroughts). Note these variables are explained in (section 14.8, Appendix 8).

7.5.4.2 Principal components analysis with Varimax rotation

The quantitative variables were linked together. Linear models cannot deal with collinear variables, and a variable selection needed to be undertaken. The problem with variable selection, is that it is impossible to have a global overview of the importance of all the variables in a single model. To deal with this, a principal components analysis with Varimax rotation was used. This technique allowed us to build a new set of variables by grouping the collinear variables into Principal Components (PC), where the PCs are unlinked from each other. Five independent components were extracted from the original set of 20 variables. Three components explain 70% of the total variance of the original variables as shown in the table below.

85

PC	Eigen value	Variance %	Cumulative %
1	7.1	35.6	35.6
2	4.1	20.7	56.4
3	2.5	12.7	69.1
4	1.5	7.4	76.5
5	1.3	6.7	83.2

7.5.4.3 Multivariate Linear model with the principal components

The dependent variable was the plot integral average MOE at 17 years using 5PL sigmoid on cambial age. When analysed by the five principal components, only PC1 and PC4 are significant (shown below).

Coefficients	Estimate	Std. Error	t value	Pr(>|t|)
(Intercept)	9276.15	139.48	66.507	< 2e-16
PC1	167.03	78.77	2.121	**0.040**
PC2	-86.63	68.56	-1.264	0.213
PC3	23.31	91.84	0.254	0.801
PC4	-319.66	102.41	-3.121	**0.003**
PC5	-44.6	117.59	-0.379	0.706

The characteristics of the final model with PC1 and PC4 are shown below (R^2=0.21). The interaction term in the model was not found to be significant. Note that PC4 (-278.32) has more influence on the MOE than PC1 (146.95) see below.

Coefficients	Estimate	Std. Error	t value	Pr(>|t|)
(Intercept)	9276.15	138.15	67.148	< 2e-16
PC1	146.95	67.58	2.174	0.035
PC4	-278.32	93.04	-2.991	0.004
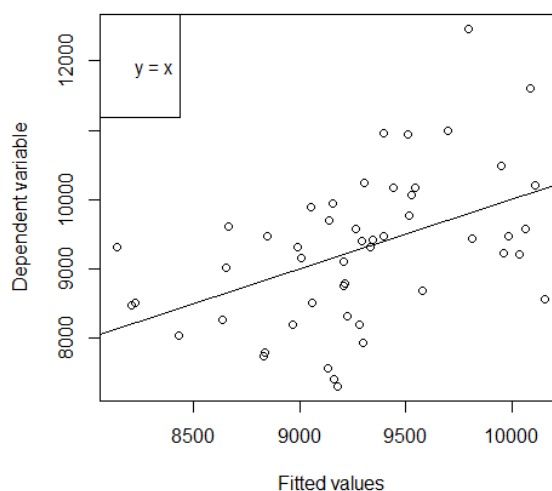
Figure 78 shows the importance of each original variable within the 1st and 4th principal components. For PC1 the collinear moisture related variables: RHmaxT (r=+0.9), Rain

(+0.8), Evap (-0.7), Wetindex (+0.8), Raindays (+0.8), and DryMonths (-0.9). The main component of PC4 is formed by: Stocking (r=-0.7), MaxDrought (+0.7) and NoDroughts (+0.9) with these later two variables being collinear.
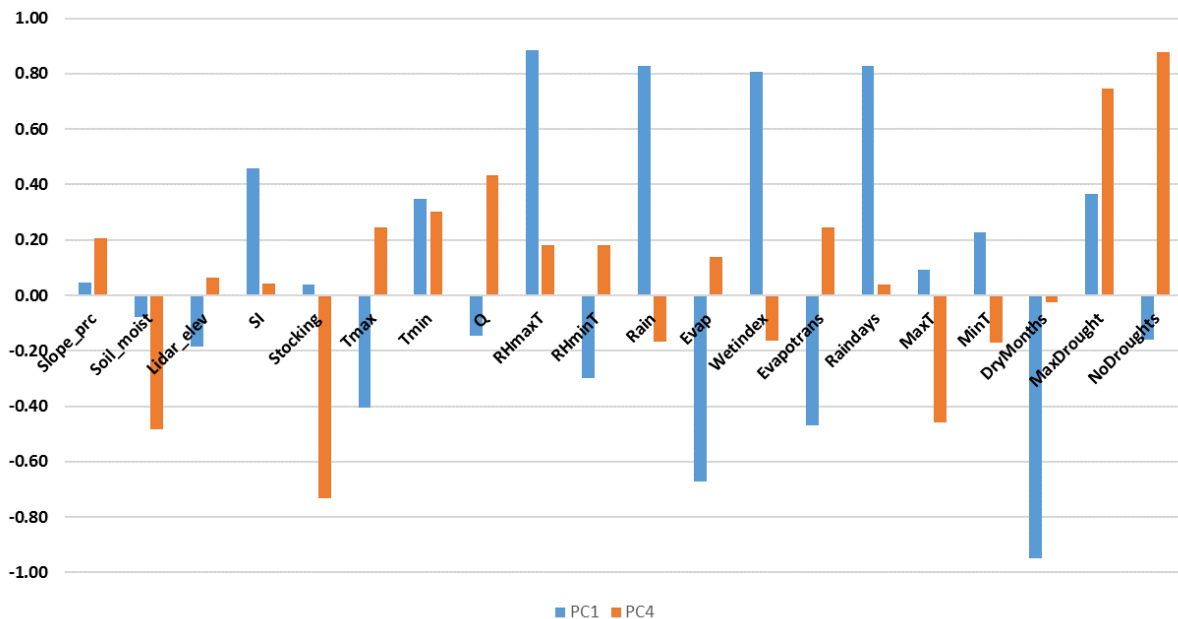
Figure 78. Bilateral correlations with the two significant Principal Components (PC)

7.5.4.4 Analysis of variance of the categorical factors

Number of factors = 6 (Taxon, Aspect, PriorUse, Pruned, PCT, Thinned)
Modalities (Categorical or qualitative variables within a factor that may explain USMOE performance).

- Taxon (modalities: F_1, F_2, PCH, PEE)
- Aspect (modalities:1=nil, 2=N, 3=E, 4=S, 5=W)
- PriorUse (modalities: 1R=prior softwood rotation, N=native forest, P=pasture, U=unknown)
- Pruned (modalities: yes/no)
- PCT (modalities: yes/no)
- Thinned (modalities: yes/no)

The analysis (factor by factor) shows that "Taxon", "PriorUse" and "PCT" have significant variations of means between the modalities.

Factor	F-statistic	residuals DF	p-value
Taxon	5.001	46	**0.004**
Aspect	2.013	45	0.109
PriorUse	3.161	46	**0.033**
Pruned	0.051	48	0.822
PCT	9.008	48	**0.004**
Thinned	1.275	48	0.265

A Tukey's HSD test was applied to identify the differences between means for the factors "Taxon" and "PriorUse". The figures below (Figure 79a) highlight these differences: Taxon

(F1-PCH) differ; PriorUse (1R-P) differ; PCT(Yes-No) differ. The associated groups, obtained by a Duncan test, are also included in Figure 79.

Taxon	diff	p adj
F2-PCH	741.2	0.106
PEE-PCH	840.5	0.309
F1-PCH	**1507.0**	**0.004**
PEE-F2	99.3	0.997
F1-F2	765.7	0.313
F1-PEE	666.4	0.645

PriorUse	diff	p adj
U-P	208.4	0.970
N-P	328.5	0.848
1R-P	**1156.9**	**0.041**
N-U	120.2	0.992
1R-U	948.5	0.142
1R-N	828.3	0.122
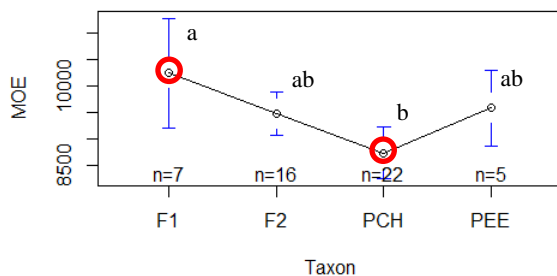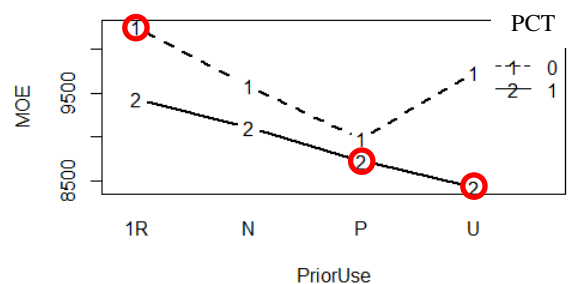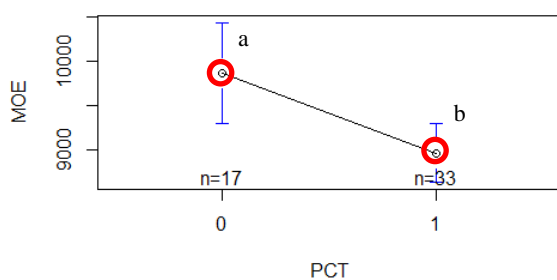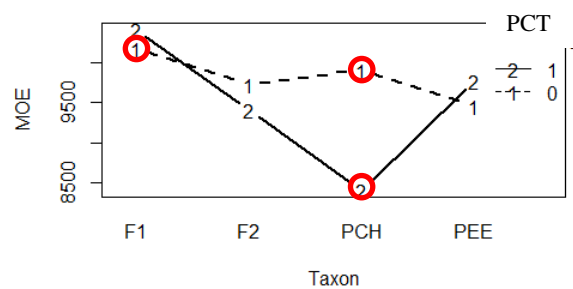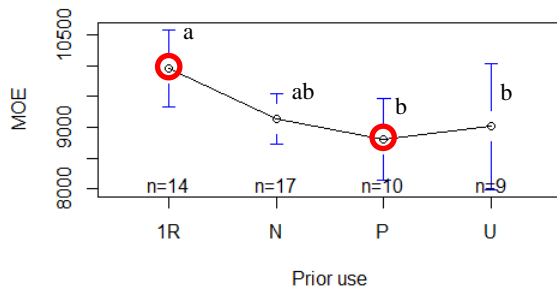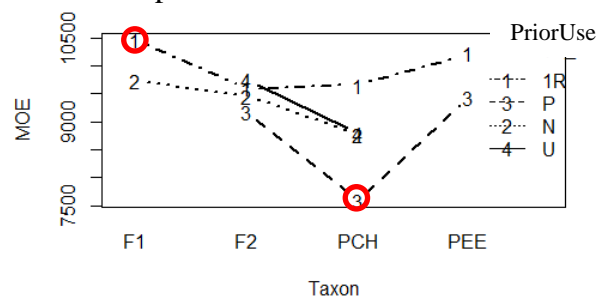
Figure 79. (a) Significant categorical factors. (b) Significant interaction of categorical factors. In these figures the red circles indicate significant differences between modalities.

Interactions
The Tukey's HSD test was also used to test the interactions between factors. The associated bivariate interactions plots are shown above (b).

- "Taxon" with "PriorUse", the only difference was for the pair F_1:1R - PCH:P.
- "Taxon" with "PCT", differences are found in the cases F_1:0 (no PCT) - PCH:1 (PCTed) and PCH:0 (no PCT) - PCH:1 (PCTed).

- "PriorUse" with "PCT", differences for 1R:0 (no PCT) - U:1 (PCTed) and 1R:0 (no PCT) - P:1 (PCTed).

If the complete interaction is tested in the same way, no combination of modalities were found to be significantly different (the lowest probability p=0.11 was for F1:1R:0-PCH:P:1). Investigating how the current whole of growing period climate factors and the monthly and yearly climate factors impact on the annual growth of trees in the plots is recommended.

7.5.5 Key Points from the factor analysis

The factorial analysis of genetic and environmental relationships with wood stiffness indicated that the moisture related variables have the biggest impact on MOE, with variates associated with making moisture available (e.g. Rain, Raindays and RHmaxT - Mean relative humidity at the mean daily maximum temperature) being positive and drought related factors (e.g. DryMonths - Average annual number of dry months with <= 30 mm of rain and NoDroughts - Total number of dry months) having the largest negative effect on MOE. Stocking rate had a positive effect, whereby high stocking rates were correlated with higher average MOE of stands. In the single factor analysis, the primary factor was taxon, where the F_1 hybrid was shown to rank higher on average for MOE, followed by the F_2 hybrid and slash pine, then Caribbean pine with the lowest MOE on average. The second ranked factor was prior land use, with first rotation sites producing higher MOE wood on average compared to former pasture sites. The third ranked factor in this analysis was the silvicultural practice of early, pre-commercial thinning where stands that had been thinned early in the rotation showing lower MOE on average.

7.6   Comparison between tools

The three technologies: the wood value platform, ST300 and IML Resistograph can all predict the MOE of the trees (logs) with varying degrees of accuracy. However it is how accurately they predict the range of MOE of boards within the trees /logs that is the real measure of value for each technology. The reason for this is the value of the products in the market are dictated by the products performance. Here we compare and contrast each of the technologies evaluated in terms of:

- accuracy and precision of predicting trees, plots, boards and related trees not sampled
- price multiplied by number trees sampled, etc.
- key data obtained from each of the tools and level of usefulness for the forest grower or processor.
- benefits of the technology for growers and wood processors.
- the minimum level of data/information needed to predict stiffness (and at what level – stand, plot, tree etc.) and link that into pros and cons of each tool.

Note, the wood value platform was developed as an experimental platform and is an output of this project. The level of data needed by future users may be considerably lower than the high intensity of measurement and data collection undertaken here. Neither ST300 nor Resitool are able to predict trees outside the sample trees. The assumption with these tools is that the sample trees represent the whole stand, in other words this sub-population has exactly the same performance as the whole population of trees of the stand. No information from the rest of the stand is combined to predict the trees outside the sample trees' data. In our approach, we use the cambial age information of the sample trees (fingerprint curve) combined with the growth information of the rest of the stand to be able to better predict (through reconstruction) the whole stand.

Indicative purchase prices of main pieces of equipment used in the study
- IML Resistograph: $18,000 - $20,000 (with expanded memory and precision drill bits).
- Hitman ST300: $17,000 - $18,500
- NIR spectrometer: there are a range of options depending on the accuracy needed: $6,000 - $100,000
- Ultrasound kit: $6,000 - $8,000
- Electronic scales: $500
- Hilti 36-volt drill: $2,500
- Coring drill bits: $300 - $400 each (includes cost of extension tubes and adapter for the Hilti).

In Table 5, travel times and work associated with plot access due to weeds, etc. are ignored as they would be similar for each technology. For brevity USMOE is used as a substitute for the wood value platform in this table.

Training industry in the use of the wood value platform
The team at DAF can demonstrate and train staff from the industry in the collection of cores and the capture of data from these cores. Currently the analysis of this data requires expert knowledge but developing a user friendly interface is possible if properly funded. Similarly simplifying the technology platform and increasing the speed of data collection can be customised to end-user specific requirement. The current project used the platform to focus

on accuracy, but this does not preclude a focus on increasing efficiency of the data collected and processed.

Table 5. Evaluation and comparison of each technology investigated

Comparison evaluated	USMOE (coring) (Platform)	ST300MOE (ST300)	ResiMOE (Resistograph)
Type of MOE measurement or prediction	Analytical reconstruction, not calibration based	Calibration based (depends on training samples)	Calibration based (depends on training samples)
Internal rate of return	Positive: high potential to increase the amount of MPG10 and above boards in the value chain	NA	NA
Field data collection	15 trees/plot	15 trees/plot	15 trees/plot
Sample rate	Slow	Moderate	Quick
Samples per hour	4	27	40
Pre-processing of samples to collect data	Slow, but the platform has not been optimised for time at the moment. Instead it was optimised for accuracy: core cambial age data collection, edged cores and number, data collection: 8% density, NIR for resin, ultrasound with care needed to maintain data alignment form different modules. Intricate analysis but can be simplified and automated in the future.	Quick: Download and analyse immediately.	Moderate: Download allocate growth rings and pith then analyse.
Estimated time to collect and prepare data/plot			
MOE only	• Currently approximately 8 hours • With additional automation and larger segments approximately 5 hours, but this could be reduced further using NIR calibrations based on the over 13,000 segments measured	Approximately 1 hour	Approximately 1 hour

Comparison evaluated	USMOE (coring) (Platform)	ST300MOE (ST300)	ResiMOE (Resistograph)
	and scanned in this study.		
Full analysis MOE, age referencing, density, extractives,	Approximately 11.5 hours	NA	NA
Ease of data analysis	Expert data analysis currently needed but this can be simplified and automated in the future.	Simple application of a single formula	Expert data analysis currently needed. This should become easier with the new interface being developed.
Accuracy and bias for tree or log MOE			
Logs	Accurate measure of MOE, 78% of variance explained with a low bias (9%).	Over predicts MOE, 42% of variance explained with a large bias (41%)	Moderate-high prediction of MOE, 68% of variance explained with a low bias (9%).
Plots	High (ranks plots) and moderate estimation of value of boards.	Moderate (ranking of plots) low estimation of value of boards.	Moderate (ranking of plots) low estimation of value of boards. Some plots appear to be poorly estimated. Possibly due to the wood properties falling outside the calibration set for the equipment.
Prediction of boards			
Average of boards' MOE vs the logs' MOE	High: explains 70% of the variance of boards' average MOE from that of the log	Moderate: explains 44% of the variance of boards' average MOE from that of the log	Moderate: explains 50% of the variance of boards' average MOE from that of the log
Individual board MOE vs log MOE	Low: explains 28% of the individual board MOE variance from the log MOE	Low: explains 22% of the individual board MOE variance from the log MOE	Low: explains 23% of the individual board MOE variance from the log MOE

Comparison evaluated	USMOE (coring) (Platform)	ST300MOE (ST300)	ResiMOE (Resistograph)
Individual boards vs individual boards	Moderate: explains 53% variance of the individual boards' variance. Given the reconstruction is based on clear wood samples and the inherent relative inaccuracy of the standard static MOE measurement this is quite good.	NA	NA
Related trees outside of the sampled trees from their growth characteristics	Reconstruction of all trees in a stand is possible using the cambial sigmoid (fingerprint) from sampled trees and growth curves of the trees not sampled.	Cannot predict trees outside the sample trees without local information along the radius (cambial age versus MOE) from the sample trees.	Cannot predict trees outside the sample trees without local information along the radius (cambial age versus MOE) from the sample trees.
Benefits for growers	Rank plots for measured MOE and this is directly related to value and processing parameters. Identify when plots/coupes will start producing high value wood allowing silvicultural interventions including: • Identifying plots that will never produce high value products so these can be felled and replanted with improved genetics that will produce high value products. • Identifying plots that start producing high value products at an early age that could be harvested at a younger age resulting in increased rotations from the same piece of land. • Allowing better log allocation to different processors e.g. High MOE	Rank plots for predicted MOE (of the outer wood) but does not link this to value. Will help identify very low or very high MOE plots.	Rank plots for predicted MOE but does not link this to value. Will help identify very low or very high MOE plots. As the calibration is based on radiata pine some of the plots appear to be poorly ranked e.g. plots 288 and 61 which are ranked high by USMOE and ST300MOE but low by ResiMOE.

Comparison evaluated	USMOE (coring) (Platform)	ST300MOE (ST300)	ResiMOE (Resistograph)
	logs to solid wood processors and low MOE logs to other processors that don't require the same stiffness. • Can be extended to other products without any alteration, calibration or modification e.g. veneer, resin, energy, fibre and woodchips. • Facilitates dendrochronology and composition analysis, impact of climate change and fertilisation studies • The wood samples are in a collection that can be revisited for verification, complementary or further analysis.		
Benefits for processors	Knowledge about the end value of logs they are receiving will allow them to better manage the feedstock to maximise value recovered. Adjustment of the processing parameters to maximise value (e.g. sawing patterns). Assistance to select plots or logs to be sawn for improving process efficiency. Decrease the risk of sawing logs from coupes that will not produce profitable products. The wood samples are in a collection that can be revisited for verification, complementary or further analysis.	Very poor or very high MOE plots can be identified but those in the middle cannot be ranked for value.	Very poor or very high MOE plots can be identified but those in the middle cannot be ranked for value. As the calibration is based on radiata pine some of the plots appear to be poorly ranked e.g. plots 288 and 61 which are ranked high by USMOE and ST300MOE but low by ResiMOE.

8 Virtual log reconstruction

In this section we discuss a method for reconstructing a virtual timber billet (see Figure 9) for peeling, including internal features such as knots, after it has been peeled into a full veneer ribbon. This reconstruction process was the first stage in developing a mathematical model for the variation in timber properties within a given tree. The reconstruction of internal timber features can be achieved through the use of computed tomography (CT) scanning. However, this requires the use of equipment that may be cost-prohibitive. Here we discuss an alternative approach that utilises more readily available and accessible equipment for timber processors, including a spindleless lathe and digital single-lens reflex (SLR) camera.

In comparison to conventional scanning methods, this reconstruction method based on a destructive process has the key advantage of delivering high-resolution colour images. This reconstruction serves two purposes. Firstly, we are able to generate three-dimensional visualisations of the timber billet, to uncover internal structures such as knots, defects, insect or fungi attack, discoloration and resin. Secondly, the reconstruction allows us to map timber properties measured for 10 cm strips of the veneer at 1 metre intervals to their original location within the billet. This allows us to locally populate the mapping with wood properties and subsequently derive their distribution throughout the billet. From this information, it is then possible to extract any part of the billet and obtain the appearance and extrapolated wood properties of processed products. To validate our reconstruction process, we show that we can obtain reasonable agreement between our predicted billet Modulus of Elasticity (MOE) and that measured on the original billet.

The internal features of a tree have direct impacts on the physical, mechanical and appearance properties of wood products. For example the knots (remnants of the branch architecture) detract from strength, creating a site of potential rupture under load (Hanhijärvi, *et al.*, 2005). Grain deviations developed during wood formation can result in sloping grain in a sawn board which can also have a negative impact on wood properties. The internal core of wood in a tree is commonly referred to as juvenile wood, as it forms in the early development of the crown. This zone of wood provides important support for the young tree, and for the tops of growing trees, for example allowing the tree to bend under wind pressure without breakage. Although important for the survival of the tree, this juvenile zone of wood typically has low stiffness and low wood density, making it unsuitable for structural wood products (Zobel and Sprague, 1998). The outer cylinder of wood formed during the mature stage of a tree's life is typically higher in density and stiffness properties. Again, these are evolutionary traits developed to ensure survival of the tree, providing the structure to support the weight of the tree's branches and foliage and withstand lateral wind pressure.

The physical, mechanical and visual properties of timber products are of critical importance to the forest and timber industry. These properties are directly linked to the value of the timber. However, accurately determining these properties prior to cutting the tree is difficult. The first stage in developing a mathematical model for the properties within the tree is to develop a virtual reconstruction of any given tree. Typically, this is done by either computed tomography (CT) scanning (Berglund *et al.*, 2013; Fredriksson, 2015; Fredriksson *et al.*, 2015; Schmoldt *et al.*, 1996), or the so-called flitch method, where logs are sawn into sections (Knapic *et al.*, 2011; Lin *et al.*, 2011; Pinto *et al.*, 2003; Pinto *et al.*, 2005) (flitches) and each section is scanned to build up a three-dimensional image of the log. However, these approaches may be deemed too expensive, cumbersome or inaccurate, and it therefore becomes difficult to create a virtual representation of a log. Here we investigate a method of

building a virtual reconstruction of timber billets based on their peeled ribbon, as the first step towards a mathematical model of property variation within the southern pines.

For this section, we focus on the 30 trees from a 29-year-old, F_2 hybrid pine plantation near Maryborough in south-east Queensland. These 30 trees were cross-cut into two peeler billets (approximately 1.2 m each), one sawlog (approximately 4.0 m) and discs from four different heights in the tree (Figure 9). Prior to sawing, a reference cut was made along the length of the tree. The peeler billets were drilled on the reference cut through the diameter at the butt end to facilitate alignment of images for stitching and for reconstruction. The billets were peeled on an Omeco spindleless veneer lathe at a thickness of approximately 2.5 mm to 3.0 mm. An initial rounding-up peel was conducted to remove significant variation from the surface of the billet and to obtain a near-cylindrical billet, however we were careful not to remove too much timber from the outside of the billet. This is because the highest quality timber (i.e. the highest stiffness) is generally found in the outer layers (Lachenbruch *et al.*, 2011). The rounded-up billet was then peeled until a core of approximately 50 mm diameter remained. Following peeling of the billet, the ribbon was placed over a light table to provide illumination through the veneer, allowing features to be easily detected.

Figure 80 shows the set-up for the photography of the ribbon. The light table was positioned at the end of a conveyor belt to allow for easy handling of the full ribbon. A Perspex sheet was placed on top of the light table to diffuse the light evenly across the sections of ribbon. An adjustable rig was constructed to position the camera, and this was attached to the steel frame of the workshop housing the equipment. This ensured consistent positioning of the camera across all images. High resolution images of the ribbon were captured using a Canon EOS 600D, ensuring approximately 25% overlap with each subsequent frame.
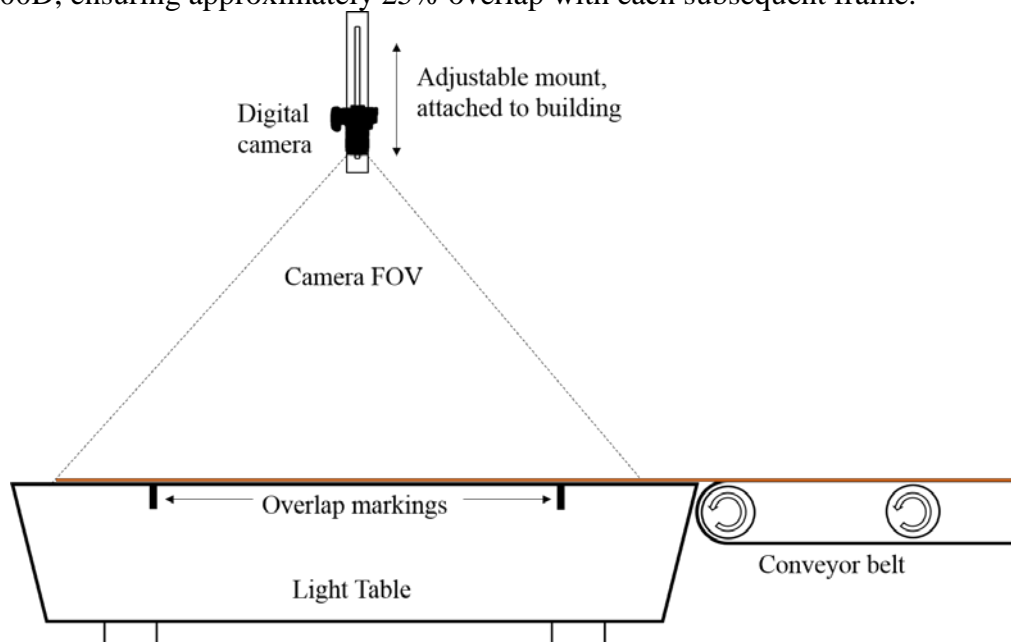
Figure 80. Diagram showing the camera setup and light table.

An example image of one section of the ribbon is shown in Figure 81.
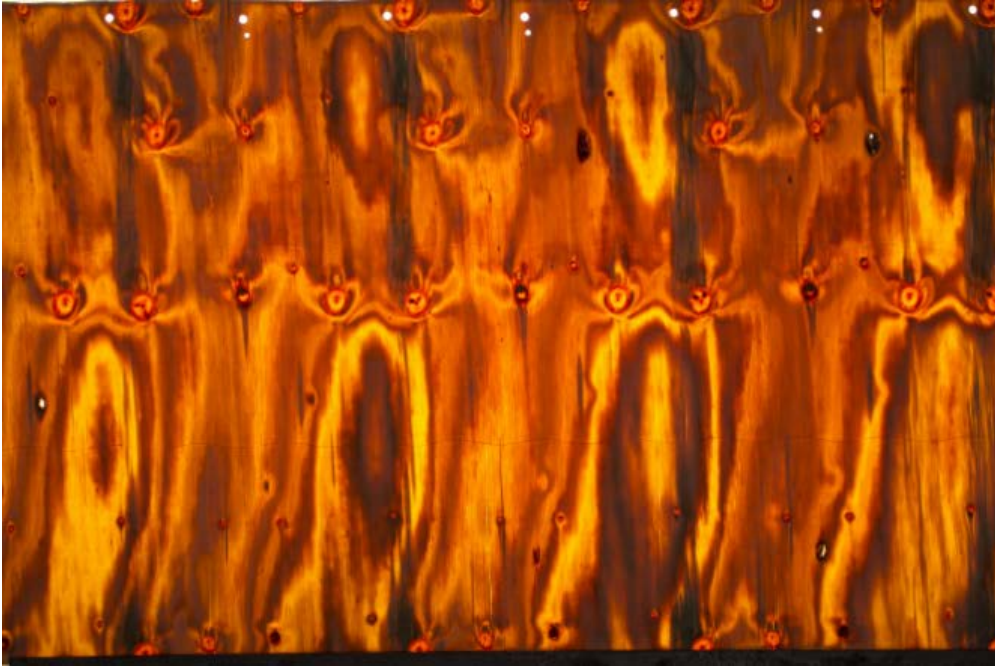
Figure 81. Example of a digital veneer ribbon image captured over the light table.
Notes: Dark tones show latewood, bright regions show earlywood; white holes along top are drill holes to locate the tree's relationship to the row direction in the stand; dark circles are knots.

Following photographing, strips of the ribbon (100 mm width) were clipped at one metre intervals, with every fifth strip being centred over the nearest reference hole. These strips were further processed to obtain measurements for density and modulus of elasticity (MOE), MOE measurements were obtained using the vibrational technique known as Bing (Beam Identification by Non-destructive Grading; Faydi *et al*., 2017; Paradis *et al*., 2017).

Before stitching the images to form a full ribbon image, the captured images were corrected for lens distortion using RawTherapee (Horváth, 2016) by way of the appropriate lens profile. We utilised Microsoft Research's Image Composite Editor (ICE) (Gutierrez *et al*., 2015) for stitching of the images due to the high resolution of each individual image. Our stitched ribbon images can exceed 700 megapixels, and ICE is designed to handle gigapixel panoramic images and can easily generate our stitched images at full resolution.

Figure 82 shows an example of a full stitched ribbon, where the radial position of the billet increases from left to right (i.e. the left-hand edge of the image is located in the centre of the log). Note that the stitched image itself is not rectangular, it instead appears that the peeled ribbon is curved in nature.

Figure 82. Complete stitched image of full billet ribbon. The white scale bar represents one metre.

Figure 83 shows a representation of how a truncated cone will trace a circular path if peeled. This indicates that the billet may be considered as a truncated cone, where the butt end radius is greater than the top end.

97
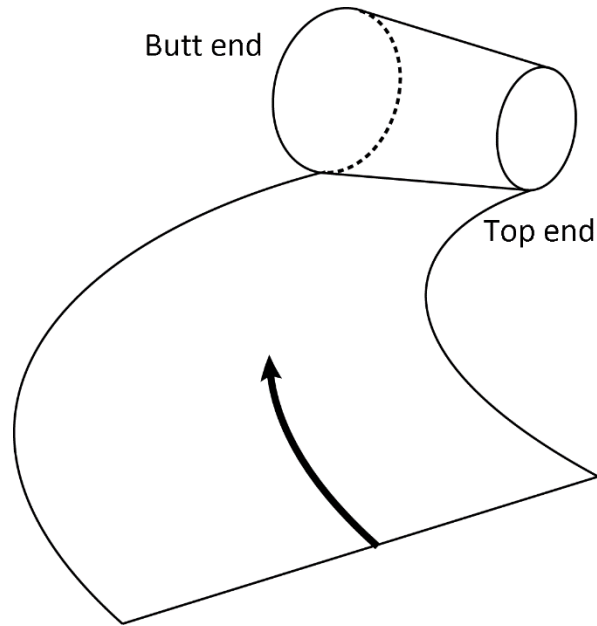
Figure 83. Representation of the path traced out by a truncated cone. We assume that the stitched peel is formed by peeling a truncated cone (the billet), where the butt end radius is greater than the top end.

Possible explanations for this are that the billet was not a perfect cylinder following the initial round-up peel, or due to the initial configuration of the lathe. If the pressure bar that holds the billet against the blade is not perfectly parallel to the blade then this would lead to a non-cylindrical billet. Here we assume that regardless of the cause, the billet can be represented as a truncated cone. In a latter part of this section we will discuss how we utilise the shape of the billet for our reconstruction process.

8.1   Image analysis

We now outline the image processing techniques that have been utilised to analyse the stitched ribbon images and to assist us in the billet reconstruction. Image processing in this project has been done using the distribution of ImageJ, Fiji (Schindelin *et al.*, 2012), which is an open-source platform for analysis of biological images.

8.1.1   Hole detection

Recall that prior to peeling the billet into a ribbon, a reference hole was drilled through the diameter of the billet. This was carried out to provide a reference for the reconstruction. To use this reference hole, we must locate the resulting holes in the peeled ribbon. To do this, we developed a custom macro in Fiji that identifies the hole locations in the stitched ribbon image. This process relies on the fact that the holes in the ribbon are brightly illuminated due to the light table, and are (near) circular in nature. Note that due to damage close to the edges of some sections of ribbon (tearing etc.), manual image manipulation was required to ensure the holes were closed.

The first stage in detecting the hole locations was to set the correct scale for the image. We took reference images with a steel ruler placed on the light table, and from this we were able to calculate the conversion from image pixels to mm. The stitched image was then converted to an 8-bit grayscale image prior to thresholding the pixel intensities, η. The range for thresholding was set to $220 \leq \eta \leq 255$, and the pixels with intensities within the range were set to be coloured in red. An example of this thresholding process is shown in Figure 84. We can

see that the desired hole locations are detected, however in some cases we also pick up other regions that we do not wish to consider. Note the larger dark circles below the highlighted holes near the top edge, which are due to a core that was taken from the standing tree in the field. This core was plugged in the field, however during peeling the plug can become dislodged, causing additional holes to become visible and therefore selected during thresholding.
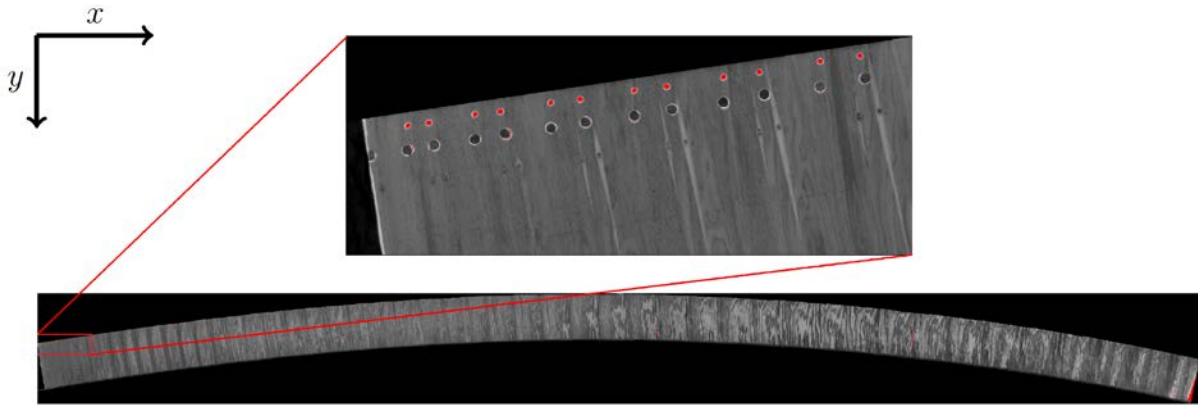
Figure 84. Thresholded image used for hole location identification. The small holes are the reference holes.

Applying the thresholding to the image allowed for Fiji's automatic particle analysis to detect the holes. To remove the regions not of interest that were identified during thresholding, we specify the size and degree of circularity of the regions we wish to detect. Circularity is defined as $(4\pi \times \text{area}) / \text{perimeter}^2$, with circularity equal to unity for a perfect circle (Ferreira and Rasband, 2012). Setting circularity to be greater than or equal to 0.7 and the size of the regions to be between 70 and 220 mm^2 allowed us to successfully detect the locations of the reference holes, as shown in Figure 85. We obtained the x and y coordinates of the centroids of these regions to use for our reconstruction.
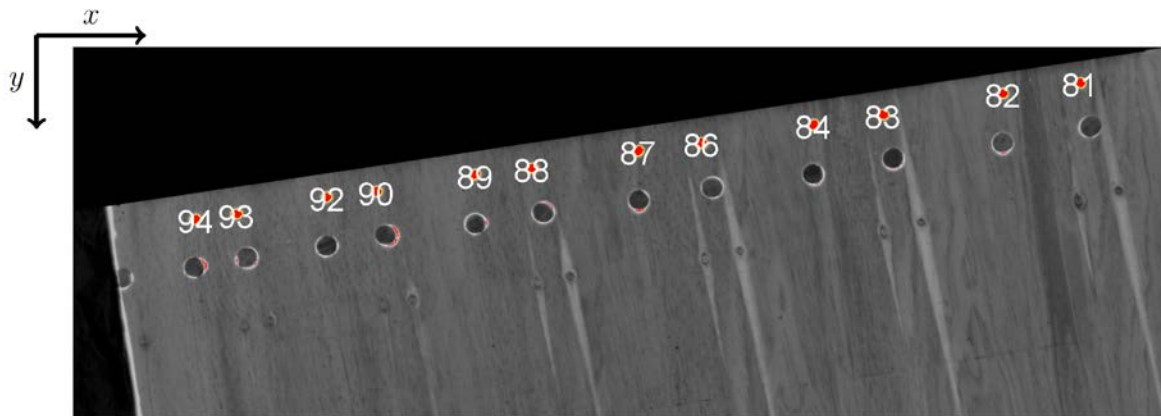
Figure 85. Identification of holes through analysing particles in the image. The particle size range was set to only capture the holes of interest. The numbers indicate the number of each individual hole that was detected. Note that adjacent holes are not always numbered consecutively.

8.1.2 Boundary detection

To detect the boundary of the peel from the full stitched image, we again use image processing techniques through Fiji to obtain the coordinates of each pixel on the boundary of the peel. However, it is not sufficient to only have the boundary coordinates. We must also

determine which of the four boundaries of the ribbon each point lies on. To automate this process, we utilise a spectral clustering approach based on the gradient between adjacent points. We use a two-pass approach, where the first pass clusters the points based on whether they lie on a curved or straight boundary, and the second pass separates each of these clusters into the two sub-clusters. This allows us to cluster the points into four distinct sets, each corresponding to one of the four boundaries of the ribbon (top, bottom, left, right), as shown in Figure 86.
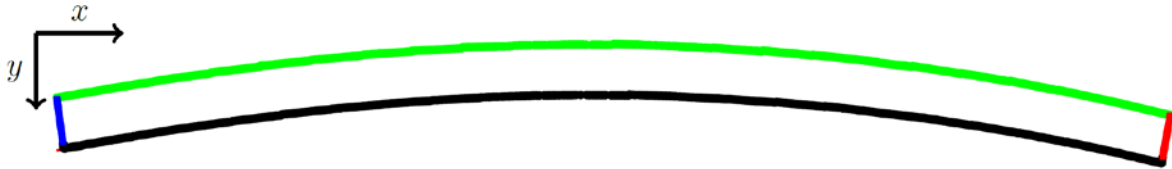
Figure 86. Each of the four individual boundaries identified by clustering. Note that the aspect ratio is not 1:1.

8.2   Reconstruction

The work developed in the preceding sections now allows us to consider reconstructing the peeled ribbon. Here we describe the process of transforming the full stitched image of the peel into a three-dimensional visualisation of the billet. The main steps involved in this process are:

- fitting functions through the hole locations and boundaries of the peel
- determining the intersections of the fitted boundary functions to define a series of circular arcs through the peel
- transformation of the circular arcs from the peel into a spiral cross-section of the billet.

Figure 87 shows a flowchart of the process required to transform the stitched ribbon images into a series of cross sections representing the full billet.
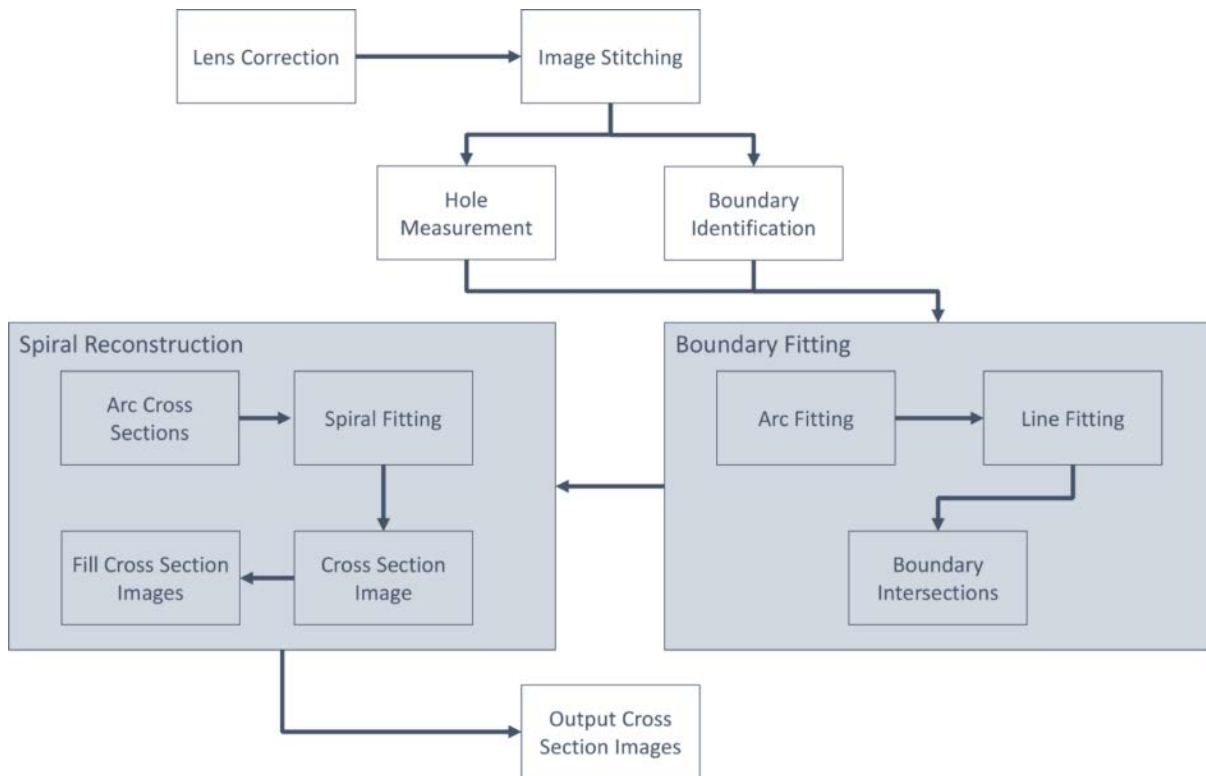
Figure 87. Flowchart describing the process of moving from the stitched images of the ribbon to a series of cross-sectional images representing the three-dimensional billet.

8.2.1 Boundary function fitting

We consider the process of peeling the billet similar to that of rolling out a truncated cone, where the radii of the cone continue to decrease at an equal rate. This does not affect the shape of the path scribed by the cone, merely the rate at which it is laid out.

Using the assumption that the billet can be represented as a truncated cone, the top and butt ends of the peel must lie on arcs of two concentric circles, while the left and right-hand ends lie on rays that intersect at the centre of these circles. We further assume that all pixels in the full stitched image can be represented by a sequence of concentric circular arcs of decreasing radii (from the butt end to the top). This idea is shown in Figure 88.
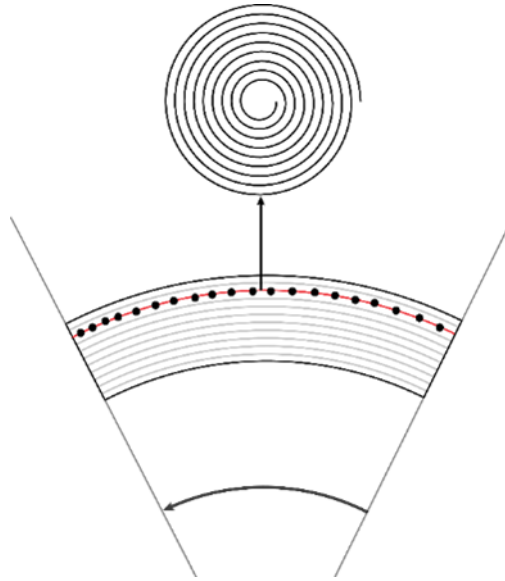
Figure 88. Circular arcs passing through the peel are transformed into a spiral cross-section. The dots denote the reference holes, and the red line shows the circular arc fitted to the reference holes.

8.2.2   Boundary intersections

Given the equations for each of the four boundaries, we can then find the intersection points of the rays with the circular arcs. This allows us to calculate the limits on the polar angle needed to describe the peel, and the length of each circular arc through the peel. This enables us to describe every location on the peel in terms of a radius, r_{arc}, and angle, θ_{arc}. To reconstruct the peel into a three-dimensional representation of the billet, we must transform each circular arc into a cross-sectional slice of the billet. To do this, we assume that we can represent each slice as a spiral, emulating the cutting of the knife during the peeling process.

8.2.3   Spiral transformation

To map the coordinates on the peel to a location in the billet, we assume a form for the spiral function that allows for the possibility of a varying thickness (distance between arcs of the spiral for a given angle, θ_s). For the spiral corresponding to the circular arc passing through the holes, we utilise two constraints to formulate a system of nonlinear equations. The first constraint is that the arc length (distance) between each hole for the computed spiral must match the measured distance on the peel. The second constraint is that the holes must lie along a straight line when mapped onto the spiral. This is because we assume that when the reference hole through the billet was drilled, there was no deflection in the drill bit. Note that this line does not necessarily pass through the centre of the assumed circular billet cross-section.

Given the spiral function corresponding to the arc that passes through the holes, we can then calculate the appropriate spiral parameters for every arc passing through the peel. We assume that the radius of the billet decreases linearly as we move from the butt end to the top. Therefore, we can linearly decrease (or increase in the case where we move towards the butt end) the radius of the spiral function as we move along the billet. We assume that the range of θ_s remains constant for every spiral function. This ensures that the start and end points of each spiral will be aligned vertically.

Examples of the spiral fitted through the reference holes for billets of varying radius are shown in Figure 89. The dot markers represent the locations of the holes when mapped

according to the spiral function. We can see that they do not lie perfectly along the line. We believe this may be due to the thickness variation in the ribbon, and the non-circular nature of the billet cross-section.
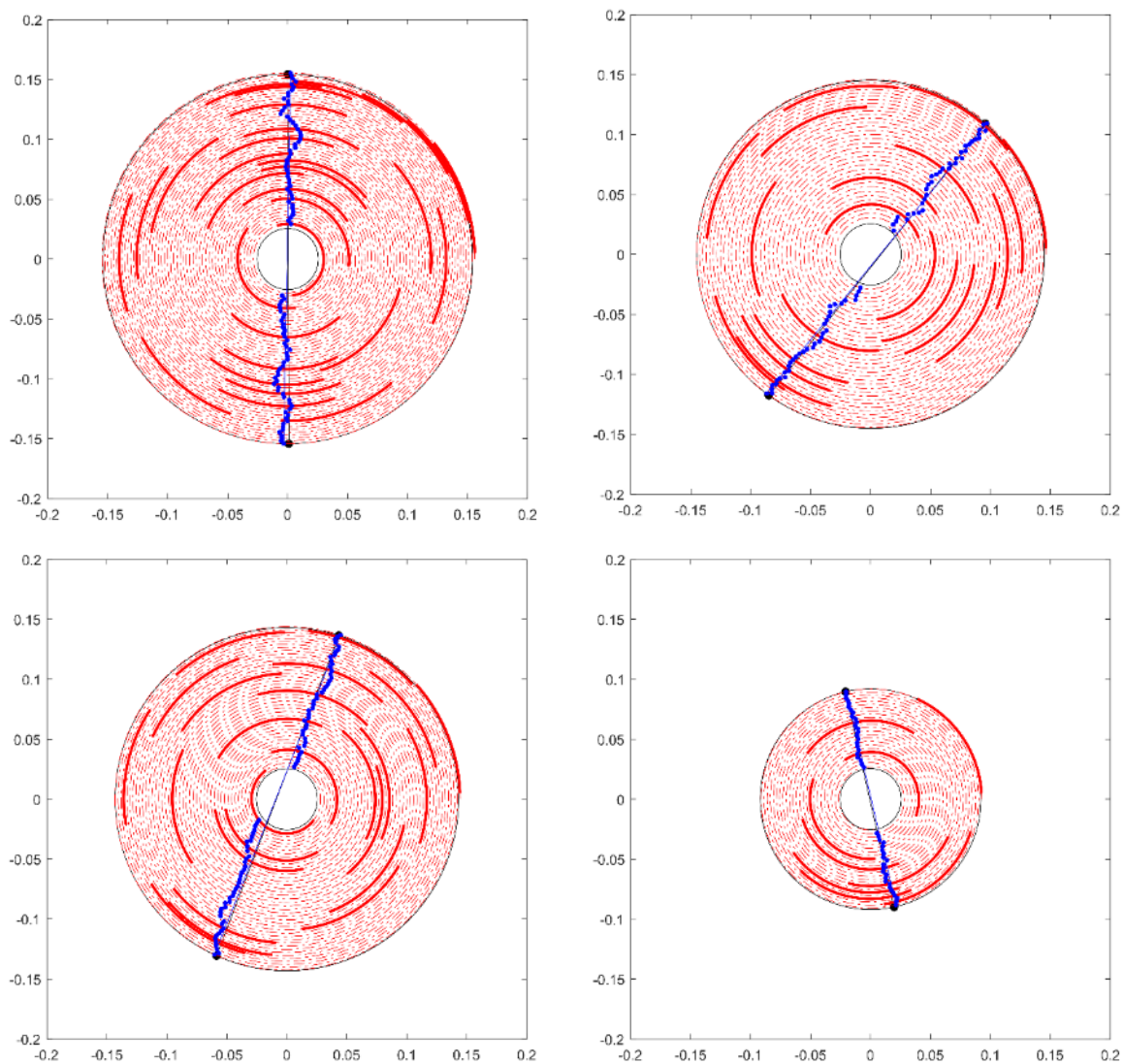
Figure 89. Examples of fitted spiral functions (- - -) with hole locations (·) and strips (——) mapped to original position in the billet. The initial estimate for the drill hole line is shown by the straight, diametrical line together with the location following fitting.

Figure 90 shows a comparison of the variation in the ribbon thickness for the example billets given in Figure 89, between our fitted spiral function and thickness measured from the veneer strips. We can see that near the outside of the billet (at the beginning of the ribbon), our spiral function underestimates the veneer thickness. However, we see that after approximately half-way along the ribbon reasonable agreement is obtained between our estimated thickness and the measured thickness.

103
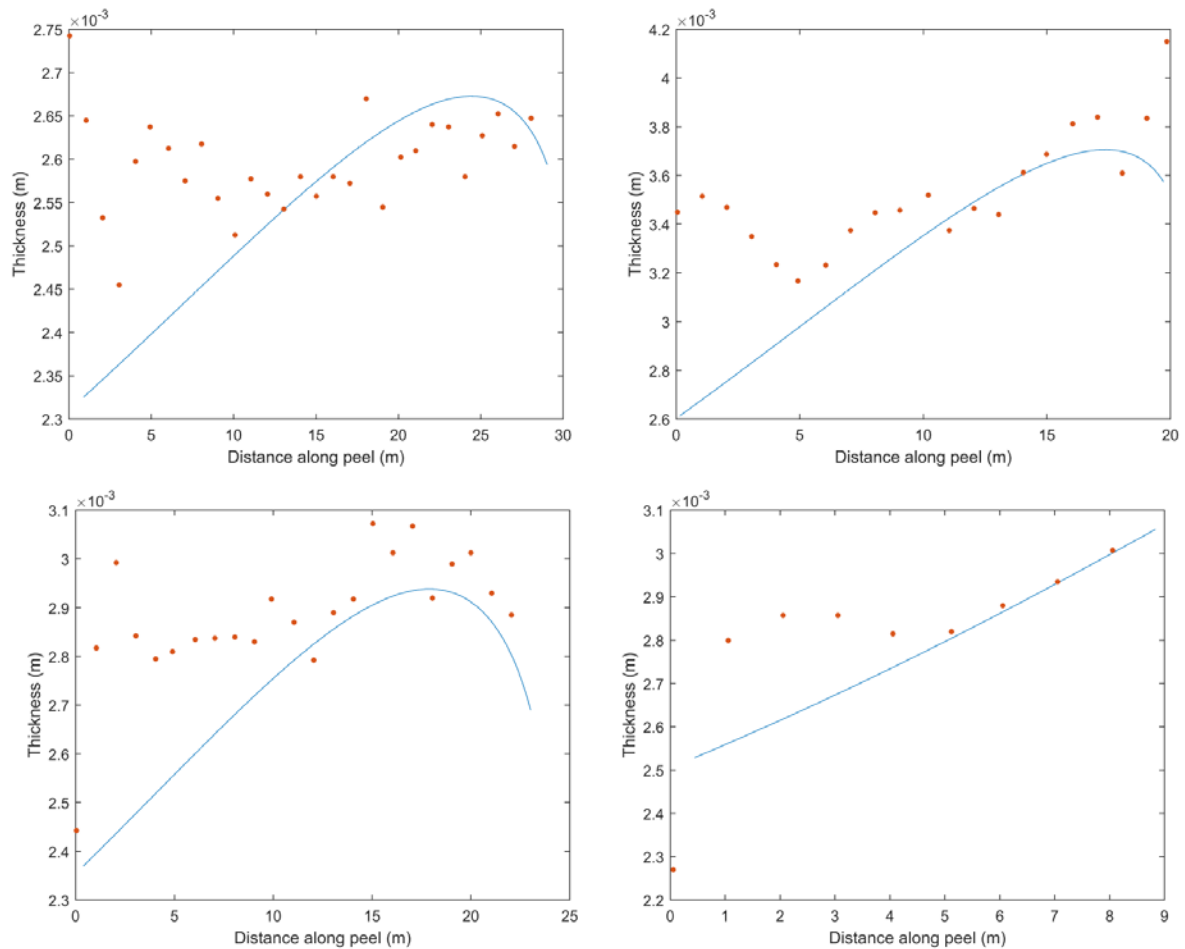
Figure 90. Thickness of ribbon based on fitted spiral functions shown in Figure 84 (—), compared with the average thickness of the veneer strips (·). Increasing distance along the ribbon represents moving from the outside of the billet towards the centre.

We now have a function that maps each circular arc through the ribbon into a spiral-shaped cross section of the billet. Therefore, we can generate a series of images by mapping the pixel intensity values along the arcs onto the spiral, leading to a set of cross-sectional images of the billet. The result of reconstruction using the fitted spiral function is a series of cross-sectional slices representing different heights within the billet. However, due to the nature of the spiral, there are voids between the arcs of the spiral. To overcome this we utilise an algorithm akin to ray-marching (Hart *et al.*, 1989) to propagate the RGB values towards the centre of the spiral.

8.2.4   Slice generation

We take a series of rays passing through the centre of the spiral, and traverse these rays from the outside towards the centre. Beginning from the outer arm of the spiral, we initialise rgb_{curr} to be the current RGB value of the image corresponding to where the ray intersects with the edge of the spiral. We then move along the ray towards the centre of the spiral, copying the RGB value into the image pixels that are currently black. When we encounter a non-black pixel, we reset the value of rgb_{curr} to the new RGB value, and continue the process. The result of this process is shown in Figure 91. We can clearly see the existence of knots within the billet, however there are also some artefacts introduced due to the discrete nature of the pixels. This means that some pixels are processed more than once.

104
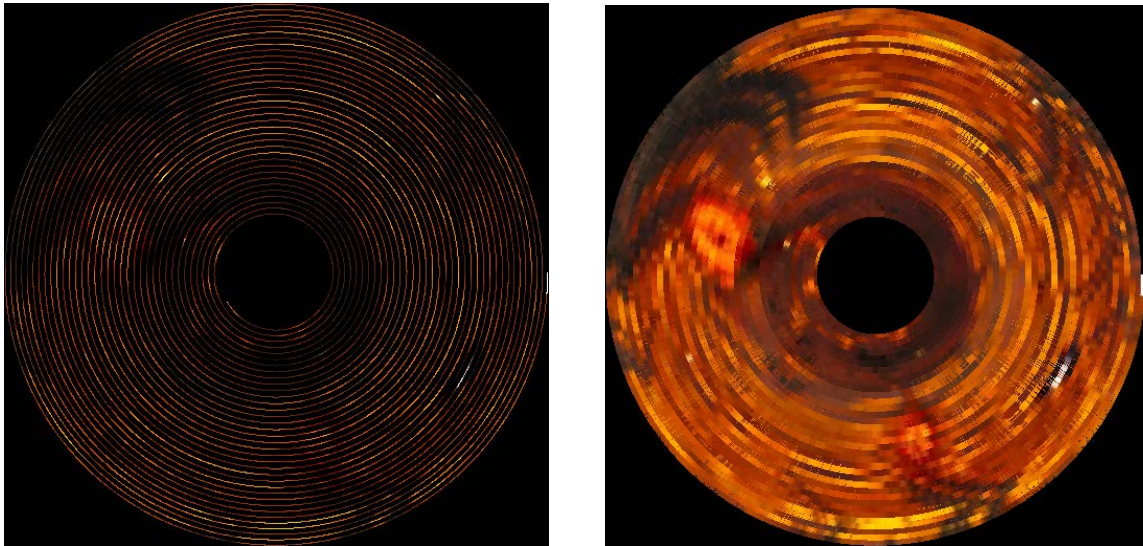
Figure 91. Spiral reconstruction with RGB values mapped from the stitched ribbon image.

Figure 92. Filled image generated using our algorithm. Applying our algorithm to each spiral mapped from the stitched ribbon image, we obtain approximately 2,500 cross-sectional images describing the full billet volume. We can then use these images to generate volumetric visualisations of the reconstructed billet.

To visualise the reconstructed billet we utilise the volume rendering package, Drishti (Limaye, 2012). Developed by Ajay Limaye at ANU (Australian National University), Drishti is a powerful rendering tool that can be used to visualise complex datasets. This allows us to obtain a volumetric rendering of the billet as shown in Figure 93. We are able to slice through the data to reveal the internal structure of the billet or to cut a board from within it, as shown in Figure 94. One of the major advantages of this approach is that we are able to represent the three-dimensional billet in full colour.

Figure 93. Volume visualisation of reconstructed billet using Drishti. The internal knots are clearly visible.

Figure 94. Representative board cut from the reconstructed billet.

8.3 Property reconstruction

Utilising the spiral reconstruction of the timber billet, we can map the properties measured from the veneer strips back to their original locations. Here we restrict consideration to only the Modulus of Elasticity (MOE) of the timber, as it is the key timber property determining value in the case of plantation-grown southern pines.

Figure 95 shows the variation in MOE in the radial direction across the billet, as measured from the veneer strips, together with a fitted sigmoid function. We see that generally the highest stiffness (high MOE) timber is located towards the outer edge of the billet, whilst the timber closest to the pith has low stiffness.
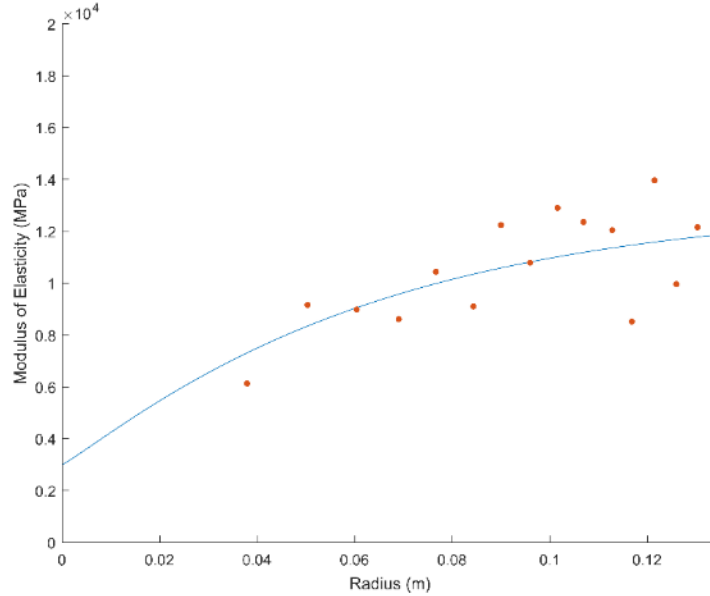
Figure 95. Radial distribution of MOE based on measured veneer strips. A sigmoid function (—) has been fitted to the data (·) to obtain a continuous distribution of MOE with radial position.

To model the variation in the MOE with radial position, we have assumed a five parameter logistic function (Gottschalk and Dunn, 2005) of the form:

$$f(r) = \alpha_0 + \frac{\alpha_1 - \alpha_0}{\left(1 + \left(\frac{r}{\alpha_3}\right)^{\alpha_2}\right)^{\alpha_4}}. \tag{7}$$

where r is the radial position, α_0 represents the minimum asymptote, α_1 is the maximum asymptote, α_2 controls the rate of increase of MOE with r, α_3 governs the inflection point, and α_4 is an asymmetry factor. We have utilised MATLAB's nonlinear least squares fitting (MathWorks, 2013) to solve:

$$\min_{\alpha} \sum_{j=1}^{m} \left[f(r_j; \alpha) - M(r_j)\right]^2, \tag{8}$$

where α is the vector of parameters $\alpha_0, \ldots, \alpha_4$, $M(r_j)$ are the data points shown in Figure 96, and m is the number of data points.

Given the least-squares solution to Equation (9), we can utilise Equation (10) to estimate the value of MOE throughout the billet, and obtain an average value for the MOE of the entire billet. To obtain the average MOE for the billet, we utilise the mean value theorem (Anton *et al.*, 2005) and integrate the fitted *f(r)* across the volume of the billet. Note that we assume that MOE is independent of θ and z (height in the billet). It is important to calculate the average in this way to correctly account for the radial dependence of MOE and timber volume.

From the mean value theorem, we form the integral:

$$\text{MOE}_{avg} = \frac{1}{V} \int_0^{2\pi} \int_0^h \int_0^{g(z)} f(r)\, r \ \ dr\, dz\, d\theta \tag{9}$$

where $V \ = \ \frac{1}{3}\pi\big(R_{\text{butt}}^2 + R_{\text{butt}}\, R_{\text{top}} + R_{\text{top}}^2\big)h$

is the volume of the truncated cone-shaped billet, R_{butt} and R_{top} are the radius of the butt and top end of the billet respectively, and h is the length of the billet. The function $g(z)$ describes how the billet radius varies linearly with height, z, and is given by:

$$g(z) \ = \ R_{\text{butt}}\left(1 \ - \frac{(1-\gamma)}{h} \right) \tag{10}$$

with $\gamma \ = \ R_{\text{top}}/R_{\text{butt}}$. allows the average MOE to be calculated for each individual billet, and we compare this to the billet MOE measured using acoustic methods (Faydi *et al.*, 2017; Paradis *et al.*, 2017). This comparison is shown in Figure 74. We see that overall, we obtain good correlation between our predicted billet MOE and the measured values, with an R^2 value of approximately 0.63. Out of the 60 billets analysed here, our estimate for MOE is within 10% of the measured value for 45 of them, with only one billet showing greater than 20% difference (26.3%), as shown in Figure 96.
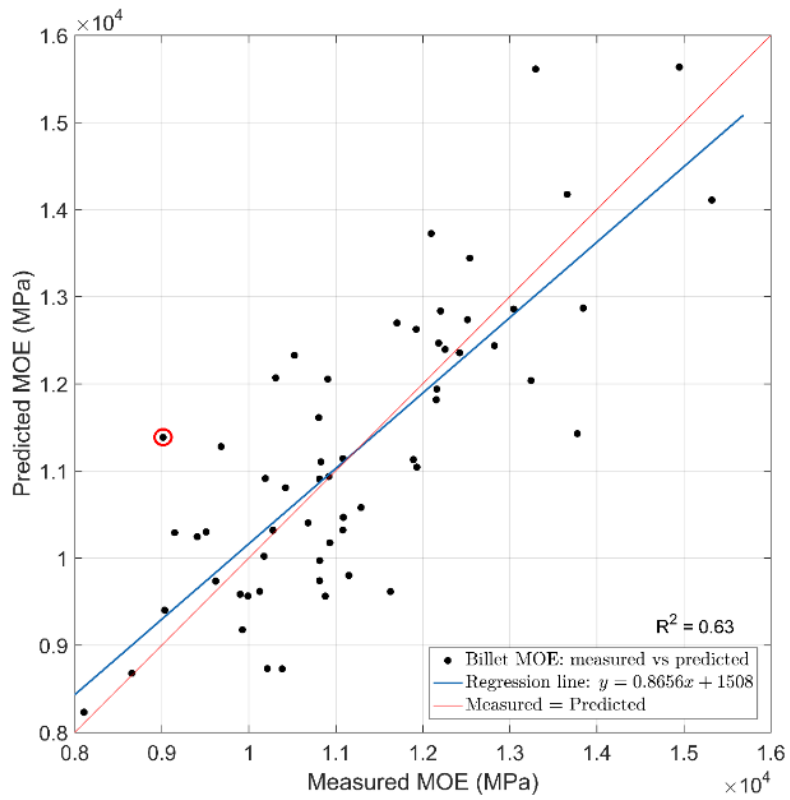
Figure 96. Correlation between measured and predicted billet MOE (·), fitted regression line (—) and line of perfect correlation (—). The red circled data point shows the point with the largest relative error (26.3%).

9   Other traits investigated that influence value

In section 6 we discussed the main driver of value (i.e. MOE). Here we discuss other traits that influence value particularly resin and permeability. Shrinkage of the core segments was also evaluated during the project, however no significant findings were made. Hence we have focussed this section on resin and permeability.

9.1   Resin and extractives variability

Data on resin and extractives were captured on the core segments for two reasons:
- To correct the density data used in the calculation of the USMOE. This allowed more accurate measurement of this trait on the cores and therefore reduce the bias indicating that USMOE was a more accurate way to scale up to product value in the southern pine estate as measured on the boards than either the ST300 or Resistograph tools.
- To evaluate the variation of resin and extractives across the southern pine estate to see the variation at a taxon, site (state forest) and age level.

This second dot point is the focus of this section of the report.

The sampling strategy was designed to obtain training samples from the full range of site indices for the ages and taxa of interest to provide calibration data (based on wet chemistry) for NIR analysis. A similar strategy to that used for the ST300 and coring plots (section 14.3) was applied. To set up the calibration, 28 locations were identified covering the range and of site indices and age classes for each taxon at locations in SEQ and northern NSW. Two trees adjacent but not closer than 3 rows to a growth plot were selected for destructive sampling, involving the extraction of a single 200 mm disc from each tree, collected at breast height. The aim was to select a highly resinous tree (obvious resin exudation) and a non- or low resinous tree (no visible resin exudation) from each location.

Details of the sites selected for the resin and extractives NIR calibration study were:

- hybrids: 13 sites × 2 trees.   age classes: 15-20 years, 25-31 years.
- PCH: 7 sites × 2 trees.   age classes: 15-20 years, 25-31 years.
- PEE: 8 sites × 2 trees.   age classes: 15-20 years, 25-31 years.

The wet chemistry wood extractives content method is detailed in section 14.2.8.

9.1.1   Variability between taxon and plots

Resin content expressed as a percentage of oven dried mass was scaled up to the tree level using the 2D sigmoid curves from the breast height cores (i.e. area / disc basis) discussed in Section 6. Overall the tree level resin did not vary much across the 54 plots with resin within the tree ranging from a minimum of 2 to 20.3 % of the oven dried mass with a mean of 7.6 % and median of 7.2 %. At the taxon level the median resin content across all taxon was similar with PEE having a slightly lower median and slightly less variation (shorter tails) than the other taxon. This may be due to the fact that fewer PEE trees were evaluated for resin content (only 5 plots) compared to the other taxon (9 F_1, 18 F_2, and 22 PCH plots). In all trees resin was more likely to occur close to the pith and not near the bark (Figure 98).
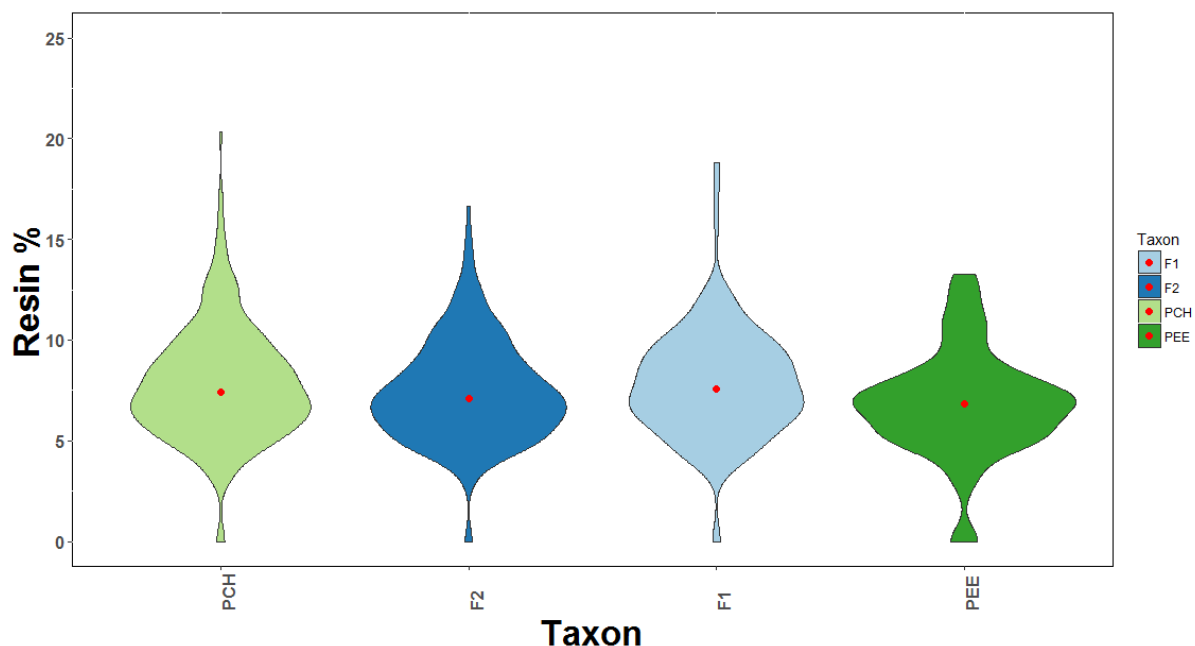
Figure 97. Violin plot showing the variation in percentage of resin (on an oven dried mass basis) in southern pine taxon sampled across multiple plots. The red dot is the median for that taxon. Width of the violin plot indicates the number of trees in that resin class.
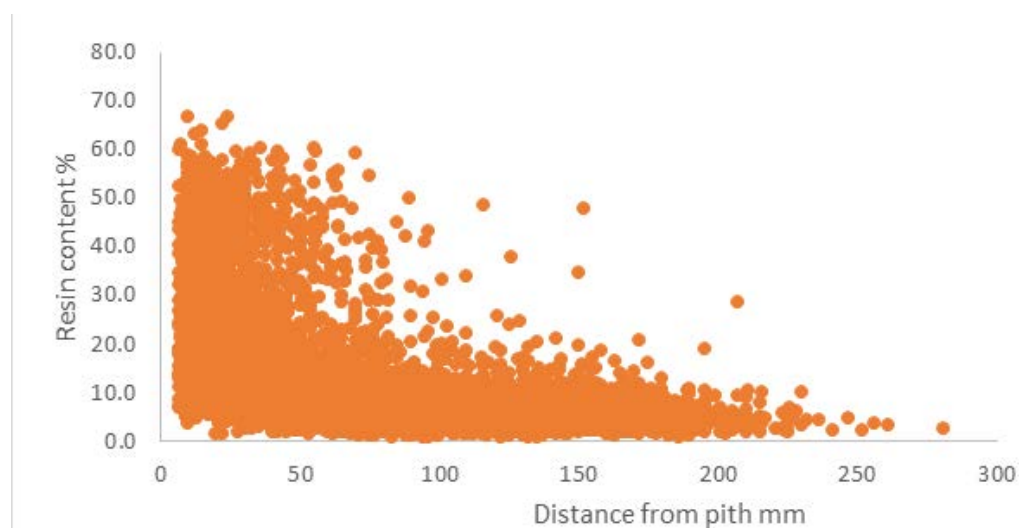
Figure 98. Expression of radial resin content % for all increment cores from 54 plots (all taxa combined). Each data point corresponds to one 20 mm segment from a core.

At the plot level, the average resin content as a percentage of oven dried mass was similar across all the plots sampled with median resin % across all plots being between 5-10% of the oven dried mass. Overall, neither taxon nor site (state forest) appeared to impact resin content; however age did impact this trait with the older plots generally having higher resin content than the younger plots (Figure 99).

9.1.2   Key points from the resin study

The results indicate that neither taxon nor site appear to have an impact on resin development in the trees, however age appears to have an impact on all taxa. Therefore, if resin is a factor of importance for either the growers or processors, then stand age should be taken into consideration, as a potential indicator of elevated resin content.

110
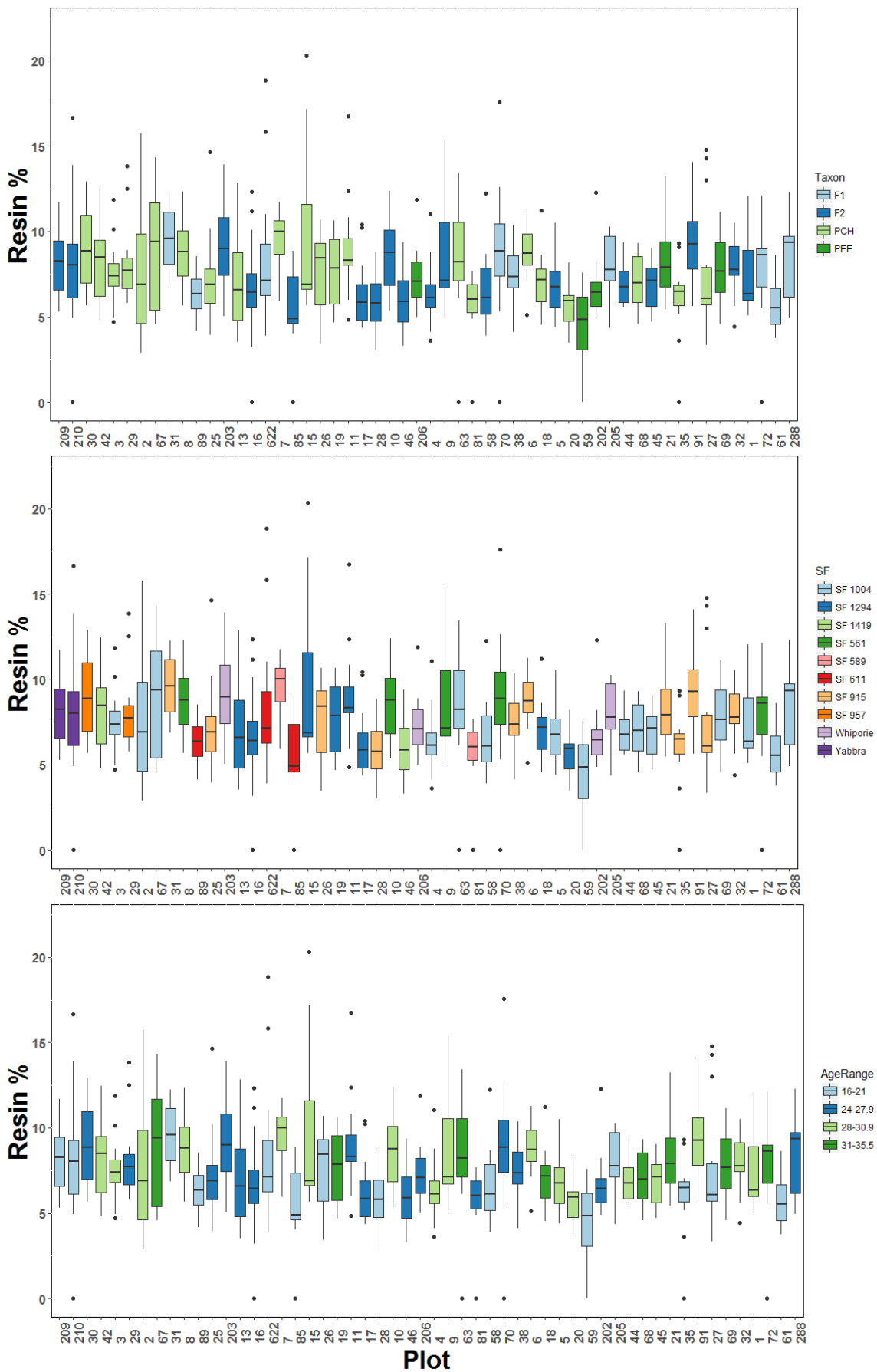
Figure 99. Variation in resin content using the 2D sigmoid curves from the breast height cores expressed as a percentage of oven dried mass of the segments across 54 southern pine plots.

9.2 Permeability results and discussion

Permeability is the property of a material that indicates how freely fluids flow in response to a pressure gradient and for liquids, it is determined by measuring the rate of flow of fluid through a wood specimen of known length and cross-sectional area when a known pressure difference is applied (Booker, 1977). The permeability of wood to liquids influences many important processes including treatment with preservatives, wood modification systems, drying, chemical pulping, gluing, finishing and durability (Booker, 1977, Zimmer *et al.,* 2014, Sandberg and Salin, 2012).

Permeability was measured on two separate sets of samples to assess variability in typical southern pine resources. Wood is very permeable in the longitudinal direction and less so in the radial and tangential directions, so we focussed on these latter two directions as they are the limiting dimensions for treatment of southern pine. One set of samples was prepared for radial liquid permeability and the other for tangential liquid permeability.

9.2.1 Radial permeability

The radial permeability of the F_1 hybrid pine (*Pinus elliottii* var. *elliottii* [PEE] $\times$ *Pinus caribaea* var. *hondurensis* [PCH]) was investigated for wood samples (at three radial positions: near the pith, mid radius and near the bark of the tree) from 30 trees at age 19, representing three F_1 genotypes planted at five different stocking rates (Experiment 622NC, Beerburrum). Tree mean radial permeability varied within and between F_1 hybrid genotypes; however, the differences in permeability between three genotypes was not statistically significant (Figure 100). For all data combined, the ranking was F_1 seedling most permeable, followed by clone C625 and then clone C887 (least permeable).
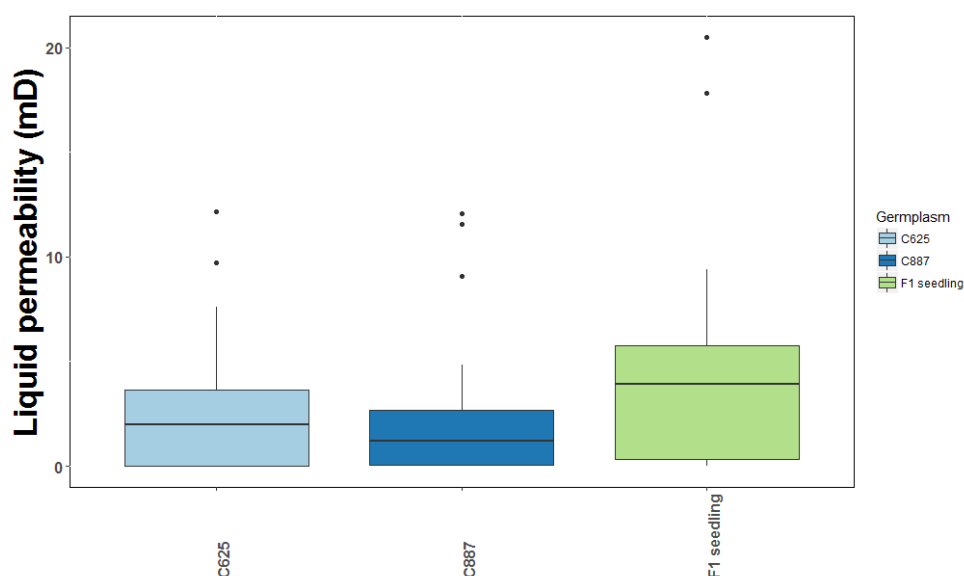
Figure 100. Box plot representation of liquid radial permeability by three F_1 genotypes (averaged across 5 stocking rates)

Tree mean radial permeability varied slightly between different stocking rates (Figure 101). Again the differences were not statistically significant with a large overlap for all stocking rates.
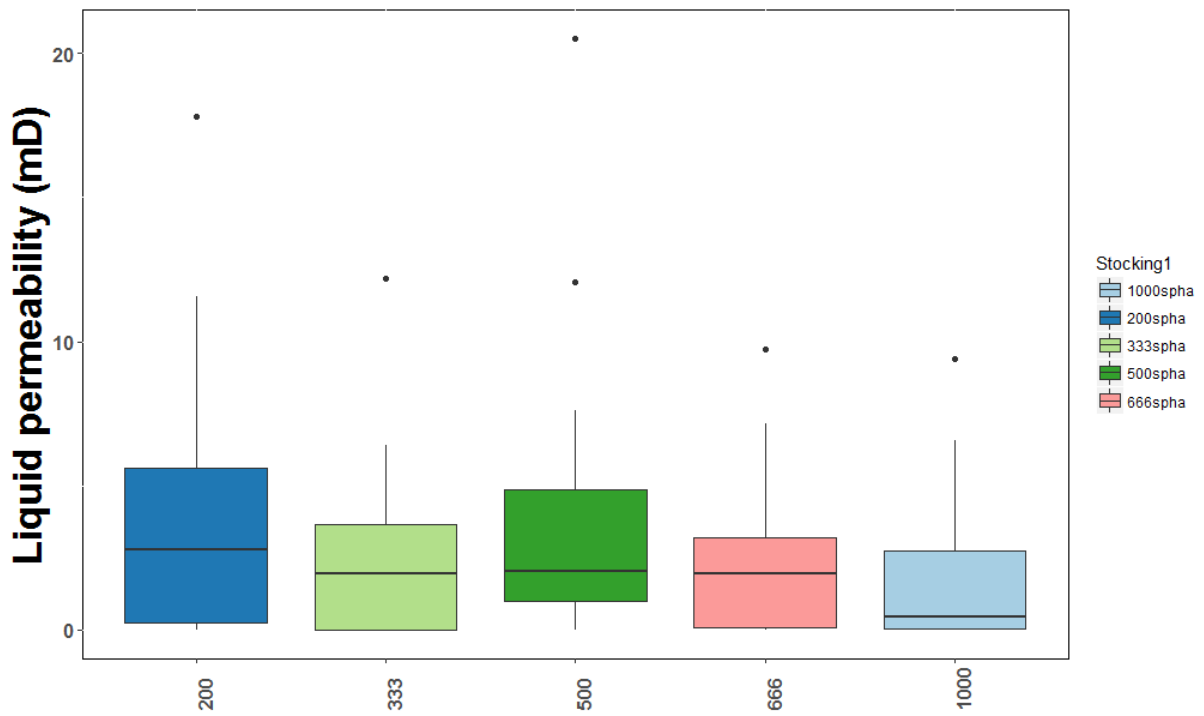
Figure 101. Liquid radial permeability for five stocking rates (averaged across three F₁ hybrid genotypes).

Figure 102 show the radial gradient of liquid permeability. Permeability was highest in the outer wood and lowest (effectively zero) nearer the pith where some samples were impermeable.
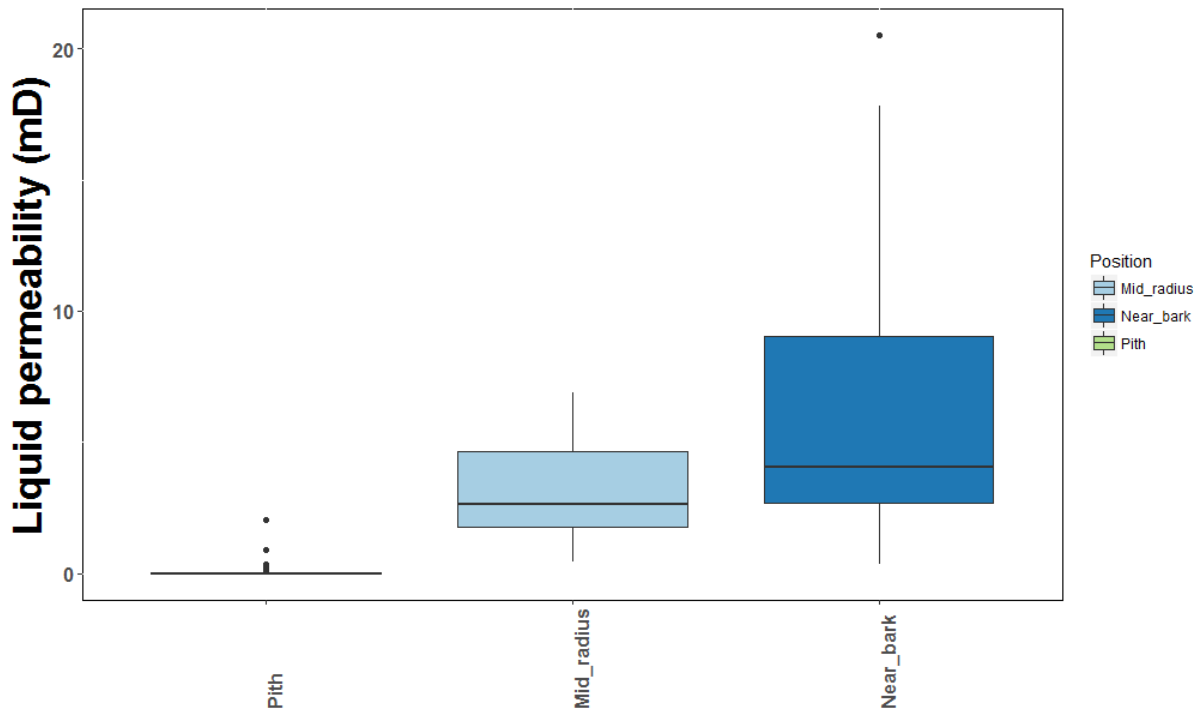
Figure 102. Liquid permeability of wood samples across the radial axis.

Overall, mean liquid permeability decreased radially from near the bark moving towards the pith and the differences between radial positions were statistically significant at $p < 0.001$.

Excluding the near pith results, a significant relationship ($p<0.05$) was found between distance from the pith and liquid radial permeability.

Nineteen percent of liquid radial permeability samples registered zero permeability. These results are most likely due to local anatomical characteristics associated with heartwood formation, or wood chemistry that restricted fluid flow. For example, in most cases it was the resinous samples closest to the pith which registered zero permeability.

9.2.2 Tangential liquid permeability

Tangential liquid permeability was tested on a wider range of taxa resulting in a higher variability of results. For all data combined, in order from highest to lowest tangential permeability, the ranking was loblolly pine (Taeda; however this is represented by only two trees), F_2, PEE, PCH and F_1 (Figure 103).
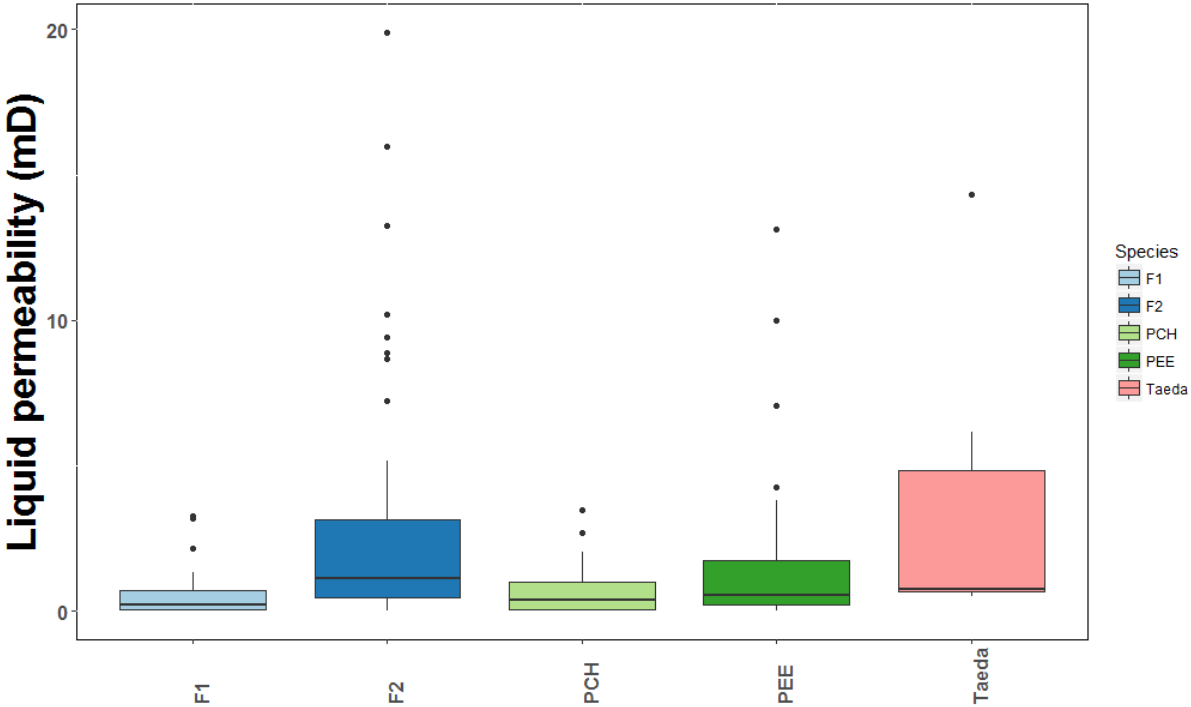
Figure 103. Tangential permeability of each southern pine taxon.

Mean tangential permeability also varied considerably within and between state forests from which the samples were collected (Figure 104). For all data combined, in order from highest to lowest tangential permeability the ranking was Yabbra (NSW), Whiporie (NSW), Toolara (Qld), Tuan (Qld), Beerburrum (BBM, Qld) and Wongi (Qld).

114
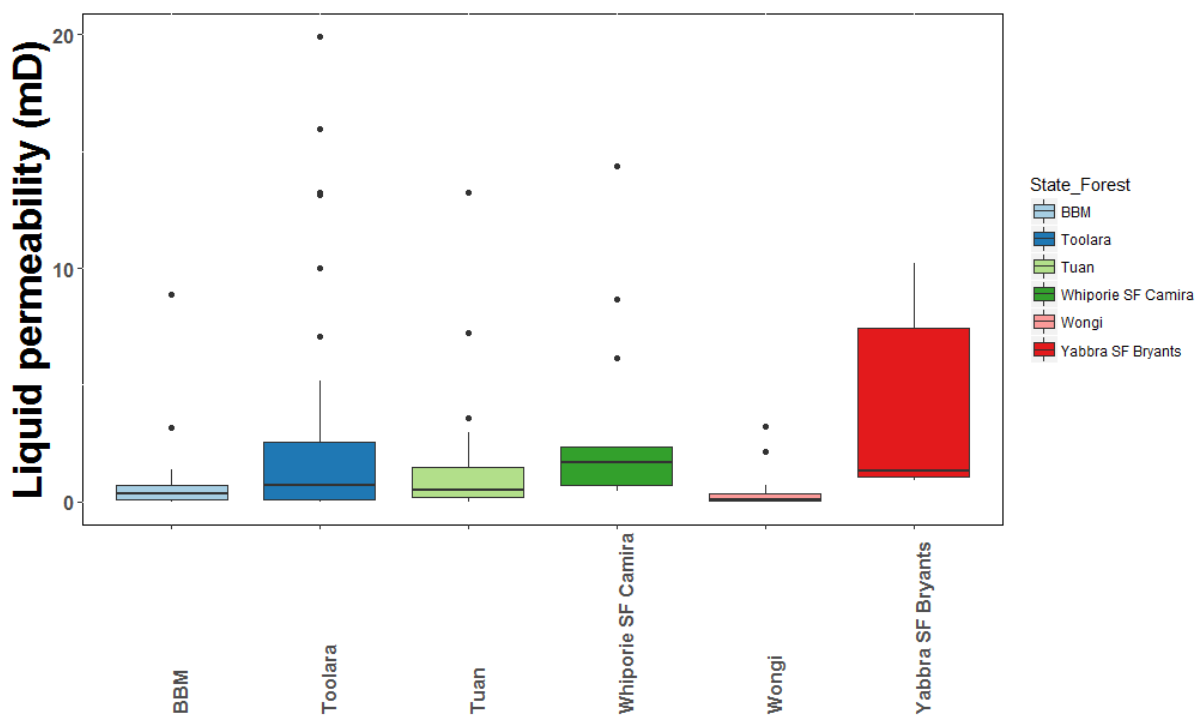
Figure 104. Tangential permeability of wood samples from state forest.

The differences in tangential permeability within and between taxa, sites and plantation ages would most likely be related to wood anatomical differences influenced by many factors including genetics and growing conditions. Treatability is closely linked to permeability and can vary between stands due to variation in wood anatomical characteristics influenced by factors such as geographic origin, climate, position in the stand, growth increments and intra-tree competition. Apart from wood anatomical variation, differences in wood chemistry (e.g. wood extractives or resin content) could also explain some of the variation.

Figure 105 shows differences in tangential permeability according to radial position from pith to bark for all samples combined. As for radial permeability, there was a gradient from pith to bark with lower permeability being observed near the pith and highest permeability in the outer wood nearer the bark. However the variation was much lower. This can be explained by the trend of reducing heartwood content radially from the pith to the bark (or increasing transformation of sapwood to heartwood from the bark inwards) although the extent of heartwood formation varies with age. The heartwood of most species is less permeable due to higher extractives content, greater pit aspiration, pit encrustation and reduced size and frequency of pits.
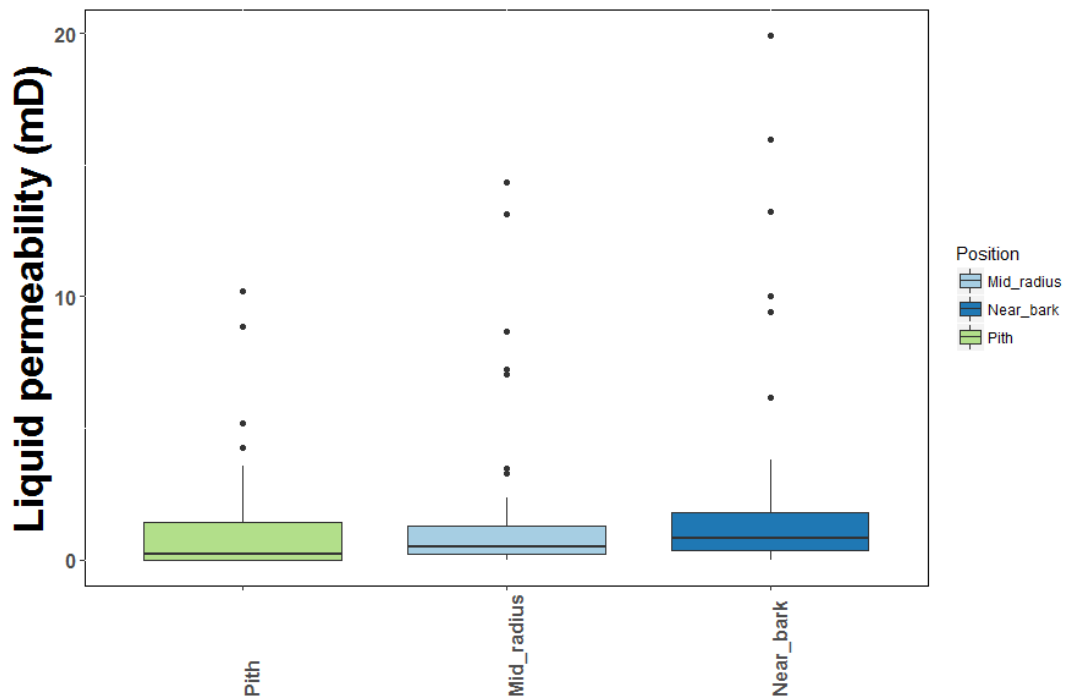
Figure 105. Tangential liquid permeability of wood samples along the radial axis.

For all data combined, no significant relationships were found between tangential permeability and cambial age (adjusted[2] R^2 =0.002); tree age (adjusted R^2 =0.002); density (adjusted R^2 =0.008) or DBHOB (adjusted R^2 =0.002).

Overall, 7% of the samples registered zero tangential permeability even after a repeat measurement. These results could be due to anatomical or chemical features of the wood that restricted fluid flow.

9.2.3 Key points from the permeability study

There was no significant variability in liquid radial permeability between different genotypes of the F_1 hybrid, nor different stocking rates as tested in this study. Permeability does however display a pattern with higher permeability measured nearer the outer wood, and low or no permeability near the pith.

---

[2] Adjusted R^2 is the R^2 corrected for the sample size and numbers of coefficients

10 Key findings and recommendations

10.1 Key findings from the study were:

- Sigmoid curves (S-shaped curves) capture the variation in wood properties from the pith to the bark.
  - The cambial age versus ultrasound MOE (USMOE) sigmoids, referred to here as 'fingerprint curves', measured along sampled cores, are believed to be independent of the silviculture, size and growth of the trees. Variation of these curves is dependent on genetics and environment. They allow the grower and processor to determine the performance potential of genetic material in a given environment (e.g. the age when a stand will produce 10,000 MPa wood).
  - The radial growth versus USMOE curves, referred to as 'radial sigmoids', are influenced by silviculture as well as genetics and environment. These curves can be processed to estimate the quantity of wood of a given performance (e.g. >10,000 MPa).
  - Both of these curves provide valuable information on product performance. This information is useful to manage plantation growth and processing, improving the growers' and processors' abilities to value stands of trees.

- The USMOE using a 2D reconstruction approach can estimate MOE for individual boards that can be sawn from trees with moderate accuracy ($R^2 = 0.53$) and very little bias (2%). Similar accuracy and bias were achieved using 3D approaches. However, board MOE estimation using the 3D static bending simulation had a better prediction capacity for rating the boards. These correlations are robust, since they are based on a deterministic approach that directly connects products to the trees from which they were derived. This has potential to improve the growers' and processors' abilities to value stands of trees and the trees within these stands. The choice of the method of board MOE estimation is dependent on the objective and the level of accuracy required by the grower or processor.
- An initial characterisation of the southern pine resource has been completed. This study highlighted that some plots or stands will produce high MOE wood (>10,000 MPa) at a young age (e.g. 5-10 years old) and other stands will not produce this quality of wood during a typical rotation. The drivers of the geographical variation of the wood properties has to be better understood to be able to map this variation spatially and temporally, and to optimise the sampling strategy.
- Of the three technologies tested, the USMOE provided the most accurate measure of sawlog MOE ($R^2 = 0.78$) and the least biased (9% bias). The Resistograph was the second most accurate tool at predicting log MOE ($R^2 = 0.68$) and a 9% bias. The ST300 was the least accurate tool to predict log MOE ($R^2 = 0.42$) and had a large bias of 41%. The large bias on the ST300 resulted in this tool over-predicting the MOE of the trees in the stands.
- The ST300 (time-of-flight of stress waves) and Resistograph (resistance to drilling) technologies only give a single measurement or prediction for each sawlog MOE, and this number is based on calibrations and approximations. Hence, they cannot be used to accurately predict the value of different parts of the plantation estate, but they may be useful for a general ranking of stands. They are useful at segregating plots in the extreme high or low MOE range.
- Changing the sawing pattern used on a log can have a dramatic impact on the recovery of MGP10 or better boards. This could improve product value with flow-on effects across the whole value chain.

- In the factorial analysis, moisture related variables had the biggest impact on MOE, with variates associated with making moisture available (e.g. rain and increased number of rain days) having a positive impact on MOE and drought related factors (e.g. number of months with low rainfall (≤ 30 mm of rain) and the total number of dry months) having the largest negative effect on MOE. Higher stocking rates were positively correlated with higher MOE.
- Neither taxon nor site appear to have an impact on resin development in the trees, however age appears to have an impact on all southern pine taxa investigated, with older trees generally having more resin.
- There was no significant variability in liquid radial permeability between different genotypes of the F_1 hybrid, nor different stocking rates as tested in this study. Permeability does however display a pattern with higher permeability measured nearer the outer wood, and low or no permeability near the pith.

10.2 Key recommendations

- The sawlog and board MOE estimated by the USMOE should be further validated by destructively sampling a broad range of the plots. It is recommended that destructive processing of plots / stands with predicted average poor board MOE (< 10,000 MPa) and good board MOE (> 10,000 MPa) be undertaken to validate the project findings. In addition, for those regions where a number of plots in the lower end of the predicted MOE range occur, we recommend the industry should undertake additional surveying to see how reflective the results observed here are for these regions.
- Southern pine growers could use the fingerprint curves obtained from USMOE measured on cores at age 17, along with LiDAR information to better manage their plantation estates to maximise sales of high value products.
- Processors could use the USMOE to optimise their settings to maximise recovery of high value products improving returns across the whole value chain.
- Costly silvicultural interventions should be made after the trees in a plot or stand have started producing structural wood to maximise the recovery of high value products. This needs further investigation.
- Improving the calibration of the IML Resistograph should be undertaken to try to improve its MOE prediction capacity, particularly the MOE of younger plots. Further investigations on the traces would inform on the potential to extract local MOE values and its ability to predict board performances. In addition, metrological evaluation of the tool should be undertaken.
- If resin is a problem, try to harvest coupes earlier. If resin is desirable then delaying harvest may result in more resin being accumulated in the plots.
- Variation in wood properties above the height where we assessed to in this study (approximately 8 m) should be investigated (e.g. the MOE of the top logs may be highly impacted by the greater proportion of knots).
- We have only started to "mine" this large dataset, which warrants much further investigation over the coming years to provide on-going benefits to all stakeholders across the forest value chain.
- Site and environmental drivers of wood properties should be evaluated at a finer scale than was possible in this study, where we worked on interpolated average climate data between planting and sampling age for each plot. For the climate data, it should be possible to align this to the cambial age of the cores to directly compare the impact of climate (on a yearly or monthly basis) on wood value.
- Soil and genetics should be included as factors in future studies to explain more of the variation in MOE than that possible in this study.

- Plantation growers need to capture soil and genetics data and accurately link this to stands, to better understand the impact of these factors on wood value. This will facilitate a better understanding of the effect of these factors on wood value and will help inform the decision making process.
- Quantification of the importance of genetics and environment on the cambial age sigmoids needs to be investigated to further understand the influence of both of these factors on cambial age. This will help answer the question 'how can we select for or manage the trees to maximise production of high value wood?'
- Sensitivity analysis should be undertaken on the results and models developed during this project to provide confidence in the results and models by quantifying the uncertainty in any results or model, and secondly by evaluating how much each input is contributing to the output uncertainty.
- This initial resource characterisation should be expanded to provide tangible benefits across the southern pine resource value chain.
- The reconstruction of log and board MOE from the USMOE should be applied across other pine resources in Australia to maximise value in these supply chains.
- The same approach can be applied to other products such as veneer and/or other performance criteria such as fibre length or calorific power.
- We have presented a useful approach based on the models developed in this project. With its current accuracy, it can be implemented on southern pine and other pine resources to assess the performances and value of any stand. However, there is great potential to improve this approach and make it more user friendly. One avenue for further work is around investigating faster means of obtaining useful data so the resource can be better understood.
- Future work should focus on developing user-friendly algorithms into a predictive decision support tool to assist the future management of southern pine, radiata pine and pinaster pine resources. Eucalyptus plantation resources could as well benefit from the project approach (e.g. fibre length). This would deliver technological and economic benefits to the timber industry and provide insights about the resource, facilitating design of new industrial technologies and optimising current forestry operations under changing market and environmental conditions.
- We propose that a suite of logical follow-on projects would bring growers and processors further towards the mutually-beneficial target of **Precision Forestry Chain**. We propose that extending the modelling work and performing further analysis of genetic and environmental factors and use of GIS and LiDAR technologies will improve the logistics and field management, stand allocation and timing of harvesting, information for replanting (second/third-rotation) decisions, impacts of climate change on wood production (structure and properties) and processing and product development.

11 References

Achim, A., Paradis, N., Carter, P. and Hernández, R.E. (2011). Using Acoustic Sensors to Improve the Efficiency of the Forest Value Chain in Canada: A Case Study with Laminated Veneer Lumber. *Sensors*. 11(6): 5716-5728.

Anton, H., Bivens, I., and Davis, S. (2005). CALCULUS - EARLY TRANSCENDENTALS. John Wiley and Sons, Inc.

Alves, A.M.M., Simões, R.F.S., Santos, C.A., Potts, B.M., Rodrigues, J. and Schwanninger, M. (2012). Determination of *Eucalyptus globulus* Wood Extractives Content by near Infrared-Based Partial Least Squares Regression Models: Comparison between Extraction Procedures. *Journal of Near Infrared Spectroscopy*. 20:2, pp 275-285.

Arciniegas, A., Prieto F., Brancheriau, L. and Lasaygues, P. (2014). Acoustic and ultrasonic tomography of standing trees: Literature review and signal processing open problems. *Trees - Structure and Function*. 28(6): 1559–1567.

Arciniegas, A., Brancheriau, L. and Lasaygues P. (2015). Tomography in standing trees: revisiting the determination of acoustic wave velocity. *Annals of Forest Science*, 72(6): 685-691.

Australian/ New Zealand Standards (2000). AS/NZS 1080.3:2000. Timber: Methods of test for timber: density. SAI Global.

Australian/ New Zealand Standards (2010). AS/NZS4063.1:2010. Characterization of structural timber – test methods. SAI Global.

Baillères, H., Hopewell, G. and Boughton, G. (2009). MOE and MOR assessment technologies for improving graded recovery of exotic pines in Australia. Forest and Wood Products Australia Limited. Research Report PNB040-0708. 85p.

Baillères, H., Hopewell, G., Boughton, G., and Brancheriau, L. (2012). Strength and stiffness assessment technologies for improving grading effectiveness of radiata pine wood. *BioRes*. 7(1): 1264-1282.

Baillères, H., Vitrac, O. and Ramananantoandro, T. (2005). Assessment of continuous distribution of wood properties from a low number of samples: application to the variability of modulus of elasticity between trees and within a tree. Holzforschung 59(5):24-530. DOI:10.1515/HF.2005.087.

Barnett, J. and Jeronimidis, G. (2003). WOOD QUALITY AND ITS BIOLOGICAL BASIS. Wiley-Blackwell. 240p.

Berglund, A., Broman, O., Grönlund, A., and Fredriksson, M. (2013). Improved log rotation using information from a computed tomography scanner. *Computers and Electronics in Agriculture*, *90* (Supplement C): 152–158. https://doi.org/https://doi.org/10.1016/j.compag.2012.09.012

Blakemore, P., Cown, D. Dumbrell, I. McKinley, R. Lyon, A. Barr, B. and Northway, R. (2010). Western Australian Softwood Resource Evaluation: a survey of key characteristics of

the *Pinus radiata* and *Pinus pinaster* resources in Western Australia with links to product performance of trees sampled from each resource, as determined by a processing study. Melbourne, Victoria, Forest and Wood Products Australia Research Report PNC059-0809. 82p.

Bodig, J. and Jayne, B.A. (1982). MECHANICS OF WOOD AND WOOD COMPOSITES. Van Nostrand Reinhold. 712p.

Boggs, P. T., and Rogers, J. E. (1990). ORTHOGONAL DISTANCE REGRESSION. NISTIR 89-4197, Gaithersburg, MD, United State of America.

Booker, R.E. (1977). Problems in the measurement of longitudinal sapwood permeability and hydraulic conductivity. *New Zealand Journal of Forestry Science* 7(3) 297-306.

Brancheriau L. and Baillères H. (2002). Natural vibration analysis of wooden beams: a theoretical review. *Wood Science and Technology*, Springer – Verlag (Ed), 36(4) 347-365.

Brancheriau, L. (2011). Corrections for Poisson effect in longitudinal vibrations and shearing deformations in transverse vibrations applied to a prismatic orthotropic body. In: Galloway, A. L. (Ed.). MECHANICAL VIBRATIONS- TYPES, TESTING AND ANALYSIS. Nova Science Publishers. ISBN-13: 978-1616682170, 205-223.

Brancheriau, L. (2014). An alternative solution for the determination of elastic parameters in free-free flexural vibration of a Timoshenko beam, *Wood Science and Technology*, 48(6):1269-1279.

Brancheriau, L., Paradis, S., and Baillères, H. (2007). Bing: Beam Identification by Non-destructive Grading. CIRAD. https://doi.org/10.18167/62696E67.

Bruneau M. and Potel C. (2009). MATERIALS AND ACOUSTICS HANDBOOK. Wiley. 960p.

Carr, J. C., Beatson, R. K., Cherrie, J. B., Mitchell, T. J., Fright, W. R., McCallum, B. C., and Evans, T. R. (2001). Reconstruction and representation of 3D objects with radial basis functions. In *Proceedings of the 28th annual conference on Computer graphics and interactive techniques* (pp. 67–76).

Carr, J. C., Fright, W. R., and Beatson, R. K. (1997). Surface interpolation with radial basis functions for medical imaging. *IEEE Transactions on Medical Imaging*, 16(1): 96–107.

Carter P., Briggs D., Ross R.J., Wang X. (2005) Acoustic testing to enhance western forest values and meet customer wood quality needs. USDA Forest Service General Technical Reports PNW 642:121–129.

DAF (2015). The drill corer- a field manual for taking tree cores using the large-bit drill corer. ACIAR project report FST/2012/043.

Dinulica, F., Marcu, V., Borz, S. A., Vasilescu, M.-M., and Petritan, I. C. (2016). Wind contribution to yearly silver fir (*Abies alba* Mill.) compression wood development in the Romanian Carpathians. *iForest-Biogeosciences and Forestry,* 9(6): 927.

Dossing, O. (1988). STRUCTURAL TESTING. PART 1—MECHANICAL MOBILITY MEASUREMENTS. Bruel and Kjaer, Denmark.

Downes, G.M.; Hudson, I.L.; Raymond, C. A.; Dean, G. H.; Michell, A. J.; Schimleck, L. R.; Evans, R.; Muneri, A. (1997). SAMPLING PLANTATION EUCALYPTS FOR WOOD AND FIBRE PROPERTIES. 132 p. CSIRO Publishing. Melbourne, Australia.

Downes, G. and Lausberg, M. (2016). User Manual for the software tool for the prediction of Acoustic Velocity (HM200) from traces collected from *Pinus radiata* using the IML Resistograph PD-400. Tasmania, Forest Quality Pty Ltd.

Downes, G. M., Lausberg, M., Potts, B. M., Pilbeam, D., Bird, M. and Bradshaw, B. (Accepted). Application of the IML Resistograph to the infield measurement of basic density, in plantation eucalypts. Australian Forestry.

Downes, G., Hogg, B. and Lee, D. (2017). Evaluating the application of the IML Resistograph to the prediction of key wood properties of the Southern Yellow Pine. University of the Sunshine Coast. In Milestone report 5a-d FWPA PNC361-1415

Dunn, J., and Wild, D. (2013). Calibration Curve Fitting. In THE IMMUNOASSAY HANDBOOK: THEORY AND APPLICATIONS OF LIGAND BINDING, ELISA AND RELATED TECHNIQUES (pp. 323–329). Elsevier Ltd.

Eberhardt, T. L., and Samuelson, L. J. (2015). Collection of wood quality data by X-ray densitometry: a case study with three southern pines. *Wood Science and Technology,* 49(4): 739-753.

Essien, C., Via, B. K., Cheng, Q., Gallagher, T., McDonald, T., Wang X. and Eckhart L. G. (2017). Multivariate modeling of acoustomechanical response of 14-year-old suppressed loblolly pine (*Pinus taeda*) to variation in wood chemistry, microfibril angle and density. *Wood Science and Technology,* 51(3): 475-492.

Faydi, Y., Brancheriau, L., Pot, G. and Collet, R. (2017). Prediction of oak wood mechanical properties based on statistical exploitation of vibrational response, *BioResources*, 12(3):5913-5927.

Ferreira, T., and Rasband, W. (2012). ImageJ User Guide.

Francis, L. (2016). Southern pine timber extractives measurement: solvent extraction at ESP. DAF in-house procedure document.

Fredriksson, M. (2015). Optimizing sawing of boards for furniture production using CT log scanning. *Journal of Wood Science*, 61(5): 474–480.

Fredriksson, M., Berglund, A., and Broman, O. (2015). Validating a crosscutting simulation program based on computed tomography scanning of logs. *European Journal of Wood and Wood Products*, 73(2): 143–150.

Fries, A., and Ericsson, T. (2006). Estimating genetic parameters for wood density of Scots pine (*Pinus sylvestris* L.). *Silvae Genetica,* 55(1-6): 84-92.

Gantz, C. (2002). Evaluating the efficiency of the Resistograph to estimate genetic parameters for wood density in two softwood and two hardwood species. Dissertation, College of Natural Resources, North Carolina State University.

Gao, S., Wang, X., Wiemann, M. C., Brashaw, B. K., Ross, R. J., and Wang, L. (2017). A critical analysis of methods for rapid and non-destructive determination of wood density in standing trees. *Annals of Forest Science, 74*(2), 27p. doi:10.1007/s13595-017-0623-4.

Giroud, G., Bégin, J., Defo, M., and Ung, C.-H. (2017). Regional variation in wood density and modulus of elasticity of Quebec's main boreal tree species. *Forest Ecology and Management,* 400: 289-299. doi: https://doi.org/10.1016/j.foreco.2017.06.019.

Gottschalk, P. G., and Dunn, J. R. (2005). The five-parameter logistic: A characterization and comparison with the four-parameter logistic. *Analytical Biochemistry*, 343(1): 54–65.

Grissino-Mayer, H. D. (2003). A MANUAL AND TUTORIAL FOR THE PROPER USE OF AN INCREMENT BORER. *Tree-ring research*.

Gutierrez, R., Kang, S. B., and Joshi, N. (2015). Image Composite Editor (ICE). Retrieved from https://www.microsoft.com/en-us/research/project/image-composite-editor/.

Hart, J. C., Sandin, D. J., and Kauffman, L. H. (1989). Ray Tracing Deterministic 3-D Fractals. *Computer Graphics*, 23(3): 289–296.

Hein, P.R.G., Brancheriau, L., Trugilho, P.F., Lima, J.T. and Chaix G. (2010a). Resonance and near infrared spectroscopy for evaluating dynamic wood properties, *J. Near Infrared Spectrosc*., 18(6): 443-454.

Hein, P., Brancheriau, L., Lima, J.T., Rosado, A.M., Gril, J. and Chaix, G. (2010b). Clonal and environmental variation of structural timbers of *Eucalyptus* for growth, density, and dynamic properties. *Cerne*, 16 (Suplemento) 74-81.

Hong, Z., Fries, A., and Wu, H. X. (2015). Age trend of heritability, genetic correlation, and efficiency of early selection for wood quality traits in Scots pine. *Canadian Journal of Forest Research*, 45(7): 817-825.

Horváth, G. (2016). RawTherapee. Retrieved from http://rawtherapee.com/

Isik, F. and Li B. (2003). Rapid assessment of wood density of live trees using the Resistograph for selection in tree improvement programs. *Canadian Journal of Forest Research* 33(12): 2426-2435.

Ivković, M., Gapare, W. J., Abarquez, A., Ilic, J., Powell, M. B., and Wu, H. X. (2008). Prediction of wood stiffness, strength, and shrinkage in juvenile wood of radiata pine. *Wood Science and Technology*, 43(3): 237. doi:10.1007/s00226-008-0232-3

Jordan, L., Clark Iii, A., Schimleck, L. R., Hall, D. B., and Daniels, R. F. (2008). Regional variation in wood specific gravity of planted loblolly pine in the United States. *Canadian Journal of Forest Research*, 38(4): 698-710.

Kahl, T., Wirth, C., Mund, M., Bohnisch G. and Schulze E. (2009). Using drill resistance to quantify the density in coarse woody debris of Norway spruce. *European Journal of Forest Research* 128: 367-473.

Kimberley, M. O., Cown, D. J., McKinley, R. B., Moore, J. R., and Dowling, L. J. (2015). Modelling variation in wood density within and among trees in stands of New Zealand-grown radiata pine. *New Zealand Journal of Forestry Science*, 45(1): 22. doi:10.1186/s40490-015-0053-8

Kimberley, M. O., McKinley, R. B., Cown, D. J., and Moore, J. R. (2017). Modelling the variation in wood density of New Zealand-grown Douglas-fir. *New Zealand Journal of Forestry Science*, 47(1): 15. doi:10.1186/s40490-017-0096-0

Koch, P. (1972). UTILIZATION OF THE SOUTHERN PINES. VOLUME I- THE RAW MATERIAL. USDA Forest Service. Agriculture Handbook No. 420.

Kollmann, F.F.P. and Côté, W.A.Jr. (1968). PRINCIPLES OF WOOD SCIENCE AND TECHNOLOGY – PART I: SOLID WOOD. Springer-Verlag. 592p.

Knapic, S., Seppä, I. P., Usenius, A., and Pereira, H. (2011). Stem modeling and simulation of conversion of cork oak stems for quality wood products. *European Journal of Forest Research*, 130(5): 745–751.

Lachenbruch, B., Moore, J. R., and Evans, R. (2011). RADIAL VARIATION IN WOOD STRUCTURE AND FUNCTION IN WOOD PLANTS, AND HYPOTHESES FOR ITS OCCURRENCE. In F. C. Meinzer, B. Lachenbruch, and T. E. Dawson (Eds.) (pp. 131–164). Springer.

Legg, M. and Bradley S., (2016). Measurement of stiffness of standing trees and felled logs using acoustics: A review. *Journal of the Acoustical Society of America,* 139(2): 588-604.

Lenz, P., MacKay, J., Rainville, A., Cloutier, A., and Beaulieu, J. (2011). The influence of cambial age on breeding for wood properties in *Picea glauca*. *Tree Genetics & Genomes*, 7(3), 641-653.

Limaye, A. (2012). Drishti: a volume exploration and presentation tool. In *Proc. SPIE 8506, DEVELOPMENTS IN X-RAY TOMOGRAPHY VIII*.

Lin, C., Wang, S., Lin, F. C. and Chui C. (2003). Effect of moisture content on the drill resistance value in *Taiwania* plantation wood. Wood and Fiber Science 35(2): 234-238.

Lin, W., Wang, J., and Thomas, E. (2011). Development of a 3D log sawing optimization system for small sawmills in central Appalachia, US. *Wood and Fiber Science*, 43(4): 379–393.

MathWorks. (2013). Matlab Curve Fitting Toolbox® User's Guide. Natick, MA.

MATLAB. (2016). *version 9.0.0.341360 (R2016a)*. Natick, Massachusetts: The MathWorks Inc.

Moore, J. R., Lyon, A. J., Searles, G. J., Lehneke S. A. and Ridley-Ellis D. J. (2013). Within- and between-stand variation in selected properties of Sitka spruce sawn timber in the UK: implications for segregation and grade recovery. *Annals of Forest Science* 70(4): 403-415.

Murphy, G. and Cown, D. (2015). Stand, stem and log segregation based on wood properties: a review. *Scandinavian Journal of Forest Research*, 30(8): 757-770.

Nester, M. R. (2014). Southern pine resource characterisation 2014/2015 sampling strategy discussion paper, Unpublished Report HQPlantation Pty Ltd: 14p.

Paradis N., Auty D., Carter P. and Achim A. (2013). Using a Standing-Tree Acoustic Tool to Identify Forest Stands for the Production of Mechanically-Graded Lumber. *Sensors*. 13(3):3394-3408.

Pinto, I., Pereira, H., and Usenius, A. (2003). Analysis of log shape and internal knots in twenty Maritime pine (*Pinus pinaster* Ait.) stems based on visual scanning and computer aided reconstruction. *Annals of Forest Science*, *60*: 137–144.

Pinto, I., Usenius, A., Song, T., and Pereira, H. (2005). Sawing simulation of maritime pine (*Pinus pinaster* Ait.) stems for production of heartwood containing components. *Forest Products Journal*, *55*(4).

Pokharel, B., Dech, J. P., Groot, A., and Pitt, D. (2014). Ecosite-based predictive modeling of black spruce (*Picea mariana*) wood quality attributes in boreal Ontario. *Canadian Journal of Forest Research*, 44(5), 465-475.

Pokharel, B., Groot, A., Pitt, D., Woods, M., and Dech, J. (2016). Predictive Modeling of Black Spruce (*Picea mariana* (Mill.) B.S.P.) Wood Density Using Stand Structure Variables Derived from Airborne LiDAR Data in Boreal Forests of Ontario. *Forests*, 7(12): 311.

Rinn, F., Schweingruber, F. H. and Schär, E. (1996). Resistograph and X-Ray Density Charts of Wood. Comparative Evaluation of Drill Resistance Profiles and X-ray Density Charts of Different Wood Species. *Holzforschung - International Journal of the Biology, Chemistry, Physics and Technology of Wood.* 50: 303-311.

Roth, B. E., Li, X., Huber, D. A. and Peter, G. F. (2007). Effects of management intensity, genetics and planting density on wood stiffness in a plantation of juvenile loblolly pine in the southeastern USA. *Forest Ecology and Management,* 246(2–3): 155-162.

RStudio (2016). Version 1.0.136 – © 2009-2016 RStudio, Inc.

Sandberg, K. and Salin, J. (2012). Liquid water absorption in dried Norway spruce timber measured with CT scanning and viewed as a percolation process. Wood Science and Technology (46) 207-219.

Schindelin, J., Rueden, C. T. and Hiner, M. C. (2015). The ImageJ ecosystem: an open platform for biomedical image analysis. *Molecular Reproduction and Development*, Google Scholar PMID 26153368.

Schmoldt, D. L., Li, P. and Araman, P. A. (1996). Interactive simulation of hardwood log veneer slicing using CT images. *Forest Products Journal*, 46(4): 41–47.

Ukrainetz, N. K. and O'Neill G. A. (2010). An analysis of sensitivities contributing measurement error to Resistograph values. *Canadian Journal of Forest Research*, 40(4): 806-811.

Waghorn, M. J., Mason E. G. and Watt, M. S. (2007). Influence of initial stand density and genotype on longitudinal variation in modulus of elasticity for 17-year-old *Pinus radiata*. *Forest Ecology and Management*, 252: 67-72.

Wang, X., Ross, R.J., McClellan, M., Barbour, R.J., Erickson, J.R., Forsman, J. W. and McGinnis, G.D. (2001). Non-destructive evaluation of standing trees with a stress wave method. *Wood and Fiber Science* 33(4):522-533.

Wang, X., Ross, R.J. and Carter P. (2007). Acoustic evaluation of wood quality in standing trees. Part 1- acoustic wave behaviour. Wood and fiber science 39(1) 28-38.

Wang X., Carter P., Ross R.J. and Brashaw B.K. (2007). Acoustic assessment of wood quality of raw forest materials - A path to increased profitability. *Forest Products Journal* 57(5):6-14.

Watt, M. S. and Trincado, G. (2014). Modelling between tree and longitudinal variation in green density within *Pinus radiata*: implications for estimation of MOE by acoustic methods. *New Zealand Journal of Forestry Science* 44(1): 1-10.

Watt, M. S. and Zoric B. (2010). Development of a model describing modulus of elasticity across environmental and stand density gradients in plantation-grown *Pinus radiata* within New Zealand. *Canadian Journal of Forest Research* 40(8): 1558-1566.

West, G.B., Brown, J.H. and Enquist, B.J. (2001). A general model for ontogenetic growth. Nature Oct 11; 413(6856):638-31. DOI: 10.1038/35098076.

Wielinga, B., Raymond, C. A., James R. and Matheson A. C. (2009). Genetic parameters and genotype by environment interactions for green and basic density and stiffness of *Pinus radiata* D. Don estimated using acoustics. *Silvae Genetica* 58(3): 112-122.

Zeller, L., Ammer, C., Annighöfer, P., Biber, P., Marshall, J., Schütze, G., Rio Gaztelurrutia, M. and Pretzsch, H. (2017). Tree ring wood density of Scots pine and European beech lower in mixed-species stands compared with monocultures. *Forest Ecology and Management,* 400: 363-374.

Zimmer. K.P., Hoibo, O.A., Vestol, G.I. and Larnoy, E. (2014). Variation in treatability of Scots pine sapwood: a survey of 25 different northern European locations. Wood Science and Technology (48) 1049-1068.

Zobel, B. J., and Sprague, J. R. (1998). JUVENILE WOOD IN FOREST TREES (21–55). Berlin Heidelberg, Springer-Verlag 304p.

Zobel, B. J. and van Buijtenen J.P. (1989). WOOD VARIATION ITS CAUSES AND CONTROL. Berlin Heidelberg, Springer-Verlag. 363p.

12 Acknowledgements

13 Researcher's disclaimer

The information contained herein is subject to change without notice. The authors shall not be liable for technical or other errors or omissions contained herein. The reader/user accepts all risks and responsibility for losses, damages, costs and other consequences resulting directly or indirectly from using this information.

14 Appendices

14.1 Appendix 1. Site and location information for the study

14.1.1 Selection of growth plots in Queensland

The initial basis for the development of a sampling strategy in Queensland was informed by a report by Nester 2014 (internal report commissioned by HQPlantations in the lead up to the project). He recommended a stratified sampling approach be adopted across plantation nodes including: taxa, site index, age class and prior land use history.

In the adopted sampling strategy, we limited the project to the three major southern pine taxa (PCH = *P. caribaea* var. *hondurensis*, PEE = *Pinus elliottii* var. *elliottii* and hybrid pine (PEE x PCH, both F_1 and F_2 hybrids) across age ranges: thinning age (15 to 20 years old) and harvest age (25-36 years). Three southern pine nodes in SEQ were included in the study: Wongi (north of Maryborough), Tuan-Toolara (Maryborough to Gympie region: the largest node) and Beerburrum (south of Caloundra) accounting for approximately 100,000 ha of southern pine plantations (Figure 106).

Given we were sampling three distinct locations in Queensland (Wongi, Tuan-Toolara and Beerburrum), up to three taxa at each location and a range of site index classes and age classes, the decision was made to locate existing growth plots covering as many of the combinations as possible. In addition we included ex-pasture, ex-native forest and second rotation sites to examine the impact of prior land use on wood quality.

In SEQ, we selected trees from four site index classes (site index is based on the height of the tallest 50 trees per hectare at age 25 years). The site index classes targeted were: 22-24 m, 25-27 m, 28-30 m and 31-33 m. In addition five age classes; one being post thinning (15-20 years old) and four representing harvest age (25-36 years) for each of the three taxa included in the study. Selected plots were then overlayed on taxa and planting age maps which showed an excellent distribution of plots across the range of the plantings for the respective taxon and planting ages. In total 79 plots were measured and sampled in Queensland.

14.1.2 Selection of growth plots on the NSW estate.

In the FCNSW estate, site index, age, location and southern pine taxa were also considered when selecting sites to measure, assess and core. As permanent growth plots were not available, compartments were nominated based on their age profile of 15-20 years (similar to the thinning age plots in Queensland) and older compartments (25-27 years old) representing the oldest plantings of the hybrid pine (F_1 and F_2), the focus of the work in NSW. Other factors considered included the distribution of the compartments across the estate, the ability to compare and contrast the wood properties of different southern pine taxa (pine hybrid, PEE and *P. taeda*) and the potential to value add to the project by including compartments already assessed in previous wood properties studies (e.g. Palmer and Brown 2013, FCNSW internal report, no date). Based on this, 12 plots were established in NSW: eight in the region near Whiporie and four near Yabbra (Figure 8).

14.1.3 Sampling in genotype × spacing trials

This component of the study involved measures and assessments of two Genotype × spacing trials in Queensland.

• Experiment 622NC, a taxon (three F_1 clones and a single F_1 family) × spacing trial planted during March 1997 at SF 611 Beerburrum. The trees were 19 years old at the time of measurement and sampling in October 2016 and represent a broad range of stocking rates: 200, 333, 500, 666 and 1,000 spha. These are low to moderately high stocking rates

representing a range of low to intermediate inter-tree competition effects. Thirty trees were also destructively sampled from this trial (see section 5.2.2).

• Experiment 288GYM a taxon (10 F_1 clones) × spacing trial (Nelder Wheel trial) planted in May 1993 in SF 1004 Toolara in the Fraser Coast, Queensland. The trial was established with the research objective to quantify the effect of spacing on F_1 hybrid performance (growth, branch, crown and stem characteristics). The trees were approximately 24 years old when measured and sampled during February 2017 and represent a broad range of stocking rates: 229, 314, 423, 552, 1,006, 1,404, 2,020 and 2,660 spha. These range from very low to very high stockings rates for southern pine. Eight trees of the clone F_1 hybrid clone 887 (which was sampled in the other genotype × spacing trial) were also destructively sampled from this trial.
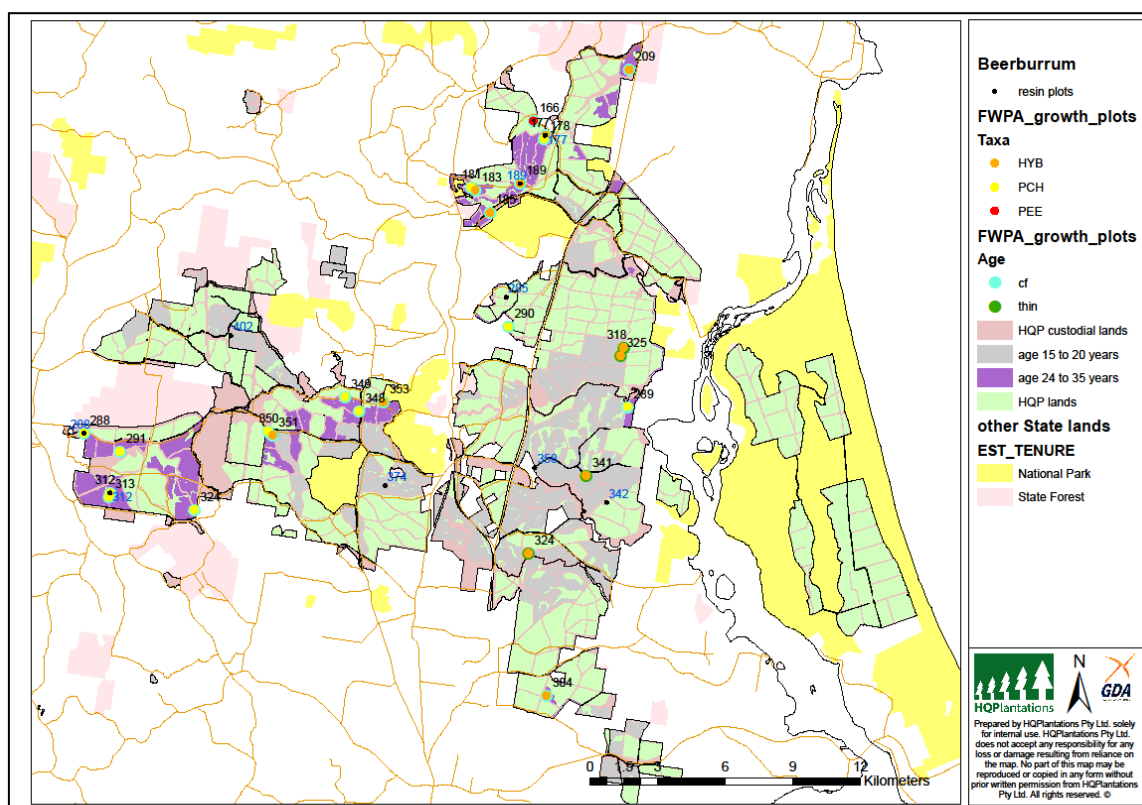
Figure 106. Example map detailing the plots to be sampled for ST300, cores and resin on HQPlantations land near Beerburrum. Age classes of interest are grey (15-20 years old) and purple (24-35 years old).

130

14.1.4 Sampling within the growth plots

Across all growth plots measured, assessed and sampled we used a stratified sampling strategy to capture data on the trees.

Collection of ST300, core samples and IML Resistograph data

The initial 10 plots assessed were used as a pilot study to determine the sampling intensity for the remainder of the trial. For these plots, two cores per 15 selected trees were extracted. One core was taken at 1.2 m above ground, parallel to the row and the second core at 0.7 m above ground perpendicular to the row. In addition, ST300 data were collected for the 300 pilot study trees. The results from the ST300 trial are presented in Figure 107 and Figure 108 which shows a strong correlation between the two measures taken for each tree. A simple linear regression forced through the origin shows a 1:1 relationship which explained 80% of the variation.

Figure 107 shows that the plot means were very similar for the two sampling positions (along and across the planting row. Based on an analysis of the results from these cores it was decided that only a single core was required from each tree, and all remaining plots were cored only at the 1.2 m height parallel to (along) the row direction.
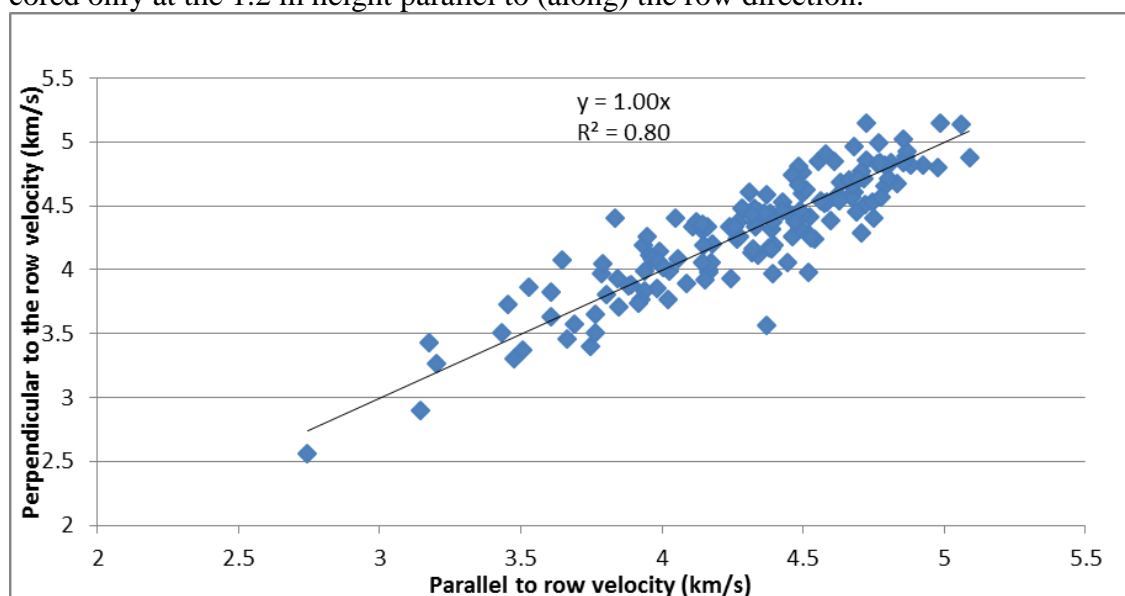
Figure 107. ST300 acoustic velocity perpendicular to the row (Y-axis) versus velocity parallel to the row (X-axis) for the trees measured in the pilot study (10 plots × 15 trees × two axes).
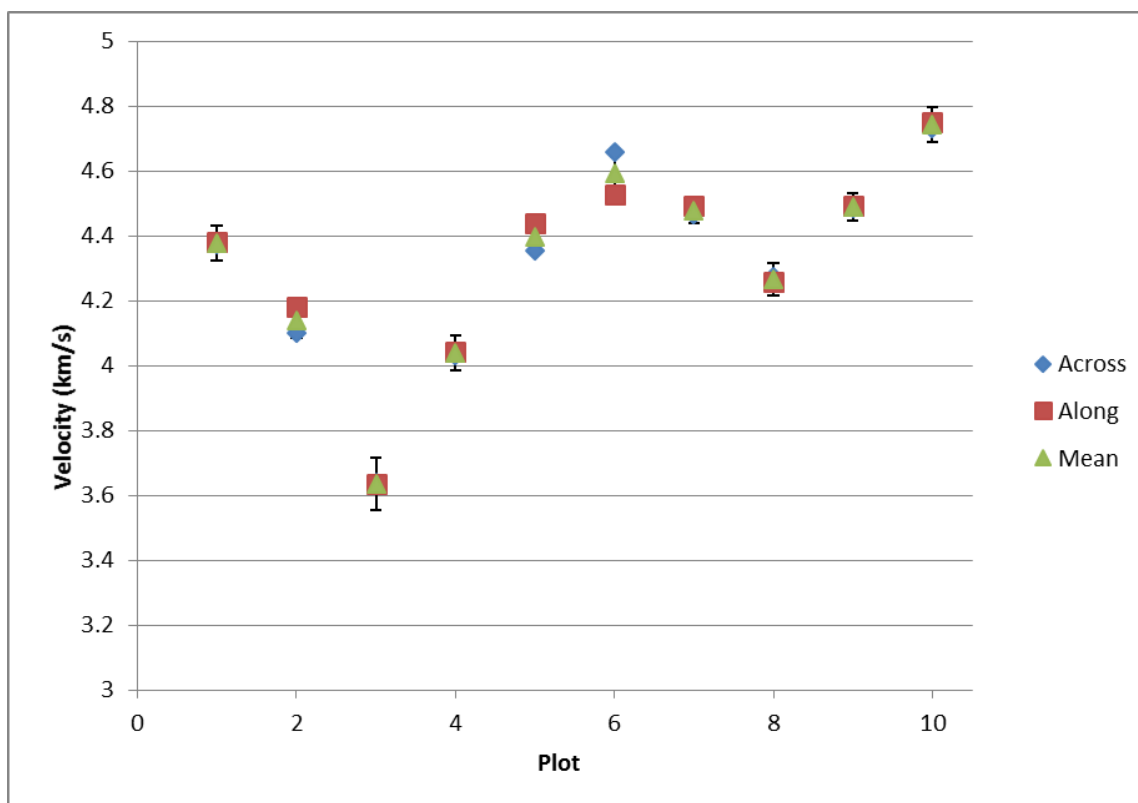
Figure 108. Average ST300 velocity of the 30 trees in each pilot study plot. Bars indicate standard error of the 'Mean' plot velocity

Data was collected from 91 growth plots

- In these 91 growth plots (79 in Qld and 12 in NSW), field data on row direction, aspect, slope and moisture was collected. A stratified sampling was used to select ~30 trees, representing the full range of diameter classes available from the plot. Each tree was measured for total height with a Vertex IV (Haglof, Sweden AB), DBHOB, lean (degrees), height to and type of limiting defect, ovality of the tree at 1.3 m (using callipers) and time of flight (ToF) acoustics using the Director ST300 (Fibre-gen, Christchurch, New Zealand).

- In a subset of 54 growth plots, 15 trees (of those measured and assessed using the ST300), had bark-to-bark cores collected at 1.2 m above ground level, with cores collected along the planting row. Selection of these trees to core was also based on stratified sampling to ensure the full range of diameter classes available within the plot were sampled.

- IML Resistograph traces were collected from the same 30 trees sampled using the ST300, for 81 growth plots. This data was captured approximately four months following the end of the previous measures and sampling. During this time, 10 growth plots had been harvested, so Resistograph traces / data are not available for these plots. Resistograph traces were collected within 10 cm of 1.2 m point above ground level along the planting row and parallel to any previous cores taken from the trees, to allow direct comparison between cores and Resistograph predictions of density and MOE.

14.1.5 Sampling within the Genotype × spacing trials

In Experiment 622NC data was collected across the whole trial with 15 trees × each genotype (three F_1 clones [clones 522, 625 and 887] and one F_1 family [Batch 4957 ex Beerburrum nursery]) × five spacing treatments (200, 333, 500, 666 and 1,000 spha). Selection of trees to measure and assess in each field plot was based on stratified sampling to ensure the full range

of diameter classes available within the plot were sampled. For each tree total height, DBHOB, lean (degrees), height to and type of limiting defect, ovality of the tree at 1.3 m, time of flight (ToF) acoustics using the Director ST300 (Fibre-gen, Christchurch, New Zealand) and IML Resistograph traces were collected.

In Experiment 288GYM data was collected from two replicates in the trial across eight stocking rates: 229, 314, 423, 552, 1006, 1404, 2020 and 2660 spha. For each tree total height, DBHOB, lean (degrees), height to and type of limiting defect, ovality of the tree at 1.3 m, time of flight (ToF) acoustics using the Director ST300 (Fibre-gen, Christchurch, New Zealand) and IML Resistograph traces were collected.

14.1.6 Sacrificial plots: destructive sampling on commercial and experimental plots

The first batch comprised 30 sacrificial trees from a growth plot located within a typical commercial plantation, compartment 25B Cowra Logging Area (LA) in State Forest 915 Tuan, near Maryborough, Queensland (Figure 109). These trees provided a proportional representation of the range and distribution of diameter stem classes for the compartment. The taxon was F_2 hybrid (second filial hybrid, *Pinus elliottii* var. *elliottii* × *P. caribaea* var. *hondurensis,* PEE × PCH cross) and the site was planted during May 1987 giving the trees an age of 29 years old at the time of harvest in April 2016. The stocking rate at the time of harvest was 388 stems per hectare (spha) which provided representative trees from a relatively open plantation with typical post-thinning spacing and minimal inter-tree competition.

Figure 109. The F_2 hybrid 30 logs, selected from a typical commercial plantation at Tuan.

The remaining trees for destructive sampling were sourced from two separate spacing trials. These trials were included to provide an insight to the effects of cambial age and levels of inter-tree competition on development of wood properties and characteristics. Eight trees were harvested in February 2017 from a Nelder Wheel format spacing trial of ten F_1 hybrid clones. This Nelder Wheel trial (Experiment 288GYM; Figure 110) is located in Compartment 81B Elliott LA, SF 1004 Toolara in the Fraser Coast region of south-east

Queensland. The trial was established in May 1993 on a second rotation site with the research objective to quantify the effect of spacing on F_1 hybrid performance (branch, crown and stem characteristics). The trees were approximately 24 years old when harvested during February 2017. The four stocking rates represented by the selected trees were 1,006 spha, 1,404 spha, 2,020 spha and 2,660 spha which are relatively high to very high stockings, representing strong inter-tree competition. All trees were of the same genetic origin (clone C887).
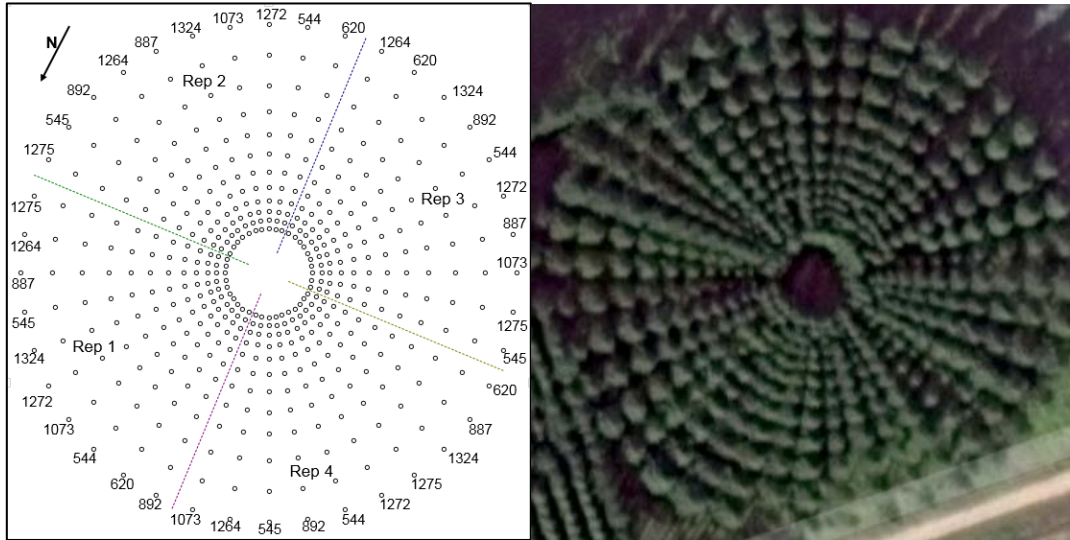
Figure 110. Experiment 288GYM- Nelder Wheel plot layout showing high inter-tree competition near the centre and wide spacing near the periphery.

The second spacing trial provided 31 trees of which one was later rejected due to its small size and another was unable to be fully tested as it was broken during harvesting and handling. The trees were extracted from Experiment 622NC, an F_1 taxon × spacing trial planted during March 1997 within Compartment 202 Donnybrook LA, SF 611 Beerburrum, north of Brisbane, Queensland (Figure 111). The trees were 19 years old at the time of harvest in October 2016 and represent material from three different genetic origins (F_1 seedling, clone C887 (same as that collected in the other spacing trial) and clone C625) and a broad range of stocking rates, from wide spacing at 200 spha and 333 spha, medium stocking rates of 500 spha and 666 spha, to high stocking at 1,000 spha.

Figure 111. Selecting trees for destructive sampling from Experiment NC622 spacing trials, Beerburrum.

Table 5. Site descriptions and types of wood quality data collected.

Experiment	Growth plot	State Forest	Location	Latitude	Longitude	Taxon	Measure age	ST300 data	Core data	Resistograph data	Broad location	Age range
Resource characterisation plots sampled												
1FWP	641	1004	Cpt 202A Nth Dempster LA, SF 1004	-26.00	152.82	F2	29.3	yes	yes	yes	Toolara	28.0 to 30.9
2FWP	623	1004	Cpt 103 Nth Dempster LA, SF 1004	-26.00	152.80	PCH	29.3	yes	yes	yes	Toolara	28.0 to 30.9
3FWP	622	1004	Cpt 102A Nth Dempster LA, SF 1004	-26.00	152.81	PCH	29.3	yes	yes	yes	Toolara	28.0 to 30.9
4FWP	643	1004	Cpt 112 Sth Dempster LA, SF 1004	-26.09	152.86	F2	28.4	yes	yes	yes	Toolara	28.0 to 30.9
5FWP	634	1004	Cpt 201A Sth Dempster LA, SF 1004	-26.00	152.84	F2	29.3	yes	yes	yes	Toolara	28.0 to 30.9
6FWP	604	915	Cpt 10B Hakea LA, SF 915	-25.82	152.84	PCH	29.5	yes	yes	yes	Tuan	28.0 to 30.9
7FWP	324	589	Cpt 18 Woodford LA, SF 589	-26.97	152.84	PCH	29.3	yes	yes	yes	Beerburrum	28.0 to 30.9
8FWP	181	561	Cpt 201 Bluegum LA, SF 561	-26.85	152.97	PCH	30.4	yes	yes	no	Beerburrum	28.0 to 30.9
9FWP	185	561	Cpt 203A Bluegum LA, SF 561	-26.86	152.98	F2	28.3	yes	yes	yes	Beerburrum	28.0 to 30.9
10FWP	189	561	Cpt 206 Bluegum LA, SF 561	-26.85	152.99	F2	29.4	yes	yes	no	Beerburrum	28.0 to 30.9
11FWP	239	1294	Cpt 6 Duckinwilla LA, SF 1294	-25.39	152.39	PCH	26.7	yes	yes	yes	Wongi	24.0 to 27.9
13FWP	223	1294	Cpt 20 Harwood LA, SF 1294	-25.43	152.48	PCH	27.8	yes	yes	yes	Wongi	24.0 to 27.9
14FWP	189	1294	Cpt 6 Harwood LA, SF 1294	-25.46	152.45	F2	30.3	yes	no	yes	Wongi	28.0 to 30.9
15FWP	188	1294	Cpt 5 Harwood LA, SF 1294	-25.46	152.45	PCH	29.7	yes	yes	yes	Wongi	28.0 to 30.9
16FWP	218	1294	Cpt 001B Harwood LA, SF 1294	-25.45	152.51	F2	27.7	yes	yes	yes	Wongi	24.0 to 27.9
17FWP	220	1294	Cpt 001B Harwood LA, SF 1294	-25.45	152.50	F2	27.7	yes	yes	yes	Wongi	24.0 to 27.9
18FWP	143	1294	Cpt 45 Saltwater LA, SF 1294	-25.45	152.54	PCH	33.4	yes	yes	no	Wongi	31.0 to 35.5
19FWP	147	1294	Cpt 034B Saltwater LA, SF 1294	-25.46	152.59	PCH	33.4	yes	yes	yes	Wongi	31.0 to 35.5
20FWP	176	1294	Cpt 16 Bruce LA, SF 1294	-25.44	152.65	PCH	30.8	yes	yes	yes	Wongi	28.0 to 30.9
21FWP	618	915	Cpt 19 Melaleuca LA, SF 915	-25.59	152.74	PEE	31.7	yes	yes	yes	Tuan	31.0 to 35.5
24FWP	680	915	Cpt 30 Boonooroo LA, SF 915	-25.62	152.82	F2	26.9	yes	no	yes	Tuan	24.0 to 27.9
25FWP	649	915	Cpt 75 Talegalla LA, SF 915	-25.71	152.68	PCH	27.6	yes	yes	yes	Tuan	24.0 to 27.9
26FWP	769	915	Cpt 228 Magnolia LA, SF 915	-25.70	152.73	PCH	18.7	yes	yes	yes	Tuan	16.0 to 21.0
27FWP	770	915	Cpt 228 Magnolia LA, SF 915	-25.70	152.74	PCH	18.7	yes	yes	yes	Tuan	16.0 to 21.0
28FWP	777	915	Cpt 220A WEST LA, SF 915	-25.72	152.75	F2	18.8	yes	yes	yes	Tuan	16.0 to 21.0
29FWP	671	957	Cpt 10 Baker LA, SF 957	-25.77	152.69	PCH	26.8	yes	yes	yes	Tuan	24.0 to 27.9
30FWP	674	957	Cpt 8 Baker LA, SF 957	-25.76	152.69	PCH	26.8	yes	yes	yes	Tuan	24.0 to 27.9
31FWP	751	915	Cpt 203A Tahiti LA, SF 915	-25.75	152.81	F1	19.8	yes	yes	yes	Tuan	16.0 to 21.0
32FWP	610	915	Cpt 023B Cowra LA, SF 915	-25.75	152.93	F2	29.9	yes	yes	yes	Tuan	28.0 to 30.9
33FWP	626	915	Cpt 023A Cowra LA, SF 915	-25.75	152.93	PEE	30.7	yes	no	yes	Tuan	28.0 to 30.9
34FWP	572	915	Cpt 022A Cowra LA, SF 915	-25.76	152.92	PEE	33.6	yes	no	yes	Tuan	31.0 to 35.5
35FWP	834	915	Cpt 209 MissingS LA, SF 915	-25.82	152.73	PCH	16.8	yes	yes	yes	Tuan	16.0 to 21.0
36FWP	661	915	Cpt 60 Lomatia LA, SF 915	-25.82	152.75	F1	27.8	yes	no	yes	Tuan	24.0 to 27.9
37FWP	659	915	Cpt 58 Lomatia LA, SF 915	-25.83	152.75	PCH	27.8	yes	no	yes	Tuan	24.0 to 27.9
38FWP	654	915	Cpt 061A Lomatia LA, SF 915	-25.82	152.77	F1	27.8	yes	yes	yes	Tuan	24.0 to 27.9
39FWP	665	915	Cpt 021B Hakea LA, SF 915	-25.84	152.81	F2	27.9	yes	no	yes	Tuan	24.0 to 27.9
40FWP	662	915	Cpt 018B Hakea LA, SF 915	-25.83	152.81	F2	27.9	yes	no	yes	Tuan	24.0 to 27.9
41FWP	637	915	Cpt 64 MissingS LA, SF 915	-25.89	152.76	PCH	28.9	yes	no	yes	Tuan	28.0 to 30.9
42FWP	45	1419	Cpt 15 Tinana LA, SF 1419	-25.88	152.76	PCH	28.0	yes	yes	yes	Toolara	24.0 to 27.9
43FWP	657	1004	Cpt 47 Ulirraba LA, SF 1004	-25.88	152.77	PCH	28.9	yes	no	yes	Toolara	28.0 to 30.9
44FWP	658	1004	Cpt 49 Ulirraba LA, SF 1004	-25.89	152.78	F2	28.9	yes	yes	yes	Toolara	28.0 to 30.9
45FWP	661	1004	Cpt 51 Ulirraba LA, SF 1004	-25.90	152.78	F2	28.9	yes	yes	yes	Toolara	28.0 to 30.9
46FWP	37	1419	Cpt 4 Taurus LA, SF 1419	-25.90	152.75	F2	27.8	yes	yes	yes	Toolara	24.0 to 27.9
47FWP	87	1419	Cpt 16 Bungawatta LA, SF 1419	-25.95	152.72	F2	26.0	yes	no	yes	Toolara	24.0 to 27.9
49FWP	91	1419	Cpt 17 Bungawatta LA, SF 1419	-25.94	152.73	F1	26.0	yes	no	yes	Toolara	24.0 to 27.9
50FWP	633	1004	Cpt 94 Nth Dempster LA, SF 1004	-25.94	152.79	F2	29.9	yes	no	yes	Toolara	28.0 to 30.9
54FWP	71	1419	Cpt 23 Red Ridge LA, SF 1419	-25.98	152.77	F1	20.0	yes	no	yes	Toolara	16.0 to 21.0
55FWP	70	1419	Cpt 23 Red Ridge LA, SF 1419	-25.98	152.77	F1	20.0	yes	no	yes	Toolara	16.0 to 21.0
56FWP	628	1004	Cpt 98 Nth Dempster LA, SF 1004	-25.96	152.79	PCH	30.0	yes	no	yes	Toolara	28.0 to 30.9
57FWP	765	1004	Cpt 213A Kelly LA, SF 1004	-25.95	152.84	F1	17.3	yes	no	yes	Toolara	16.0 to 21.0
58FWP	726	1004	Cpt 217A Kelly LA, SF 1004	-25.97	152.83	F2	19.2	yes	yes	yes	Toolara	16.0 to 21.0
59FWP	779	1004	Cpt 211 Elliott LA, SF 1004	-25.99	152.87	PEE	17.0	yes	yes	yes	Toolara	16.0 to 21.0
60FWP	730	1004	Cpt 210A Sth Dempster LA, SF 1004	-26.04	152.83	PEE	19.2	yes	no	yes	Toolara	16.0 to 21.0
61FWP	731	1004	Cpt 210A Sth Dempster LA, SF 1004	-26.04	152.83	F1	19.3	yes	yes	yes	Toolara	16.0 to 21.0
63FWP	573	1004	Cpt 106 Sth Dempster LA, SF 1004	-26.10	152.88	PCH	33.0	yes	yes	yes	Toolara	31.0 to 35.5
64FWP	575	1004	Cpt 105 Sth Dempster LA, SF 1004	-26.11	152.87	PCH	33.0	yes	no	yes	Toolara	31.0 to 35.5
65FWP	574	1004	Cpt 102 Sth Dempster LA, SF 1004	-26.13	152.87	PCH	33.0	yes	no	yes	Toolara	31.0 to 35.5
66FWP	571	1004	Cpt 65 Como LA, SF 1004	-26.16	152.89	PCH	33.0	yes	no	yes	Toolara	31.0 to 35.5
67FWP	566	1004	Cpt 48 Como LA, SF 1004	-26.15	152.89	PCH	34.0	yes	yes	yes	Toolara	31.0 to 35.5
68FWP	565	1004	Cpt 43 Como LA, SF 1004	-26.15	152.91	PCH	34.0	yes	yes	yes	Toolara	31.0 to 35.5
69FWP	603	1004	Cpt 70 Como LA, SF 1004	-26.17	152.90	PEE	32.9	yes	yes	no	Toolara	31.0 to 35.5
70FWP	209	561	Cpt 9 Landsborough LA, SF 561	-26.80	153.04	F1	26.1	yes	yes	yes	Beerburrum	24.0 to 27.9
72FWP	177	561	Cpt 210A Bluegum LA, SF 561	-26.83	153.00	F1	32.2	yes	yes	yes	Beerburrum	31.0 to 35.5
73FWP	178	561	Cpt 210A Bluegum LA, SF 561	-26.83	153.00	PCH	32.2	yes	no	no	Beerburrum	31.0 to 35.5
74FWP	183	561	Cpt 201 Bluegum LA, SF 561	-26.85	152.97	F1	31.2	yes	no	yes	Beerburrum	31.0 to 35.5
76FWP	291	589	Cpt 5 Woodford LA, SF 589	-26.95	152.81	PCH	35.1	yes	no	no	Beerburrum	31.0 to 35.5
80FWP	351	589	Cpt 201 Twins LA, SF 589	-26.95	152.88	F2	28.0	yes	no	yes	Beerburrum	24.0 to 27.9
81FWP	349	589	Cpt 210 Tibrogargan LA, SF 589	-26.93	152.91	PCH	27.4	yes	yes	yes	Beerburrum	24.0 to 27.9
82FWP	348	589	Cpt 210 Tibrogargan LA, SF 589	-26.94	152.92	PCH	27.4	yes	no	yes	Beerburrum	24.0 to 27.9
83FWP	353	589	Cpt 215 Tibrogargan LA, SF 589	-26.93	152.93	F2	28.1	yes	no	yes	Beerburrum	28.0 to 30.9
84FWP	290	611	Cpt 002D WARNES LA, SF 611	-26.90	152.98	PCH	28.0	yes	no	yes	Beerburrum	24.0 to 27.9
85FWP	325	611	Cpt 207 Black Swamp LA, SF 611	-26.91	153.03	F2	20.1	yes	yes	yes	Beerburrum	16.0 to 21.0
86FWP	318	611	Cpt 207 Black Swamp LA, SF 611	-26.91	153.04	F1	20.1	yes	no	yes	Beerburrum	16.0 to 21.0
88FWP	341	611	Cpt 215 Tripconys LA, SF 611	-26.96	153.02	F2	19.1	yes	no	yes	Beerburrum	16.0 to 21.0
89FWP	324	611	Cpt 210 Donnybrook LA, SF 611	-26.99	152.99	F1	20.4	yes	yes	yes	Beerburrum	16.0 to 21.0
90FWP	304	611	Cpt 201A Toorbul LA, SF 611	-27.05	153.00	F2	27.1	yes	no	yes	Beerburrum	24.0 to 27.9
91FWP	630	915	Cpt 025B Cowra LA, SF 915	-25.79	152.91	F2	28.9	yes	yes	no	Tuan	28.0 to 30.9
93FWP	93	1419	Cpt 14 Bungawatta LA, SF 1419	-25.94	152.73	PCH	26.3	yes	no	no	Toolara	28.0 to 30.9
201FWP	201	Whiporie	Cpt 359 Whiporie (Camira) NSW	-29.21	152.96	F2	25.4	yes	no	yes	Whiporie	24.0 to 27.9
202FWP	202	Whiporie	Cpt 357 Whiporie (Camira) NSW	-29.22	152.95	PEE	24.4	yes	yes	yes	Whiporie	24.0 to 27.9
203FWP	203	Whiporie	Cpt 360 Whiporie (Camira) NSW	-29.22	152.96	F2	24.4	yes	yes	yes	Whiporie	24.0 to 27.9
204FWP	204	Whiporie	Cpt 111 Whiporie SF	-29.28	153.01	F2	25.4	yes	yes	yes	Whiporie	24.0 to 27.9
205FWP	205	Whiporie	Cpt 140 Whiporie NSW	-29.26	153.00	F1	20.4	yes	yes	yes	Whiporie	24.0 to 27.9
206FWP	206	Whiporie	Cpt 357 Whiporie (Camira) NSW	-29.22	152.95	PEE	25.4	yes	yes	yes	Whiporie	24.0 to 27.9
207FWP	207	Whiporie	Cpt 353 Whiporee (Camira) NSW	-29.24	152.98	F2	26.4	yes	yes	yes	Whiporie	24.0 to 27.9
208FWP	208	Whiporie	Cpt 351 Whiporie (Camira) NSW	-29.24	152.98	LBP	26.4	yes	no	yes	Whiporie	24.0 to 27.9
209FWP	209	Yabbra	Cpt 755 Yabbra (Bryants) NSW	-28.51	152.49	F2	20.4	yes	yes	yes	Yabbra	16.0 to 21.0
210FWP	210	Yabbra	Cpt 755 Yabbra (Bryants) NSW	-28.51	152.49	F2	20.4	yes	yes	yes	Yabbra	16.0 to 21.0
211FWP	211	Yabbra	Cpt 765 Yabbra (Bryants) NSW	-28.50	152.51	F2	19.4	yes	yes	yes	Yabbra	16.0 to 21.0
212FWP	212	Yabbra	Cpt 765 Yabbra (Bryants) NSW	-28.50	152.50	F2	19.4	yes	no	yes	Yabbra	16.0 to 21.0
999FWP	640	1004	Cpt 202A Nth Dempster LA, SF 1004	-26.00	152.82	F2	29.2	yes	no	no	Toolara	28.0 to 30.9
Genotype x spacing trials												
288FWP	288GYM	1004	Cpt 81B Elliott LA, SF 1004	-25.98	152.88	F1	23.8	yes (162 trees)	yes (8 trees)	yes (162 trees)	Toolara	24.0 to 27.9
622FWP	622NC	611	Cpt 201 Donnybrook LA, SF 611	-26.98	152.98	F1	19.6	yes (622 trees)	yes (31 trees)	yes (621 trees)	Beerburrum	16.0 to 21.0

135

14.2 Appendix 2. Components of the wood value platform

14.2.1 Increment cores

Introduction and literature review

Increment borers are used to extract cores from living and dead trees for analysis of growth trends of tree ring patterns and to evaluate wood quality. The coring method is relatively inexpensive, rapid and simple.

Increment coring is the most widely used sampling technique for wood density analysis (Gao *et al.*, 2017). Kimberley *et al.*, (2015) developed a wood density model using historical wood density dataset values obtained from increment cores and stem discs from almost 10,000 trees at over 300 sites of radiata pine (*P. radiata*) grown in New Zealand. They developed two sub models: one for predicting radial variation in breast height wood density and another for predicting distribution of density along the height. The model using both ring number and ring width predicted wood density better than the model that only considered ring number. In a separate study, they also developed models to explain the variation of wood density among sites and among trees within stands and radial and longitudinal variation of wood density (Kimberley *et al.*, 2017).

Similarly increment coring has been used to analyse wood density and annual ring width in Scots pine (*P. sylvestris*) (Fries and Ericsson, 2006; Pokharel *et al.*, 2016). Gao *et al.* (2017) cited that increment corers have been used as a standard method for assessing wood density in trees, whereas other methods such as torsiometer, Pilodyn, and nail withdrawal tools have had very limited success and cannot replace increment corers. Analysis of annual ring specific gravity of breast height (1.37 m) increment cores from 3,957 trees representing 147 plantations across the natural range of loblolly pine (*Pinus taeda*) showed that ring specific gravity increases with increasing age and varies significantly among physiographic regions (Jordan *et al.*, 2008).

Pokharel *et al.* (2014) extracted 127, 12 mm increment core samples at breast height from black spruce (*Picea mariana*) trees to model wood quality characteristics. Their models explained over 32% of variance, with estimated root mean squared errors of 40.4 kg/m^3 and 5.6% for density and latewood percentage, respectively.

Apart from density modelling, increment cores extracted from breast height have also been used to analyse other properties and factors affecting wood quality. Dinulica *et al.*, (2016) determined how wind regime affects the incidence of compression wood in silver fir (*Abies alba*) and found stronger wind effect in trees growing at higher elevation.

Hong *et al.*, (2015) investigated the efficiency of early selection for wood quality in forty year old Scots pine (*P. sylvestris*). A total of 778 wood increment cores were sampled from 179 full-sib families. They found that wood density, fibre coarseness, fibre wall thickness, and MOE increased from the pith to bark and plateaued around ages 24–27, whereas annual ring growth and microfibril angle exhibited a declining trend from the pith to bark, reaching a minimum around ages 24–27.

Zeller *et al.* (2017) investigated whether tree species mixing modifies tree ring wood density in Scots pine (*P. sylvestris*) and European beech (*Fagus sylvatica*). They analysed increment cores from 322 trees for tree ring width and tree ring wood density using a

LIGNOSTATION™ and found that tree ring width was 14% wider in mixed stands compared to pure stands for Scots pine, whereas, for European beech, tree ring widths were similar for both mixed and pure stands.

Wood density and MoE variation in boreal softwoods (black spruce, balsam fir, jack pine) and hardwoods (paper birch, trembling aspen) were estimated using near-infrared spectroscopy on 30,159 increment cores from 10,573 inventory plots (Giroud, Bégin, Defo and Ung, 2017). Higher temperature and precipitation increased overall wood density and MoE for all species.

Increment cores from white spruce (*Picea glauca*) analysed from 375 trees were extracted to investigate the influence of cambial age correlations between different wood traits and the possibility of early selection in order to help decision-making for the improvement of juvenile wood (Lenz *et al*., 2011). They found most correlations became stronger in magnitude in rings closer to the bark.

Ivković *et al.* (2008) collected 12 mm bark-to-bark increment cores at breast height (1.3 m) for basic density analysis and bark-to-pith cores were assessed by SilviScan to obtain individual ring value MOE, and ring-area weighted averages. The objective of the study was to examine the variability and relationship between stiffness, strength, shrinkage and basic wood properties. They found that the variability in wood stiffness and strength from pith-to-bark was very high with greatest change near the pith. For the prediction of billet MOE, the combination of ring width, density and microfibril angle showed good correlation (R^2=0.506). They concluded that although multiple regression can achieve good prediction (R^2=0.42) in billet stiffness, it has weak potential to predict wood strength and shrinkage (R^2=0.22).

Since the annual rings are readily distinguished for pines (*Pinus* spp*.,* Eberhardt & Samuelson, 2015), an increment borer is an efficient tool for dendrochronological analyses for these species (Grissino-Mayer, 2003).

Increment coring has been widely used for density analysis and developing correlation between properties. However, limited studies have been conducted to predict wood value with a focus on MOE. For example, in southern pine, Harding (2008) used 12mm diameter increment cores to assess extracted and un-extracted basic density, spiral grain and microfibril angle from a range of southern pine genetics and silvicultural trials. He reported moderate correlations between core MFA measured on Silviscan and stress wave velocity of the Fakopp and Wood Spec instruments. Kain (2003) also used a 12mm diameter increment core to assess spiral grain and variation in earlywood and lower latewood density and the ability to select for density in southern pine trials.

14.2.2 Tree coring

Taking a 12 mm core from a tree at breast height is a non-destructive method for collecting a large number of wood specimens to determine wood age, rates of growth and wood properties without the need to harvest the tree. Although less invasive tools are available, they cannot provide the same level of information as a full diametrical core of solid wood. Most non-destructive evaluation (NDE) methods provide indications of the qualities of the outer wood which is often the highest quality within the stem due to its typical higher stiffness and density and straighter grain. However, this zone of wood is often removed during conventional processing techniques and measurements taken from the periphery of the tree may not correlate well to the performance of the inner wood. Therefore transverse cores provide the most accurate, and greater breadth, of information across the full diameter.

For this project 1,130 transverse cores were extracted from representative trees across 54 plots. Plot selections were based on age classes to include thinning age (15 to 20 years old) and final harvest age plantations (25 to 36 years old). Within the plots trees were selected from a stratified sample based on the range and distribution of tree diameters.

Diametrical cores (bark-to-bark), were extracted using a cordless hammer drill fitted with the patented DAF 16 mm tree corer bit (DAF, 2015; Figure 112).

Figure 112. DAF tree corer system comprising a rechargeable hammer drill (top) and extension bar and corer bits (bottom).

The initial 10 plots accessed were used as a pilot study to determine the sampling intensity for the remainder of the project. For these pilot study plots, two cores per 15 selected trees were extracted. One core was taken at 1.2 m above ground, parallel to the row direction and the other was taken at 0.70 m above ground level perpendicular to the row. Based on an analysis of the results from these cores it was decided that only a single core was required from each tree, and all remaining plots were cored only at the 1.2 m height parallel to row direction.

Each core was placed in a vacuum-sealed bag to maintain its moisture content and to protect it from moulds and fungi. Of the 1,130 cores extracted, 1,018 were processed through the wood value platform to provide data for this report. Examples of an intact core and a segmented core are depicted in Figure 113.
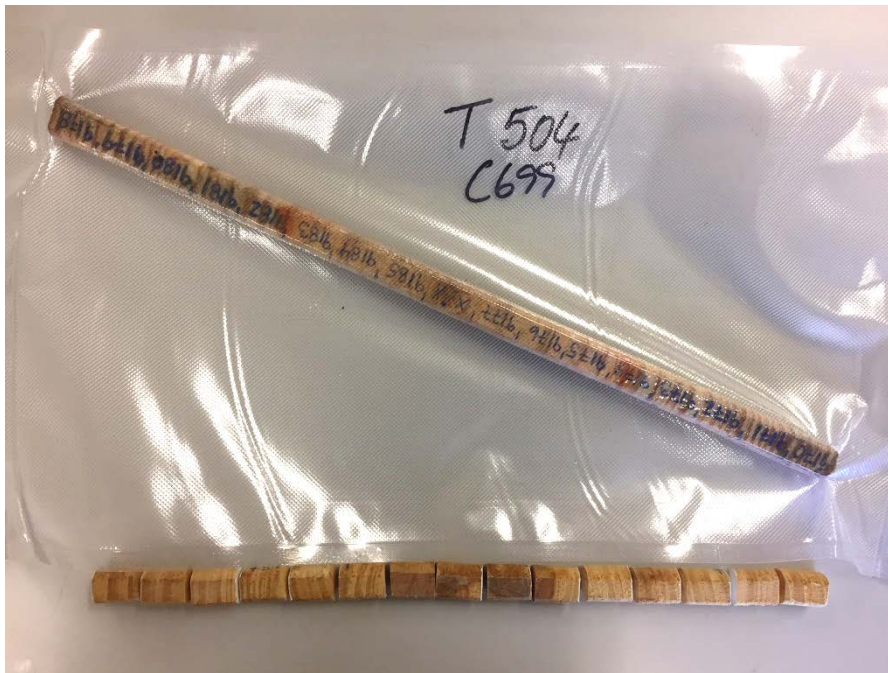
Figure 113. Increment core sample (top) and segmented core (bottom).

14.2.3 Diametrical samples from discs

Additional cores from four heights along the stem were cut out of discs retrieved from 68 destructively sampled trees (refer to section 5.2.2). These stems also provided sawlogs and peeling billets for extracting commercial products (boards and veneer sheets) which were subsequently tested according to Australian and New-Zealand standards. The diametrical cores cut out of these 272 discs were segmented and processed through the wood value platform as for the increment cores from the standing trees.

14.2.4 Referencing and age mapping

Cambial age refers to the age of the cambium when the wood was formed. On a seasonal basis it corresponds to the ring number when counting outwards from the pith. Cores were edged on two sides to provide flat contact surfaces for subsequent ultrasound testing. A high-definition colour scan was archived to retain a record of the full core. The cores were marked out at 20 mm intervals starting at the outer end (bark side) and a unique number marked on each segment. Based on the planting date for each plantation, the chronological age at the time of core extraction was determined and an allowance made for the position of the core (distance from ground level, apical age). Growth rings were transposed onto a booking sheet and the minimum, mean and maximum cambial and chronological ages for each 20 mm segment recorded (Figure 114). After mapping, the cores were segmented into 20 mm sections using a guillotine, ensuring no wood fibre was lost. As indicated above, each segment had a unique identifier to maintain chain-of-custody traceable to its original core, tree, plot, compartment and logging area. Numbering of core segments was from the outside toward the pith of the tree for each side of the tree. For example segment 1 = directly under the bark on the side of the tree where drilling into the tree was initiated. When the pith of the tree is reached number restarts from the first segment on the opposite side of the tree (directly under the bark) so the segments with the highest number from each side are closest to the pith.
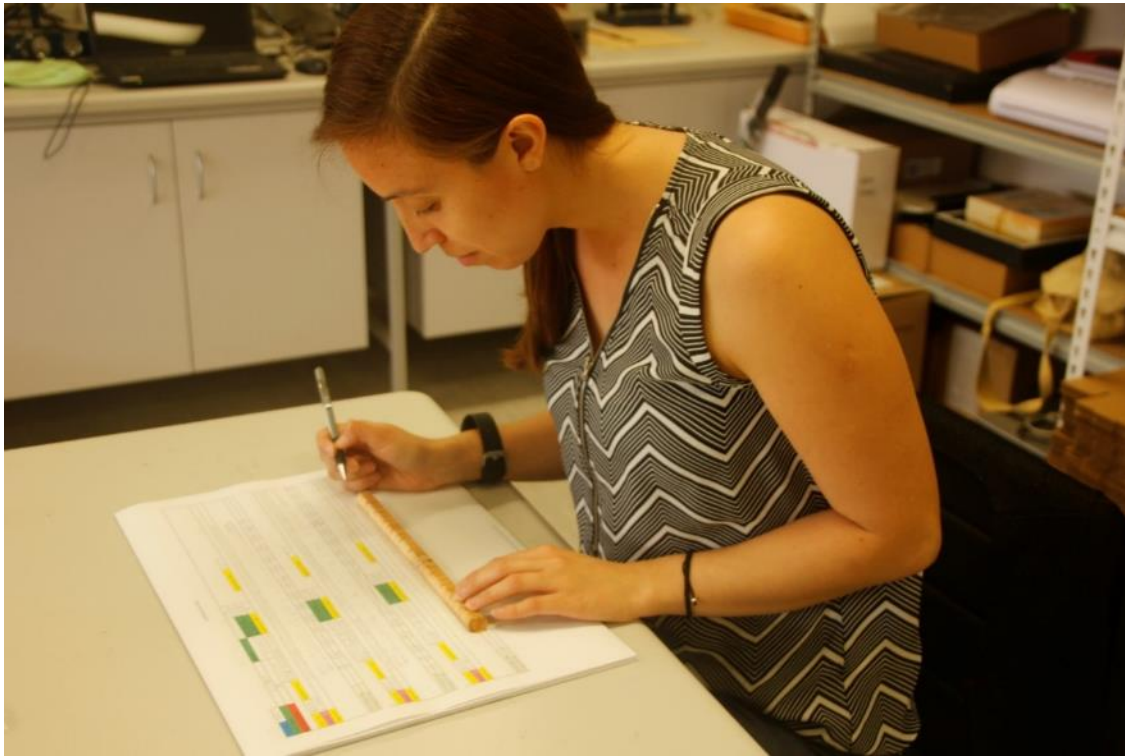
Figure 114. Producing a cambial age map from an increment core.

14.2.5 Wood stiffness (Modulus of Elasticity, MOE)

Stiffness refers to a board's ability to resist deflection under load and is a function of combined wood properties (mainly moisture content, density, microfibril angle) and the anatomical structure of the wood. Higher stiffness properties for boards are more valuable due to their capacity for longer spans in service. Boards with high stiffness properties can also be used in a smaller cross-sectional dimension than boards of lower stiffness. MOE is determined directly via standardised static methods in compression, in tension and in bending. Non-destructive evaluation (NDE) via resonance acoustics overcomes the problems induced by static tests which are time consuming and destructive.

Acoustic techniques provide some of the most accurate methods for non-destructively extracting fundamental material information. Pulse-echo ultrasonic methods are commonly used to determine the speed of sound in solids, where a single short pulse of high frequency sound is applied to one surface and a time-of-flight record of the reflected ultrasonic wave from the solid is analysed to estimate the speed of sound given the distance travelled in the round trip. Various methods for velocity measurement using pulse-echo methods have been previously described in a number of reviews. Among them, ultrasonic, acoustic and resonance methods are widely used for wood properties characterisation.

In this project, the mean wood stiffness value for each segment was determined using an ultrasound device (Figure 115). The segments were placed between two transducers, with their thickness recorded. Measurements were performed in transmission mode at 1 MHz with a dry coupling (thin elastomer). The device ensured a constant, light contact pressure. The output signal was digitised to calculate the propagation time. The equipment used for this test includes a Picoscope oscilloscope (Pico 3224), Olympus 5077PR square wave emitter/receiver, two contact transducers (V103 Videoscan, Olympus) and a computer. The software version used was CIRAD Ultrasound Transmission Velocity 2015.
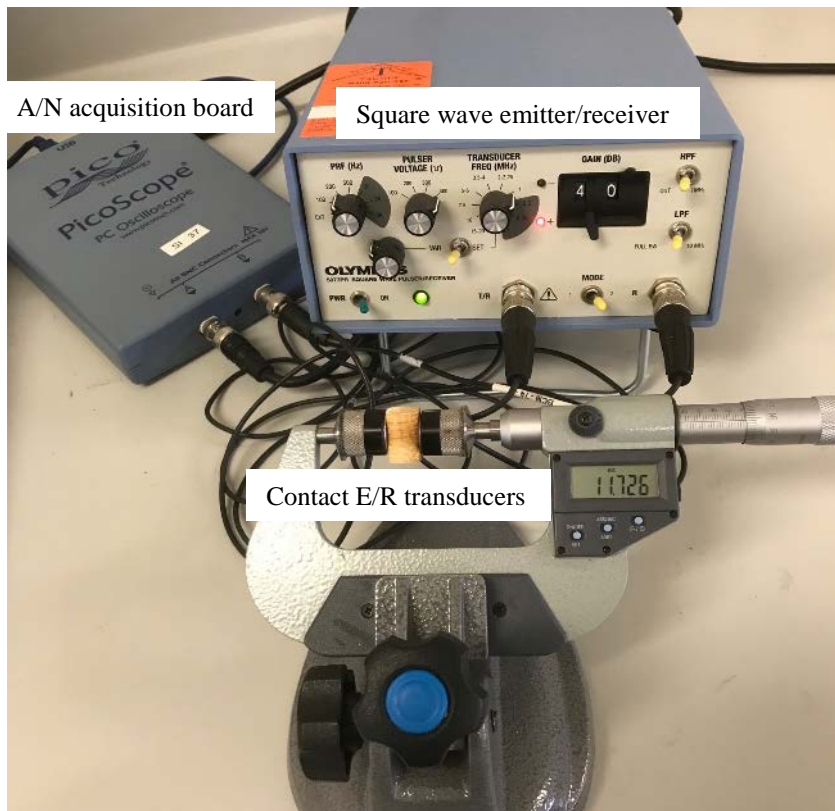
Figure 115. Ultrasound apparatus for calculation of wood stiffness properties (USMOE).

The stiffness of each segment, expressed as MOE in megapascals (MPa), was determined through a corrective formula of the conventional equation:

$$MOE = \rho V^2 = \rho \left(\frac{L}{\tau}\right)^2$$

(11)

Where ρ = the density, V = the wave velocity, L = the segment thickness, τ = the propagation time. This last equation is only valid for guided waves in a freely bound slender beam.

The corrective formula takes into account the Poisson ratios in longitudinal-tangential and longitudinal-radial planes, the shape and the dimensions on the specimen.

To establish the correction formula, it was assumed that:
1. The natural resin within the wood tissue does not alter the wave propagation in the wood
2. The presence of free water over and above fibre-saturation point (FSP, set as a constant value of FSP=30%) will alter wave propagation.

These assumptions have been verified.

14.2.6 Wood density

Wood is a porous solid with a similar cell wall density across all species of approximately 1,500 kg/m³. Different species have different cell wall thicknesses and void sizes so the actual range of dry wood densities (12% moisture content) varies from as low as 130 kg/m³ for balsa wood (*Ochroma pyramidale*) up to 1,350 kg/m³ for gidgee (*Acacia cambagei*). Although density by itself is not a self-sufficient index of wood quality, wood density is the most commonly studied wood property due to its importance in determining general end-use. Density is relatively inexpensive and simple to measure including on small samples such as the segments from increment cores used in this project. Segment densities were calculated at green, 16%, 8% and oven dry moisture conditions. The water displacement method was used

according to the immersion method described in Australian Standard *AN/NZS 1080.3:2000 Timber—Method of test density*. A Mettler Toledo MS 204TS laboratory balance was used for all sample weighing (Figure 116).

Figure 116. Wood segment density determined in accordance with Australian Standards.

To prevent surface tension on the green wood segments and to provide a stable wet environment during immersion, three drops of a wetting agent (Pervitro 75%) were added to the water. At 8% moisture content, the segments were treated with a light spray of 3M Scotchguard™ fabric and upholstery protector. This prevented instability caused by the occurrence of air bubbles during weighing in water. Densities were calculated using the formula:

$$\rho 2 = \frac{A}{A - B} \times \rho o \qquad (12)$$

where:

$\rho 2$ = the density of the segment in grams per cubic centimetre
A = the mass of the segment in air in grams
B = the mass of the segment when immersed in water in grams
ρo = the density of the water in grams per cubic centimetre.

The density results were corrected for resin content using predictions for each segment gathered by near infrared spectroscopy (NIR) at 8% moisture content (Francis 2016).

14.2.7 Wood shrinkage

Wood is a biological product formed in an aqueous environment. Freshly harvested southern pines typically have moisture content in excess of 100% of the dry wood mass. The removal of moisture during drying imparts stability and improves mechanical properties, but results in dimensional changes. After drying, wood products can continue to shrink or swell in correlation with changing micro-climate conditions, sometimes leading to distortion (spring,

twist and bow). One of the objectives of the project was to develop a relatively inexpensive alternative method to provide comparative shrinkage data from the 20 mm segments.

The process involved painting one tangential longitudinal face of the 20 mm segments in the green condition with white correction fluid and scanning to produce a benchmark digital image (Figure 117). Scanning was repeated after drying to 8% moisture content and the two areas analysed with the image analysis freeware program ImageJ (Schindelin *et al.*, 2015) by first removing artefacts using a threshold function, then selecting a position within the region of interest to calculate the number of pixels at a set resolution. The difference in the two areas expressed as a percentage provides a comparative indication of the magnitude of shrinkage.
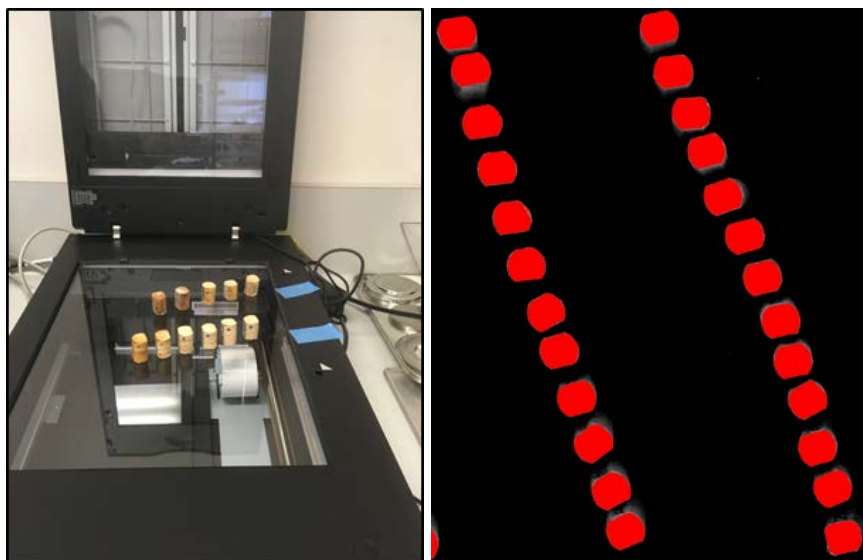
Figure 117. Digital scanning of segments (left); ImageJ plot of scan for area analysis (right).

No significant findings were made and hence we have excluded further discussion on shrinkage to concentrate on the more important issue of wood MOE.

14.2.8 Wood extractives' content

Extractives are naturally-occurring compounds produced by plants, often for the purposes of wound repair and bio-chemical defence against insect pests. In pines, the best-known extractives are collectively referred to as 'resin', evident as a semi-solid exudate containing aromatic hydrocarbons such as the pinene group of terpene compounds (Figure 118) which give pines their distinctive odour.

Figure 118. Resin in the core of a log (left) and exuding from freshly sawn pine boards right).

Extractives impact on wood density measurements, which in turn are used in the calculation of wood stiffness using data collected during ultrasound testing. Extractives were accounted for in this study by predicting the extractives content from core segments enabling an extractives content correction factor to be applied to the density values. Near infrared spectroscopy (NIR) was selected to indirectly predict the extractives content in diametrical cores. A multivariate NIR calibration model was developed from wet chemistry extraction data, which enabled rapid predictions of the extractives. The triple extraction wet chemistry process was conducted in accordance with the method described by Alves *et al.*, 2012. This process involves percolation and extraction steps for each of three solvents: dichloromethane (DCM), 96% ethanol and deionised water (Figure 119).
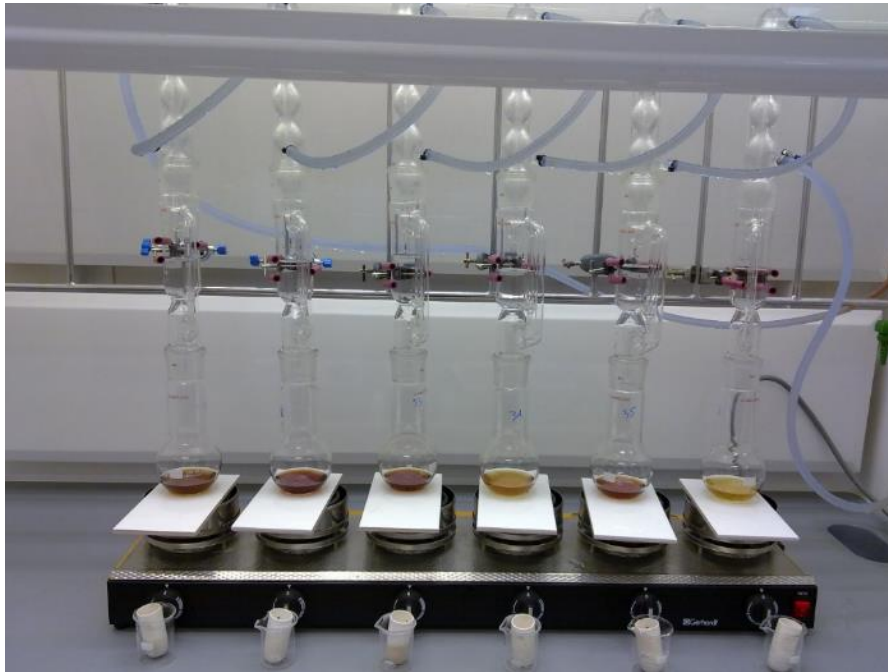
Figure 119. Wet chemistry solvent extraction processing of southern pine material.

Fifty-eight sacrificial trees representing different age classes for five southern pine taxon growing on a range of sites (n=28) were selected from Queensland and New South Wales plantations to develop the NIR calibration models. Disc specimens were collected from breast height then sub-sampled from the sapwood, intermediate wood and inner heartwood (close to pith). The preliminary step involved scanning of both sawdust (wood ground through a 1×1 mm mesh) and solid wood samples using Bruker MPA NIR (Bruker Optics, Ettlingen, Germany) to obtain diffuse reflectance spectra. Spectra were acquired between 800 nm to 2,500 nm and the spectral resolution of 16 cm^{-1}. To minimise the effect of moisture, sample storage and NIR processing were carried out in a constant environment room set to conditions equivalent to an equilibrium moisture content of 8%. These data were then interrogated using Bruker OPUS software which enabled selection of 87 specimens to be further processed and analysed through the wet chemistry laboratory for development of the multivariate calibration model. The multivariate NIR calibration model was developed using MATLAB software (MATLAB R 2016b).

The DCM extraction resulted in the best calibration with a coefficient of determination $R^2 =$ 0.98, whereas the ethanol and deionised water extractions yielded less extractives (<8%) and were more sensitive to extraction measurement uncertainties. This means that the DCM wet chemistry and NIR predictions could be used with more prediction power than either the ethanol or water extractions. The statistical method of root mean square error of calibration

(RMSEC) was used to measure how well the calibration model fitted the calibration set. The result was RMSEC = 2.2085. Bias is a measure of how far the curve is away from a line forced through the origin and for this calibration bias was 0. Cross validation is a useful tool enabling an assessment of the optimal complexity of a model (for example, the number of principal components in a Principal Components Analysis (PCA) or Principal Components Regression (PCR) model. Similarly it is used to calculate the number of latent variables in a Partial Least Squares (PLS) model and it allows the estimation of the performance of a model when it is applied to unknown data. A venetian-blind cross (splitting data into groups) validation with 16 splits was run on the NIR predicted data, providing the following results:

- coefficient of determination (cross validation) $R^2 = 0.97$
- root mean square error of cross validation (RMSECV) = 2.54
- cross validation bias = -0.056.

The multivariate NIR calibration model was used to rapidly predict resin contents within 20 mm solid wood segments of diametrical cores collected from 54 plots. A near infrared spectrum representing each core segment was collected using the integrating sphere of a Bruker MPA and a custom made sample oscillator for sample presentation (Figure 120). The sanded radial surface of each 20 mm segment was scanned using the microsample option of a Bruker MPA. Again, the constant environment room was used for storage of core segments and collection of NIR spectra.
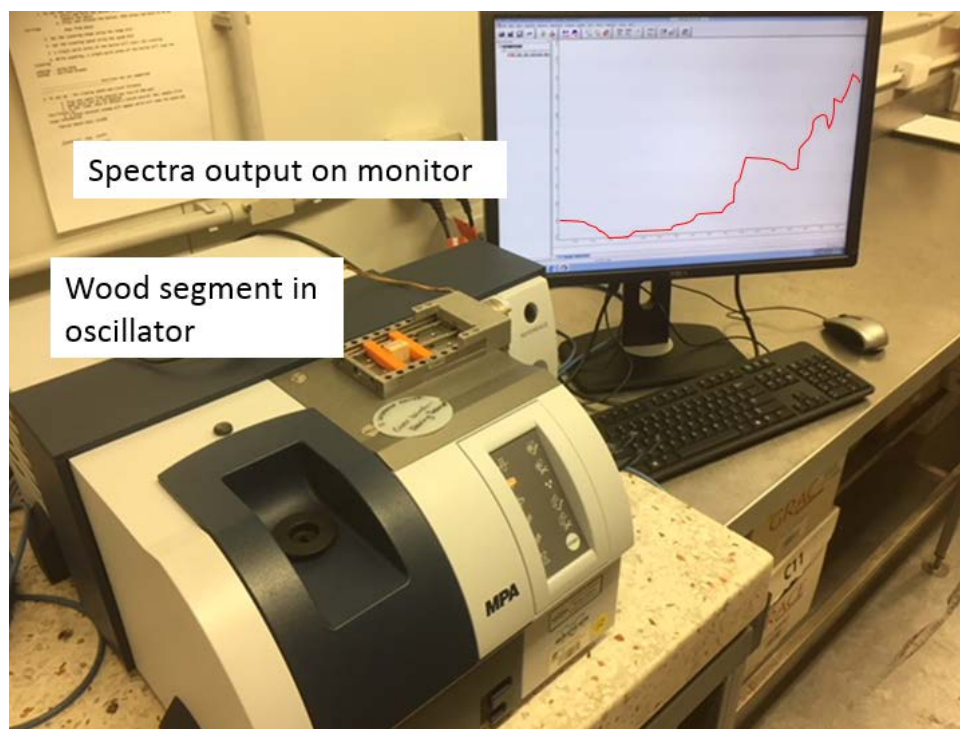
Figure 120. Rapid scanning of segments using the Bruker MPA near infrared spectroscope (NIR).

14.2.9 Permeability

Permeability is the property of a material that indicates how freely fluids or gases flow in response to a pressure gradient. Growth features (such as ring width), anatomical features (such as tracheid pitting) and wood chemistry (for example, the incidence of resin) impact permeability. The permeability of wood to liquids influences many processes including treatment (e.g. with preservatives), modification, drying, pulping, gluing and finishing. In the case of permeability by liquids, permeability is measured as the rate of flow of fluid through a

wood specimen of known length and cross-sectional area while a known pressure gradient is applied. Permeability is expressed in milliDarcy units (mD) where 1 mD = 1.01×10^{-15} m².

Tangential permeability measurements were conducted on a sample from fifty-seven trees harvested from 28 sites. These were selected to represent the range of taxa, age classes, sites across south-east Queensland and northern New South Wales.

Radial permeability was measured on specimens from 30 F_1 hybrid trees from a spacing trial (622NC, refer to Appendix 1)

Each tree sampled provided a transverse disc from breast height (1.3 m above ground level). The discs were conditioned to 8% moisture content, then three specimens at 22 mm diameter $\times$ 8.5 mm thickness were cut out using a hole-saw drill attachment from positions near pith, mid-radius and near bark (Figure 121, tangential permeability and Figure 122, radial permeability).

Figure 121. Tangential permeability sample positions.
The range of cambial ages (ring number from the pith) was recorded for each specimen and they were coated with epoxy resin on all surfaces except the surface facing the direction of flow. This was done to minimise any liquid movement through surfaces other than the tangential or radial surface, so permeability could be measured in one direction only.

Wood liquid permeability measurements were undertaken on all the samples using a Porolux 1000 Porometer. This wood value platform module measures the pore size and liquid permeability. Samples were subjected to water flowing at a constant pressure of 4,200 millibars for five minutes. In some cases, where the sample registered zero permeability after five minutes, a second permeability test of up to one hour was implemented. Figure 123 shows a permeability test being undertaken using the Porolux 1000 porometer equipment.

146
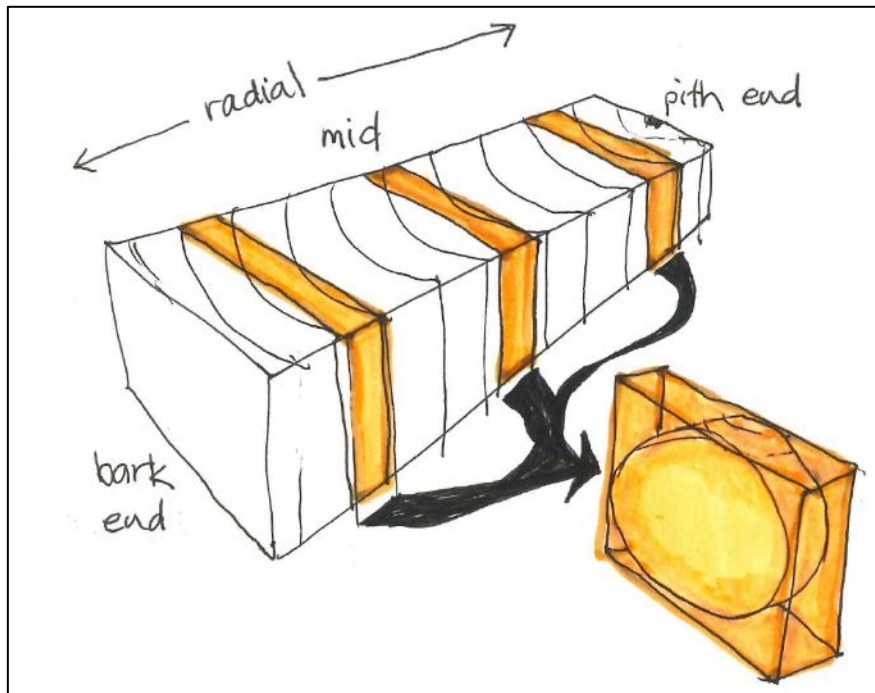
Figure 122. Radial permeability specimen locations.

Figure 123. Permeability module in the wood value platform: Porolux 1000 porometer.

Permeability was calculated from Booker's equation (Booker, 1977):

$$K = QL\eta/A\Delta P \tag{13}$$

Where K = permeability (mD)

Q = flow rate (m/s)

L = length of the specimen (m)

η = viscosity (Pa.s)

A = cross-sectional area of flow (m^2)

ΔP = pressure difference across the specimen (Pa)

Resin contents for each permeability specimen were predicted using the NIR module described earlier section 5.1.1.7). Wood density was measured using the immersion method also described earlier (section 5.1.1.5).

14.3 Appendix 3. Propagation time of acoustic waves in solids using the ST300 (Fibre-gen, New Zealand)

Measurement methodology

The experimental setup consisted of two acoustic probes (accelerometers), a hand-held hammer, and a portable digital oscilloscope (Figure 124). The two probes were inserted into the tree trunk at about 45° to the trunk surface (pierce the bark and cambium and extend into the sapwood) and aligned within a vertical plane on the same face approximately 1.2 m apart from 60-70 cm above ground level. A laser guided ultrasound rangefinder measured the exact distance between the probes. Acoustic waves were introduced into the tree in the longitudinal direction by impacting the lower probe with the hand-held hammer. The receiver probe recorded the acoustic signal passing through the tree and a propagation time (Time-of-fight, TOF) was determined. The distance between probes and TOF were sent by wireless communication to a PDA (personal digital assistant) that calculated the acoustic velocity (Wang *et al.,* 2001; Carter *et al.* 2005; Wang *et al.*, 2007). Wang *et al.* patented the principle of measurement in 2008.

Figure 124. Experimental setup used for testing standing trees (ST300, Fibre-gen, Inc.)

14.3.1 Time-of-flight: rationale and literature review

Analysis fundamentals

The distance between probes (L) divided by the propagation time (TOF) is equal to the calculated acoustic velocity (V):

$$V = \frac{L}{TOF} \tag{14}$$

Theoretically, the acoustic velocity (V) is linked to the apparent modulus of elasticity (MOE) and density of the material (ρ) by the one-dimensional wave equation: (Wang *et al*., 2001; Paradis, 2013)

$$MOE = \rho V^2 \tag{15}$$

This equation is valid for homogeneous material (e.g. steel) and planar compressional waves. This type of one-dimensional wave propagation is encountered in very slender beams where the distance L is much greater than the diameter (e.g.$10 \times$ diameter). In a tree this does not often apply (Brancheriau and Bailleres 2002) due to the large tree diameters. Still, many authors report good velocity readings when the velocity is measured over 1.2-1.3 m (Wang *et al.,* 2001; Carter *et al*. 2005; Paradis, 2013). This distance is used as it allows rapid measurement, and from practical concerns for operators reaching a comfortable height.

An estimation of the apparent MOE requires a measure of tree density, but density is not usually measured in the field. Still, many authors hypothesised that the acoustic velocity is related to the mechanical properties of wood in the tree (Wang *et al.,* 2001). Researchers therefore concentrated on correlating the velocity with quality criterion defined for trees, logs and boards (Carter *et al*. 2005; Wang *et al.,* 2007; Paradis, 2013). At this point, it is important to remind readers of this report, that neither a correlation coefficient (r), nor a coefficient of determination (R^2), are good indicators to compare different regression results from different studies because the R^2 depends on the variance of the trait (the standard deviation of the residuals should be used and compared in this case).

As the acoustic velocity (V) is linked to the specific modulus (MOE/ρ), it is normal to find that V mainly varies according to: the moisture content within the tree (from pith to bark and from base to top of tree that is associated with the formation processes of juvenile and mature wood); with the grain angle and with the microfibril angle. Variation observations of the MOE and the density can be found in many references (see for example Kollmann and Côté 1968, Bodig and Jayne 1982, Barnett and Jeronimidis 2003).

When the trunk is impacted with a hammer, low frequency waves are induced in the medium (Arciniegas *et al.*, 2014). These waves are of different types (compressional, shear and surface waves) (Bruneau and Potel, 2009). The acoustic velocity is defined as the apparent velocity of the fastest compressional wave. 'Apparent' velocity is used here, as different methods of time propagation analysis lead to different results (Arciniegas *et al.*, 2014, 2015). For the specific case of the ST300, the user can visually evaluate the quality of the acoustic signal. A waveform with a sharp-rising pulse (high slope) in the beginning is deemed as a good signal and hence the ToF is determined by measuring the time difference between two rising start points of the waveforms (Wang *et al.*, 2007). The slope-detection method, as cited by Wang (2007), is not documented in the literature.

To improve the accuracy of the ToF determination, Wang *et al*. (2007) performed tree measurements on a randomly selected side of the tree trunk, and three readings were collected to obtain an average acoustic velocity. In comparing the results between ST300 and HM200 Carter *et al*., 2005 stated that the correlation is improved as one acquires and averages more samples around the stem circumference with the ST300. The best prediction of log velocity was achieved by averaging 27 hits/tree (three positions × nine hits). More recently, Paradis *et al.* (2013) chose eight successive hits to limit the variability between successive readings on the same tree.

When using the ST300, the distance between probes is generally 1.2 m, but the equation is only valid for distances which are approximately 10 times the diameter (as an example, for a tree of 30 cm diameter, the probes should be placed 3.0 m apart). If the distance between probes is shortened, the configuration of the test changes progressively from one-dimensional waves to volume waves. Christoffel's equation should therefore be used, where the stiffness matrix in the longitudinal direction is superior to the corresponding modulus of elasticity. Since the physical assumptions for these tools (based on equation 15) are violated, the ToF is higher than that which would be measured if the correct configuration was used.

Issues to consider when using ToF acoustics to estimate MOE include:
- Acoustic velocity varies with moisture content and hence season, with longitudinal velocity reducing with increased moisture content whereas radial and tangential velocities become variable (Legg and Bradley, 2016). Density also varies with moisture content which will impact on the predicted MOE. Note that above fibre saturation point MOE is relatively constant.
- Acoustic velocity decreases with increased temperature (Legg and Bradley, 2016).
- Reaction wood can cause variations in acoustic velocity measurements (Legg and Bradley, 2016).
- Branches, knots, grain angle and spiral grain can all reduce acoustic wave velocity (Legg and Bradley, 2016).
- There may be a negative correlation between acoustic wave velocity and DBH, with some authors suggesting tree stiffness should be compared to slenderness (height/DBH) rather than DBH (e.g. Legg and Bradley, 2016 Watt and Zoric, 2010).
- Acoustic velocity increases with increasing age of a tree in a non-linear way (Legg and Bradley, 2016).
- ToF acoustic tools over-estimate the stiffness compared to resonance acoustics (e.g. HM200 or Beam Identification by Non-destructive Grading (BING) or bending techniques (Legg and Bradley 2016; Wang, 2013).
- ToF measurements are over approximately 1 m compared to resonance acoustics measured over a whole log, hence ToF measurements are more prone to errors from localised variation in the wood properties (grain angle, knots / branches, spiral grain, reaction wood, etc). This can partially be compensated for by using multiple hammer hits (Legg and Bradley, 2016).
- ToF acoustic measurements more closely correspond to the MOE of the outerwood than the corewood (Legg and Bradley, 2016).
- Thinning is thought to reduce ToF velocities of some species e.g. *P. radiata* but not Douglas fir, *Pseudotsuga menziesii* (Legg and Bradley, 2016).
- Increased stocking is positively correlated with increased ToF acoustic velocities and predicted MOE in *P. radiata* and *Cryptomeria japonica* (Japanese cedar; Legg and Bradley, 2016), *P. taeda* when stocking increased from 1,334-2,990 stems/ha (Roth *et al.*, 2007) and *P. radiata* when stocking increased from 275 to 2,990 stems/ha (Waghorn *et al.*, 2007).

- Standing tree ToF acoustic tools can be operationally used for indicative stand level comparisons of stiffness. They are also useful for comparative tests, such as in the selection of genetic material and assessment of thinning impacts. Further work is needed for widespread application e.g. sorting compartments for wood quality and value (Murphy and Cown, 2015).
- Field based acoustic tools are practical and show promise, however they cannot detect resin blemishes, decay, intra-ring checks and reaction wood (Murphy and Cown, 2015).
- Using constant (assumed) densities may result in substantial over estimation of MOE from acoustic tools, particularly at the log level (Wielinga *et al.*, 2009, Watt and Trincado, 2014).
- There is often more variation in MOE within a Sitka spruce (*Picea sitchensis*) stand than between stands (Moore *et al.*, 2013). Given this, Moore *et al.*, (2013) suggested that ToF acoustic tools could be used to segregate trees that have potential to produce high stiffness timber.

A recent study has highlighted that the theoretical operations of ToF acoustic tools are still not completely understood with Essien *et al.* (2017) observing that whole disc density explained a higher portion of variation in acoustic velocity than just examining the outer wood density. In their study of 14 year old *P. taeda*, they found a moderate but significant correlation (0.48) between cellulose and log velocity measured using an ST300. They also found cellulose content was strongly associated with acoustic velocity and MOE providing molecular level support for the capability of ToF tools to estimate stiffness.

Studies evaluating the characterisation of plantation estates using ToF acoustic tools have been underway for the last 15 years following the development of portable ToF acoustic tools such as the Director ST300, IML Hammer, TreeTap and Fakopp. The reason these tools have been included in these resource characterisation studies is due to the ease of data collection in the field and the ease of analysing this data to rank plots / compartments for wood properties (but not necessarily value at the board level as described in section 6.4).

14.3.2 Repeatability and operator effects

Previous characterisation studies (e.g. Blakemore *et al.*, 2010) have found that ToF stress wave tools were subject to errors associated with poor tool calibration and variation between operators. To account for this we have undertaken several studies to minimise the variation and understand what is being measured and how good the tools are at predicting MOE of the log and of the boards.

To overcome calibration issues with the ST300 tool it was calibrated on a regular basis to ensure that it was providing accurate data. We also undertook a range of supplementary tests as follows:
- Effect of operator. We found there was variation for the ToF velocity when three operators used the same equipment on the same tree. Hence we decided to use only one operator to collect all ST300 data.
- Similarly, we found that when using two calibrated ST300 tools there was up to a 12% difference in acoustic velocity readings between the two instruments. Hence we decided to only use one ST300 tool for the whole study.
- To ensure good repeatability of the ST300 across seasons, we conducted a season of sampling study within a single growth plot with 47 trees. There were very strong correlations between the four repeated measures over an 11 month period with R^2 ranging from 0.91 to 0.95. For example, Figure 125 shows correlations between acoustic velocity measures 11 months apart for the same trees.

In addition we evaluated what part of the logs the ST300 was measuring and how this data corresponded to ST300 measurements of $30 \times 30 \times 1,800$ mm boards cut from these logs. In this small study we evaluated two logs from a 38 year old PEE plantation. We found that the acoustic velocity of the outer boards were highly correlated with the ST300 acoustic velocity of the logs ($R^2 = 0.92$). However, the acoustic velocity of the inner boards was not correlated to the log results (see blue circle, Figure 126). Hence the ST300 is not predicting the wood properties or value of the inner boards that will be cut from a log even though these generally constitute the majority of the boards.
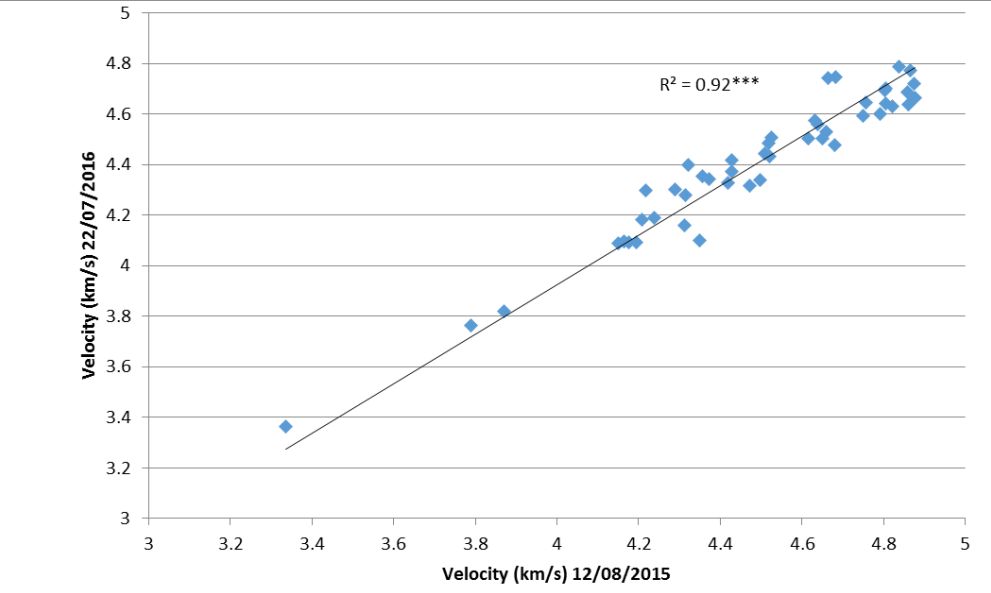

Figure 125. Repeatability of ST300 acoustic velocity measures between two measure dates (11 months apart) for 47 trees in Growth Plot 640 at Toolara. Data was collected by a single operator using the same ST300 tool.
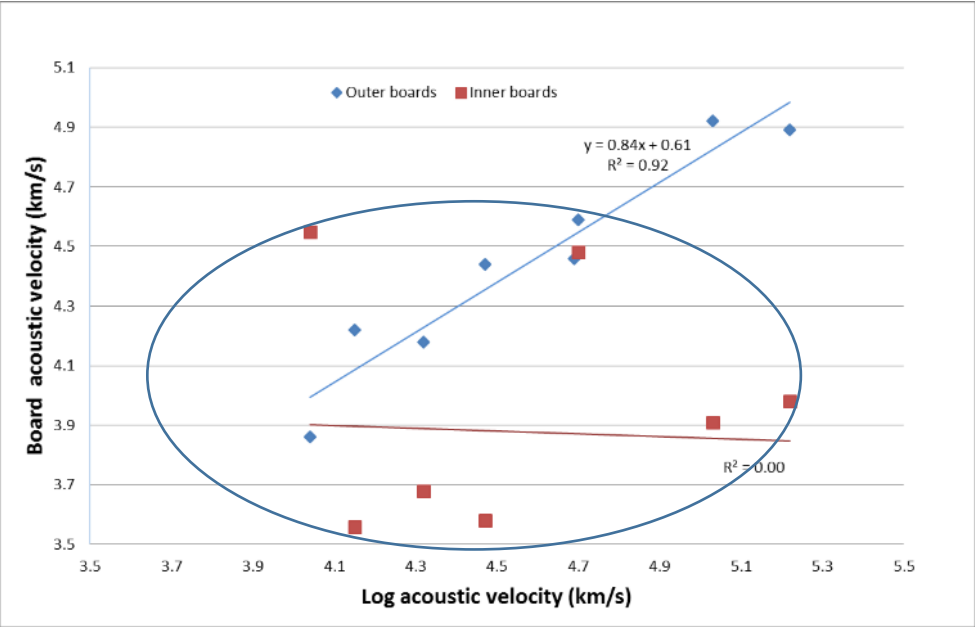

Figure 126. Comparison of ST300 acoustic velocity data collected from two 38 year old PEE logs with the acoustic velocity of boards cut from these logs.

14.4 Appendix 4. Resonance frequencies of acoustic waves in solids (HM200, Fibre-gen, New Zealand)

14.4.1 Measurement methodology

An acoustic probe is put in contact with one end of the log. The user hits the end of the log with a hammer (Figure 127). The probe records the resulting acoustic signal, and a built-in Fast Fourier Transformation (FFT) program analyses this signal to determine the fundamental resonance frequency of the log. Once the user enters the log length, or selects the length from a pre-loaded list, the acoustic velocity is determined. (Wang *et al.*, 2005; Carter *et al.*, 2005). The user can also program the HM200 to recognise up to three grade categories based on the displayed velocity. These are signalled to the operator by a colour code in the display and by a unique sound signal. The operator can then suitably colour spray or otherwise mark the log for subsequent sorting (Carter *et al.* 2005).
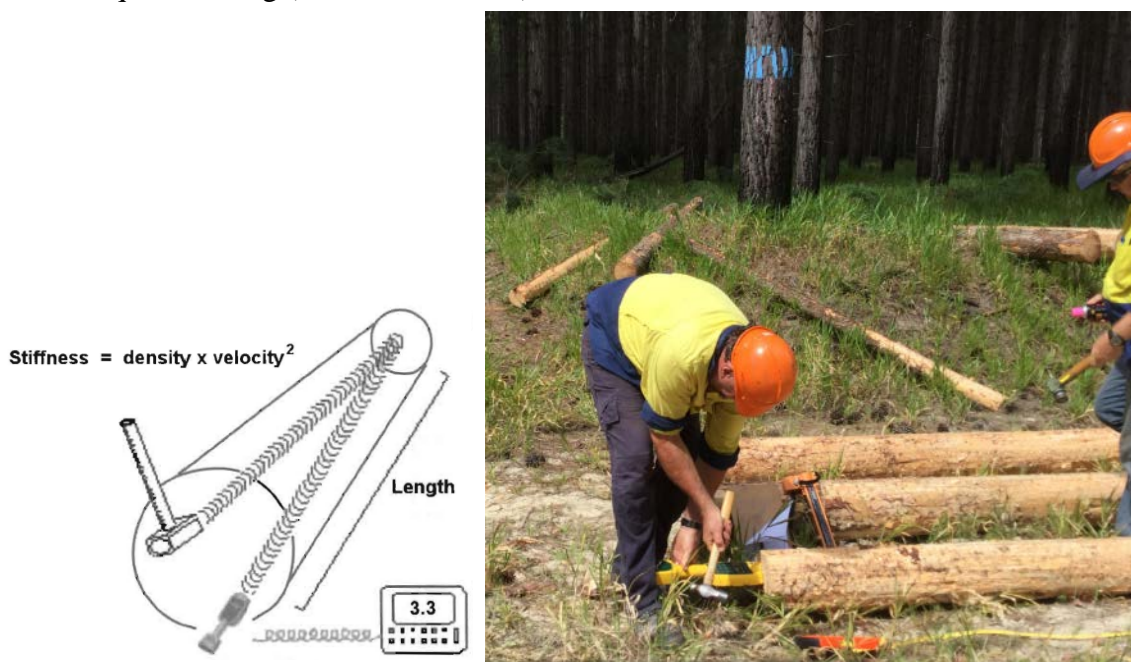
Figure 127. (Left) Experimental setup used for testing logs (HM200, Fibre Gen, Inc., Carter *et al.* 2005). (Right) Collecting HM200 data in the field.

14.4.2 Analysis fundamentals

The log acoustic velocity is determined using the following equation:

$$V = 2Lf \tag{16}$$

Where:
V = acoustic velocity
f = the fundamental natural frequency, and
L = the log length (Wang *et al.*, 2005).

This equation is valid for homogeneous materials (e.g. steel) and planar compressional waves (one-dimensional wave-guide) in a slender beam, which can be characterised as having a length $L \geq 10 \times$ diameter. The resulting velocity is linked to the global dynamic behaviour of the beam (Achim *et al.*, 2011). This resonance velocity measures the whole log whereas ToF velocity only measures a local dynamic MOE. Furthermore, the vibration should occur in free

boundary conditions with negligible effect of the log supports which is different from a simply supported beam (Brancheriau and Bailleres, 2002). However this rarely applies in the field or mill. Ideally, acquisition settings of acoustic signals (sampling frequency and duration of acquisition) for the HM200 should be recorded and the probe should be firmly connected to the surface (Dossing, 1988).

Tree acoustic velocity (ST300) was compared with log acoustic velocity (HM200) by Carter *et al*. (2005) and Wang *et al.* (2007). They found that in most cases the correlation between standing tree velocities and log velocities increases as age and diameter decrease (Carter *et al*. 2005). Therefore, for small diameters, the resonance velocity is better linked with the ToF velocity.

This phenomenon was partially approached by Wang *et al.* (2007) in isotropic material. The trial data showed that acoustic velocity measured on standing trees by ToF method is generally higher than the acoustic velocity measured in the butt logs by resonance method (Wang *et al*. 2007). Their results were consistent with previous findings on standing trees and logs, and concluded that deviation of tree velocity from log velocity seems be influenced by species, stand age and DBH of the trees. They proposed a correction of the form (Wang *et al.* 2007):

$$C_L = a\left(\frac{DBH}{S}\right)^b C_T^c \qquad (17)$$

Where:

C_T is the acoustic velocity of a tree

C_L is the acoustic velocity of a butt log

a, *b*, and *c* are coefficients determined by regression analysis

S is the span between two probes.

In the trial studies discussed in this paper, S was kept constant and was 1.2 m (Wang *et al*., 2007). The HM200 was used in the study, as it is one of the traits predicted by the Resistograph. As the physical principle (measure of longitudinal resonance frequency) for both the HM200 and BING is the same, they were highly correlated ($R^2 = 0.95$) and any difference would be attributed to operator effect. In this study, we have provided data from BING (discussed next) because it can also be used on boards and veneers.

14.5 Appendix 5. Resonance frequencies of acoustic waves in solids (BING, CIRAD, France)

14.5.1 Measurement methodology

The BING consists of a microphone, an acquisition card (Pico Technology), two elastic supports and a hand-held hammer (Figure 124). The geometric characteristics and the mass of the sample were measured with a calliper and a weight scale. This device, originally designed for small samples (360 mm × 20 mm × 20 mm), can be used with a wide range of shapes and sizes. The sample was placed on the two elastic supports to ensure free vibrations. An impulse was generated by hitting one end of the sample and the acoustic sensor recorded the induced vibrations on the other end. The acquisition card was an analog-to-digital converter (12 bit resolution for the Pico card) and the main settings were a sampling frequency of approximately 40 kHz with an acquisition duration less than one second depending on the size of the sample, and the test configuration. The BING software allowed the automatic detection of resonance frequencies and the computation of the results (Baillères *et al*., 2009; Brancheriau, 2014; Faydi *et al*., 2017).
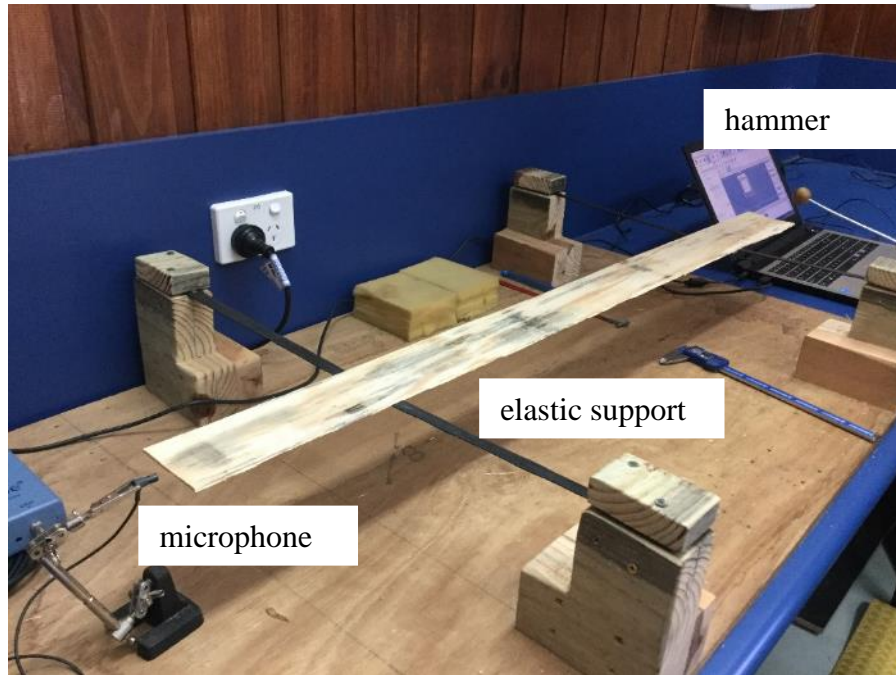
Figure 128. BING resonance module determining stiffness (MOE) on a veneer strip.

14.5.2 Analysis fundamentals

For longitudinal vibrations, the following equation is used to determine the axial modulus of elasticity:

$$MOE = 4L^2\rho \left(\frac{f_n}{n}\right)^2$$

(18)

> Where:
> > L = length of the beam
> > ρ = density
> > f_n = vibration frequency of rank n.

This equation is valid for slender beams ($L/h \geq 10$, h: the height of the beam) and only for the fundamental frequency (Brancheriau and Bailleres, 2002). For higher ranks, the Poisson's effect induces a bias and a correction was proposed by Brancheriau (2011).

The BING technique has been used and tested with other NDE techniques to improve the stress grading of piece of timber (Baillères *et al*., 2009; Hein *et al*., 2010a; Bailleres *et al*., 2012; Faydi *et al*., 2017) or to study the environmental and progeny effects on quality properties (see for example Hein *et al*., 2010b).

Bing used in this study to measure the MOE of logs, boards and veneer.

14.6 Appendix 6. Resistance of drilling (torque): Resistograph IML-RESI PD-Series

14.6.1 Introduction and literature review

There is a range of publications over the last 20 years about micro-drill resistance tools to non-destructively evaluate wood properties of tree species. However, widespread adoption of these tools has not occurred, although several Australian forest growers have recently purchased Resistograph tools. These tools measure variations in drilling resistance of a thin needle when driven into a tree at a constant force. Measured variables include: power consumption, torque, depth penetration through time and are reported to relate well to variation in tree density and the tools can detect growth rings based on the variation in drilling resistance (Rinn *et al.*, 1996). Resistance tools have also been used to detect wood rot in trees (Kahl *et al.*, 2009).

Isik and Li (2003), evaluated an older version of the IML Resistograph tool in four 11 year old loblolly pine (*Pinus taeda*) progeny trials; directly comparing density measured on bark to bark cores to the Resistograph reading (amplitude) and found significant, weak to moderate phenotypic correlations between wood density and the Resistograph amplitude regression equation (r=0.29 to 0.65 across the four sites), however the correlation across all sites was weak (r=0.12). Given this they found a high family mean correlation between density and Resistograph amplitude, leading to them concluding the Resistograph could be used to rank loblolly pine families for wood density. In another study Gantz (2002) found that phenotypic correlations between Resistograph amplitudes and wood density was moderate for four species (two *Pinus* and two *Eucalyptus* species), R^2 ranging from between 0.30 to 0.78. Recently, strong linear correlations (R^2 range 0.66 to 0.87) have been found with the basic density of increment cores of eucalypts species (*E. nitens* and *E. globulus*) across 8 sites in southern Australia (Downes *et al.,* submitted).

Variation in air temperature, flexing of the drill bit during drilling and presence of knots are reported to impact the quality of the Resistograph traces and data of interior spruce (*Picea* spp.; Ukrainetz and O'Neill, 2010). In addition, moisture content of the wood may affect drilling resistance (Lin *et al*. 2003). The development, use and ability of the Resistograph to predict basic density is well described in Goa *et al*. (2017).

No published papers were found on the ability of the IML Resistograph to predict log MOE and log HM200 acoustic velocity, however Downes and Lausberg (2016) have report a moderate relationship between these traits and the trace from the Resistograph for *P. radiata*.

14.6.2 Analysis Fundamentals

This technology is protected by confidentially agreements and we cannot analyse the fundamentals of how it operates.

14.7 Appendix 7. Destructive standard static bending tests

Static bending tests were performed using a testing method in accordance with AS/NZS 4063.1:2010 Characterization of structural timber - Test methods (AS/NZS 4063). Random position tests were used on every board. MOE and MOR were calculated for each board.

The load for the reference testing was applied and measured with a Shimadzu Autograph AG-X 100 kN (10 tonne) universal testing machine depicted below (Figure 129).
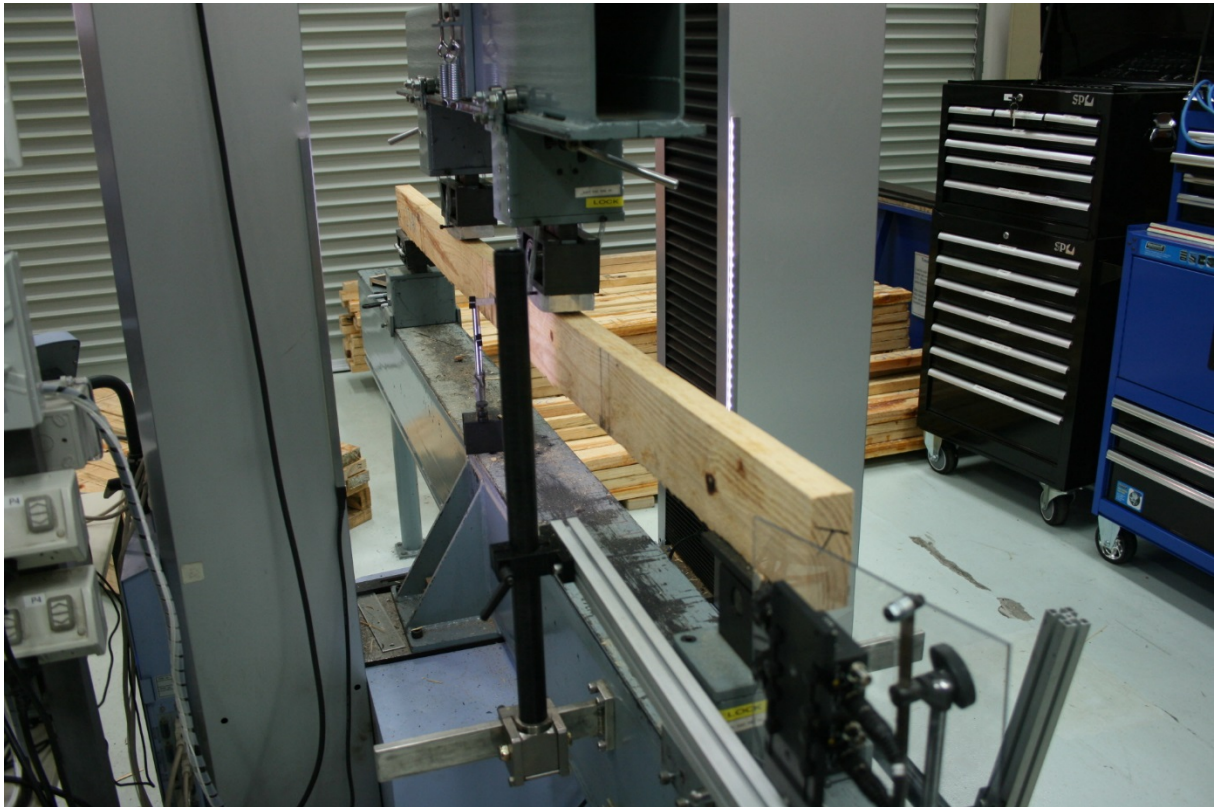
Figure 129. Shimadzu Autograph AG-X 100 kN (10 tonne) universal testing machine.

The term 'universal' indicates that the machine is capable of performing a range of tests including static bending, tension, compression, shear and hardness tests on large samples. The support consists of a solid steel roller 240 mm long by 50 mm diameter and a flat mounting plate. The mounting plates have two holes which are used to locate the plate over machine bolts situated in the centre of the supports. The roller, and to a lesser extent the mounting plate, are held in place by two springs which attach to bolts protruding from the centre of the load roller.
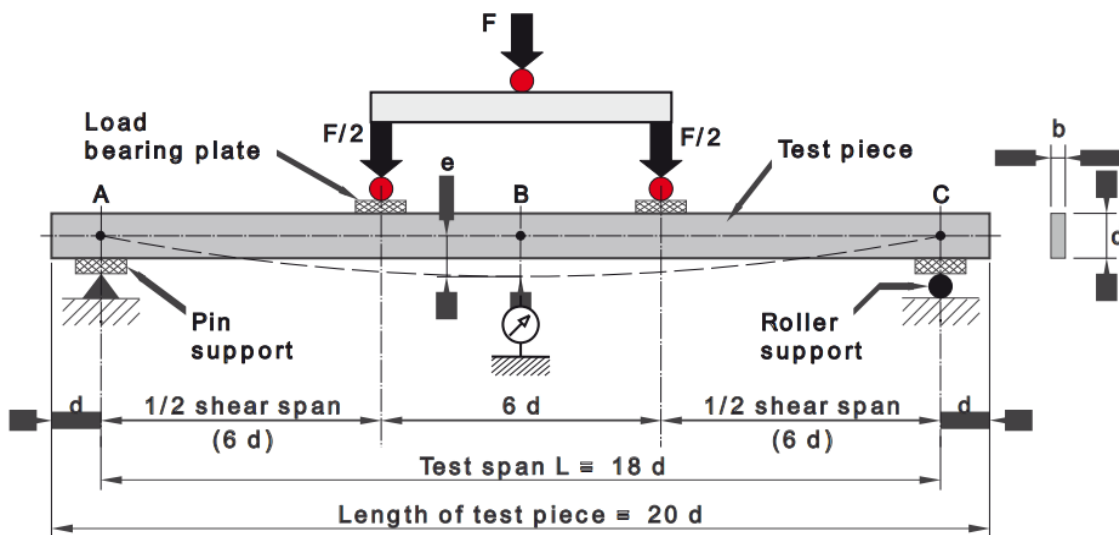

Figure 130. Diagram of the 4-point bending method.

The Shimadzu UDH-30 is a 'Grade A' testing machine in accordance with Australian Standard AS 2193-2005 (R2017) Calibration and classification of force-measuring systems.

The Australian and New Zealand Standard (AS/NZS 4063.1:2010) requires that the specimens shall be conditioned to a temperature of 20 ±3°C and in an environment having a relative humidity of 65 ±5%. This conditioning shall continue until the moisture content is stable within each piece (10-15%).

Moisture content was checked using an electric resistance moisture meter to confirm that the boards had conditioned to the range specified in the standard. Bending strength and stiffness were then tested according to the methods specified in AS/NZS 4063.

In the middle of the span the deflection was measured with a strain gauge type linear displacement transducer. The bending test span was 18 times the height of the board with load applied at four points. The load deflection curve was measured on the linear part of the loading curve for all specimens. The modulus of elasticity can be determined from the slope of the linear relationship between the applied load (P) and the resulting deflection (ε) using the following equation:

$$MOE = \frac{23}{108} \cdot \frac{l_s^3}{bh^3} \cdot \frac{\Delta P}{\varepsilon} \tag{19}$$

The loading continued until failure of the specimen. The modulus of rupture was calculated using the following equation:

$$MOR = \frac{l_s P}{bh^2} \tag{20}$$

The following equation gives an estimation of the relative maximal error on static bending MOE:

$$\frac{|\Delta MOE_{stat}|}{MOE_{stat}} = \frac{|\Delta b|}{b} + 3\frac{|\Delta h|}{h} + 3\frac{|\Delta l_s|}{l_s} + \frac{|\Delta k|}{k} \tag{21}$$

The relative errors on the measurements are based on a sample of 60 specimens and are:

$$b = h = \pm 1\,\text{mm}$$

$$l_s = \pm 10\,\text{mm}$$

k is calculated using the 95% confidence interval from the slope of the force-deflection diagram. This method ensures the maximum relative error in the calculation of static MOE using Equation 12.

The coefficient $\frac{|\Delta k|}{k}$ is calculated as 3 % and due to the similar methodology used in this study the same value was used. Thus the maximal relative error for static MOE is:

$$\frac{|\Delta MOE_{stat}|}{MOE_{stat}} \approx 11\%$$

The maximal relative error of the MOR can be calculated by the following equation:

$$\frac{|\Delta MOR|}{MOR} = \frac{|\Delta b|}{b} + 2\frac{|\Delta h|}{h} + \frac{|\Delta l_s|}{l_s} + \frac{|\Delta P|}{P}$$

The relative error of the load applied is known as 1 % for the machine used. Therefore the maximal relative error of the modulus of rupture is:

$$\frac{|\Delta MOR|}{MOR} \approx 6\%$$

14.8 Appendix 8. Factors evaluated for impact on wood property performance variability (sorted by abbreviation).

Factors	Abbreviation
Age	Age
Cardinal aspect of slope (flat, north, south, east or west)	aspect
Diameter at breast height	DBH
Variation in diameter at beast height measure using callipers	dbh_eccent
Average annual number of dry months with <= 30 mm of rain	DryMonths
Average yearly evaporation	Evap
Average yearly evapotransporation	Evapotrans
Total height to highest green shoot	Ht
Latitude	Lat
Lean (%)	Lean
Elevation measure by Lidar for the plot	Lidar_Elev
Longitude	Long
Number of consecutive drought seasons	MaxDrought
Extreme maximum temperature for the growing period	MaxT
Extreme minimum temperature for the growing period	MinT
Total number of dry months	NoDroughts
Pre-commercial thin completed	pct
Prior land use	Prior use
Has the plot been ground pruned	pruned
Mean daily solar radiation	Q
Average yearly rainfall	Rain
Average yearly number of rain days	Raindays
Mean relative humidity at Tmax	RHmaxT
Relative humidity at Tmin	RHminT
Compass bearing of the planting row	row_bearing
Site index	SI
Tree slenderness (ratio: Ht/DBH)	Slenderness
Percentage of slope	slope
Soil moisture at time of data collection	soil_moist
Stocking	Stocking
Taxon	Taxon
Commercial thinning operation	thinned
Mean daily maximum temperature	Tmax
Mean daily minimum temperature	Tmin
Volume	vol
Average yearly wetness index (Rain/Evap)	Wetindex

14.9 Appendix 9. Median plot MOE rankings determined by non-destructive tools.

For both the ST300 and the IML Resistograph additional plots were sampled. Here we give the MOE predicted by these tools for the full range of plots sampled by each tool. The 93 plots sampled using the ST300 are shown in Figure 131 and the 83 plots sampled by the Resistograph are shown in Figure 132.
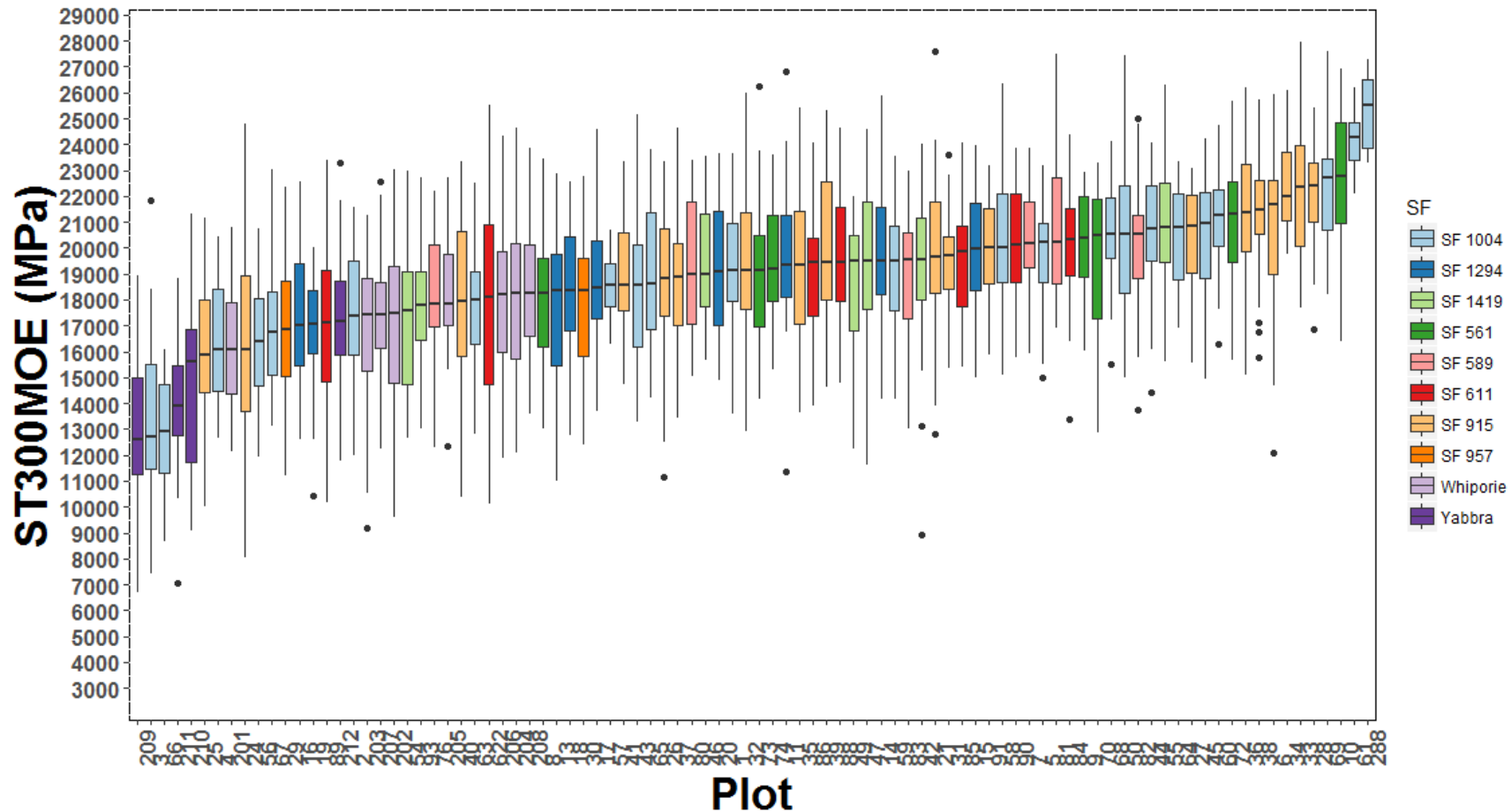

Figure 131. Plots ranked by median MOE as measured by ST300. Colour indicates the state forest (SF) where the plot is located.
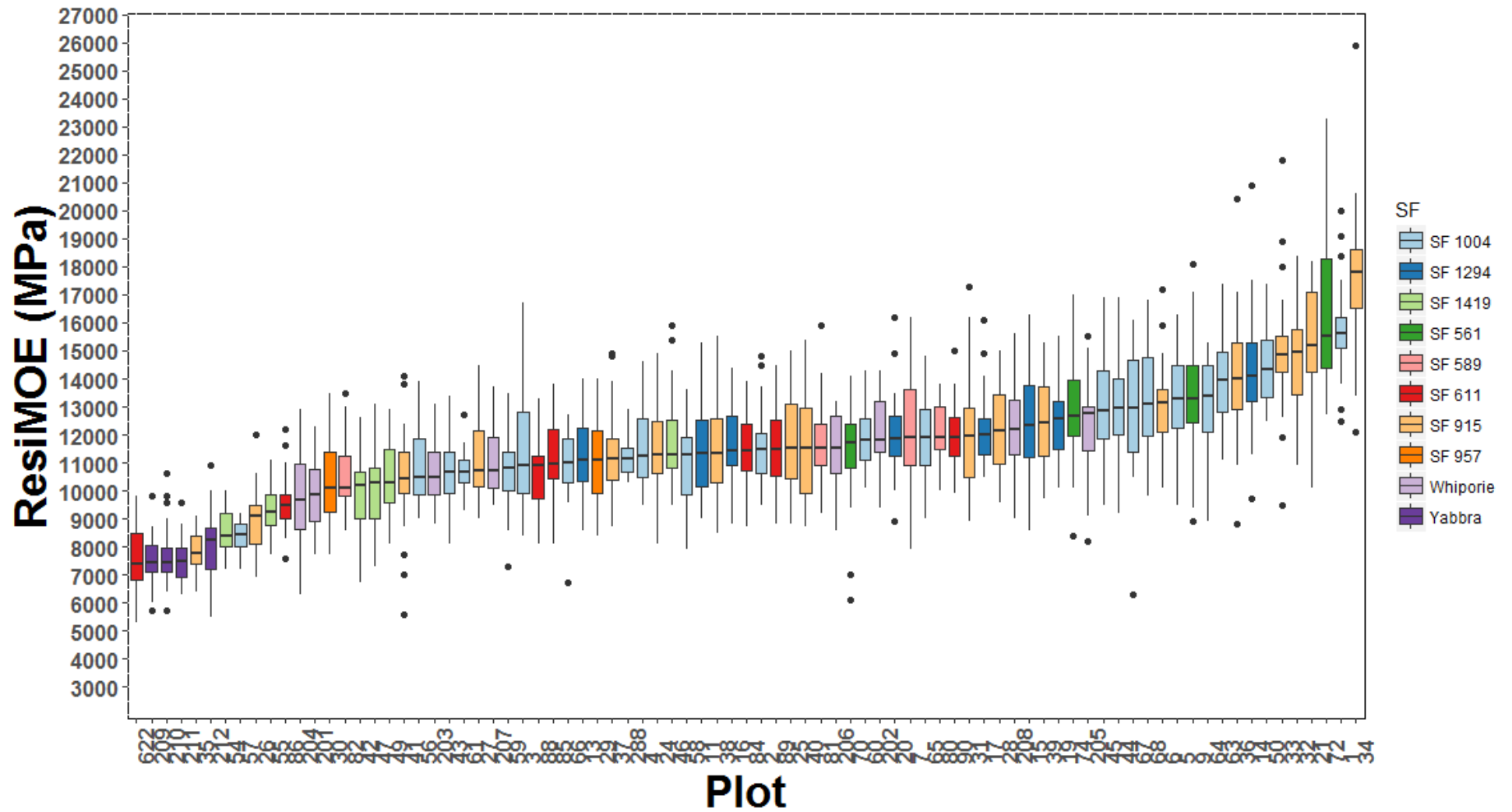
161

Figure 132. Plots ranked by median MOE as determined by the Resistograph. Colour indicates the state forest (SF) where the plot is located.